Transannular interactions in medium-ring carbocycles: Theoretical and experimental investigations

Dissertation

zur Erlangung des Doktorgrades der
Naturwissenschaften im Fachbereich Chemie
der Universität Duisburg-Essen

vorgelegt von

Parveen Choudhary Mohr

Chandigarh, India

2006

This work was carried out between January 2004 and July 2006 at the Fachbereich Chemie, Universität Duisburg-Essen, Germany. The systems discussed in chapter 7 (section 7.2) and 10 (section 10.2) have been studied using Gamess under supervision of Prof. Dr. Harjinder Singh, Dr. Tej Vir Singh and Dr. Paloth Venugopalan at Panjab University, Chandigarh, India.

Ph.D. Advisor: Prof. Dr. Paul Rademacher

Referee: Prof. Dr. Dr. h.c. Reiner Sustmann

Date of the oral examination and defense of the Ph.D. thesis: 25-10-2006

For Andreas and my family

Acknowledgments

During my research work I have been accompanied and supported by many people directly or indirectly. Today, I am very pleased to express my gratitude to all of them.

First and foremost I would like to express my sincere gratitude and thanks to my advisor Prof. Dr. Paul Rademacher at the Universität Duisburg-Essen for his valuable advice, guidance and constant encouragements throughout this research work. His editorial advice was essential to the completion of this dissertation and has given me insights on the workings of scientific research in general. Moreover, I am especially thankful to him for providing me the opportunity to work at Universität Duisbürg-Essen and carry out this research work.

Special thanks are due to Prof. Dr. Dr. h. c. Reiner Sustmann for providing generous support and opportunity to attend and discuss my research work in his research group seminars.

I would also like to give my thanks to Prof. Dr. Harjinder Singh, Dr. Tej Vir Singh and Dr. Paloth Venugopalan for the guidance and support during my stay in Panjab University. I am greatful that they have given me opportunity to work in a project under their supervision. The lessons learnt under their guidance remained helpful to me in both personal and professional life.

I would like to extend my thanks to Prof. Dr. Georg Jansen for numerous stimulating discussions and fruitful suggestions. I would also like to thank Dr. Hans -Gert Korth for his constructive comments and valuable suggestions.

For X-ray diffraction analyses I would like to thank Prof. Dr. Roland Boese and Mr. Dieter Bläser.

Of course I should not forget to mention Dr. Torsten Schaller and Mr. Heinz Bandmann for recording NMR spectra and Mr. Werner Karow and Winfried van Hoof for mass spectra. I would like to thank Dr. Holger Gollan for his support regarding running Gaussian jobs in the computing centre.

I would like to thank Prof. Dr. Sustmann and Mr. Wilhelm Sicking for allowing me to use the program Pergra. Special thanks are due to Mr. Sicking for his generous help regarding computer related problems.

Last years spent in Essen have been a wonderful experience because of the nice, sociable and helpful colleagues. I would like to take this opportunity to thank all my colleagues for their whole hearted help and Dr. Ursula Maria Lottermoser for her support in initial days of my stay in Essen.

I would also like to thank my friends some of them living thousands miles away but who have been always helpful and motivating.

I have no words to express my deep sense of gratitude to my parents for providing me unconditional support throughout my studies. The motivation and invaluable support of my family in the stressful professional and personal stages has proved a great support for me. The unquestioning faith of my family in me remained a stablising force in all the decisions made until now.

I would like to thank my family in-laws especially parents who have tried their best to make me feel comfortable in the family irrespective of wide cultural differences.

The chain of my gratitude would be definitely incomplete if I would forget to thank my husband Dr. Andreas Mohr for his love and patience during the Ph.D. period. He has shown complete understanding towards my personal and professional difficulties and tried hard to remove them. He has been a constant support and motivation throughout my research especially during hard days of thesis writing. In the end I would like to dedicate my thesis to Andreas and my family.

Table of Contents

Chapter **Page**

1 Introduction

1.1 Biological importance

Medium-ring compounds form the structural core of a large number of biologically important natural products. A few examples are given in Scheme 1.1.[1-13] More than 100 natural products belong to the structurally diverse family of cyclooctanoids.[1, 14, 15] Nature has greatly harnessed the flexibility of medium-rings for transannular cyclisation to build numerous polycyclic sesquiterpenoids and diterpenoids. Poly-functionalised medium-rings are an integral part of terpenes and a variety of other natural products, for example, ingenol, taxol and dumortenol.[1] These compounds are of immense synthetic interest worldwide and a great challenge for a synthetic chemist because of their stereochemical complexity.[3, 16] Due to high enthalpic and entropic barriers[17, 18] construction of medium-ring compounds lead to disappointingly low yields.

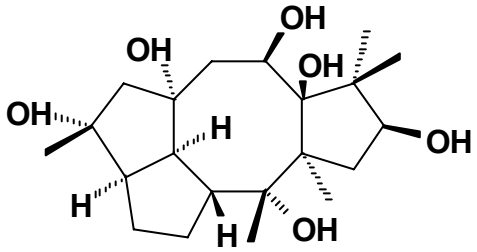

Kalmanol

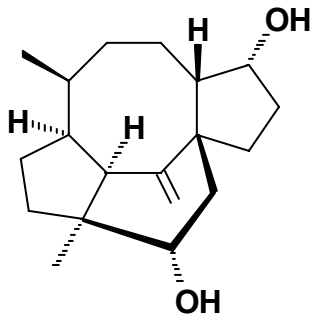

Longipenol

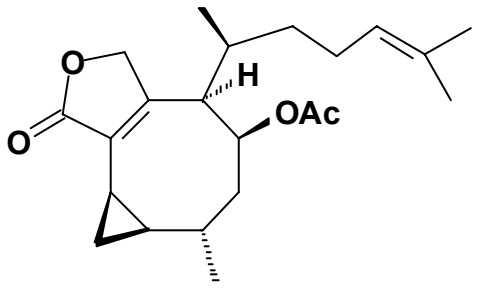

Acetoxycrenulide

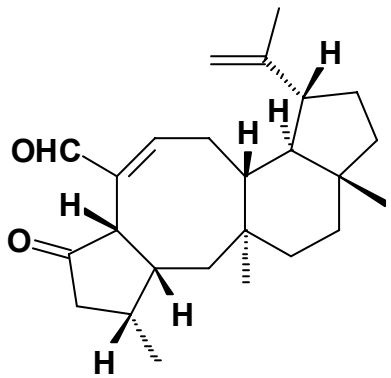

Variecolin

Scheme 1.1: Examples of biologically important natural products containing eight-membered rings.

Interest has been rapidly increased in developing new methodologies for construction of the eight-membered rings since they are found to be useful for biochemical processes.[1, 5, 18] Also, there is an intense activity aimed at producing compounds which can mimick natural compounds.[19, 20] Transannular interactions in medium-rings are an important property in drug design.[21, 22] Derivatives of eight-membered rings are used in the synthesis of macromolecules[23] and polymers.[24]

1.2 Transannular interactions

Medium-ring compounds are eight- to eleven-membered rings. These rings have large number of conformations[25-33] with low energy barriers for interconversion and only medium-ring compounds show transannular reactions.[26, 34-37] In these compounds bond angles, torsional strains and non-bonded interactions are important.[37] In commonly occurring conformations of saturated rings non-bonded hydrogen-hydrogen repulsions are present (Scheme 1.2). When hydrogen atoms are replaced with some functional groups then these non-bonded repulsions lead to transannular reactions.

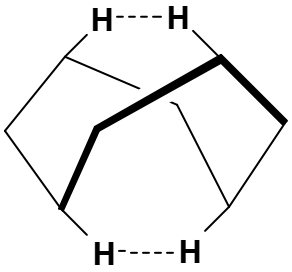

Boat-Boat

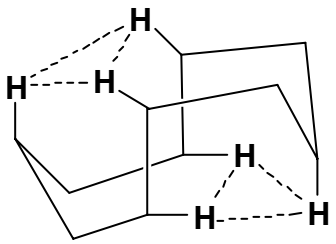

Boat-Chair-Boat

Scheme 1.2: Non-bonded hydrogen-hydrogen repulsions in cyclooctane and cyclodecane.

Due to the presence of non-bonded repulsions between atoms in medium-rings a considerable amount of Baeyer,[38] Pitzer[28, 39] and Prelog strain[28] are present (Figure 1.1). These unusual properties have made medium-rings an area of great interest in organic chemistry.[39, 40] The angle for a tetrahedral carbon atom in medium-rings is more than 109.5°. This leads to Baeyer or large angle strain.[28, 39] To avoid transannular interactions medium-rings adopt conformations in which carbon-

carbon bonds are eclipsed or partially eclipsed. This gives rise to Pitzer or torsional strain.[28, 39] Prelog strain [28] arises from interactions between non-bonded atoms in medium-ring compounds.

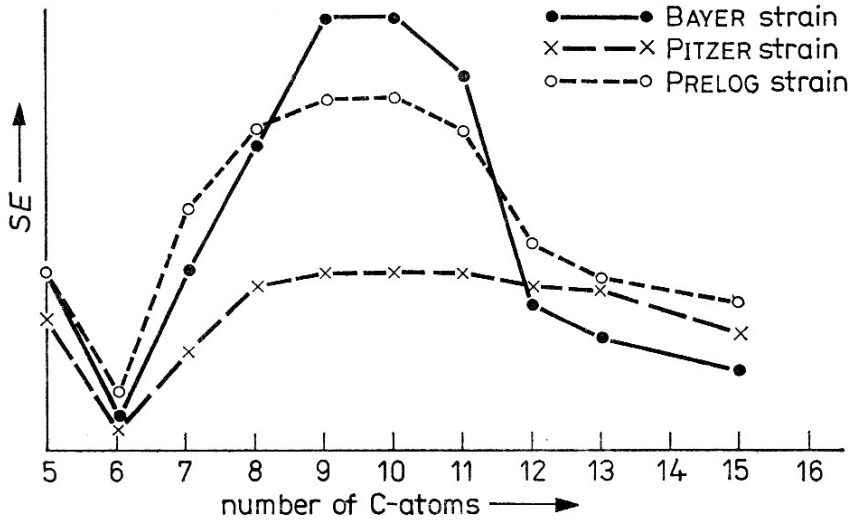

Figure 1.1: Variation of strain energy in five- to fifteen-membered rings.[28]

1.3 Methods to study transannular interactions

Because of the flexible nature of medium-sized rings and abundance of their conformations, there are few studies related to strain in conformations and transannular interactions and often they are inconclusive. A brief review of the work done both by experimental and theoretical methods is given below.

(i) X-ray diffraction studies of crystalline compounds have been reported by Bürgi and Dunitz.[41, 42] The structure correlation method used is based on non-bonded interactions but considers mainly the geometrical effects. X-ray analysis does not give a direct proof of transannular strain. Therefore, other methods such as computational calculations are required to determine the transannular strain due to the proximity of atoms on opposite sides of the ring.

(ii) Griffith and co-workers[21] have quantitatively investigated transannular amine-ketone (N···C–O) interaction in medium-sized heterocycles by force field methods. Theoretical attempts such as *ab initio* calculations and semiempirical electron density analysis have been used to understand transannular interactions in rigid system such as diketones and methyleneketones.[43]

(iii) Nuclear magnetic resonance spectroscopy (NMR) mainly ^{13}C- has been used to study such interactions.[43-46] A number of investigations have been carried out to compare changes in ^{13}C-NMR chemical shift values of the sp^2 carbon atoms in difunctional systems with those of the corresponding monofunctional congeners.[43, 47, 48] Transannular interactions have been discovered in alkanoids and were investigated by chemical, spectroscopic (IR, UV, ORD) and other physical method by Leonard and co-workers[38] in the 1950's. Experimentally, photoelectron spectroscopy[34, 47, 49-51] and electron transmission spectroscopy[52, 53] have been used to detect transannular interactions in flexible as well as rigid systems.

2 Presentation of the problem

Chemical consequences of transannular interactions have been extensively investigated by Cope and co-workers[40] in the cyclooctane series and by Prelog and co-workers[54] in the cyclodecane series. The relationship between structure and reactivity in medium-rings is still not clear due to transannular interactions. Most of the reactions in medium-rings lead to non-classical products. The ring bound functional groups show unusual reactivities. Such cases are reported for mono-functional eight-membered rings. Nucleophilic addition reactions (A_N) are either completely absent or proceed extremely slowly in these rings. Two examples of absence of the nucleophilic addition reaction in cyclooctanone are illustrated in Scheme 2.1.[28, 55, 56]

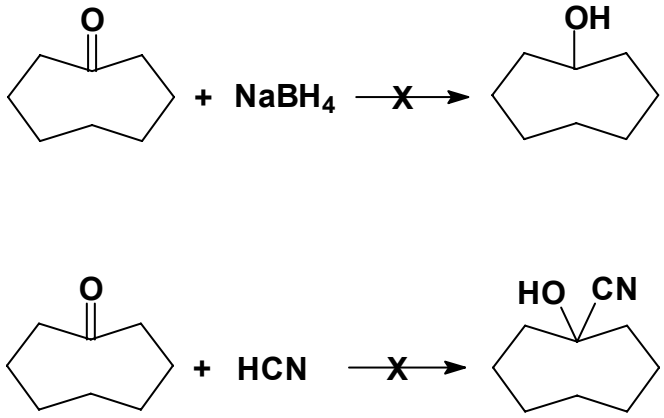

Scheme 2.1: Absence of A_N reactions in the cyclooctanone systems.

The addition of the nucleophile leads to the transformation of a C_{sp}^2 to a C_{sp}^3. This transformation is largely discouraged due to the increase in non-bonded repulsions between hydrogen atoms present in the ring. The relative reactivity of medium-rings is lowest when a $C_{sp}^2 \rightarrow C_{sp}^3$ transformation takes place in a reaction, but the reactivity is highest when the reaction involves the reverse transformation $C_{sp}^3 \rightarrow C_{sp}^2$ (Figure 2.1).

Electrophilic addition reactions (A_E) in eight- and ten-membered rings can also lead to non-classical products. For example, bromination of *cis*-cyclooctene gave *trans*-1,2-dibromocyclooctane, *cis*-1,5-dibromocyclooctane and *trans*-1,5-dibromo cyclooctane in 73, 14, and 8% yields, respectively, whereas *cis*-cyclodecene on

reaction with bromine gave *cis*-1,6-dibromocyclodecane as the sole product (Scheme 2.2).[29]

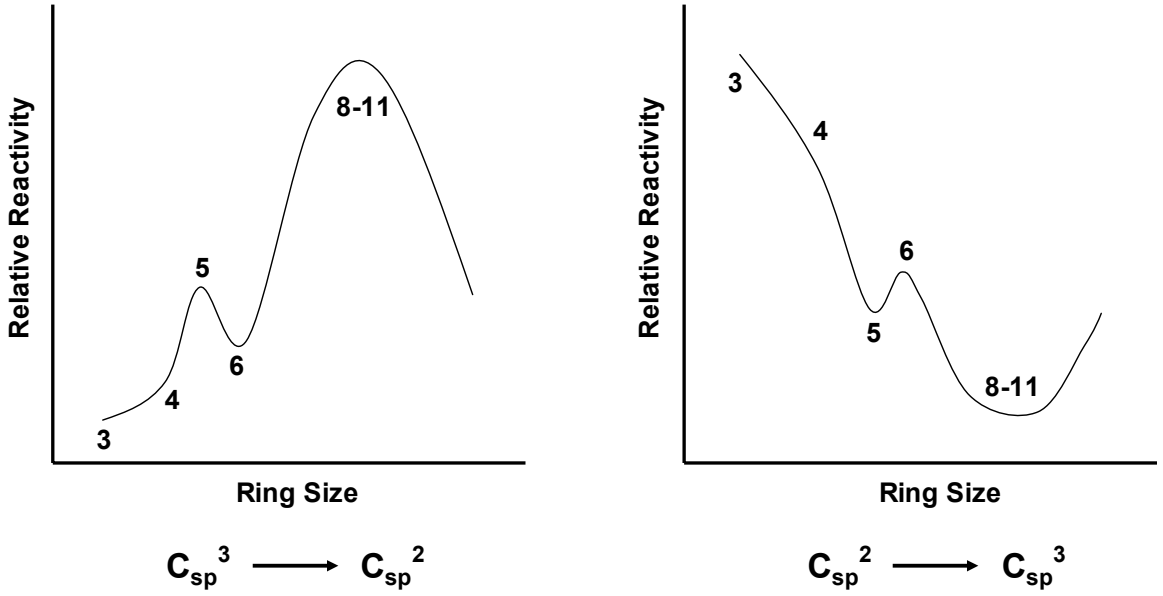

Figure 2.1: Predicted reactivity profiles for alicycles.[55]

Transannular products formed from the bromination of *cis*-cyclooctene and *cis*-cyclodecene are due to intramolecular hydride shifts. The reaction involves an intermediate, i.e., bromonium ion, which is attacked by a hydride ion from the opposite side of the ring.

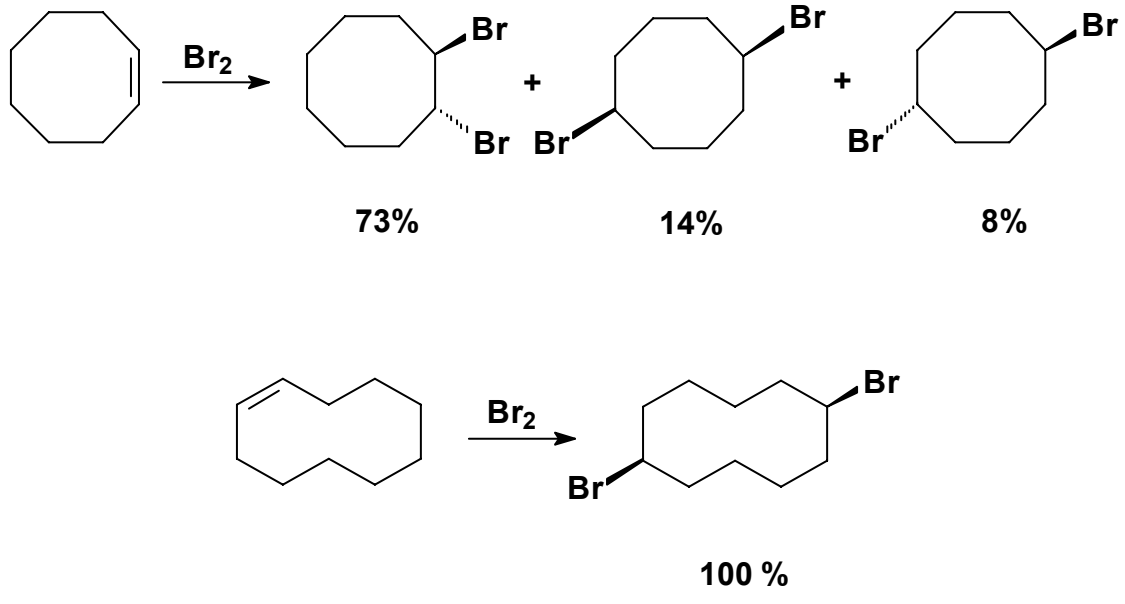

Scheme 2.2: Bromination of *cis*-cyclooctene and *cis*-cyclodecene.

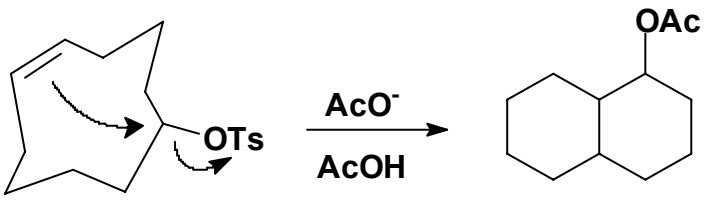

Scheme 2.3: Participation of double bond in reaction leads to transannular product.

Double bonds present in medium-ring compounds also participate in transannular reactions, e.g., acetolysis of cyclodec-5-enyl sulfonate ester leads to a transannular product resulting from π-electron participation in the displacement of the sulfonate leaving group (Scheme 2.3).[29] Catalytic hydrogenation of 1,6-cyclodecanedione gives 1,6-cyclodecanediol as a major product but a small amount of transannular product is also formed (Scheme 2.4).[57]

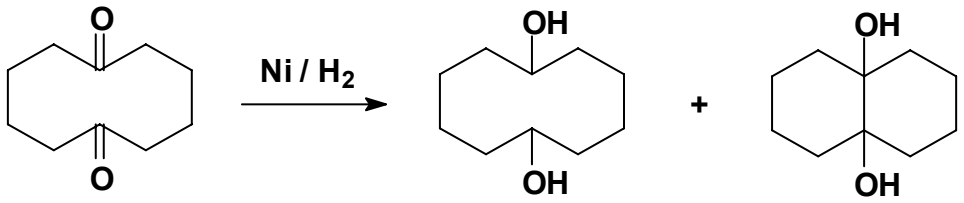

Scheme 2.4: Catalytic hydrogenation of 1,6-cyclodecanedione.

Transannular reactions are also reported for difunctional medium-rings.[34, 49, 58] Such reactions can serve as models for bimolecular reactions.[34] The tautomeric equilibrium between hydroxy-ketone and hemiacetal in difunctional medium-rings is an example of a transannular reaction (Scheme 2.5).[59-66] The formation of the hemiacetal can be related to the spatial proximity of the functional groups present in the ring, i.e., >C=O and –OH.

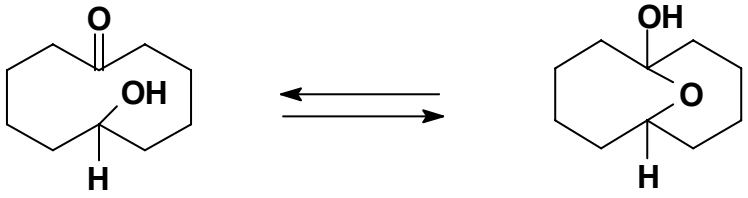

Scheme 2.5: Equilibrium between hydroxy-ketone and hemiacetal in a ten-membered ring.

Based on the spatial proximity of >C=O and –OH/H (, i.e., CHOH) in medium-rings, two competitive transannular reactions are possible, intramolecular hemiacetal formation and hydride shift. The degenerate 1,6-hydride shift has been reported[58] in unsubstituted 6-hydroxycyclodecanone (Scheme 2.6).

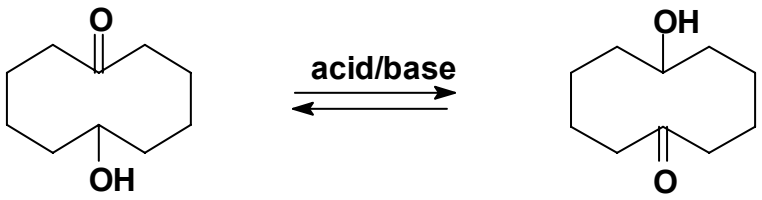

Scheme 2.6: Transannular 1,6-hydride shift in 6-hydroxycyclodecanone.

A transannular hydride shift was first reported by Prelog, Cope and their co-workers in medium-ring compounds.[40, 54] Later, a number of studies, both experimental and theoretical, have been carried out in rationally designed substrates under different acidic and basic conditions.[67-73] In these substrates the hydrogen atom is rigidly held within the spatial proximity of the electrophilic centre (carbonyl carbon or carbocation) (Scheme 2.7).[68-70, 74]

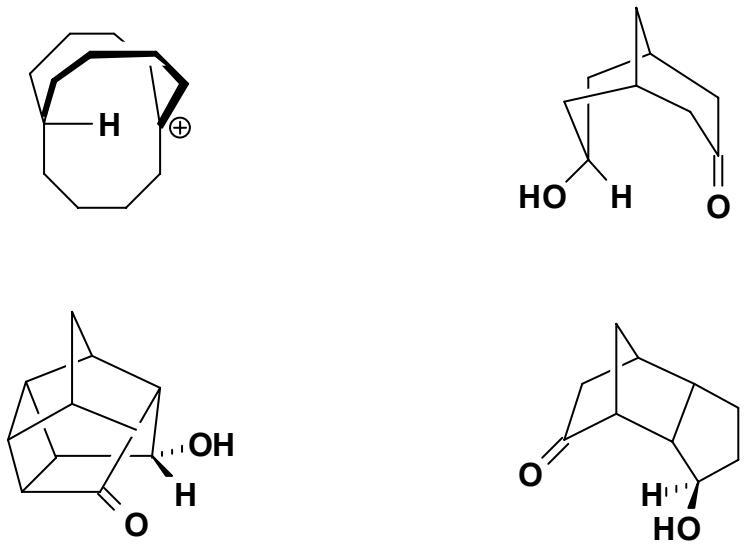

Scheme 2.7: Rigid substrates used for studying intramolecular hydride shift.

A recent example of a transannular hydride shift is reported by Paquette and co-workers[75] in a substituted nine-membered ring (Scheme 2.8). The transannular

oxidation-reduction process is observed in the presence of conjugate bases of δ-hydroxy-ketones (Scheme 2.8). This study investigates the role of various factors such as hydrogen bonding and solvent in controlling the thermodynamic equilibrium between **A** and **B**. Protic solvents interupt intramolecular hydrogen bonding, thus favoring **A** whereas an aprotic solvent such as benzene favors **B**. This is an interesting example of hydride shift where the anion is the driving force for the shift. Such intramolecular transannular hydride shift processes have implications in the synthesis of natural products.[75, 76]

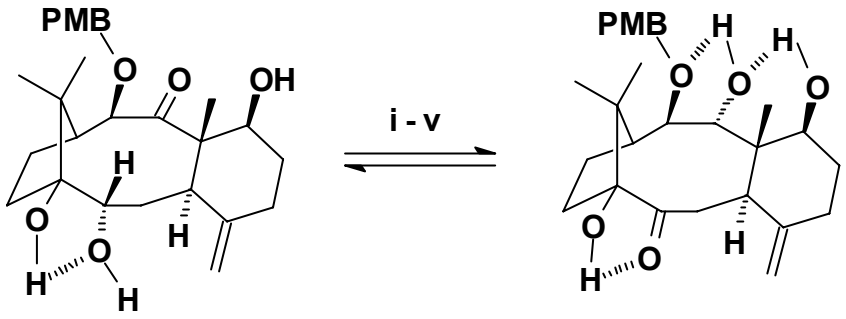

i) NaOH, MeOH, THF **6** : **1**
ii) KOMe, MeOH **7** : **1**
iii) KO*t*-Bu, THF **3** : **2**
iv) KO*t*-Bu, CH_2Cl_2 **1** : **1**
v) KO*t*-Bu, C_6H_6 **0** : **10**

Scheme 2.8: Transannular oxidation-reduction process in a poly-substituted nine-membered ring.

Protection of the hydroxy group can prevent or hinder an undesirable intramolecular reaction such as hemiacetal formation. An unusual protection method (in strong acidic conditions) was reported by McMurry and co-workers[68] in 6-hydroxycyclodecanone (Scheme 2.9). This reaction is simply a condensation of two alcohols under acidic conditions to give the keto-ether.

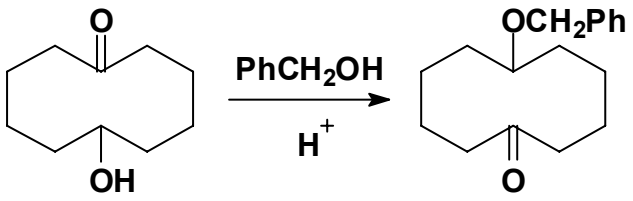

Scheme 2.9: Protection of –OH group in strong acidic conditions.

An intramolecular hydride shift was considered to be involved in the formation of the above keto-ether. This method is futher exploited for the protection of the OH group in 6-hydroxycyclodecanone under mild acidic conditions in polar solvents.[58] Since the transannular interactions lead to significant changes in geometry, charges and other electronic properties, it is important to investigate these features by quantum mechanical methods. In addition, transition-state structures and reaction pathways for hemiacetal formation and hydride shift can be effectively studied theoretically.

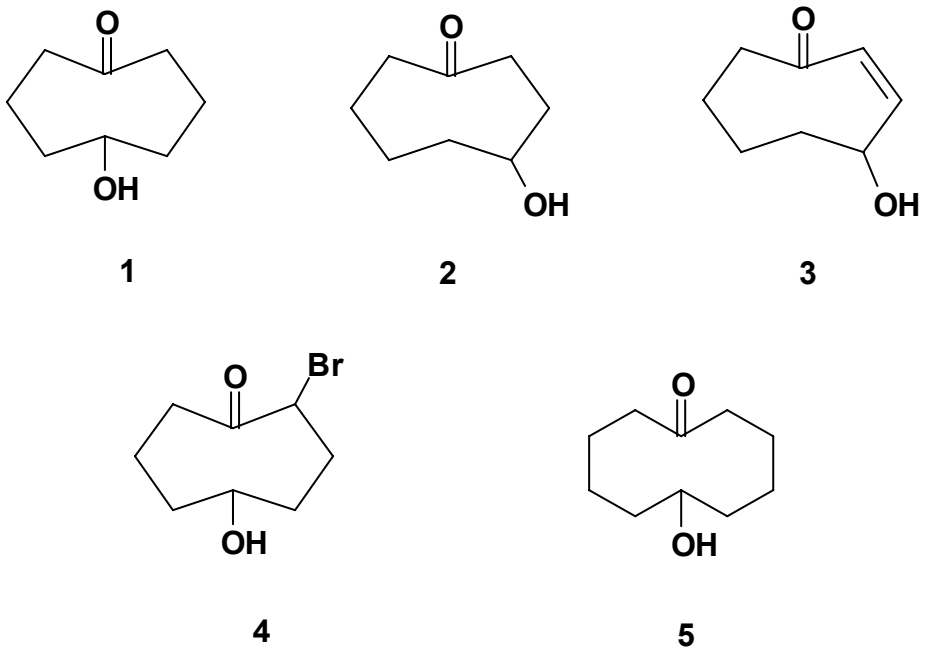

Scheme 2.10: Model compounds chosen for studying transannular reactions.

With this aim we have chosen model compounds **1** – **5** (Scheme 2.10). Despite detailed transannular interaction studies[58] reported in medium-rings, there is lack of literature available regarding transannular studies in **1** – **5**.[40] These difunctional medium-rings contain easily interconvertable groups (>C=O and –OH) and these are expected to undergo competitive transannular reactions, i.e., hemiacetal formation and hydride shift. Because of the conformational flexibility of the hydroxy-ketones, it

is not clear which factors can lead to one product selectively. We wish to study the influence of different factors such as ring size, presence of a C=C double bond and substituents on the interactions leading to transannular hemiacetal formation or hydride shift in eight- and ten-membered carbocycles. The study involves an integrated approach using experimental and modern theoretical techniques. An attempt is made to develop a predictive ability and control over the transannular reactions (Scheme 2.11). It is assumed that the knowledge obtained from this investigation can be exploited in functionalisation and expansion of the framework that is present in a variety of natural products.

Transannular hemiacetal formation

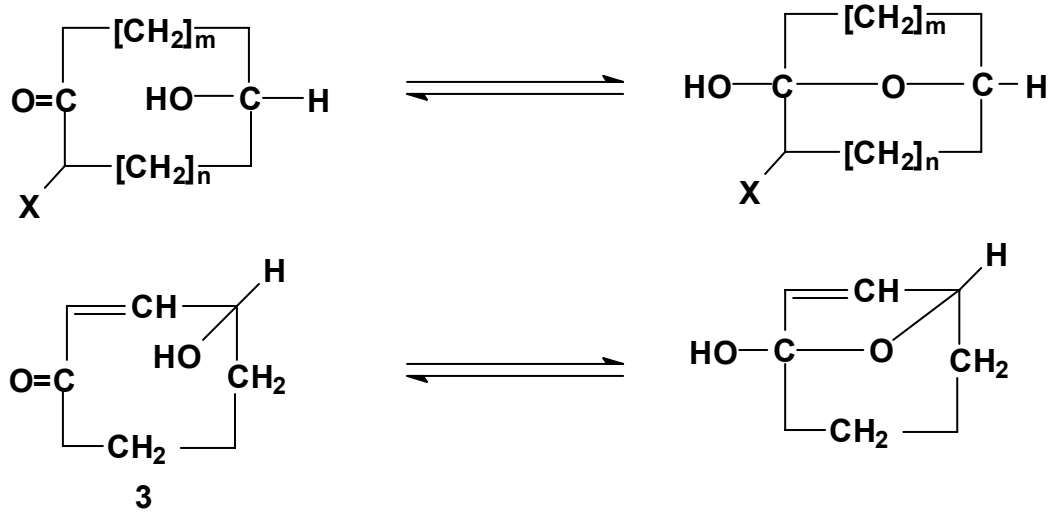

3

Transannular hydride shift

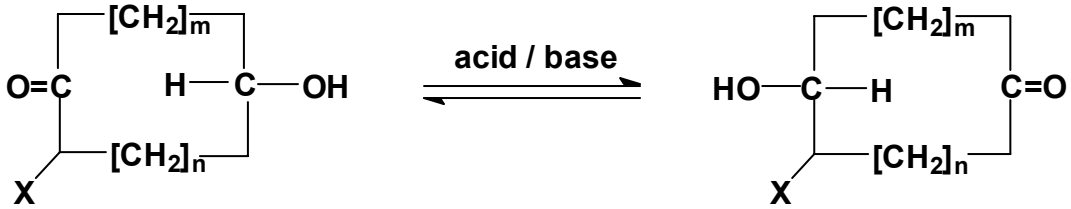

Exploiting hydride shift process for protection of hydroxy group

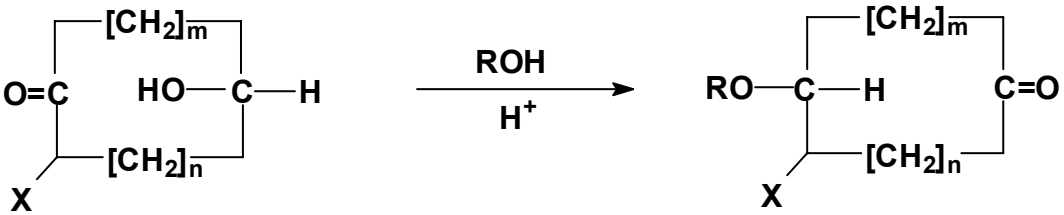

1: m=1, n=1, X=H
2: m=2, n=0, X=H
4: m=1, n=1, X=Br
5: m=2, n=2, X=H

Scheme 2.11: Transannular reactions proposed for theoretical and experimental investigations.

Objectives

1. This work investigates possible intramolecular non-bonded interactions between electrophilic and nucleophilic centres present at different positions in compounds **1** – **5**.
2. Quantum chemical studies on model compounds are carried out to locate low energy conformers. In these conformers structural features such as proximity between >C=O and –OH/H and electronic charge distribution are determined.
3. Investigations are carried out to study solvent effects on transannular interactions. The correlation between dielectric constant of the environment and conformations of model compounds are exploited in determining reaction conditions in organic synthesis since the conformation determines the reactivity of ring bound functional groups. Thus, a control of conformation leads to control of reactivity of ring bound functional groups.
4. For compound **1** reaction like transannular 1,5-hydride shift in acidic and basic conditions are carried out.
5. The hydride shift is exploited for the protection of a hydroxy group as ether in polar media.
6. Transition-states are calculated to find out the activation barriers for transannular reactions such as hemiacetal formation and hydride shift. In addition, single point calculations for studying the solvent effect are carried out to support the experimental results.

3 An introduction to computational methods

The theoretical foundation for modern chemistry was laid more than 70 years ago and today it becomes possible to use this knowledge for understanding how electrons, atoms and molecules interact. Molecular modeling is simply an art of representing molecular structures numerically and simulating their behaviour with the equations of quantum and classical physics. Theoretical calculations are very helpful tools in understanding the chemistry of reactions. Computer modeling is not a replacement for conventional experiments but it can be used to complement the experimental results. Computer simulations can be used to validate experimental results. Computer modeling has many advantages over conventional experimental methods. Careful use of computer modeling can help in predicting or optimising various physical and chemical parameters which determine reaction conditions.

The most important role of computer simulations is their use as a predictive tool in a chemical reaction. The ability to predict the outcome of a reaction provides large savings in terms of money and time. Chemists have long recognized that intramolecular forces of various types have a profound influence on the chemical and physical properties of molecules. The quest of a chemist is to understand molecular shapes and reactivity of various chemical systems. A large number of chemical systems have been extensively studied with molecular modeling but still a number of systems have not been studied in detail due to many reasons based on structure and size. The medium-ring compounds are an example of systems which are least studied because of their greater flexibility.

3.1 Methods used in calculations

The two common approaches that are used in molecular modeling are quantum mechanics[77, 78] and molecular mechanics.[26, 78, 79] The most important quantum mechanical models commonly used for calculating ground state geometries for 'organic molecules' are *ab inito* and semi-empirical techniques. Molecular mechanics are also known as force field methods. These methods do not take into consideration the electronic motions in a chemical system. This chapter gives a brief introduction to molecular mechanics, *ab intio* molecular orbital and density functional theories.[78, 80]

3.2 Molecular mechanics methods

Force field calculations use the concepts of classical physics to explain and interpret the behaviour of atoms and molecules.[26, 78, 79] They rely on force fields with embedded parameters. The energy of the system is calculated as a function of the nuclear positions only. These calculations are least extensive. They can even be used for large molecules such as enzymes.[78] However, they have several limitations. Not all molecular systems can be treated with the same force field. Molecular properties which are dependent on details of electron distribution cannot be reproduced. The MMFF methods[81] (Merck Molecular Force Field developed by Merck Pharmaceuticals) are used for conformer search in **1** – **5**. This program gives good initial geometries.

3.3 Semi-empirical methods

Semi-empirical methods do not use exact solutions of the Schrödinger equation but include empirical parameters.[82-85] These techniques are less time consuming since some of the electrons in organic systems are ignored. The major drawback of these methods is the calculation of properties, such as resonance in amides, which have not been taken into major consideration during the parameterisation process.

3.4 *Ab-initio* molecular orbital methods

Ab initio, or first principles, methods, have been an essential tool in the study of atoms and molecules during past three decades.[77, 78] They make use of no experimental parameters in their computation. The underlying core technology is to solve the Schrödinger wave equation for a given chemical system. These methods involve all the electrons in a system. The computations based on these methods provide accurate quantitative predictions for a broad range of chemical systems. But they are extremely time consuming. There are limitations of *ab initio* methods since the system to be studied cannot be very large. Therefore, *semi*-empirical and empirical methods are still used for large flexible and biological molecules. At present, systems containing hundreds of atoms can be simulated. The next generation of computers is expected to simulate systems containing thousands of atoms.

3.5 Density functional methods

The third class of methods used for the calculation of the electronic structure of atoms and molecule is based upon density functional theory (DFT).[78, 80, 86-88] DFT has allowed to study the physical properties and reaction energetics of compounds containing up to 100 or more heavy atoms with perturbation theory.[80] It is a theory of the electronic ground state based on the electronic density distribution, ρ(r). In these methods there is a relationship between the overall electron density and the total electronic energy. DFT methods include the effects of electron correlation at a much lesser computational cost compared to Hartree-Fock (HF) methods. This makes DFT quite popular for calculating organic molecules. In addition, DFT theory in particular the B3LYP functional, has shown to provide accurate equilibrium geometries for a wide range of molecules and ions.[80, 89] However, unlike perturbation theory approaches used in HF methods, DFT models are not currently improved by adding more terms or more electronic configurations to the overall molecular description, i.e., they are not iterative. So there is no 'best' DFT model.[90, 91] Thus, the results obtained from DFT approaches should be compared either with experimental data or to high-level perturbation theory results.

Currently, there are two types of functionals, i.e., gradient-corrected (BLYP)[92] and hybrid (B3LYP),[88, 92, 93] that have been tested and used for a large number of organic molecules. The B3LYP functional combines Becke's three parameter exchange functional with the correlation functional of Lee, Yang and Parr. There is no systematic way of choosing the proper functional for calculations. The most popular methods in literature are based on comparison between experimental and theoretical results. The B3LYP model is most popular method particularly among those chemists who use computational chemistry to support synthetic concepts. It has shown good agreement with structural data and with the G2 test set of data.[94] The DFT methods have greater accuracy than Hartree-Fock method at slight increase in time of computation. Lynch and Truhlar[95] have reported that B3LYP slightly underestimates the energy barriers in proton-transfer reactions.

3.6 Conformational analysis

The chemical and physical properties of a molecule depend on the three-dimensional structures or conformations. Conformational analysis[78] is the study of the

conformations of a molecule and their influence on its properties. An important component of conformational analysis is the *conformational search* which helps in finding *preferred* conformers of a molecule. These conformations generally have minimum energy on the potential energy surface. Conformational search methods can be divided into the following categories: systematic search algorithms, model-building methods and random approaches.

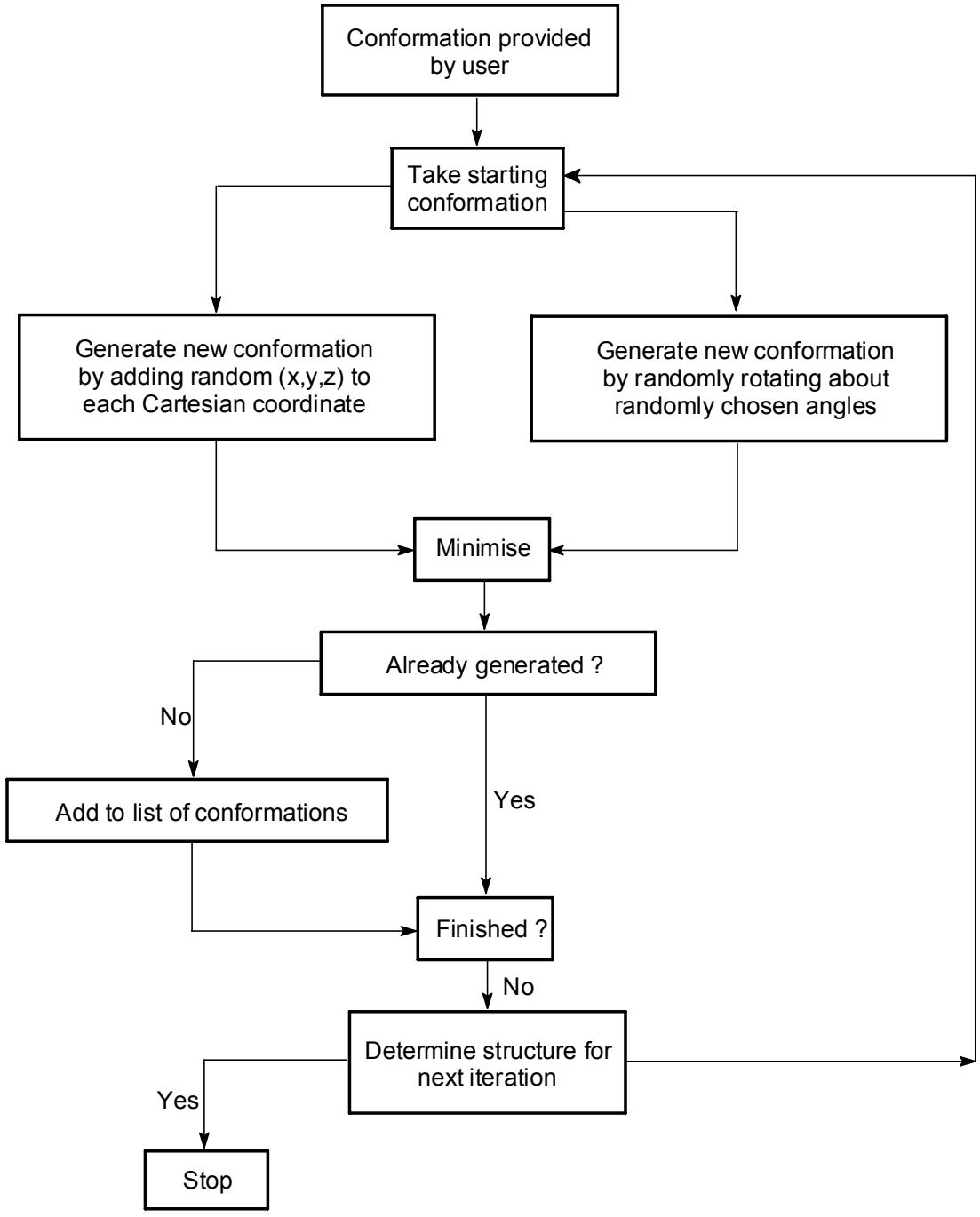

Figure 3.1: Flow chart for the steps followed by a random conformational search.[78]

A systematic search method explores the energy surface of the molecule in a predictable fashion, but in a random search method it is not possible to predict the order in which conformations will be generated. The random search method can explore the conformational space by changing either the atomic cartesian coordinates or the torsion angles of rotatable bonds.

The approach adopted by both algorithms is shown in Figure 3.1. At each iteration a random change is made to the *current* conformation. This step is followed by energy minimisation of the conformation. If the minimised structure was not found earlier it is stored, otherwise rejected. The conformation for the next iteration is chosen, and the cycle is started again. The procedure is repeated until a given number of iterations have been performed or until it is decided that no new conformations can be found. Each method has its weakness and strength. Systematic searches are not useful for cyclic molecules. However, they have a definite endpoint and one can be sure to have found all conformers for a given dihedral increment. Random search methods can require long runs to ensure that the conformational space has been covered, and they can generate the same structure many times.

3.7 Methods used for molecular orbital properties calculation

Natural Bond Orbital (**NBO**)**:** The natural bond orbital energy analysis is an important method of analysing intramolecular interactions quantitatively and to understand electronic delocalisation.[96-107] The NBO analysis has been widely used for conformational analysis of molecules[108] The investigation of intramolecular interactions in a molecule gives an insight in the reactivity, stability and other important properties. This is a complementary technique for studying the changes in bonding and electron density during the reaction.

The NBO program is used to evaluate the energies of orbitals, overlap matrix (S_{ij}) and Fock matrix (F_{ij}) elements. F_{ij} corresponds to the resonance integrals in simple MO theory. It describes electronic interaction between two orbitals Φ_i and Φ_j. The NBO analysis transforms the canonical delocalised Hartee-Fock (HF) MOs, or corresponding natural orbitals of a correlated description into localised orbitals that are closely tied to a chemical bonding concepts. This process involves sequential transformations of the non-orthogonal atomic orbitals (AOs) in sets of natural atomic orbitals (NAOs), then in natural hybrid orbitals (NHOs), and finally in natural bond

orbitals (NBOs). The energy of the interactions between filled (donor) and vacant (acceptor) NBOs represents the deviation of the molecule's energy from the energy of the Lewis structure and can be considered as a measure of the electronic delocalisation. Filled NBOs describe the hypothetical strictly localised Lewis structure. Since these interactions lead to loss of occupancy from the localised NBOs of the idealised Lewis structure into the empty non-Lewis orbitals (and thus, to deviations from the idealised Lewis structure description), they are referred to as 'delocalisation' corrections to the zeroth-order natural Lewis structure. For each donor NBO (i) and acceptor NBO (j), the stabilisation energy ($E_{i,j}^{(2)}$, i > j) associated with delocalisation ("2e-stablisation") is estimated as by the following equation.[96]

$$E_{i,j}^{(2)} = \Delta E_{i,j} = -q_i/[F_{i,j})^2(\Phi_j-\Phi_i)]$$

q_i is the donor orbital occupancy and Φ_i and Φ_j are diagonal elements (orbital energies). In the NBO program available in the Gaussian package the interaction energy is printed when it exceeds a default threshold of 0.5 kcal mol^{-1}.

Atoms In Molecules (**AIM**)**:** According to this theory, a chemical bond is described by means of the analysis of the electron density $\rho(r)$ and its Laplacian $\nabla^2\rho(r)$. It is unique since it provides a link between intuitive chemical concepts and quantum mechanics through analysis of the electron density.[109-113] It is a technique for studying the paths followed by the electron density between atoms within a molecule. AIM allows us to study the bonding properties of the system, to observe the switches in bonding and to see whether bonds are covalent or ionic.

There are a number of theoretical and experimental investigations[114-120] which have demonstrated the advantages of the AIM theory for the investigation of transannular interactions in different classes of compounds. AIM approach is based on the analysis of total electron density, ρ(r), its Laplacian, $\nabla^2\rho$(r), and contributions of the local kinetic and potential energy densities to the total local electron energy in the bond critical points (BCP) where the gradient of ρ(r) vanishes. The presence of a BCP is an indicator of a chemical bond. According to AIM theory, interatomic interactions falls into "shared" and "close-shell type". Shared (covalent) interactions are charcterised by the negative $\nabla^2\rho$(r) and high value ρ(r) values in BCP. This indicates that the electronic charge is accumulated along the bond path. In case of

closed-shell interactions (ionic bonds, some van der Waals complexes, etc.) the value of $\nabla^2\rho(r)$ is positive and the total $\rho(r)$ in BCP is small.[121, 122] The positive value indicates that the interactions are dominated by the contractions of the charge density away from the interatomic surface.

3.8 Software

The calculations of the present investigation were performed using Spartan 04,[81] Gaussian 98[123] and 03.[124] Molecular orbitals and modes of nuclear motion corresponding to imaginary frequencies have been viewed using Molden,[125] Gauss View, PCMODEL[126] and Pegra.[127]

4 Synthesis and characterisation of model compounds 1 – 3

In medium-rings many reactions take place in *non-classical* ways leading to undesired products. This is considered to be caused by close proximity of atoms present on opposite sides of the ring in certain low energy conformers. Thus, the close proximity leads to transannular reactions. These reactions present a major setback in facile interconversions or insertions of functional groups desired for synthesizing natural products. Thus, a careful investigation of the role of conformations in developing a predictive control of the reaction is required. For this purpose we have chosen very simple difunctional eight-membered rings **1** – **3** (Scheme 4.1). We have synthesized these compounds with the methods modified and reported earlier.[64, 65, 128-131]

The model compounds contain the functional groups –OH and >C=O (Scheme 4.1). These groups have been selected for two reasons. Firstly, these functional groups show transannular reactions when present in medium-rings. But the extent of interaction depends on ring size and the presence of substituent such as ring double bond. Secondly, conversion of compounds with these two functional groups to products such as alkenes is quite easy. It is expected that compounds **2** and **3** have different conformations than compound **1** because of the relative positions of the functional groups or insertion of a double bond in the ring. As a result, the extent of transannular interaction should be different in these compounds. Thus, an indepth study of these compounds can lead to better insight into the role of conformation in determining a reaction product in eight-membered rings.

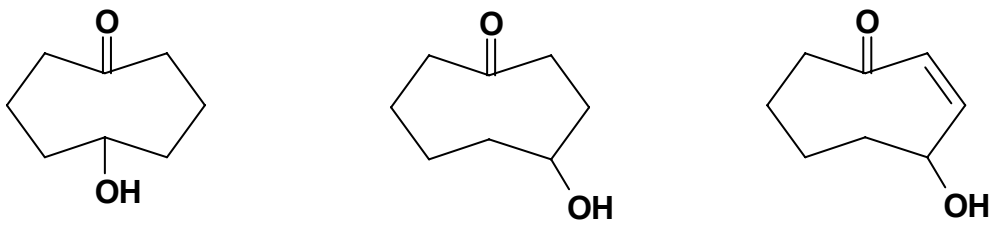

1 **2** **3**

Scheme 4.1: Model compounds **1** – **3**.

Compound **1** has been synthesised by oxidation of commercially available *cis*-1,5-cyclooctanediol with Jones reagent (Scheme 4.2).[128] A white solid was obtained

after workup of the reaction. The compound was purified by sublimation. IR and NMR studies have clearly shown the absence of a carbonyl group. The final product obtained was 9-oxabicyclo[3.3.1]nonan-1-ol (**1a**). A single crystal X-ray crystallography study has shown that compound **1** exists as the hemiacetal in a twin-chair conformation (chair-chair). The ORTEP diagram for 9-oxabicyclo[3.3.1]nonan-1-ol is shown in Figure 4.1. It is known that bicyclo[3.3.1]nonane and many of its derivatives adopt a twin-chair conformation.[132, 133] The X-ray crystal structure of derivative of **1a** synthesised and reported in chapter 18 (Figures 18.8 and 18.9) also exits in a twin-chair conformation.

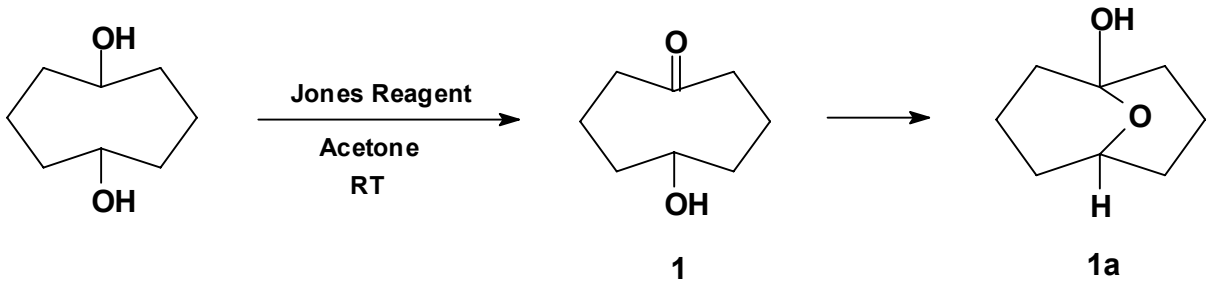

Scheme 4.2: Oxidation of *cis*-1,5-cyclooctanediol.

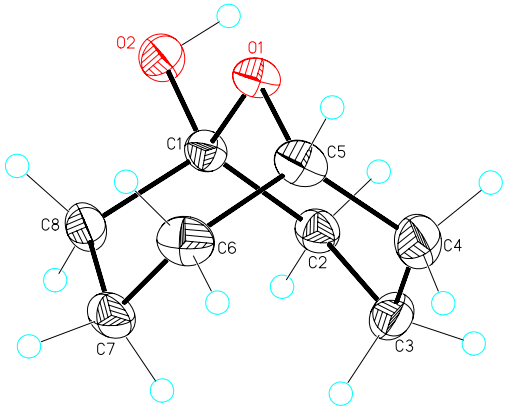

Figure 4.1: X-ray crystal structure of **1a**.

In the crystal lattice the molecules pack in such a way that there is intermolecular hydrogen bond formation due to the proximity of hydroxy hydrogen atom of one molecule of **1a** to the bridging oxygen atom of neighbouring molecule (Figure 4.2). In addition to this the oxygen bridging is also involved in hydrogen bonding. This provides stabilisation to the structure. The parameters of hydrogen bonding

between the bridging oxygen and hydroxy hydrogen atom of molecules say A and B in the lattice are O(1)A---H(2)B =1.989, O(1)B---H(2)A=1.993 Å.

In literature[129] compound **2** has been synthesised from **3c** by reduction with diimide followed by treatment with triethylamine (Scheme 4.3). Purification by column chromatography (dichloromethane:methanol, 95:5/v:v) afforded 80% yellow oil. In order to avoid purification by column chromatography we have modified this step by hydrogenation[130] in presence of 10% palladium on charcoal in methanol at 3.0 x10^5 Pa (Scheme 4.4). The compound obtained is yellow oil. Initially, compound **2** was considered to be a monocycle.[63] But later Smith and co-workers[64, 129] and others[65] have reported the ^{1}H-NMR spectrum of **2** at 300 MHz. The signals also include those of the tautomeric form **2a**.

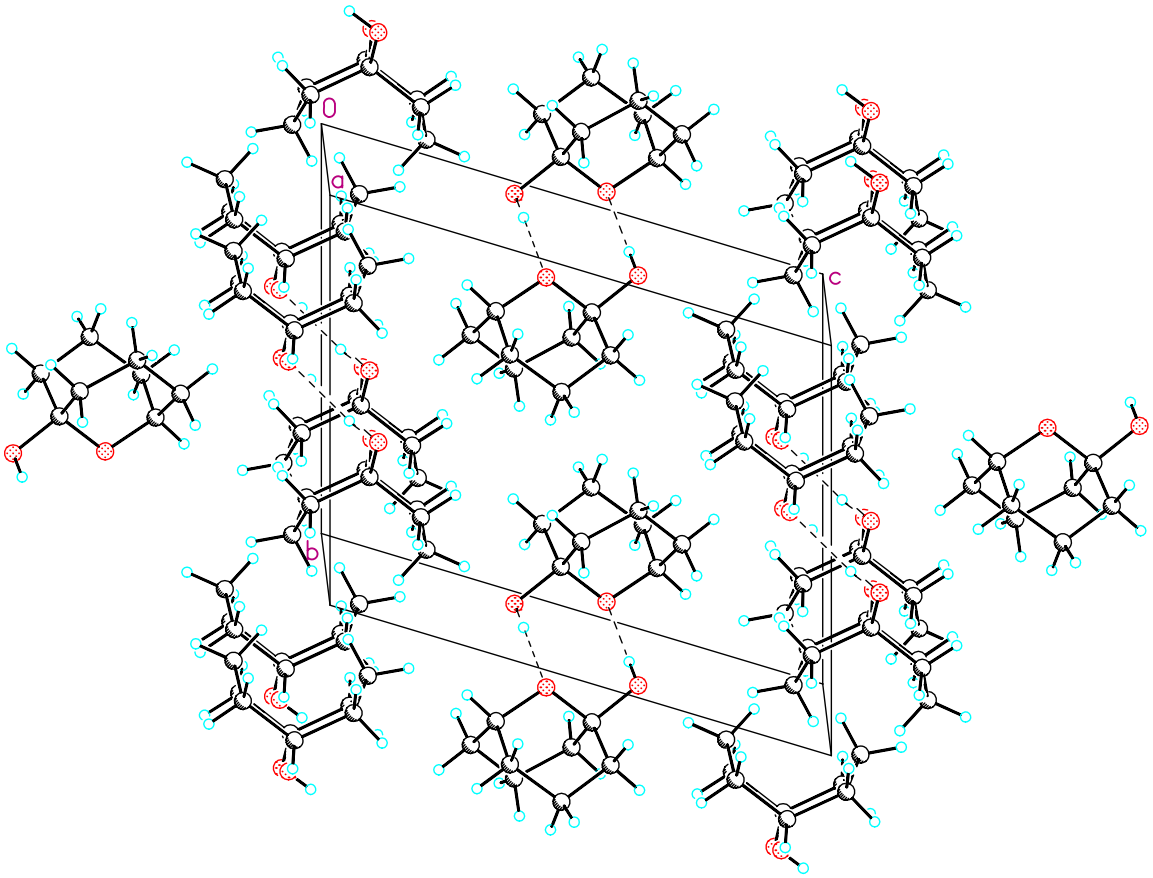

Figure 4.2: Stereoview of the packing of molecules in crystal structure of **1a**.

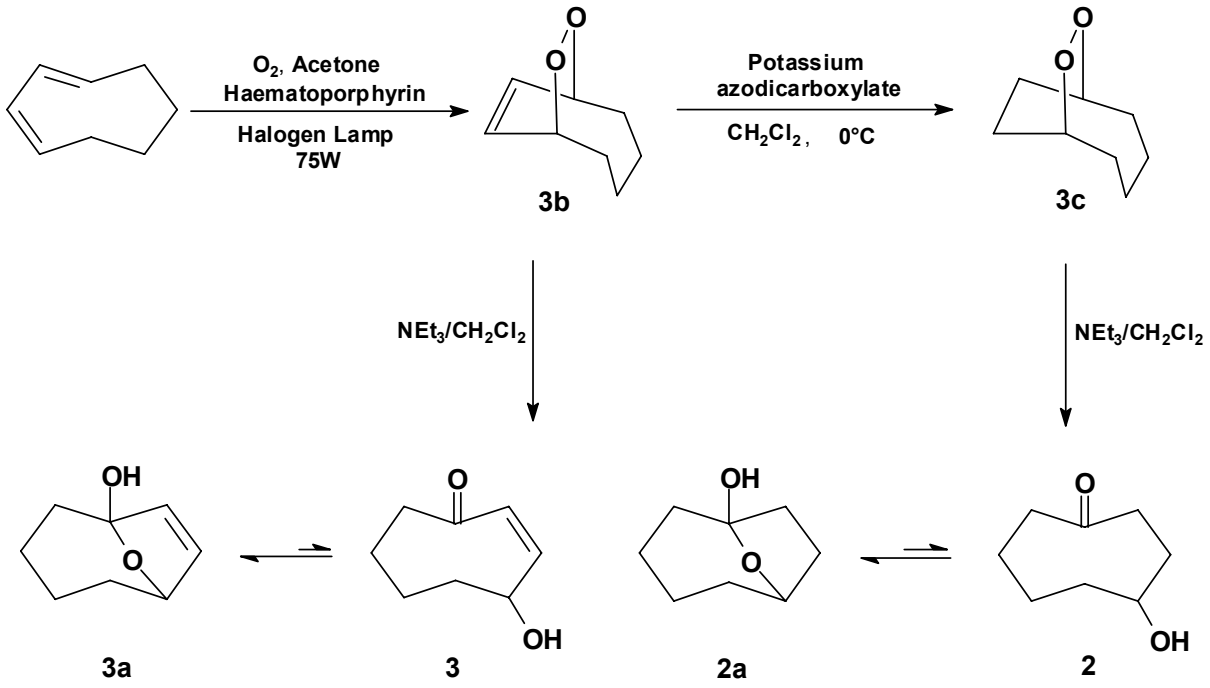

Scheme 4.3: Overall sequence of synthesis of model compound **2** and **3**.

Compound **3** is synthesised in three steps. Singlet oxygen is added to *cis*,*cis*-1,3-cyclooctanediene to yield peroxide **3b** (Scheme 4.3).[131] Kayama *et al*.[131] have used a 125 W sodium street lamp for the generation of singlet oxygen. But we have replaced it by a 75 W halogen lamp. The NMR studies done by the same group have clearly demonstrated the presence of 5% of the moncyclic form **3** in $CDCl_3$.[64] Compound **3** is absent in the solid state since single crystal X-ray structure analysis has shown the bicyclic form **3a**. An ORTEP diagram for **3a** is shown in Figure 4.3. Notably, the conformation of **3a** observed in the crystal resembles the conformation of **1a** (Figure 4.1).

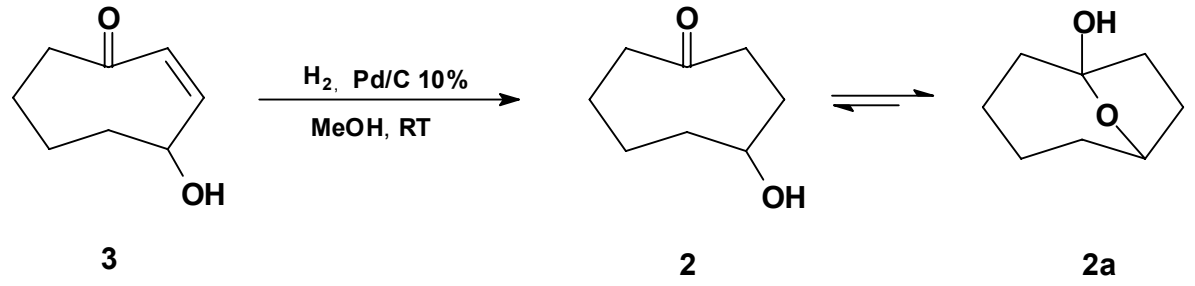

Scheme 4.4: Catalytic hydrogenation of **3**.

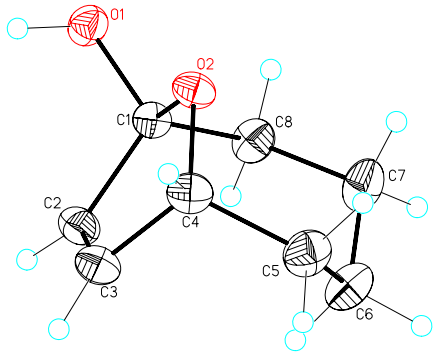

Figure 4.3: X-ray crystal structure of **3a**.

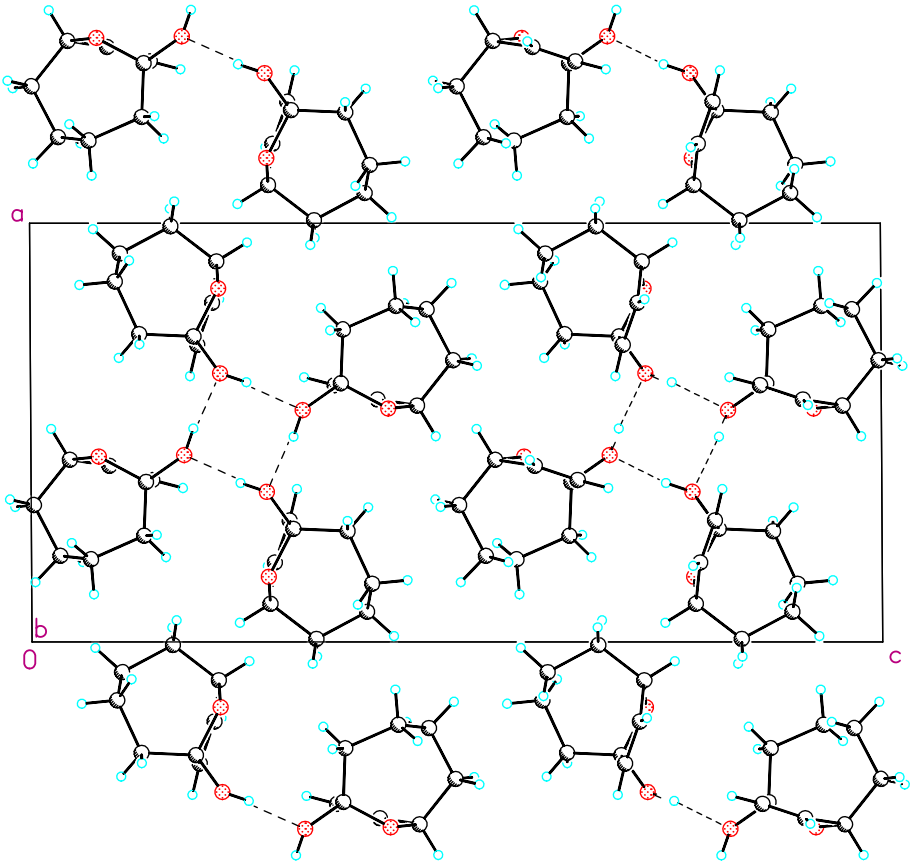

Figure 4.4: Stereoview of the packing of molecules in crystal structure of **3a**.

The packing of molecules of **3a** in crystal structure shows intermolecular hydrogen bonding between the hydroxy hydrogen atom of one molecule to the oxygen atom of the other molecule (Figure 4.4). Interestingly, unlike in **1a** the hydrogen bonding

between the bridging oxygen and the hydroxy hydrogen atom between the neighbouring molecules is absent. Compounds **1** – **3** have been used for further experimental and theoretical studies.

5 Solvent effects on transannular interactions in model compounds 1 – 3

Medium-ring carbocycles have a large number of conformations[79, 134] but only particular conformers bring the functional groups in proximity to each other necessary for a reaction to occur. A common example is the formation of hemiacetal in model compounds **1** – **5**. This is due to the transannular nucleophilic addition of –OH to >C=O. Our exhaustive literature study[59-61, 135] has shown some interesting facts about simple medium-rings containing only an –OH and a >C=O group. The difunctional compounds **1** – **5** show a variation in the tautomeric equilibrium between monocyclic and bicyclic form in deuterated chloroform. The formation of hemiacetal in **1** is an example of strong transannular interactions in difunctional medium-rings. The hemiacetal **1a** is used in the synthesis of γ- and δ-lactones present in many biologically active natural products.[61] Recently, it has been reported[136] that the presence of a hemiacetal functionality in a molecule can be utilised for the construction of polyfunctionalised medium-ring carbocyclic systems *via* alkoxy radical fragmentation reaction (ARF). There is no evidence, both experimental and theoretical, for the existence of **1** in solution or solid state. Glover and co-workers[137] have reported IR spectra of **1** in potassium bromide and carbon tetrachloride and it was found that **1** exits in its transannular form **1a** in both phases. The pure compound has always the structure **1a** and not **1**.

When the OH group is present at C-4, as in compound **2**, there is a tautomeric equilibrium between monocyclic and bicyclic forms.[64, 129] The ratio of **2** and **2a** is 31:69 in $CDCl_3$. When a double bond is present at the α-carbon atom as in compound **3** the equilibrum shifts more towards **3a**. The ratio of **3**:**3a** becomes 5:95 in the same solvent. The existence of **3** in equilibrium with **3a** has been reported earlier.[64, 129, 131]

The simultaneous existence of both functional groups is largely hindered by transannular interactions in all compounds **1** – **5**, but the effect is most severe in **1**. In the solid state, **3** exists solely in its close form while **5** occupy the open form in this state.[58] In $CDCl_3$, **5** exists in equilibrium with its hemiacetal **5a** in the ratio 54:46.[58] This indicates that the effect of transannular interaction can be altered when the positions of the functional groups are changed or a double bond is inserted. The reason for this may lie in structural or energetic features.

Compounds **1** – **5** may be considered as hydrobobic '*floppy*' rings containing the polar functional groups –OH and >C=O. Spatial interactions between the two reactive groups are only possible when they are forced into close proximity, usually by the σ framework. The geometry of the σ skeleton can be modified to a certain extent by choosing a particular environment, i.e., a suitable solvent. Thus, it is worth studying NMR spectra in solvents of different polarity. A proper choice of solvent, based on its reactivity and polarity, can help to avoid an undesired reaction. To our knowledge, until now NMR studies for compounds **1** – **3** in different solvents (except in $CDCl_3$) have not been performed. Compounds **1** – **3** are used as starting material for many biologically active natural products.[59-61] Thus, it is worth studying their NMR spectra in different solvents. With this aim in mind we have carried out an extensive NMR study. Both polar and non-polar solvents have been used. No equilibrium has been reported between **1** and **1a** in deuterated chloroform.[59-61, 135] Equilibrium between **1** and **1a** in different solvents and at different temperatures is investigated here (Scheme 5.1).

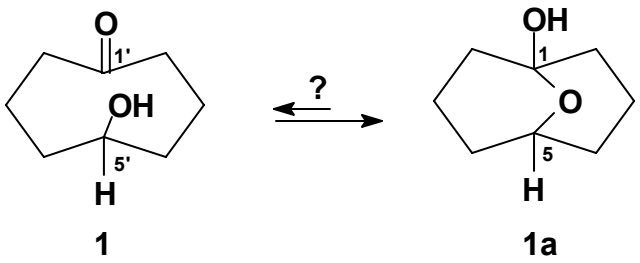

1 **1a**

Scheme 5.1: Equilibrium between **1** and **1a**

Table 5.1: Chemical equilibrium between tautomers **1** and **1a** in different solvents at different temperatures.

Solvent	**ε** [138]	**T (K)**	**1a:1**	K_{eq}**=[1a]/[1]**[a]	**Δ*G*** (**kcal mol^{-1}**)	**ΔΔG** (**kcal mol^{-1}**)
$CDCl_3$	4.81	298	≥ 99			
	4.81	323	≥ 99			
THF-*d*$_8$	7.58	298	≥ 99			
Ethanol-*d*$_6$	24.55	298	≥ 99			
Acetonitrile-*d*$_3$	37.50	298	≥ 99			
	37.50	343	≥ 99			
DMSO-*d*$_6$	46.60	298	≥ 99			
	46.60	323	≥ 99			
	46.60	373	93.9:6.1	16.5	-2.08	0.01
	46.60	403	92.0:8.0	12.5	-2.02	0.01
D_2O	80.00	298	≥ 99			
	80.00	323	96.8:3.2	31.3	-2.21	0.01
	80.00	363	90.5:9.5	10.5	-1.69	0.01

[a] Ratios were calculated from signal intensities of protons attached to C-5 and C-5'.

The X-ray structure reported in the previous chapter has shown the existence of tautomer **1a** in the solid state (Figure 4.1). The absence of a carbonyl absorption in the IR spectrum has also supported the presence of tautomer **1a**. Analysis of the ^{1}H-NMR spectrum at 500 MHz in $CDCl_3$ at room temperature has shown absence of signals corresponding to tautomer **1** (Table 5.1). The diagnostic signal for tautomer **1a** is at δ 4.33 ppm (t, 1 H) for H-5 (Scheme 5.1). The signal is a triplet since the neighbouring environment of H-5 is very symmetric due to a twin-chair conformation even in solution.[137] The signal for H-5' in **1** is expected to be more upfield as compared to the signal for H-5. The shifting of H-5' signal upfield can be explained in terms of shielding effect due to the presence of magnetic anisotropic effect generated by the carbonyl group. The conformation in **1** is not expected to be well defined, therefore the signal should appear as a multiplet. The signals for the other ring

protons come as complex multiplets at δ 1.49 – 2.16 ppm (m, 12 H) and a broad signal at δ 2.61 ppm (brs, 1 H) is assigned to the hydroxy proton in **1a**.

The equilibrium constant has been calculated by taking the ratio of the area under the signals for H-5 and H-5' for **1a** and **1**, respectively (Table 5.1). At room temperature there is no equilibrium between **1** and **1a**. In $CDCl_3$ increase of temperature has not caused any change in the NMR spectrum. Thus, there is no equilibrium between **1** and **1a** in $CDCl_3$ at room and higher temperature. This shows that ≥ 99 % of **1a** exists in $CDCl_3$. Since tautomer **1** was not observed in $CDCl_3$, NMR spectra were not recorded in solvents of lower dielectric constant.

In THF-d_8 the spectrum for **1a** remains unchanged. In solvents with a higher dielectric constant such as ethanol-d_6, acetonitrile-d_3, DMSO-d_6 and even D_2O, at room temperature no trace of **1** was detected. Following this, measurements were done at higher temperatures. In DMSO-d_6 at 373 K a multiplet at δ 3.46 – 3.48 ppm appeared. This signal is assigned to H-5'. The chemical shift of H-5' is close to the value calculated (δ 3.72 ppm) with the software ChemWindow. There are two more multiplets at δ 2.19 – 2.23 and 2.46 – 2.50 ppm assigned to the four protons on C-2' and C-8', α to the carbonyl carbon atom. Compound **1** is only 6.1% in the equilibrium mixture at this temperature and the equilibrium constant is 16.5. The Gibbs free energy is -2.08 kcal mol^{-1}. The increase in temperature to 403 K leads to a decrease of the equilibrium constant from 16.5 to 12.5. The quantity of **1** increases to 8%.

The ^{1}H-NMR spectrum at 500 MHz for the equilibrium between **1** and **1a** in D_2O is shown in Figure 5.1. It is worth noting that the signals of both **1** and **1a** are affected by the temperature. At 363 K, the equilibrium mixture contains 9.5 % of **1** while in DMSO-d_6 at 373 K the proportion of **1** is 6.1%. In D_2O there are two factors which are playing significant role - one is the high dipole moment and the other is its capability to form hydrogen bonds with the solute, whereas in DMSO-d_6 hydrogen bonding is absent, since DMSO-d_6 is an aprotic solvent.

The orientation of solvent molecules around the solute molecule in the absence of specific solute/solvent interactions is largely determined by the dipole moment. The -OH group of **1** can have two orientations which increase or decrease the proximity between the two reacting groups (Figure 5.2). The *endo*-conformer **1d** leads to hemiacetal formation **1a**, whereas the *exo*-conformer **1e** favours **1**.

The aprotic solvent DMSO-d_6 has a large dielectric constant which highly favors 5-hydroxycyclooctanone **1** as compared to its hemiacetal **1a**. In D_2O at higher temperatures both the above mentioned factors favour conformation **1e**. The effect of higher temperature on the conformational equilibrium is related to the change in entropy. This is further related to the organisation of the solvent molecules in the solvation sphere induced by the conformer.[139] A conformer with a low dipole moment has a weak effect on a polar solvent and would be better solvated in a non-polar solvent. Thus, the change in entropy would be negative, on the other hand, conformer with the higher dipole moment has a stronger effect on the polar solvent. Hence, the change in entropy would be positive.

The calculated (B3LYP/6-31+G*) dipole moments of the low energy *endo*-conformer for 5-hydroxycyclooctanone **1** and its hemiacetal **1a** in the gas phase are 4.2 and 2.5 D, respectively. Conformers with *endo*- orientation of OH group have higher dipole moments than the corresponding close form. This implies that the conformer **1d** is likely to exist in polar solvents with the high dipole moments. In non-polar solvents it is expected that mainly **1a** exist. This implies that partial control over transannular interactions between functional groups can be attained with proper selection of solvents.

The change of the position of the OH group in compound **2** has resulted in significant changes in physical and chemical properties of the molecule. The compound **2** is isolated in equilibrium with its tautomer **2a** at room temperature (Scheme 5.2). It is extracted as yellow oil (mixture of **2** and **2a**) whereas compound **1** is extracted as a white solid in its hemiacetal form **1a**. The ratio of structures **2** and **2a** in equilibrium is 31:69 in $CDCl_3$.

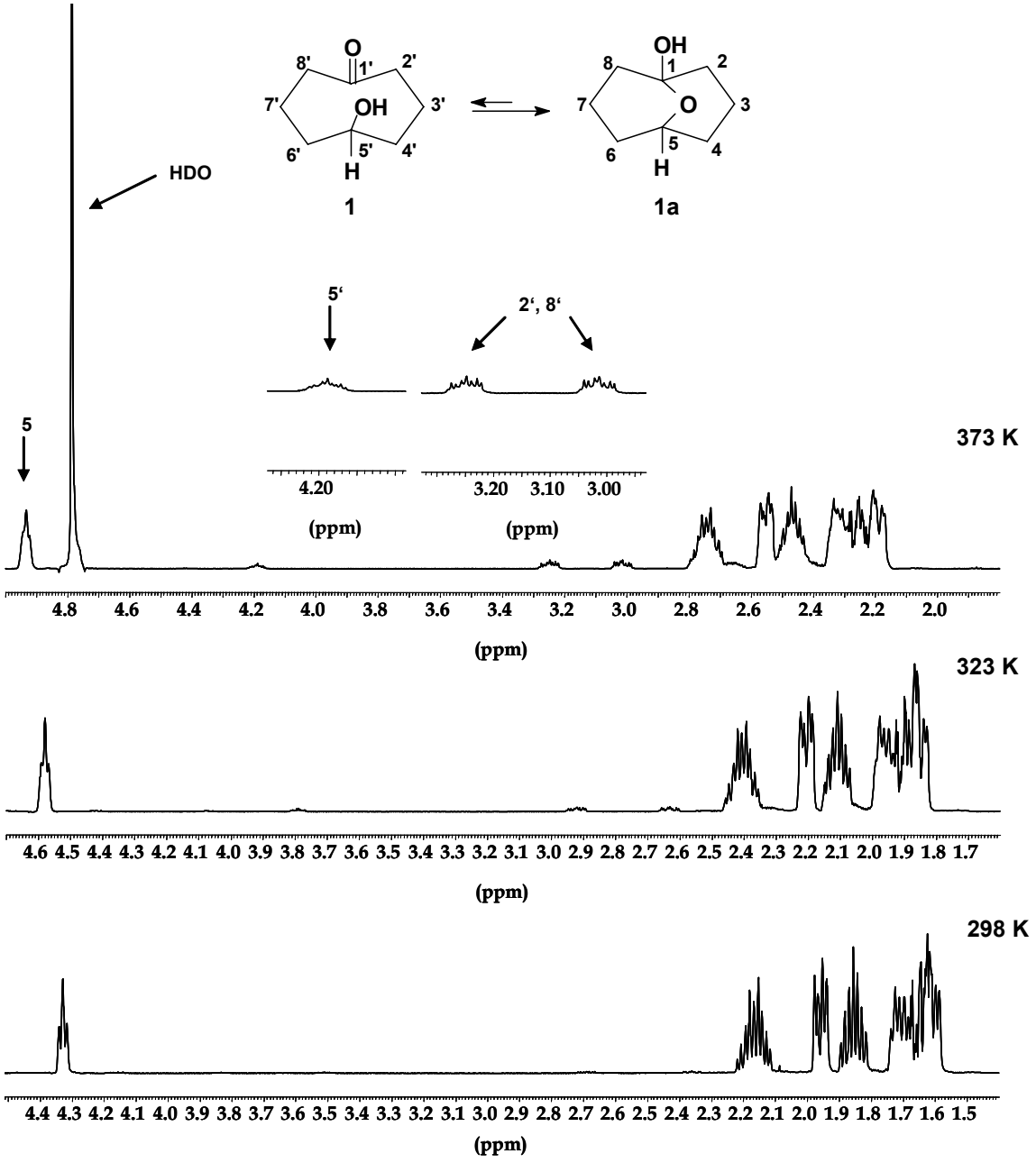

Figure 5.1: Variable-temperature NMR spectrum of tautomers **1** and **1a** determined at 500 MHz (with expansions) in D_2O at different temperatures.

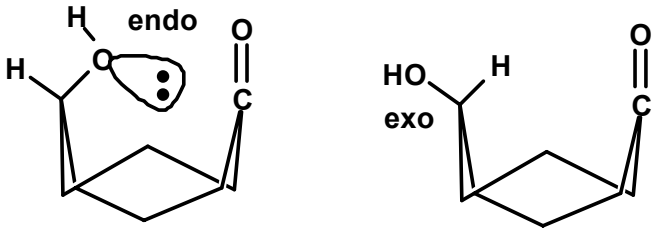

1d **1e**

Figure 5.2: Possible orientation for the OH group in **1**. Similarly, *endo*- and *exo*-conformers in model compounds (**2** – **5**) have been depticted with alphabets **d** and **e**, respectively.

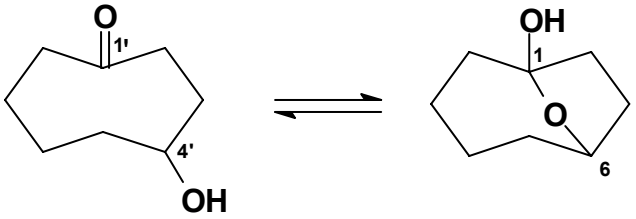

2 **2a**

Scheme 5.2: Existence of equilibrium between **2** and **2a**.

Table 5.2: Chemical equilibrium between tautomers **2** and **2a** in different solvents at different temperatures.

Solvent	**ε** [138]	**T (K)**	**2a:2**	K_{eq}**=[2a]/[2]**[a]	**Δ*G*** (**kcal mol^{-1}**)	**ΔΔG** (**kcal mol^{-1}**)
CCl_4	2.24	298	87.0:13.0	6.67	-1.12	0.012
Benzene-d_6	2.28	298	75.6:24.4	3.10	-0.67	0.024
$CDCl_3$	4.81	298	68.7:31.3	2.19	-0.46	0.034
DMSO-d_6	46.60	298	60.0:40.0	1.50	-0.24	0.050
	46.60	323	58.8:41.2	1.43	-0.21	0.06
	46.60	373	35.9:64.1	0.56	+0.34	0.17
D_2O	80.00	298	30.6:69.4	0.44	+0.49	0.17
	80.00	323	≤1:99			
	80.00	363	≤1:99			

[a] Ratios were calculated from signal intensities of protons attached to C-6 and C-4'.

Equilibrium constants for **2** and **2a** obtained from NMR data are given in Table 5.2. In $CDCl_3$ the diagnostic signals for **2** are at δ 3.72 – 3.77 ppm (m) for H-4'. The signal for H-6 appears as a multiplet at δ 4.40 – 4.43 ppm. The signals for the protons α to the carbonyl group, i.e., H-2' and H-8', appear at δ 1.86 – 2.57 ppm (m). The complex multiplet at δ 1.29 – 1.80 is assigned to the other ring protons of **2** and **2a**. The value of the equilibrium constant is calculated from the intensity ratio of the signals for H-6 in **2a** and H-4' in **2**. The equilibrium constant has its highest value 6.67 in the most non-polar solvent CCl_4. The amount of tautomer **2** increases from 13 to 69 % while going from CCl_4 to D_2O at room temperature. In the aprotic polar solvent DMSO-d_6, an equilibrium exists even at high temperature (at 323 and 373 K) whereas in D_2O at same temperatures there is no equilibrium and only **2** is found. The Standard Gibbs free energy, ΔGº, increases from a negative to a positive value with dielectric constant of the solvent (2.24 to 80.00 D).

The value of K_{eq} is less than one at 323 and 373 K in D_2O. The ability of hydrogen bonding of D_2O has completely hindered the formation of **2a** whereas in DMSO-d_6 intermolecular hydrogen bonding is absent. The molecule **2** has adopted such a conformation in water that the –OH group is projected outside the ring for intermolecular H-bonding with water and the hydrophobic ring is inside. The calculated (B3LYP/6-31+G*) dipole moments of the low energy *endo*-conformer for 4-hydroxycyclooctanone **2** and its hemiacetal **2a** in the gas phase are 3.4 and 2.6 D, respectively. The higher diople moment of *endo*-conformer **2d** is high which implies that in polar solvents the population of these conformers is large. The equilibrium between **2** and **2a** is completely shifted in one direction in D_2O at higher temperature. So we can say that with the increase of the polarity of the solvent and higher temperatures the transannular interactions are reduced. The conformational mobility of **2** seems to have similarities with the tautomeric equilibrium reported for **5**.[58] In both cases, the tautomer hydroxy-ketone exists to a significant amount in CCl_4 but exclusively in D_2O at room and higher temperature in **2** and **5**, respectively.

Compound **3** has been studied to see the effect of double bond insertion on transannular interaction. It is known to exist in equilibrium with **3a** in $CDCl_3$ (Scheme 5.3). Surprisingly, the incorporation of double bond between C-2 and C-3 directs the equilibrium towards bicyclic tautomer rather than the monocyclic tautomer. It is

speculated that the presence of double bond may lead to strain in bicyclic ring. The diagnostic NMR signals for **3** and **3a** are multiplets at δ 5.19 ppm for H-4' and at δ 4.97 – 4.98 ppm for H-6.

The equilibrium constant decreases from 19.4 in a non-polar solvent ($CDCl_3$) to 8.8 in a polar solvent (D_2O) (Table 5.3). The Standard Gibbs free energy also increases in a similar fashion. In D_2O at 363 K the ΔG value is highest, i.e., -0.50 kcal mol^{-1}. The difference in ΔG in $CDCl_3$ and D_2O at room temperature is only 0.47 kcal mol^{-1}, but the equilibrium constant difference is very high, i.e., 10.68. This implies that the equilibrium is highly dependent on the dielectric constant of the solvent. No equilibrium has been found between between **3** and **3a** in benzene-d_6 at room temperature (Figure 5.3). The ^{1}H-NMR spectrum indicates the absence of the diagnostic signal of **3** at δ 5.19 ppm for H-4'.

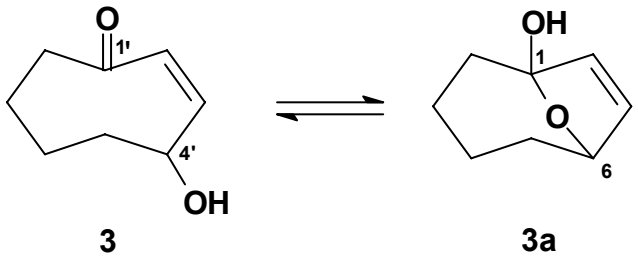

3 **3a**

Scheme 5.3: Existence of equilibrium between **3** and **3a**.

The calculated (B3LYP/6-31+G*) dipole moments for low energy *endo*-conformer for **3** and **3a** are 3.6 and 2.7 D, respectively. For the tautomeric equilibrium between **3** and **3a** the same explanation is valid as discussed above for **1**/**1a** and **2**/**2a**. The transannular interactions have been markedly increased in **3** as compared to **2**. This is due to the shortening of the bond between C-2 and C-3. Compound **3** is isolated as a white solid in its hemiacetal form **3a**. The X-ray structure was shown in the previous chapter in Figure 5.3.

Table 5.3: Chemical equilibrium between tautomers **3** and **3a** in different solvents at different temperatures.

Solvent	**ε** [138]	**T (K)**	**3a:3**	K_{eq}**=[3a]/[3]**[a]	**Δ*G*** (**kcal mol^{-1}**)	**ΔΔG** (**kcal mol^{-1}**)
Benzene-*d*$_6$	2.28	298	≥ 99			
	2.28	343	≥ 99			
CDCl$_3$	4.81	298	95.1:4.9	19.4	-1.76	0.001
	4.81	323	94.9:5.0	2.93	-1.88	0.001
Acetonitrile-*d*$_3$	37.50	298	90.3:9.7	9.30	-1.33	0.004
	37.50	343	81.8:18.2	4.50	-1.02	0.006
DMSO-*d*$_6$	46.60	298	89.0:10.0	8.86	-1.29	0.002
	46.60	323	84.0:16.0	5.25	-1.07	0.004
	46.60	373	56.0:44.1	1.27	-0.18	0.018
	46.60	403	61.1:38.9	1.57	-0.36	0.015
D$_2$O	80.00	298	89.8:10.2	8.78	-1.29	0.002
	80.00	323	81.3:18.7	4.36	-0.94	0.004
	80.00	363	66.7:33.3	2.00	-0.50	0.011

[a]Ratios were calculated from signal intensities of protons attached to C-6 and C-4'.

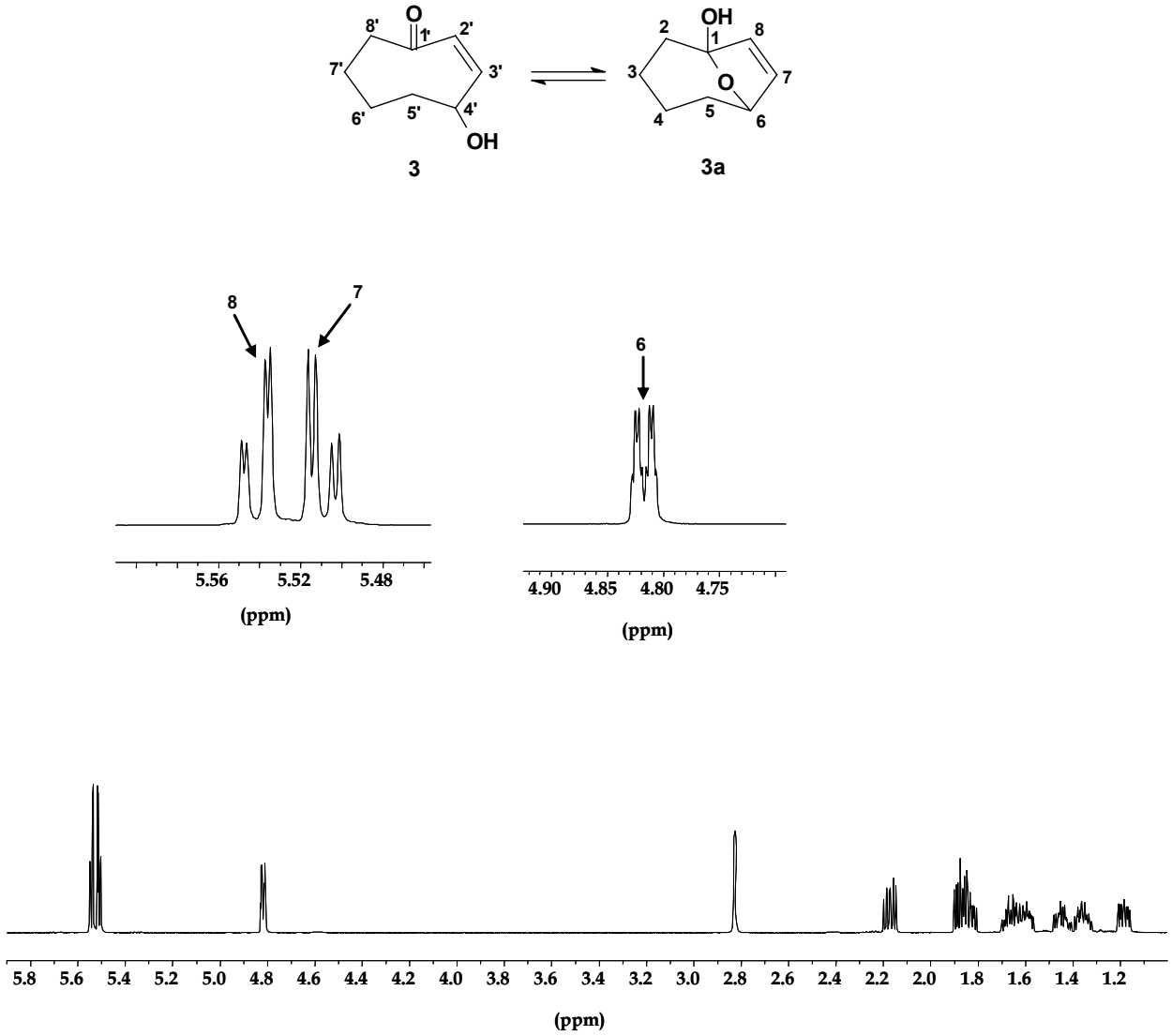

Figure 5.3: NMR spectrum of **3** determined at 500 MHz in benzene-d_6 at room temperature.

The results obtained provide evidence for the conformational mobility in model compounds **1** – **3** in solution and the relative populations of tautomers are solvent and temperature dependent. The study has certainly given a better understanding of the role of solvent in partial control of transannular interaction in **1** – **3**. The most remarkable result is the existence of monocyclic hydroxy ketone **1** in DMSO-d_6 and D_2O at higher temperatures. In the case of **2** the transannular product, hemiacetal **2a**, is ≤ 1 % in D_2O at higher temperature. The effect of the temperature on the relative position of conformational equilibrium is related to the change in entropy. Lower temperature favors the ordered system, i.e., hemiacetal. The values for the dipole moments of hemiacetal and hydroxy ketones are also in agreement with the experimental observations. The interplay of conformations can largely change the

properties of a compound. And this can be controlled by selection of a proper reaction medium. Thus, the results can be exploited in planning reactions involving compounds **1** – **3**.

6 Nucleophilic addition reaction: Hemiacetal formation

The existence of a tautometric equilibrium like the one shown in Scheme 6.1 is common in difunctional medium-ring compounds.[59-61, 63-65] The NMR studies for model compounds **1** – **3** have shown that the amount of hemiacetal formation is different in all three cases (see chapter 5). The experimental results have shown that the solvent can partially or completely control hemiacetal formation.

Numerous experimental studies have been done until now to control the transannular interactions in medium-rings.[58, 140-142] On the contrary, theoretical studies regarding the role of conformation in transannular reactions are not well investigated. Transannular interactions lead to significant changes in geometry, electron density distribution and MO energies.[34, 49, 51, 143] These changes can be studied by theoretical methods. This prompted us to investigate theoretically model compounds **1** – **5** (Scheme 6.1).

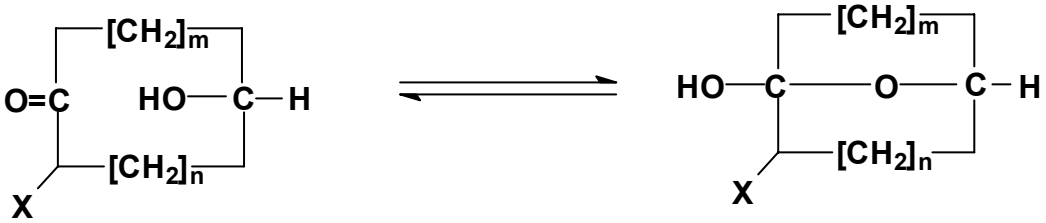

1: m=1, n=1, X=H
2: m=2, n=0, X=H
4: m=1, n=1, X=Br
5: m=2, n=2, X=H

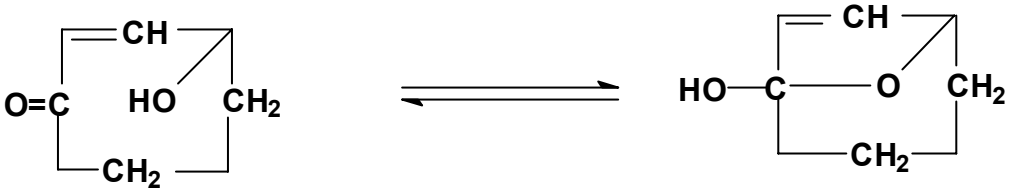

3

Scheme 6.1: Transannular hemiacetal formation in model compounds **1** – **5**.

Compounds **1** – **4** are eight-membered rings whereas **5** is a ten-membered hydroxy-ketone. The choice of these model compounds is based on factors such as ring size, position of functional groups and effect of substituents which are crucial for

investigating the role of conformation in transannular hemiacetal formation. The calculations for **1** have already been reported.[144] These calculations were done by the Gamess program[145] at different levels of theory. For comparison with other model compounds **2** – **5**, we have repeated the calculations with the B3LYP/6-31+G* level of theory. The intermolecular hydration reaction of formaldehyde can serve as a model for the intramolecular hemiacetal formation in **1** – **5**. It is the simplest example of an uncatalysed addition of water to a carbonyl compound (Scheme 6.2), and such nucleophilic addition reactions are of great importance in chemistry and biochemistry.[146-154] Examples are found in many compounds such as saccharides, containing two groups, –OH and >C=O (e.g., glucose in its cyclic pyranose form).[155]In the nucleophilic addition reaction the carbonyl C atom acts as an electrophilic centre and it is attacked by a nucleophile, i.e., –OH (Scheme 6.2).

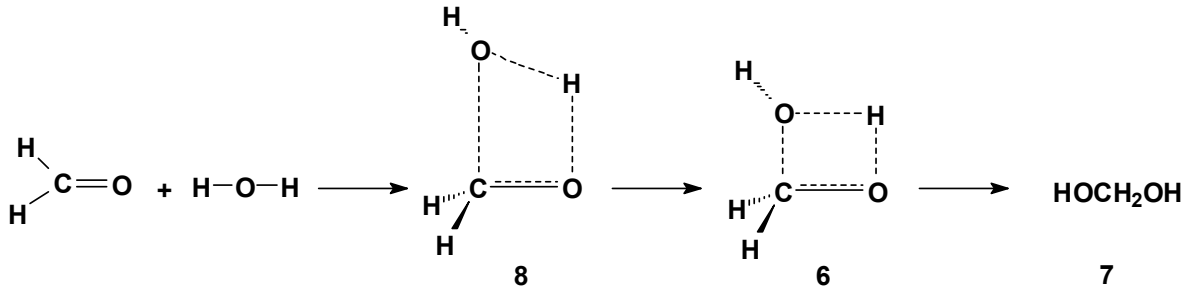

Scheme 6.2: Addition of water to formaldehyde under neutral conditions occurs *via* a four-membered transition-state (**6**).

The reaction involves conversion of the sp^2 hybridisation of the carbonyl C atom to sp^3 and in the process a weaker π bond is converted to a stronger σ bond. The reaction is entropically unfavourable, but with higher exothermic enthalpies, it is an overall favourable conversion. The equilibrium between aldehyde or ketone yielding hemiacetal or hemiketal depends on a number of factors such as the structural features of the alcohol, carbonyl compound and the adduct so formed.[154, 156] Hemiacetals and hemiketals are generally unstable compounds. In some cases stable cyclic hemiacetals and hemiketals are readily formed. The product is stable if there is ring formation, e.g., glucose. Addition of water to formaldehyde is an exception. Formaldehyde exists in its hydrated form.[157, 158]

Williams *et al*.[157] have reported *ab initio* studies for water and formaldehyde as a model for a nucleophilic addition reaction. The reaction was reported to proceeds

with a high energy barrier under uncatalysed condition with a single water molecule and formaldehyde. Numerous studies until now have been carried out for studying the mechanism.[157, 159-163] Recently, Wolfe and co-workers[160] have proposed a new mechanism in which the transition-state is not four-membered (**6**) as proposed before by Williams *et al.*[157] but contains three water molecules. In medium-rings, such as **1** – **5**, hemiacetal formation occurs by intramolecular addition of the hydroxy group present in the ring to the carbonyl group. We have carried out prototype study on formaldehyde with one water molecule in order to compare the results with those obtained for medium-rings.

We have investigated the reaction mechanism, transition-state structures and molecular complexes (van der Waals complexes) of compounds **1** – **5** and the prototype system at B3LYP/6-31+G* level of theory.[164] This level of theory has generally been found to give a good representation of reaction energies. Diffuse functions were included in order to correctly represent the electron lone pairs on oxygen. The optimisation of all conformers is done using tight convergence criteria. For transition-states the option Calcall was used for calculating the force constant in every iteration. Frequency calculations were done for all stationary points to characterise them as minima (NIMAG=0). Each transition-state structure was characterised as possessing one imaginary frequency (NIMAG=1), corresponding to the motion which carries the system over the energy barrier. Zero point energies are unscaled. The thermodynamic functions (ΔG, ΔH, ΔS) were computed in the gas phase using the B3LYP/6-31+G* frequencies within the ideal gas, rigid rotor and harmonic oscillator approximations.[165] The calculation of ΔG_{gas} uses a reference state of 1 atm (298.15 K).

Single point calculations were performed to calculate properties of all molecules at B3LYP/6-31+G**//B3LYP/6-31+G* level of theory in chapters 7-11. The natural bond order analysis (NBO)[97] was carried out to understand second order interactions and to have a deep insight of the charge distribution on atoms in reactants. The bonding properties were investigated with Bader's topologiocal electron density analysis.[109-111, 166] For each conformer the one electron density distribution ρ(r) was analysed with the aid of the Laplacian $\nabla^2\rho(r)$ which also determines the regions in space where electronic charge is concentrated or depleted. Bond critical points are

characterised by a minimum value in ρ(r) along the maximum electron density path connecting two nuclei.

6.1 Bonding and interactions

It is likely that in a hydrophobic environment the reaction between formaldehyde and water takes place through a concerted pathway (Scheme 6.2). The reaction is assumed to start from a weakly bonded complex, **8**. This complex (**8**) then leads to product **7** in one step. The complex **8** is a loose four-membered ring structure and is characterised as a true minimum on the potential energy surface. A similar structure has been reported in a nucleophilic addition of carbon monoxide and water.[153] The intermolecular interactions in adduct **8** are comparable to the intramolecular transannular interactions between the functional groups in certain low energy conformers of model compounds **1** – **5**. Some geometrical parameters of **8** and **6** summarised in Figure 6.1 and Table 6.1. In **8** the non-bonded distance C(1)···O(4) is 2.83 Å whereas the distance between the H(3) and the O(2) is 2.76 Å. These distances are less than the van der Waals (vdW) radii of C and O (3.2 Å).

As a general rule, the magnitude of transannular interactions depends on the spatial overlap between the donor and acceptor orbitals which is determined by molecular geometry. The carbonyl carbon in **8** is slightly displaced from its plane by 0.003 Å. In a series of papers Bürgi, Dunitz and co-workers[42, 167-169] have described the trajectory of the addition of a nucleophilie containing oxygen or nitrogen atoms to the carbonyl group by an angle θ with respect to the C–O axis. The approach of water towards the carbonyl group takes place in such a way that the H(3) is drawn into the plane of O(4)-C(1)-O(2) since the value of the dihedral angle O(2)–C(1)–O(4)–H(3) is only 1.4° in **8**.

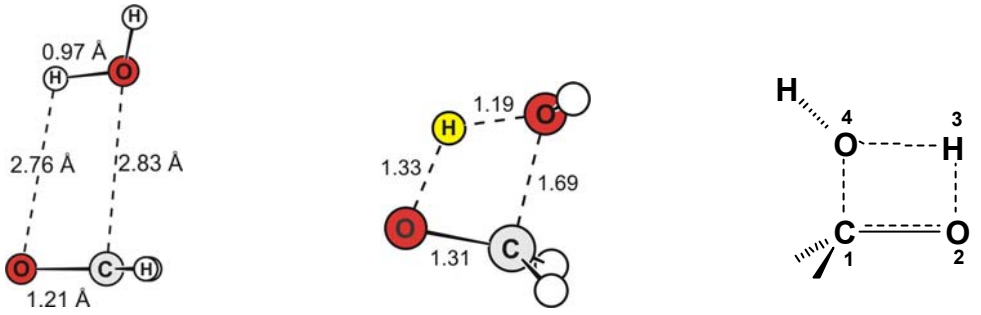

8 **6**

Figure 6.1: Some geometrical parameters [distances (Å)] of transition-state **6** and complex **8**.

Table 6.1: Some geometrical parameters [angles (°)] of the transition-state **6** and complex **8**.

	8	**6**
O(4)–C(1)–O(2)	94.9	93.0
H(3)–O(4)–C(1)	79.8	68.2
O(2)–H(3)–O(4)	106.3	120.5
H(3)–O(2)–C(1)	79.0	78.3
O(2)–C(1)–O(4)–H(3)	1.4	-0.6

Natural bond order analysis has been carried out for **8** to investigate the behaviour of interacting orbitals, i.e., n_O and $\pi^*_{C=O}$.The results are tabulated in Table 6.2. The stabilisation energy $E^{(2)}$ associated with donation of electrons from the 'filled' non-bonding nucleophilic oxygen orbital n_O to the empty $\pi^*_{C=O}$ orbital is 1.56 kcal mol^{-1}. This implies that there is electron transfer from n_o to $\pi^*_{C=O}$ in **8**. Quantum chemical properties (in a.u.) of bond path C(1)···O(4) corresponding to the intermolecular interaction is observed (Table 6.3). A bond critical point (BCP) is localised in the region of the interatomic C(1)···O(4) contact. According to AIM theory this BCP corresponds to chemical bonding. The Laplacian of the electron density ($\nabla^2\rho$) is slightly positive, 0.038. Thus, the C(1)···O(4) path shows characterstics between those of shared and closed-shell interactions (ionic bonds, some van der Waals complexes, etc.).[122, 170, 171] The ellipticity ε (0.201 a.u.) at BCP describes the spatial symmetry and spread of a bond.

Table 6.2: Natural bond order (NBO) analysis of the complex **8**. $E^{(2)}$ (kcal mol^{-1}) is the second order perturbation energy between Φ_i and Φ_j; E_j-E_i (a.u.) is the energy difference between NBOs Φ_i and Φ_j; F_{ij} (a.u.) is the Fock matrix element; only energies greater than default threshold 0.5 kcal mol^{-1} are included in the table.

	Interaction	**Second-order Interaction**			**Occupancy (ρ)**	
		$E^{(2)}$	E_j-E_i	F_{ij}	n_o	$\pi^*_{c=o}$
8	$n_o \rightarrow \pi^*_{c=o}$	1.56	0.49	0.025	1.99	0.01

Table 6.3: Properties (a.u.) calculated at bond critical point in electron density of **8**. [$\nabla^2\rho$: Laplacian of the electron density; ε: ellipticity; H(r): sum of kinetic and potential energy densities].

	Bond	$\nabla^2\rho$	**ε**	**H(r)**
8	C(1)···O(4)	0.038	0.201	-0.008

The orbital correlation diagram for water and formaldehyde is shown in Figure 6.2. The molecular orbitals HOMO-2 and LUMO for **8** are depicted in Figure 6.3. The HOMO-2 for complex **8** clearly shows the interaction between n_O of O(3) in water and $\pi^*_{C=O}$ of formaldehyde. The LUMO diagram shows a large coefficient for the C(1) atom of formaldehyde. The orbital overlap between non-bonding O(3) of water and $\pi^*_{C=O}$ of formaldehyde is highly favoured at a distance less than the vdW distance.

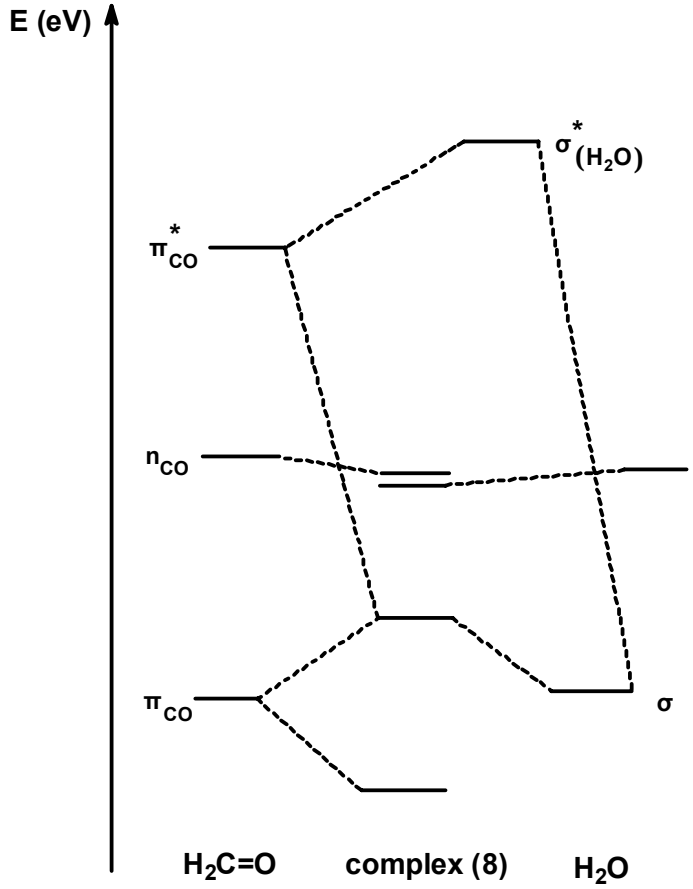

Figure 6.2: Orbital correlation diagram for a nucleophile (water) and an electrophile (formaldehyde).

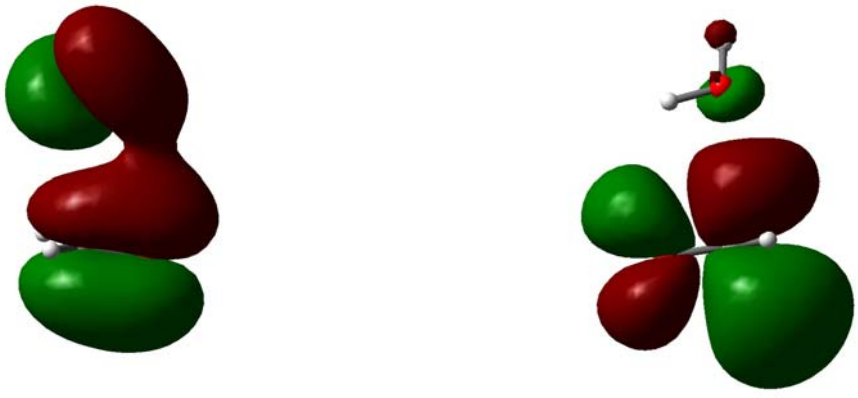

HOMO-2 **LUMO**

Figure 6.3: Graphical representation of the orbitals HOMO-2 and LUMO of complex **8**.

6.2 Transition-state calculations

The interactions between the non-bonding and antibonding orbitals of water and formaldehyde probably can initiate the nucleophilic addition reaction. The complex **8** goes to methanediol **7** through a transition-state **6** with a high activation barrier of 37.2 kcal mol^{-1} (Figure 6.4). The transition-state is characterised by an imaginary frequency. The complex **8** is only 1.5 kcal mol^{-1} more stable than the isolated reactants (Figure 6.5). This shows that the potential energy surface is rather flat in this part.

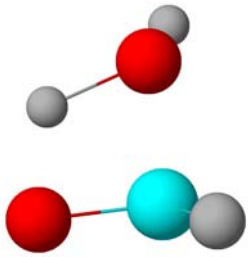

6 (-1765)

Figure 6.4: Transition-state **6**. Imaginary frequency (cm^{-1}) is given in parentheses.

The energy profile for the addition of water to formaldehyde is shown in Figure 6.5. The isolated reacting molecules initially form a vdW complex **8**. These interactions stabilise the complex by 1.5 kcal mol^{-1}, with respect to the isolated reactants. The activation energy required for going from **8** to **6** is 37.2 kcal/mol whereas the energy difference between the isolated molecules and transition-state is 35.7 kcal/mol. This energy barrier is lower than that for reported unassisted hydrolysis of formamide passing through a similar four-centred cyclic transition-state (42.0 kcal mol^{-1} at MP2(FULL)/6-31G**//4-31).[172]

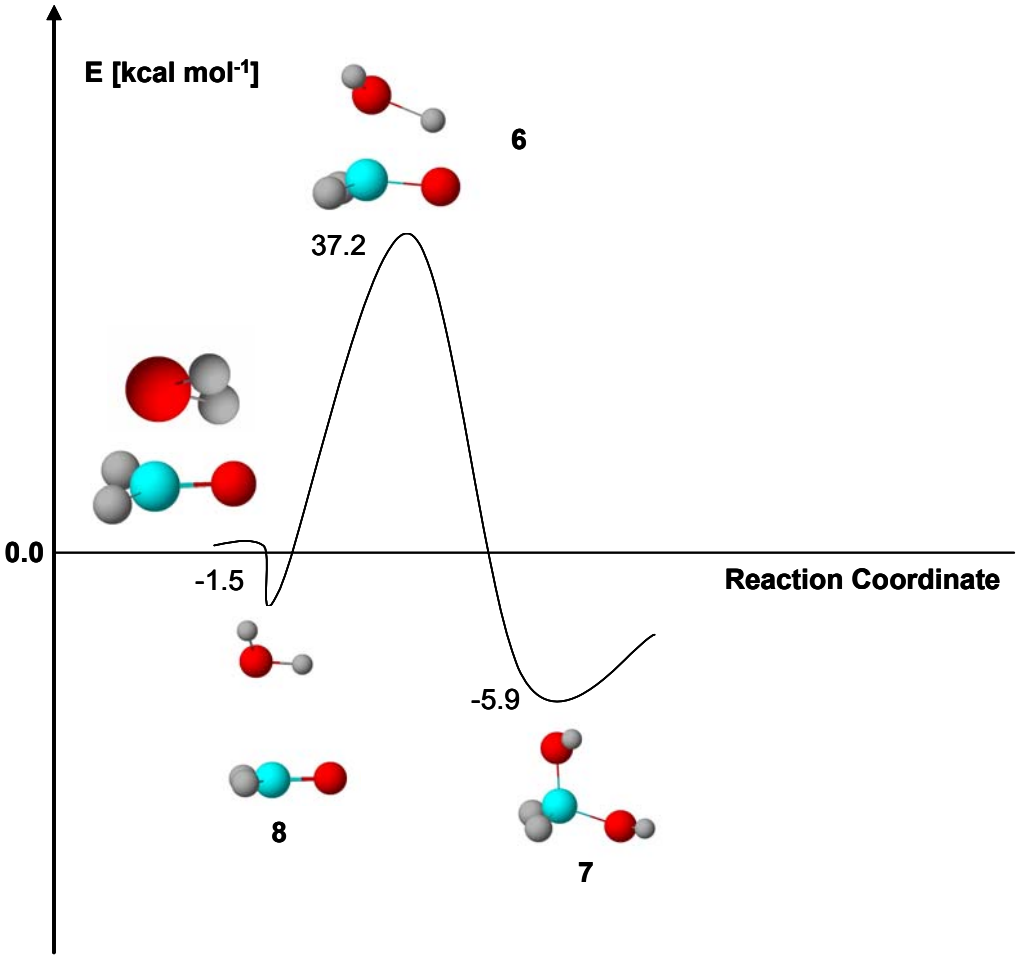

Figure 6.5: Energy profile for the gas phase addition reaction of water and formaldehyde.

The C(1)···O(4) distance is decreased to 1.69 from 2.83 Å while going from **8** to **6**. show many similarities (Figure 6.1). The attacking angle is decreased in **6** by only 1.9°. The four-membered cyclic structure in **6** is more planar than in adduct **8**. Comparison of the natural charge distribution in transition-state **6** and complex **8** also shows that the complex is close to the transition-state geometry (Table 6.4). The charge at the electrophilic carbon atom is 0.223 and 0.248 e in **6** and **8** respectively. Thus, it can be concluded that an uncatalysed nucleophilic additon of water occurs with the formation of adduct. The results presented here do not give a real picture of the hydration taking place in water but are useful in interpreting transannular hemiacetal formation in medium-ring compounds.

Table 6.4: Natural charge (e) distributions on the reacting atoms in adduct **8** and transition-state **6**.

	O(4)	C(1)	O(2)	H(3)
8	-0.992	0.248	-0.555	0.503
6	-0.853	0.223	-0.805	0.545

In the following chapters a detailed description of the hemiacetal formation in compounds **1** – **5** is given. The aim is to explore the presence of similar adducts as **8** in certain low energy conformations of difunctional medium-rings. The formation of a hemiacetal in **1** – **5** is an intramolecular reaction which is expected to be favoured by proximity factors.

7 Hydroxy-ketone – hemiacetal rearrangement: Theoretical mechanistic study

7.1 Introduction

The NMR studies reported in chapter 5 have shown that **1** exists mainly as its transannular product **1a** (hemiacetal) in solvents of different polarities at room temperature. But at higher temperature **1** is in equilibrium with **1a** in polar solvents, e.g., DMSO-d_6 and D_2O (Table 5.1). On the other hand, 13% of **2** is present in a non-polar solvent (CCl_4) at room temperature and ≥ 99 % in a polar solvent (D_2O) at 323 K (Table 5.2). Interestingly, with the introduction of a double bond in the ring as in model compound **3**, the equilibrium is shifted more in the direction of the bicyclic tautomer **3a** as compared to **2** ⇌ **2a**. The ratio of **3**:**3a** in $CDCl_3$ is 5:95 (Table 5.3). In a non-polar solvent such as benezene-d_6 the amount of **3a** is ≥99%. It seems that the conformational mobility of the tautomers is restricted due to the presence of a double bond. Compounds **1** and **2** have the same ring size but the position of the –OH group is different. Recently reported spectroscopic investigations of 6-hydroxycyclodecanone (**5**) have revealed that the conformation of this molecule in solution is a function of solvent polarity.[58] In a non-polar solvent such as hexane the favoured tautomer is the hemiacetal **5a** (88%) whereas in water tautomer **5** is favoured exclusively. The switching of equilibrium in either direction depends on the polarity of the solvent. These findings are consistent with conformational mobility in solution and rapid exchange between the tautomers, i.e., the hydroxy-ketone and hemiacetal, depending on the dielectric constant of the solvent.

We have studied **4** in order to understand at a fundamental level the steric and halogen effect on the transannular hemiacetal formation in **4**. It is speculated that the presence of a substituent like Br at the α position to the carbonyl carbon in **1** may lead to such conformations in which the optimal interaction of the electron lone-pair on the nucleophilic O atom with the π* orbital of the carbonyl group is not attained. Since the conformational biasing caused by the substituent may hinder or lead exclusively to the transannular product.[141] Cope and his co-workers[173] have reported that 5-hydroxycyclooctanone exists in the open form when a Br atom is present as a substitiuent at α carbon to the carbonyl carbon.

The formation of a hemiacetal is a simple nucleophilic addition reaction. It seems that the equilibrium favours the hemiacetal on thermodynamic grounds. For the

cyclisation to take place, an optimal distance between the atoms involved and a suitable angle of attack by the nucleophile are the obvious requirements. In other words, a suitable conformation of the ring in model compounds **1** – **5** is of paramount importance. Until now, hemiacetal formation in difunctional medium-rings has not been studied theoretically. In these compounds the nucleophile addition is an intramolecular reaction which should be favoured by proximity effects. It is important to explore the features which favour the intramolecular addition. What controls the equilibrium between hydroxy-ketone and hemiacetal, geometric or electronic factors ? Does hydrogen bonding between the carbonyl and hydroxy group play any role ? We have investigated here some of the energetic and structural aspects of this reaction in **1** – **5**.

7.2 Results for model compound 1

Eight-membered rings are flexible in nature and can exist in a number of conformers.[30, 31, 39] The conformational preference of the cyclooctyl systems is *bc* (boat-chair).[174] X-ray structure analyses of 1,5-cyclooctadione and derivatives of cyclooctadiene have shown that in the solid state the molecule exists in a *bc* conformer.[174] DFT calculations are time consuming and it is extremely difficult to perform such calculations on all possible conformations of **1** and **1a**. In keeping the complexity of the problem in mind we have carried out molecular mechanics calculations with MMFF (Merck Molecular Force Field developed by Merck Pharmaceuticals). Conformational complexity is also true for cyclooctanone[32] but the presence of a hydroxy group restricts the number of possible conformers. Initial calculations at MMFF level have generated 53 low energy conformers for **1** (Figure 7.1). The presence of a large number of conformers shows the complexity of the problem. A realistic system is a statistical assembly of various conformers. We have selected only six conformers on the basis of proximity of the reacting groups. These conformers have been subjected to optimisation at high level of calculations (B3LYP/6-31+G*).

Conformers **9** – **15** (Tables 7.1 and 7.2) were optimised within C_1 symmetry using DFT. All conformers with *exo*- orientation of OH are excluded from further investigation on the basis that in these conformers the reacting (OH and C=O) groups are not in proximity (i. e., the distance is > 4 Å) of each other which is a necessary condition for the reaction to occur. In conformers **9** – **11** (Table 7.1) hydrogen

bonding is present but absent in conformers **12** – **15** (Table 7.2). The bonding properties of all conformers **9** – **15** were investigated with Bader's topologiocal one electron density analysis (AIM). To study the solvent effects we have used a self consistent reaction field (SCRF) model proposed for quantum chemical computations on solvated molecules.[175-177] The solvent effects are estimated at the B3LYP/6-31+G* level on the gas-phase geometries for chloroform and water using the default parameters set of the Polarized Continuum Solvation Model (PCM) method as implemented in Gaussian 98. The calculations were performed with dielectric constant (ε) values 4.9 and 78.39 for chloroform and water, respectively, at 298.15 K. The PCM method has been developed in order to describe the solvent reaction field basically through the use of cavities of general shape, modeled on the solute. The cavity is defined as the union of a series of interlocking spheres centred on the atoms.

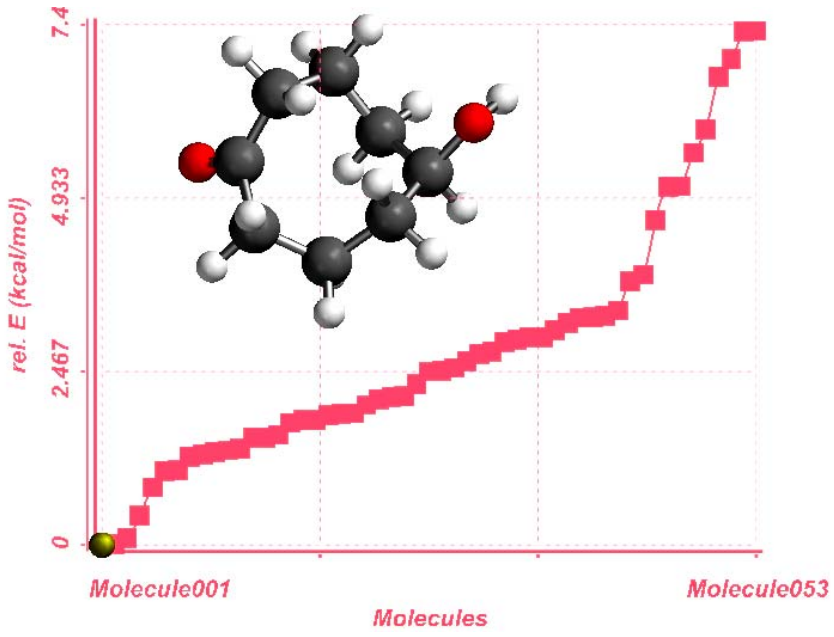

Figure 7.1: Energy profile of the conformer distribution for the *endo*-conformer of **1** at MMFF level.

7.2.1 Structural features

The structural features of the optimised conformers have been studied in detail in order to have a clear picture of the role of transannular interactions in hemiacetal formation. The most relevant parameters with respect to transannular interactions are

intramolecular non-bonded distances and angles between the electrophilic and nucleophilic groups (Scheme 7.1). Thus, we have reported here some of these relevant parameters (Tables 7.1 and 7.2). The intramolecular non-bonded distance O···C=O is represented by d_O. The nucleophilic approach trajectory may be described in terms of the attack angle θ_O between the developing C···Nu bond and the C=O bond. The distance between the carbonyl carbon and the carbon atom on which the hydroxy group is attached is represented by d_1. Since the reaction implies a $sp^2 \rightarrow sp^3$ transformation of the carbonyl carbon atom, this atom becomes pyramidal.

The deviation of carbon atom from its plane defined by three bonded neighbours is represented as Δ_O. This effect of deviation is called leaning effect and was first observed by Bürgi *et al*.[167] The leaning effect indicates the presence of a non-hydrogen bonded, non-covalent, intramolecular interaction between nucleophilic and electrophilic units present in the ring.

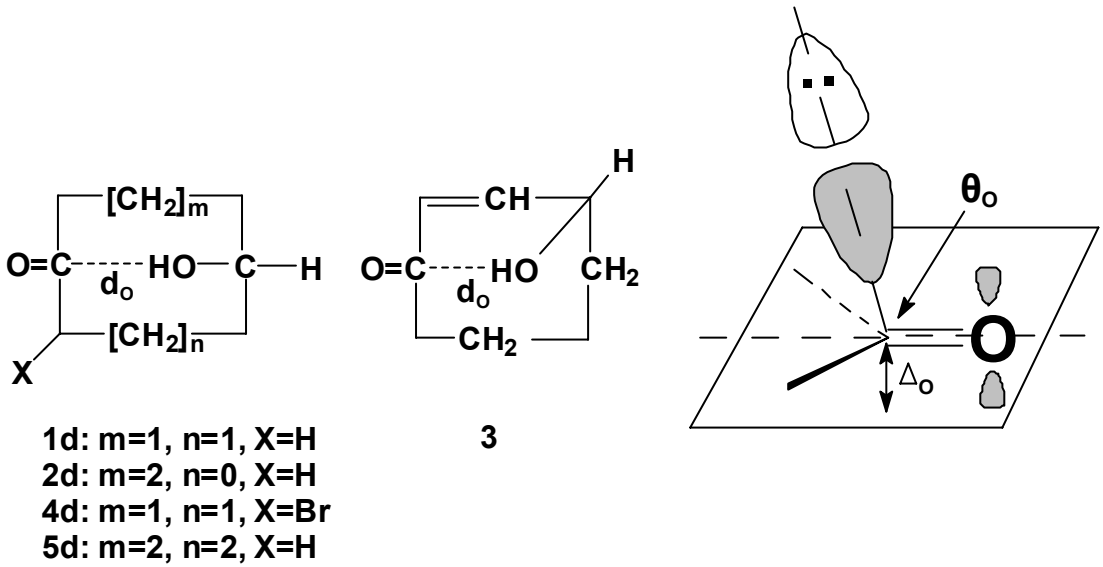

1d: m=1, n=1, X=H
2d: m=2, n=0, X=H
4d: m=1, n=1, X=Br
5d: m=2, n=2, X=H

3

Scheme 7.1: Important geometrical parameters such as non-bonded distance O···C=O (d_O), angle of attack (θ_O) and deviation of carbonyl carbon from its plane (Δ_O) are investigated in *endo*-conformers of compounds **1** – **5**.

In conformers **9** – **11** the presence of hydrogen bonding is considered. The structural features of conformers are given in Table 7.1. In these conformers the hydrogen atom of OH and the O atom of C=O are in H-bonding distance. The distance between the electrophilic C and nucleophilic O atoms in **9**, **10** and **11** are 3.2, 3.0 and 3.3 Å, respectively. These distances are near to the sum of vdW radii (3.2 Å) of carbon and

oxygen atoms. At such distances, the overlap between the orbitals of the nucleophilic and electrophilic centres is not very significant. The initial angle of approach of OH to the carbonyl carbon is not in agreement with the results of crystallographic studies on compounds with carbonyl groups in the vicinity of a base.[168, 169] Presence of hydrogen bonding has reduced the value of this angle to 74.7°, 76.4° and 74.2° in **9**, **10** and **11**, respectively. For a successful nucleophilic attack the axis of the nucleophile orbital containing the electron pair and the large lobe of the $\pi^*_{C=O}$ orbital must be coaxial during the nucleophilic attack on the C=O group. The nucleophilic attack angle given by Dunitz and Bürgi[168, 169] is near 100°. The deviation Δ_O of the carbonyl C atom from its plane in conformer **10** is smallest (0.006 Å). It shows that not only the close proximity of the reacting atoms but also the directionality of the approaching nucleophile is quite important.

In conformers **12** – **15** (Table 7.2) H-bonding is absent. The distance between the O atom of the OH group and the carbonyl C are 2.9 and 2.6 Å in **12** and **13**, respectively, whereas the distances in **14** and **15** are 3.7 Å. In **12** and **13** the distances are less than the sum of vdW radii of C and O. At such distances, the overlap between the orbitals of the nucleophilic and electrophilic centres is very significant. This small distance indicates that sizeable OITS (orbital interactions through space) are possible.

It is more likely that the cyclisation occurs in **12** or **13** with ease as compared to the cyclisation in other conformers. The nucleophilic oxygen approaches the carbonyl carbon at an angle of 102.3° to the carbon-oxygen bond in **13**. This is within the bounds for the angle of attack by a nucleophile as given by Bürgi and Dunitz.[169] In conformers **12**, **14** and **15** the attacking angles are found to be 96.8°, 97.2° and 93.2°, respectively. The displacement of the carbonyl carbon in **13** is 0.061 Å. The distance d_1 is close to 3.2 Å in **12** and **13**. Analysis of all geometric parameters has shown that conformers **12** and **13** are more likely to undergo cyclisation. In case of **9** – **11** all the geometric parameters suggest that the presence of hydrogen bonding prevents cyclisation.

Table 7.1: Important geometrical parameters investigated in **9** – **11** and relative energies including the zero point energy calculated with respect to conformer **18** (gas phase). [Distances (Å); angles (°), rel. energies (kcal mol^{-1})].

Molecular structure	**Geometrical parameters**			
	$\mathbf{d_o}$	$\mathbf{d_1}$	$\mathbf{\theta_o}$	Δ_o
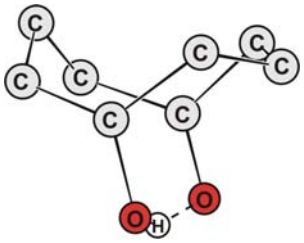 **9** (5.649)	3.171	3.197	74.7	0.024
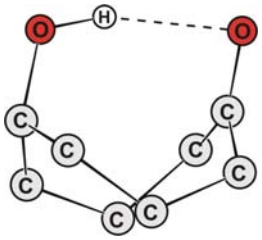 **10** (10.492)	3.042	3.108	76.4	0.006
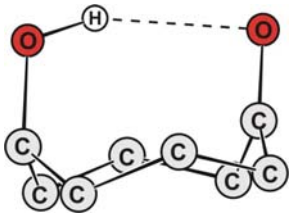 **11** (6.079)	3.338	3.238	74.2	0.039

Table 7.2: Important geometrical parameters investigated in **12** – **15** and relative energies including the zero point energy calculated with respect to conformer **18** (gas phase). [Distances (Å); angles (°), rel. energies (kcal mol^{-1})].

Molecular structure	**Geometrical parameters**			
	d_o	d_1	θ_o	Δ_o
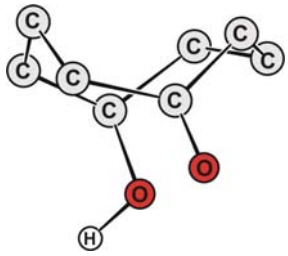 **12** (5.999)	2.898	3.297	96.8	0.032
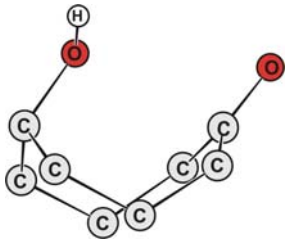 **13** (8.492)	2.636	3.208	102.3	0.061
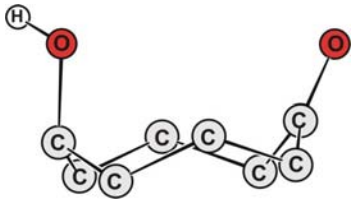 **14** (6.842)	3.690	3.555	97.2	0.010
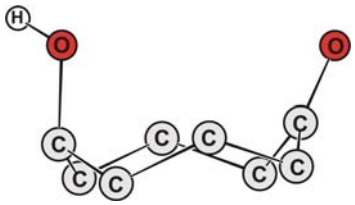 **15** (6.835)	3.683	3.530	93.2	0.038

7.2.2 Bonding and interactions

Natural bond orbital analysis was carried out to explore the interaction between the reacting groups in the different conformers **9** – **15** in their respective ground states. In this context an interesting quantity to look at is the second order interaction between the donor and acceptor orbitals. In conformers **9** – **11**, **14** and **15** interactions between the donor and acceptor orbitals were found to be absent. In conformers **9** – **11** presence of H-bonding precludes the $n_O \rightarrow \pi^*_{C=O}$ electron transfer. In these conformers the O···C=O distance d_O is quite large (>3 Å). This indicates that the intramolecular H-bonding does not facilitate cyclisation. In **12** and **13** the distances between the nucleophilic oxygen and carbonyl carbon are less than 3 Å. Therefore, interaction is expected between the two groups. As is evident from Table 7.3 the stabilisation energy $E^{(2)}$ associated with donation of electrons from the filled non-bonding nucleophilic oxygen n_O to the empty electrophilic $\pi^*_{C=O}$ orbital is strongest, i.e., 3.59 kcal mol^{-1}, in **13**. The electron occupancy in $\pi^*_{C=O}$ in **13** is higher than in **12**. This implies that there is more electron transfer from $n_O \rightarrow \pi^*_{C=O}$ in **13** than in **12**.

Table 7.3: Natural bond order (NBO) analysis of conformers **9** – **15**. $E^{(2)}$ (kcal mol^{-1}) is the second order perturbation energy between Φ_i and Φ_j; E_j-E_i (a.u.) is the energy difference between NBOs Φ_i and Φ_j; F_{ij} (a.u.) is the Fock matrix element; only energies greater than default threshold 0.5 kcal mol^{-1} are included in the table.

	Interaction	**Second-order Interaction**			**Occupancy (ρ)**	
		$E^{(2)}$	E_j-E_i	F_{ij}	n_O →	$\pi^*_{C=O}$
9	$n_O \rightarrow \pi^*_{C=O}$	-----	-----	-----	1.955	0.091
10	$n_O \rightarrow \pi^*_{C=O}$	-----	-----	-----	1.957	0.088
11	$n_O \rightarrow \pi^*_{C=O}$	-----	-----	-----	1.954	0.090
12	$n_O \rightarrow \pi^*_{C=O}$	1.13	0.34	0.018	1.955	0.084
13	$n_O \rightarrow \pi^*_{C=O}$	3.59	0.38	0.033	1.943	0.093
14	$n_O \rightarrow \pi^*_{C=O}$	-----	-----	-----	1.959	0.078
15	$n_O \rightarrow \pi^*_{C=O}$	-----	-----	-----	1.959	0.078

Table 7.4: Properties (a.u.) calculated at bond critical point in electron density for conformers **9** – **15**. [$\nabla^2\rho$: Laplacian of the electron density; ε: ellipticity; H(r): sum of kinetic and potential energy densities].

	Bond	$\nabla^2\rho$	**ε**	**H(r)**
9	O···C=O	-----	-----	-----
10	O···C=O	-----	-----	-----
11	O···C=O	-----	-----	-----
12	O···C=O	0.037	0.305	-0.007
13	O···C=O	0.058	0.122	-0.013
14	O···C=O	-----	-----	-----
15	O···C=O	-----	-----	-----

Atoms in molecule (AIM) calculations have been performed on conformers **9** – **15** to find out whether there are any electronic interactions between the donor and acceptor units. A summary of the density analysis for conformers **9** – **15** is provided in Table 7.4. A critical point corresponding to an interaction between O···C=O has been observed in both **12** and **13**, confirming that these conformers induce an interaction between OH and C=O groups in the ground state. These interactions probably are responsible for the initiation of the cyclisation reaction. Hence, it can be assumed that proximity effects initiate intramolecular interactions between nucleophile and electrophile in **12** and **13**, thus favouring the intramolecular cyclisation reaction. The electron density and the energy associated at the bond critical points between O···C=O in **13** are much stronger than in **12**, which indicate that conformer **13** probably plays a major role in the cyclisation than conformer **12**.

A significant result from the NBO and AIM data may be summarised as follows. The tendency of a molecule to exist as **1a** is influenced by the proximity and orientation of the OH and C=O groups. The lone pair of electrons present in the non-bonding orbital of OH oxygen should reach the nodal plane of the π* orbital of C=O. This is in a way similar to what happens in glucose, which with more than one hydroxy group undergoes intramolecular hemiacetal formation to form a pyranose ring rather than a furanose ring. The important aspect here is the orientation of the relevant orbitals which depends on the conformation acquired by the carbon framework. The

conformers **12** and **13** represent vdW complexes similar to the complex **8** formed in water formaldehyde addition.

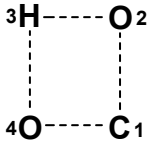

transition state

Figure 7.2: Representation of the four-membered cyclic structure formed in the transition-state during the uncatalysed transannular hemiacetal formation in **1** – **5**.

7.2.3 Reaction energies

Molecular mechanics calculations were carried out for **1a** (Figure 7.3). There are three low energy conformers for **1a**. The lowest energy conformer was *cc* and other two *bc* conformers were relatively higher in energy. According to the reported[178] conformational analysis, bicyclo[3.3.1]nonane can exist in three conformations free of angle strain, i.e., *cc* (chair-chair), *bb* (boat-boat) and *cb* (chair-boat). The conformers **16** – **18** were optimised at higher level (Figure 7.4).

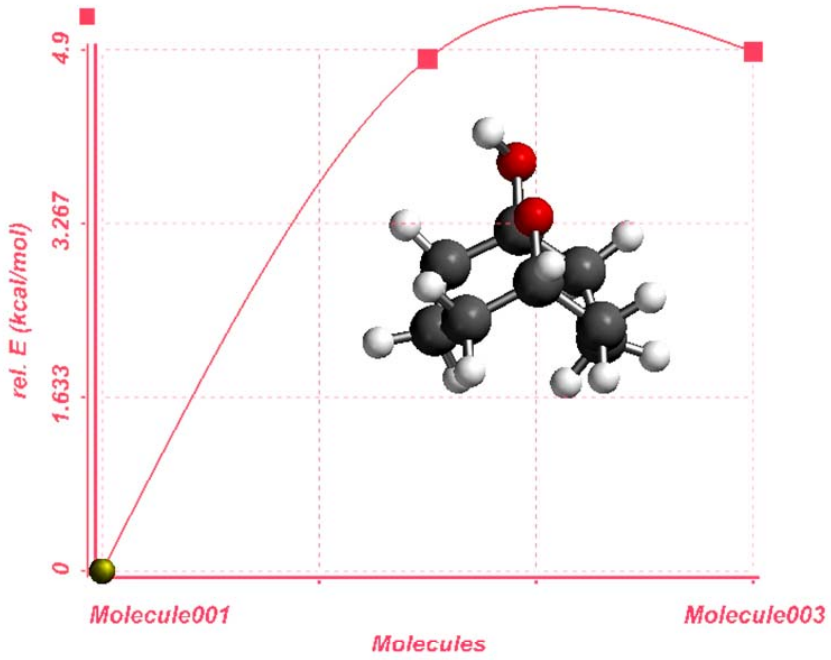

Figure 7.3: Energy profile of the conformer distribution for **1a** at MMFF level.

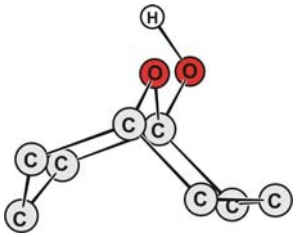

16 (2.258)

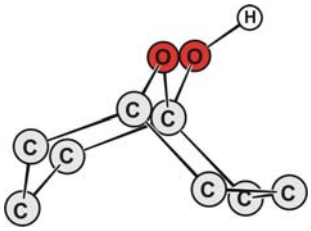

17 (1.628)

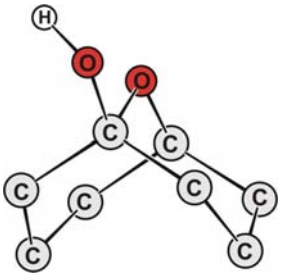

18 (0.000)

Figure 7.4: Schematic representation of the low energy conformers of hemiacetal **1a**. Relative energies (kcal mol^{-1}) are given in parentheses.

Conformer **18** was found to be the global minimum. It is in twin-chair (*cc*) conformation. Conformer **13** is more stable than the corresponding conformer **10** of hydroxy-ketone **1** suggesting that the intramolecular H-bonding does not cause significant stabilisation in **10** whereas conformer **9** is slightly more stable than conformer **12** (without H-bonding). The H-bonding structures seem to be more strained as compared to the non-bonding structures due to the close proximity of non-bonding atoms. The energetic and geometric factors in conformers **9** – **11** do not seem to play a significant role in the title reaction. The conformer **18** (*cc*) is 2.3 and 1.6 kcal mol^{-1} more stable than **16** and **17** (*bc*), respectively.

Table 7.5: Comparison of the bond angles (°) and bond lengths (Å) obtained from the X-ray crystal structure data for **1a** and optimised conformer **18**. The numbering scheme on the atoms is according to the X-ray crystal structure given in Figure 4.1.

	X-ray	**18**
C(1)–C(2)–C(3)	114.94	113.48
C(2)–C(3)–C(4)	110.93	111.44
C(3)–C(4)–C(5)	113.53	113.33
C(4)–C(5)–C(6)	116.83	116.87
C(5)–C(6)–C(7)	112.80	113.17
C(6)–C(7)–C(8)	110.53	111.15
C(7)–C(8)–C(1)	113.56	114.15
C(8)–C(1)–C(2)	116.33	116.31
C(1)–O(1)	1.452	1.438
C(5)–O(1)	1.455	1.443

The single crystal X-ray structure analysis of **1a** has shown that the conformation is *cc* (Figure 4.1). Comparison of the geometric parameters calculated for conformer **18** and experimentally obtained for **1a** has been done (Table 7.5). The parameters are in good agreement. The distance between the hydrogens at C(3) and C(7), i.e., H(3) and H(7) is 2.02 Å. Because of this the interactions between the C(3) and C(7) methylene groups are strong enough to bring about the flattening of the two rings and to increase the bond angles at atoms 2, 3, 4, 6, 7 and 8 to about 114° to compensate the resulting repulsion between these moieties. Crystallographic studies[179-181] have shown that in the solid state the *preferred* conformation of the simple bicyclic[3.3.1]nonanes is a chair-chair arrangement. Comparison of IR spectra of 9-oxabicyclo[3.3.1]nonan-1-ol in solid and solution reported[182, 183] have shown that the *cc* conformation is also an important conformation in solution. The hemiacetal conformation **18** is more stable than **13** by 8.5 kcal mol^{-1} indicating that the **13** → **18**

conversion is an exothermic process. Similarly, conformer **17** is more stable than **12** by 4.4 kcal mol^{-1} indicating that the conversion **12** → **17** is also exothermic. Finally, the intramolecular cyclisation **13** → **18** is more exothermic compared to the **12** → **17**. The relative energies of all conformers **9** – **18** have shown that hemiacetal is more stable than 5-hydroxycyclooctanone. This is consistent with our results found from NMR studies in chapter 5.

7.2.4 Transition-state calculations

The starting geometries for the transition-state calculations for hemiacetal formation are **12** and **13**. The calculated values of the activation barrier for the cyclisation reaction **12** (*bc*) → **17** (*bc*) and **13** (*cc*) → **18** (*cc*) *via* transition-states **19** (*bc*) and **20** (*bb*) are 41.2 and 38.2 kcal mol^{-1}, respectively (Figure 7.4). The activation barrier in the case of cyclisation reaction **13** → **18** is similar to the value we have obtained for the hydration of formaldehyde (37.2 kcal mol^{-1}, chapter 6). The addition of a neutral nucleophile to a carbonyl compound in the gas-phase is endothermic because the zwitterionic adduct is not stabilised by solvation as in a polar solvent or by protonation as in acidic solution.[184]

All the transition-state geometries **19** – **20** are characterised by only one imaginary frequency for each transition-state (Figure 7.4). The values of all three imaginary frequencies indicate a curved energy surface in the direction of the reaction coordinate. Here the addition is a concerted process in which nucleophilic attack by the oxygen atom takes place with simultaneous transfer of the proton. Thus, a four membered adduct is formed which has C_1 symmetry. The transition-state **19** for the cyclisation **12** (*bc*) → **17** (*bc*) has 0.5 kcal mol^{-1} higher energy barrier than transition-state **21**. Thus, the reaction **13** → **18** requires a smaller energy barrier.

The geometric parameters for the transition-states **19** and **20** are given in Table 7.6. The four-membered transition-state structure is represented in Figure 7.2. The transition-state structures **19** and **20** are similar and in the geometric parameters only slight variations have been found.

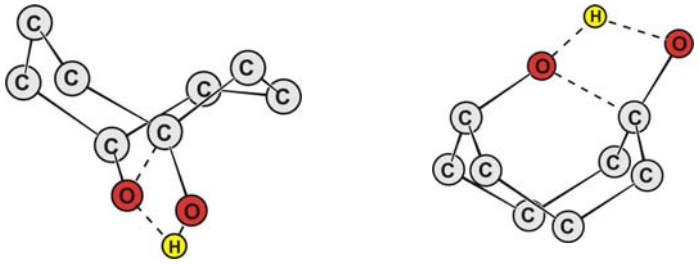

19 (-1631) **20** (-1601)
(0.478) (0.000)

Figure 7.4: Transition-states **19** and **20**, imaginary frequencies (cm^{-1}) and relative energies (kcal mol^{-1}) for the uncatalysed transannular hemiacetal formation in model compound **1**.

Table 7.6: Geometrical parameters [distances (Å) and angles (°)] of the four-membered ring in the transition-states **19** and **20**.

	19	**20**
O(4)···C(1)	1.666	1.644
C(1)···O(2)	1.319	1.320
O(2)···H(3)	1.424	1.449
H(3)···O(4)	1.144	1.139
O(4)–C(1)–O(2)	91.4	92.3
C(1)–O(2)–H(3)	78.3	77.5
O(2)–H(3)–O(4)	113.1	111.7
H(3)–O(4)–C(1)	73.6	74.7
O(2)–C(1)–O(4)–H(3)	14.5	15.4

7.2.5 Thermodynamic analysis

The equilibrium between **1** and **1a** is shifted completely towards the direction of **1a**. The energy difference between the species **13** and **18** is -8.5 kcal mol^{-1} (Table 7.2). The reaction enthalpies, ΔH°, free energy changes, ΔG°, entropy changes, ΔS°, and the corresponding equilibrium constants for the cyclisation processes **12** → **17** and **13** → **18** are shown in Table 7.7. The ΔG° values for **12** → **17** and **13** → **18** are -3.1 and -7.3 kcal mol^{-1}, respectively. In both possible conversions ΔH° is favourable (negative) but ΔS° is unfavourable (negative). The entropy is less unfavourable in **13** → **18** as compared to **12** → **17** and **13** → **18**. There is a decrease in randomness, i. e., entropy, as **1a** is formed. But the overall tendency for the cyclisation **12** → **17** and **13** → **18** is the result of the two tendencies, i.e., the tendency to acquire minimum enthalpy and state of maximum disorder. The resultant chemical potential drives the cyclisation in the forward direction. The equilibrium constant is five orders of magnitude in powers of ten towards the product for **13** → **18** and two orders of magnitude in powers of ten towards the product for **12** → **17**. The absolute free energy of **13** is lower than that of **12** by nearly 4.3 kcal mol^{-1}.

Table 7.7: Thermodynamic parameters for the processes **12** → **17** and **13** → **18**. [Reaction enthalpy (kcal mol^{-1}), free energy change (kcal mol^{-1}) and entropy (cal mol^{-1} K^{-1})].

	ΔG°	**ΔH°**	**ΔS°**	K_{eq}
12 → **17**	-3.074	-9.243	-20.7	1.79×10^{2}
13 → **18**	-7.341	-5.251	-7.0	2.42×10^{5}

In NMR studies no signal was observed corresponding to **1**. The reaction goes to complete formation of **1a** at room temperature in both polar and non-polar solvents. These results are consistent with the theoretical results since in **13** → **18** the tendency is towards the formation of hemiacetal. This is further supported by the X-ray structure (Figure 4.1). **1a** exist in a *cc* conformation in the solid state.

7.2.6 Solvent mediated calculations for the tautomeric equilibrium (1 ⇌ 1a)

Solvents often play an important role in determining equilibrium constants and stable conformers. The activation energy **13** → **18** has been calculated in water and chloroform at room temperature. The activation energies in the gas phase, chloroform and water is shown in Figure 7.5.

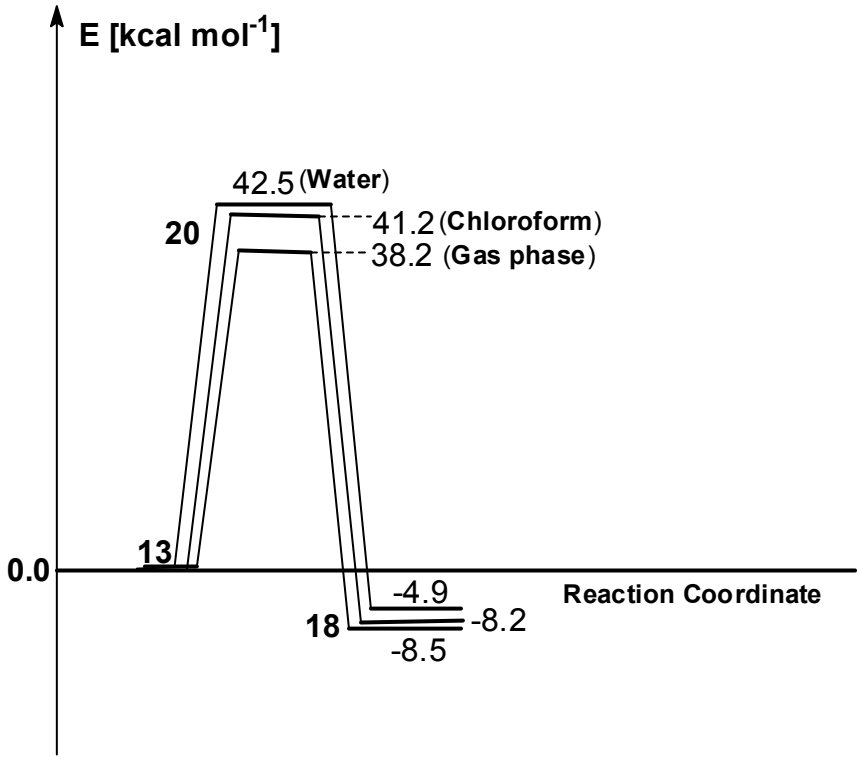

Figure 7.5: Energy profile diagram showing transannular hemiacetal formation (**13** → **18**) *via* transition-state **21** in gas phase, chloroform and water.

The activation barrier is least in the gas phase. In water the activation barrier is maximal (42.5 kcal mol^{-1}). This supports that the polar solvent disfavours the formation of the hemiacetal whereas non-polar solvent favours the conversion **13** → **18**. In the gas phase **18** is 8.5 kcal mol^{-1} more stable than **13**. In water hemiacetal **18** is only 4.9 kcal mol^{-1} more stable than **13**. The activation barrier for hemiacetal formation is very large in all cases. The hemiacetal formation is known to be acid-catalysed. Jones reagent[128] was used for the oxidation of *cis*-1,2-cyclooctanediol in the synthesis of **1**. The reaction conditions were acidic. So the formation of the hemiacetal at this stage cannot be ruled out since the isolated product is always **1a**

not **1**. After the formation of **1a** it is difficult to go back to **1** since the activation barrier is high. The calculated activation energy for an acid-catalysed reaction **13** → **18** is 27.4 kcal mol^{-1}. This energy barrier is 10.8 kcal mol^{-1} less than the activation barrier in an uncatalysed hemiacetal formation reaction. The activation barrier for the acid-catalysed hemiacetal formation is less so this reaction is possible at room temperature. These results are in accordance with the experimental condition used for the reaction.

7.3 Results for model compound 2

The investigation carried out for **1** and **1a** has shown that both structural and energetics factors favor **1a** as compared to **1**. Similar studies are reported in this section for the equilibrium between **2** and **2a**. Conformers with hydrogen bonding have not been taken into account here since in **1** we have observed that hydrogen bonding does not play any role in hemiacetal formation and because of this they are excluded from our model calculations. The MMFF calculations have generated 94 conformers for **2** (Figure 7.6). The number of conformers located in **1** was only 53.

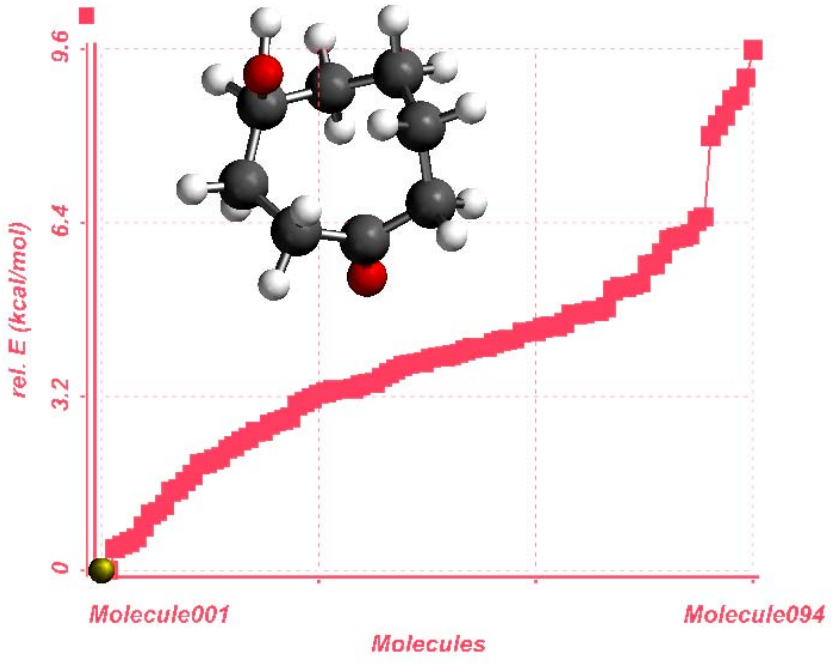

Figure 7.6: Energy profile of the conformer distribution for *endo*-conformer of **2** at MMFF level.

7.3.1 Structural features

Out of 94 conformers only conformers **21** – **25** were selected for optimisation at the B3LYP/6-31+G* level of theory (Table 7.8). The selection was done on the basis of proximity of the atoms involved in transannular hemiacetal formation. The distance between the O atom of the OH group and the carbonyl C is about 2.9 Å in **21** – **25** and is less than the corresponding sum of the vdW radii of C and O. The less the

transannular distance between the functional groups, the more is orbital overlap expected between the electrophilic C and the nucleophilic O atom.

In structures **23** and **24** the angle of attack of the nucleophile, θ_O, is 101.4° and 99.2°, respectively, in accord with angle given by Dunitz and Bürgi.[168, 169] But the deviation Δ_O of the carbonyl C atom from its plane in conformer **25** is smallest (0.002 Å). The C···C distance d_1 is less than the sum of vdW radii in conformers **21** – **25**. This implies that in **21** – **25** the proximity of the reacting functional groups is closer when the OH group is at C-4 rather than at C-5. The geometrical parameters in all the optimised conformers **21** – **25** reveal that the change of the position of the functional group has increased the proximity of the reacting atoms in 4-hydroxycyclooctanone (**2**). Thus, in this compound the cyclisation seems to be more facile than in the isomeric 5-hydroxycyclooctanone (**1**).

7.3.2 Bonding and interactions

To get a deeper insight into the effect of the change of the position of the hydroxy group in eight-membered hydroxy-ketones in the transannular hemiacetal formation we have further carried out natural bond orbital (NBO) and atoms in molecules (AIM) analyses for conformers **21** – **25** (Tables 7.9 and 7.10). It is interesting to note that all the conformers **21** – **25** show a significant amount of interaction between the donor and acceptor orbitals. This can be explained in terms of closer proximity of the reacting atoms in all optimised conformers of **2** as compared with **1**. The stabilisation energy $E^{(2)}$ associated with donation of electrons from the filled non-bonding nucleophilic oxygen n_O to the empty electrophilic carbonyl carbon $\pi^*_{C=O}$ orbital is strongest, i.e., 2.12 kcal mol^{-1} in **24** and weakest in **22**. The electron occupancy of the $\pi^*_{C=O}$ orbital in **21** is maximal (0.089 e) and minimal (0.080 e) in **22**. This implies that there is more electron transfer from $n_O \rightarrow \pi^*_{C=O}$ in **21** than in **22**.

Table 7.8: Important geometrical parameters investigated in **21** – **25** and relative energies including the zero point energy calculated with respect to conformer **29** (gas phase). [Distances (Å); angles (°), rel. energies (kcal mol^{-1})].

Molecular structure	Geometrical parameters			
	d_o	d_1	θ_o	Δ_o
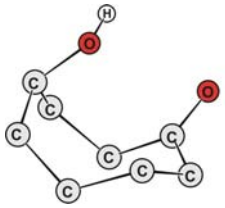 **21** (3.595)	2.821	3.049	91.7	0.027
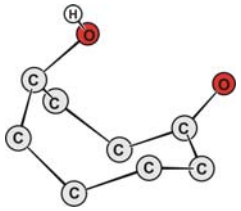 **22** (5.957)	2.883	3.120	96.3	0.041
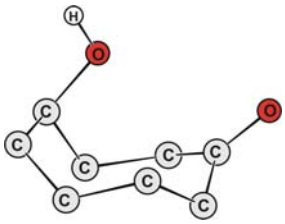 **23** (6.730)	2.824	3.181	101.4	0.035
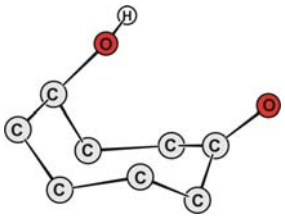 **24** (6.121)	2.773	3.126	99.2	0.038
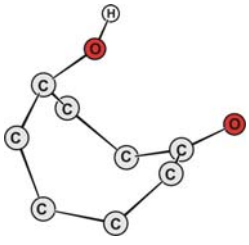 **25** (7.713)	2.915	3.101	109.0	0.002

Table 7.9: Natural bond order (NBO) analysis of conformers **21** – **25**. $E^{(2)}$ (kcal mol^{-1}) is the second order perturbation energy between Φ_i and Φ_j; E_j-E_i (a.u.) is the energy difference between NBOs Φ_i and Φ_j; F_{ij} (a.u.) is the Fock matrix element; only energies greater than the default threshold 0.5 kcal mol^{-1} are included in the table.

	Interaction	**Second-order**		**Interaction**	**Occupancy** (**ρ**)	
		$E^{(2)}$	E_j-E_i	F_{ij}	$n_o \rightarrow \pi^*_{c=o}$	
21	$n_o \rightarrow \pi^*_{c=o}$	1.78	0.33	0.022	1.948	0.089
22	$n_o \rightarrow \pi^*_{c=o}$	0.74	0.35	0.014	1.956	0.080
23	$n_o \rightarrow \pi^*_{c=o}$	0.82	0.35	0.015	1.957	0.082
24	$n_o \rightarrow \pi^*_{c=o}$	2.12	0.34	0.024	1.948	0.088
25	$n_o \rightarrow \pi^*_{c=o}$	1.34	0.34	0.019	1.955	0.085

Unlike NBO, AIM analysis has shown no electronic interactions between donor and acceptor units in **23** – **25** (Table 7.10). No bond critical point corresponding to an interaction between O···C=O has been observed in conformers **23** – **25** indicating that these conformers did not induce an interaction between –OH and >C=O groups. Hence, these conformers have no role to play in initiation of cyclisation reaction.

The electron density and the energy associated at the bond critical point O···C=O in **21** are much stronger than in **22** which indicates that the conformer **21** probably plays a major role in the cyclisation. After taking all the important factors such as energetic, geometric mainly proximity of the reacting groups conformer **21** can be considered to be comparable to the adduct leading to hemiacetal formation.

Table 7.10: Properties (a.u.) calculated at bond critical point in electron density for conformers **21** – **25**. [$\nabla^2\rho$: Laplacian of the electron density; ε: ellipticity; H(r): sum of kinetic and potential energy densities].

	Bond	$\nabla^2\rho$	**ε**	**H(r)**
21	O···C=O	0.042	0.213	-0.009
22	O···C=O	0.037	0.380	-0.006
23	O···C=O	-----	-----	-----
24	O···C=O	-----	-----	-----
25	O···C=O	-----	-----	-----

7.3.3 Reaction energies

The molecular mechanics calculations have generated 4 conformers for **2a** (Figure 7.7). These are optimised at B3LYP/6-31+G* level of theory (Figure 7.8).

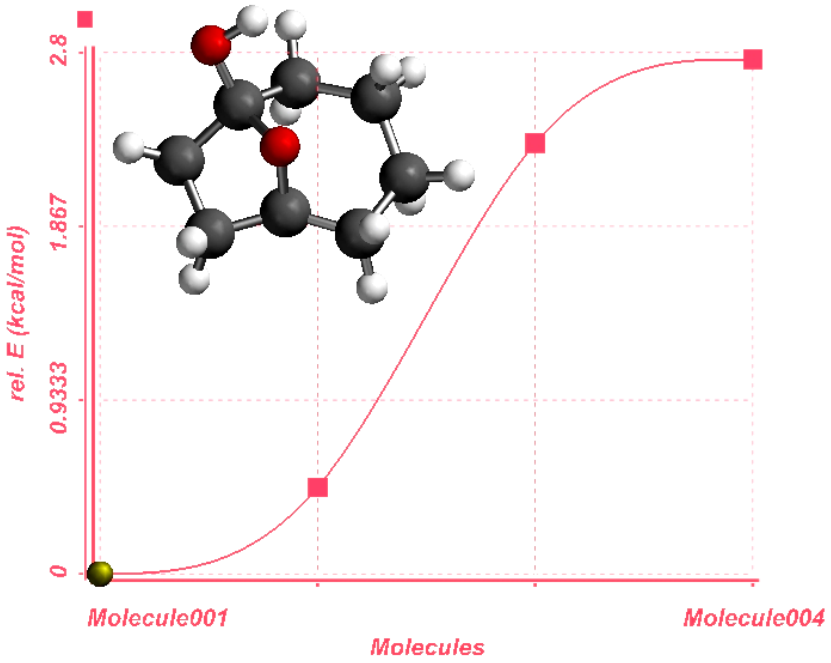

Figure 7.7: Energy profile of the conformer distribution for hemiacetal **2a** at MMFF level.

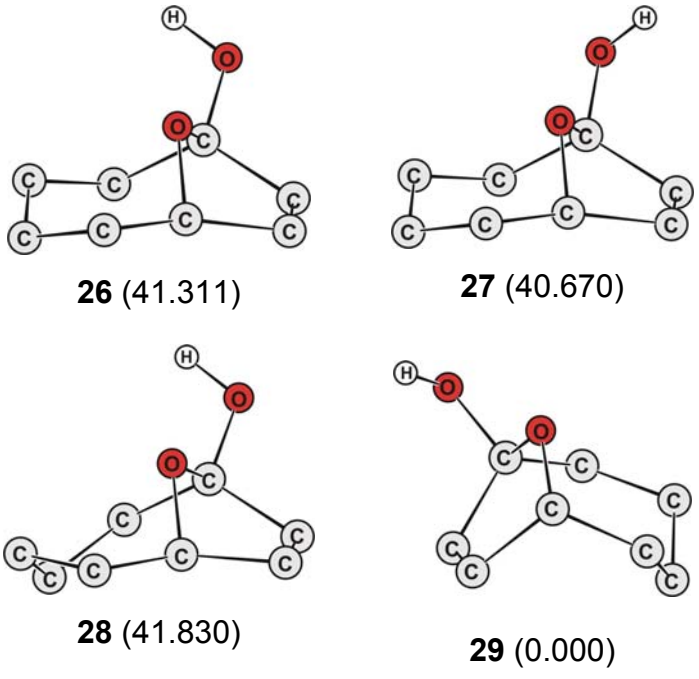

Figure 7.8: Schematic representation of the low energy conformers of hemiacetal **2a**. Relative energies (kcal mol^{-1}) are given in parentheses.

The most stable conformer is **29**. All other conformers corresponding to the hemiacetal were found to be more than 40 kcal mol^{-1} higher in energy. So at room temperature only one conformer is stable and interconversion into other conformers is highly unfavourable. But in the case of optimised conformers **16** – **18** (Figure 7.4) corresponding to the hemiacetal of 5-hydroxycyclooctanone, relative energies are low and this implies that interconversion is highly favorable even at room temperature. As compared to the relative energies of hemiacetal conformers **16** – **18** the relative energies of the hemiacetal conformers **26** – **29** are very high. The energy difference between the 4-hydroxycyclooctanone **21** and the hemiacetal **29** is only 3.6 kcal mol^{-1}. This implies that the tautomers **21** and **29** exist in equilibrium. The NMR experiment in CCl_4 shows the presence of 13% of 4-hydroxycyclooctanone (Table 5.2).

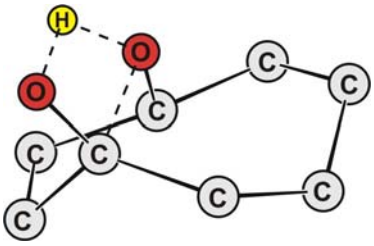

30 (-1690)
(54.360)

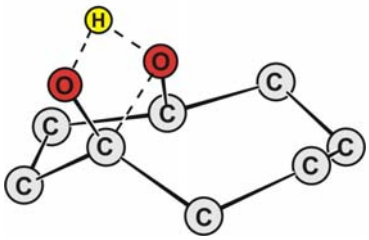

31 (-1678)
(55.387)

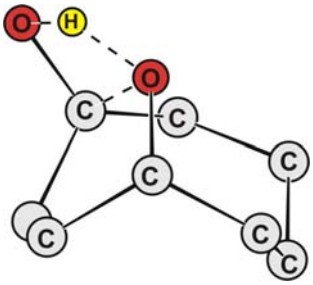

32 (-1768)
(0.000)

Figure 7.9: Calculated transition-states **30** – **32** and imaginary frequencies (cm^{-1}) for the uncatalysed hemiacetal formation in model compound **2**.

7.3.4 Transition-state calculation

Although it is likely that a number of transitions state geometries exist on the potential energy surface in an uncatalysed hemiacetal formation, we have located only three geometries **30** – **32** (Figure 7.9). The transition-states are characterised by a single imaginary frequency corresponding to the vibrational mode of nuclear motion involving the H-O and C=O bonds of the reacting atoms. The geometrical parameters of the four-membered ring in **30** and **31** are similar to each other but differ from those of **32** (Table 7.11). The distance O(4)···C(1) in **32** is larger than in **30** and **31**. The angle O(4)–C(1)–O(2) in **32** is smaller than in **30** and **31**. The distance H(3)···O(4) is largest in **32**. The structural parameters of **32** indicate that it is closer to the hemiacetal than **30** and **31**.

The activation barrier for the cyclisation **21** → **29** *via* **32** is 35.2 kcal mol^{-1}. On the other hand, in case of **21** → **29** *via* **30** or **31** the energy barriers are very high, 92.9 and 90.7 kcal mol^{-1}, respectively. This implies that the cyclisation **21** → **29** is more likely to take place *via* **32**. The high energy barriers in case of **21** → **29** *via* **30** or **31** can be explained in terms of the tight transition-state geometries. Thus, the *preferred* transition-state is **32**.

Table 7.11: Geometrical parameters [distances (Å) and angles (°)] of the four-membered ring in the transition-states **30** – **32** (see Figure 7.2).

	30	**31**	**32**
O(4)···C(1)	1.571	1.554	1.729
C(1)···O(2)	1.327	1.326	1.322
O(2)···H(3)	1.456	1.478	1.329
H(3)···O(4)	1.155	1.151	1.192
O(4)–C(1)–O(2)	96.4	96.7	91.1
C(1)–O(2)–H(3)	73.5	72.8	78.6
O(2)–H(3)–O(4)	111.6	109.7	121.1
H(3)–O(4)–C(1)	73.5	74.5	67.3
O(2)–C(1)–O(4)–H(3)	18.0	20.1	-10.1

7.3.5 Thermodynamic analysis

There is no equilibrium between **1** and **1a** at room temperature. Contrary to this the equilibrium exists between **2** and **2a** even at room temperature in both polar and non-polar solvents. The energy difference between **21** and **29** is 3.6 kcal mol^{-1} (Table 7.8). This is not large enough to drive the reaction completely in one direction and as a result 4-hydroxycyclooctanone exists in equilibrium with its hemiacetal. For the cyclisation **21** → **29** the reaction enthalpy, ΔH^o, free energy change, ΔG^o, entropy change, ΔS^o, and the corresponding equilibrium constant are shown in Table 7.12. The ΔG^o value is -2.8 kcal mol^{-1}. The experimental value of ΔG^o in CCl_4 for the cyclisation of 4-hydroxycyclooctanone to the corresponding hemiacetal is -1.12 kcal mol^{-1}. Thus, the experimental and theoretical values of ΔG^o are in agreement. The entropy is less unfavourable in **21** → **29** as compared to the process **13** → **18** (Table 7.7). There is a decrease in randomness, i. e., entropy when **2a** is formed. But the overall tendency for the cyclisation **21** → **29** is the result of the two effects, i.e., the tendency to acquire minimal enthalpy and the state of maximal disorder. The resultant chemical potential drives the cyclisation in the forward direction more than to reverse. The equilibrium constant is two orders of magnitude in powers of ten towards the product **29** which implies a small amount of **21** in the equilibrium. From NMR studies, the equilibrium constant in CCl_4 at room temperature is 6.67. The reaction goes in the direction of **2a** at room temperature both in non-polar and polar solvents.

Table 7.12: Thermodynamic parameters for the process **21** → **29**. [Reaction enthalpy (kcal mol^{-1}), free energy change (kcal mol^{-1}) and entropy (cal mol^{-1} K^{-1})].

	ΔG^o	ΔH^o	ΔS^o	K_{eq}
21 → **29**	-2.81	-4.23	-5.0	1.14 x 10^2

7.3.6 Solvent mediated calculations for the tautomeric equilibrium (2 ⇌ 2a)

A polarisable continuum model (PCM) was used to investigate the solvent effect on hemiacetal formation in **2**. The activation energy for the process **21** → **29** was calculated in water and chloroform at room temperature. Comparison of activation energies is shown in Figure 7.10. The activation barrier is least in the gas phase and

highest in water with an increase by 4.0 kcal mol^{-1}. This increase can be due to a change of conformation. In water the conformation may not have enough proximity between the reacting atoms for the cyclisation. This supports that a solvent polarity disfavours the formation of the hemiacetal whereas a non-polar solvent favours it.

In the gas phase **29** is 3.6 kcal mol^{-1} more stable than conformer **21**. In water hemiacetal **29** is only 3.4 kcal mol^{-1} more stable than **21**. The activation barrier for hemiacetal formation is very large in all cases. These results show that equilibrium exists between **2** and **2a** even in polar solvents at room temperature which is in good agreement with experimental results. The equilibrium drives in one direction with the combined effects, i.e., solvent polarity and temperature. Hemiacetal **2a** is more stable than hydroxy-ketone **2**. The energy difference between **2** and **2a** (3.6 kcal mol^{-1}) is less as compared to the energy difference between **1** and **1a** (8.5 kcal mol^{-1}) in the gas phase. But interestingly, in water and chloroform the differences in energy between **2** and **2a** do not change significantly.

This shows that the equilibrium exists in both polar and non-polar solvents. These results are consistent with the results obtained from the NMR experiments. Although the PCM usually well describes bulk solvent effects it seems that this model is not very appropriate for our compounds.

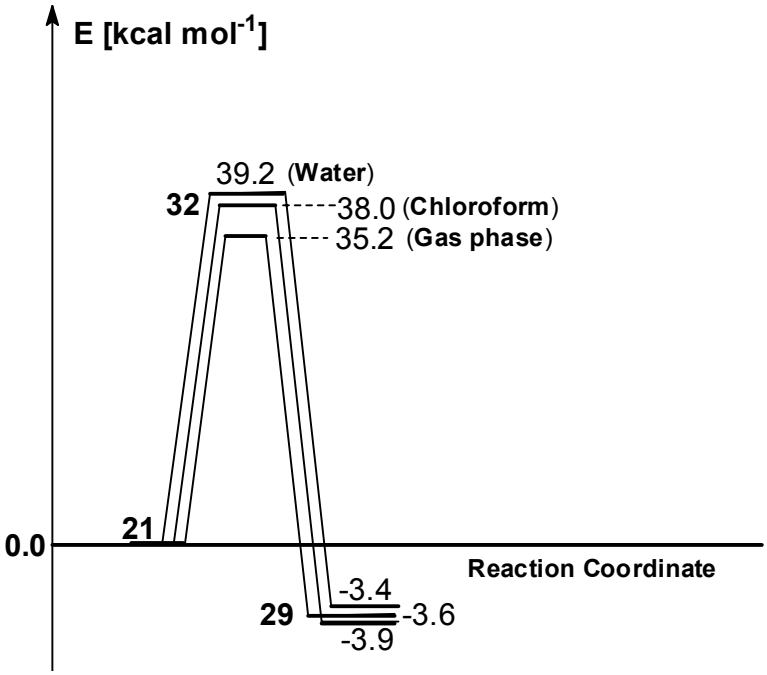

Figure 7.10: Energy profile diagram showing transannular hemiacetal formation (**21** → **29**) *via* transition-state **32** in gas phase, chloroform and water.

7.4 Results for model compound 3

The presence of double bond in **3** is expected to reduce the number of conformers as compared to the number of conformers for **2** due to the reduction in flexibility of the eight-membered ring. Conformational analysis starting with the *endo*-conformer of **3** has generated 37 conformers (Figure 7.11).

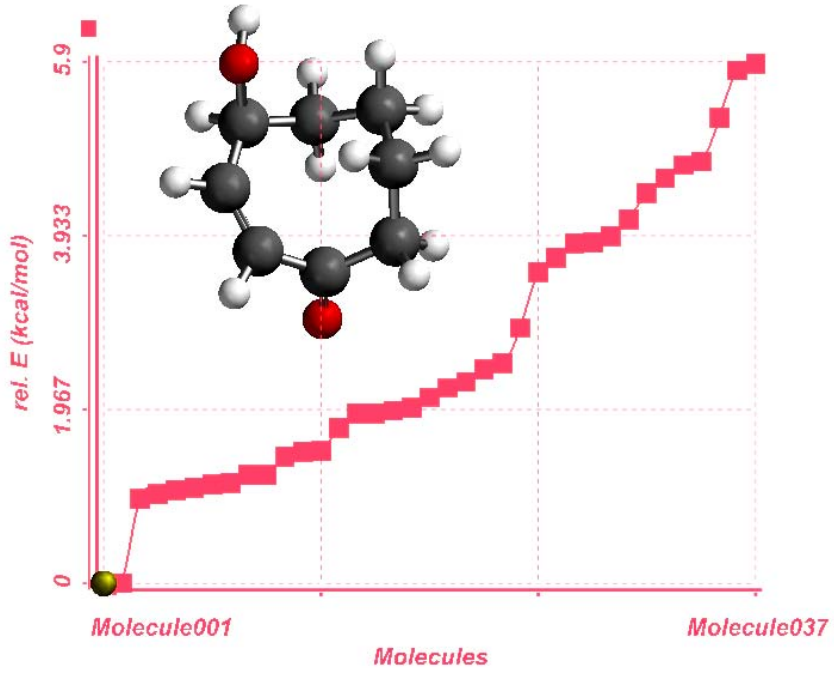

Figure 7.11: Energy profile of the conformer distribution for *endo*-conformer of **3** at MMFF level.

7.4.1 Structural features

We have performed optimisation at the B3LYP/6-31+G* level of theory on selected conformers **33** – **36** (Table 7.13). The proximity of the reacting atoms d_O is less than the sum of vdW radii of carbon and oxygen atoms in **33** and **35**. The angle of attack of the nucleophile θ_O is 101.2° and 108.0° in **33** and **35**, respectively. This is in agreement with the reported[168] nucleophilic attack angle. The C···C distance d_1 is less than the vdW distance in **33** and **35**. In case of **36** all relevant parameters indicate absence of transannular interactions between the reacting groups. The deviation of the carbonyl carbon from its plane, i.e., Δ_O is 0.058 and 0.077 Å in **33** and **35**, respectively. These deviation values are largest among all conformers of **1**, **2** and **3**. The large values of Δ_O indicate the possibility of transannular interactions in **33** and

35. The NBO and AIM analyses were done for a better insight into the interactions present in optimised conformers.

Table 7.13: Important geometrical parameters investigated in **33** – **36** and relative energies including the zero point energy calculated with respect to conformer **38** (gas phase). [Distances (Å); angles (°), rel. energies (kcal mol^{-1})].

Molecular structure	**Geometrical parameters**			
	d_o	d_1	θ_o	Δ_o
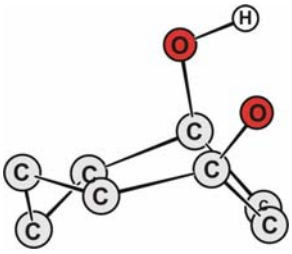 **33** (4.607)	2.771	3.081	101.2	0.058
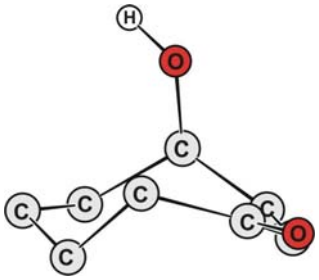 **34** (5.945)	3.321	3.349	145.2	0.019
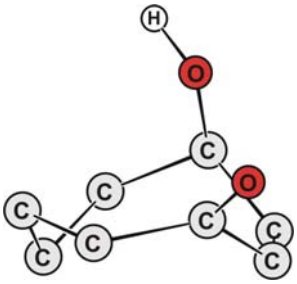 **35** (7.567)	2.800	3.137	108.0	0.077
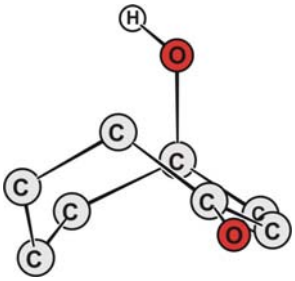 **36** (5.382)	3.478	3.340	166.0	0.001

7.4.2 Bonding and interactions

The natural bond orbital (NBO) and atoms in molecules (AIM) analyses were carried out for conformers **33** – **35** (Tables 7.14 and 7.15). The stabilisation energy $E^{(2)}$ associated with the donation of electrons from the filled non-bonding nucleophilic oxygen n_O to empty electrophilic carbonyl carbon $\pi^*_{c=o}$ orbital is strongest, i.e., 2.67 kcal mol^{-1} in **33**. The interaction between HOMO of the nucleophile and LUMO of the electrophile is found to be absent in conformer **36**. This also supports the idea that a transannular reaction is related to suitable geometric proximity of the reacting atoms. In **36** none of the geometric parameters are suitable for an interaction. The stabilisation energies in **34** and **35** are 1.11 and 1.12 kcal mol^{-1}, respectively.

Table 7.14: Natural bond order (NBO) analysis of conformers **33** – **36**. $E^{(2)}$ (kcal mol^{-1}) is the second order perturbation energy between Φ_i and Φ_j; E_j-E_i (a.u.) is the energy difference between NBOs Φ_i and Φ_j; F_{ij} (a.u.) is the Fock matrix element; only energies greater than the default threshold 0.5 kcal mol^{-1} are included in the table.

	Interaction	**Second-order Interaction**			**Occupancy (ρ)**	
		$E^{(2)}$	E_j-E_i	F_{ij}	$n_o \rightarrow \pi^*_{c=o}$	
33	$n_o \rightarrow \pi^*_{c=o}$	2.67	0.33	0.027	1.946	0.089
34	$n_o \rightarrow \pi^*_{c=o}$	1.11	0.36	0.018	1.955	0.089
35	$n_o \rightarrow \pi^*_{c=o}$	1.12	0.36	0.018	1.955	0.089
36	$n_o \rightarrow \pi^*_{c=o}$	-----	------	------	1.958	0.011

Table 7.15: Properties (a.u.) calculated at bond critical point in electron density for conformers **33** – **36**. [$\nabla^2\rho$: Laplacian of the electron density; ε: ellipticity; H(r): sum of kinetic and potential energy densities].

	Bond	$\nabla^2\rho$	**ε**	**H(r)**
33	O···C=O	0.047	0.514	-0.013
34	O···C=O	----	----	----
35	O···C=O	0.046	1.993	-0.083
36	O···C=O	----	----	----

AIM analysis shows that there are no electronic interactions between donor and acceptor groups in **34** and **36**. No bond critical points corresponding to O(4)···C(1) interaction have been observed in conformers **34** and **36** indicating that they do not participate in hemiacetal formation. The electron density and the energy associated at the bond critical points at O···C=O in **33** are much stronger than in **35**, which indicates that conformer **33** probably plays a major role in the cyclisation than conformer **35**. This is also supported by the strong stabilisation energy value $E^{(2)}$ associated with the donation of electrons from the filled non-bonding nucleophilic oxygen n_O to the empty electrophilic carbonyl carbon $\pi^*_{C=O}$ orbital in **33** (Table 7.14).

7.4.3 Reaction energies

The molecular mechanics (MMFF) calculations have generated four conformers for **3a** (Figure 7.12) which were optimised at the B3LYP/6-31+G* level of theory. The hemiacetal conformers **37** – **40** are more stable than open forms **33** – **36**. Conformer **38** was found to be the global minimum. Conformers **37** and **40** are merely 0.3 kcal mol^{-1} higher in energy than **38**. On the other hand, conformer **39** is 1.9 kcal mol^{-1} higher in energy than **38**. The geometrical parameters of structure **3a** obtained from X-ray analysis are given in Table 7.16. A comparison is made between some of the geometrical parameters of **3a** and **38**. The calculated and experimental bond angles and lengths of **3a** and **38** are in good agreement. It seems that the incorporation of a double bond between C-2 and C-3 has given more stability to the bicyclic tautomer.

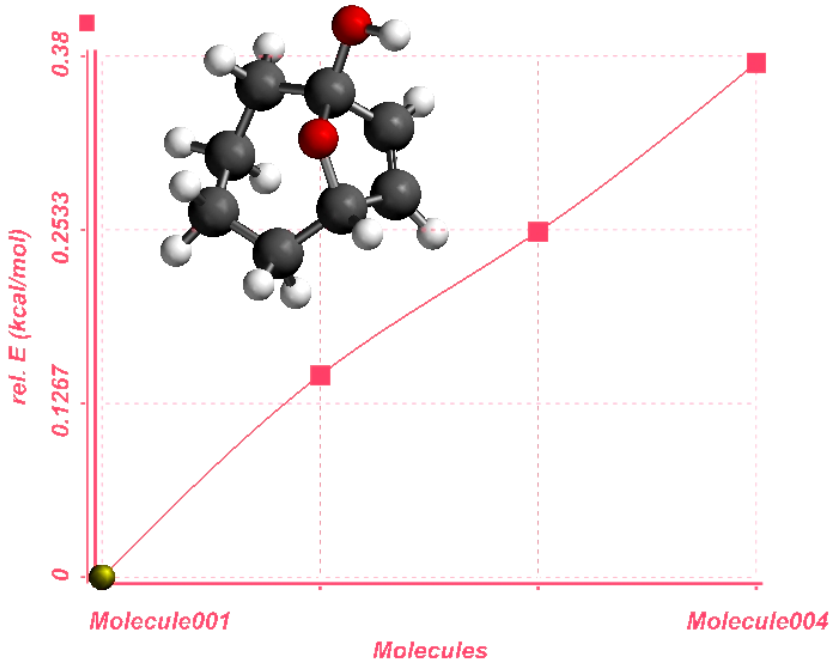

Figure 7.12: Energy profile of the conformer distribution for **3a** at MMFF level.

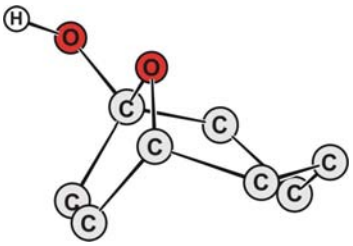

37 (0.326)

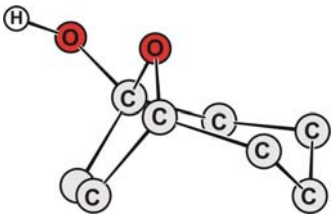

38 (0.000)

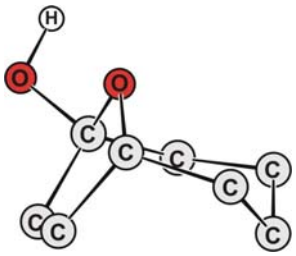

39 (1.914)

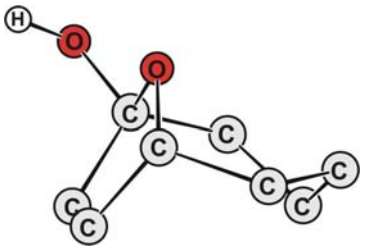

40 (0.325)

Figure 7.13: Schematic representation of the low energy conformers of hemiacetal **3a**. Relative energies (kcal mol^{-1}) are given in parentheses.

Table 7.16: Comparison of the relevant parameters [bond lengths (Å) and angles (°)] obtained from the crystal structure data for **3a** and optimised conformer **38**. The numbering scheme on the atoms is according to the X-ray crystal structure given in Figure 4.3.

	C(1)–O(2)	O(2)–C(4)	C(1)–O(2)–C(4)
3a (X-ray)	1.436	1.443	107.8
38	1.442	1.438	108.5

7.4.4 Transition-state calculations

The activation barrier for the formation of hemiacetal **38** from the starting geometry **33** *via* transition state **41** is 36.5 kcal mol^{-1} (Figure 7.14). The transfer of the hydroxy

hydrogen to the carbonyl oxygen atom occurs simultaneously with nucleophilic attack on the carbonyl carbon *via* a four-membered cyclic structure.

The geometrical parameters for **41** are very similar to the transition-state geometry **32** (Tables 7.11 and 7.17). The O(4)···C(1) distance in **41** is 1.700 Å which is near to the corresponding distance (1.729 Å) found in **32**. The H(3)···O(4) distance of the transferred hydrogen atom is 1.350 and 1.329 Å in **41** and **32**, respectively.

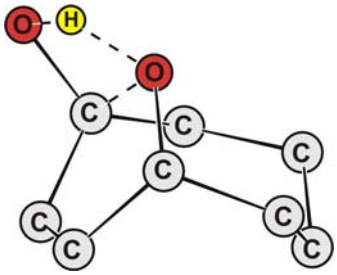

41 (-1777)

Figure 7.14: Transition-state **41** for the uncatalysed transannular hemiacetal formation *via* a four-membered ring. Imaginary frequency (cm^{-1}) is given in parenthesis.

Table 7.17: Geometrical parameters [distances (Å) and angles (°)] for the four-membered cyclic structure in the transition-state **41** (see Figure 7.2).

41			
O(4)···C(1)	1.700	O(4)–C(1)–O(2)	92.2
C(1)···O(2)	1.322	C(1)–O(2)–H(3)	77.4
O(2)···H(3)	1.350	O(2)–H(3)–O(4)	119.2
H(3)···O(4)	1.192	H(3)–O(4)–C(1)	68.0
		O(2)–C(1)–O(4)–H(3)	-12.9

7.4.5 Thermodynamic analysis

At room temperature the equilibrium between **3** and **3a** is more in the direction of **3a**. The energy difference between the species **33** and **38** is 4.6 kcal mol^{-1} (Table 7.13). This is not large enough to drive the reaction in one direction and as a result 4-hydroxycyclooct-2-enone exists in the equilibrium. For the cyclisation process **33** →

38 the reaction enthalpy, ΔH^o, free energy change, ΔG^o, the entropy change, ΔS^o, and the equilibrium constant are shown in Table 7.18. In **33** → **38** ΔG^o is -3.3 kcal mol^{-1}. ΔH^o is slightly favourable (negative) whereas ΔS^o is unfavourable (negative) in the former process. The equilibrium constant is two orders of magnitude in powers of ten towards the product for **33** → **38**.

Table 7.18: Thermodynamic parameters for the processes **33** → **38**. [Reaction enthalpy (kcal mol^{-1}), free energy change (kcal mol^{-1}) and entropy (cal mol^{-1} K^{-1})].

	ΔG^o	ΔH^o	ΔS^o	K_{eq}
33 → **38**	-3.27	-4.96	-5.67	2.5 x 10^2

7.4.6 Solvent mediated calculations for the tautomeric equilibrium (3 ⇌ 3a)

The activation energy for the reaction **33** → **38** has been calculated in water and chloroform at room temperature. The comparison of activation energies in gas phase, chloroform and water is shown in Figure 7.15. The activation barrier for hemiacetal formation is least (36.5 kcal mol^{-1}) in the gas phase and highest (40.1 kcal mol^{-1}) in water.

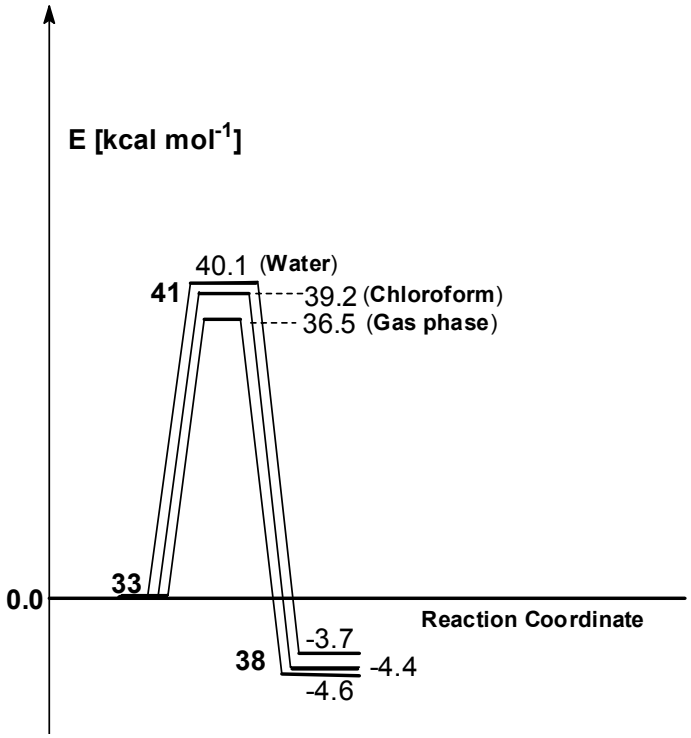

Figure 7.15: Energy profile diagram showing transannular hemiacetal formation (**33** → **38**) *via* transition-state **41** in gas phase, chloroform and water.

7.5 Results for model compound 4

This compound has been selected in order to evaluate the steric effect of a large atom (Br) in α position to the carbonyl group. Due to the presence of a substituent in the ring configurational isomerism arises. The two possible orientations of Br atom, i.e., *cis* or *trans* with respect to OH. For simplicity we have taken only one type of isomers in which Br and OH are *cis* to each other. The molecular mechanics calculations have generated 95 conformers for **4** (Figure 7.16).

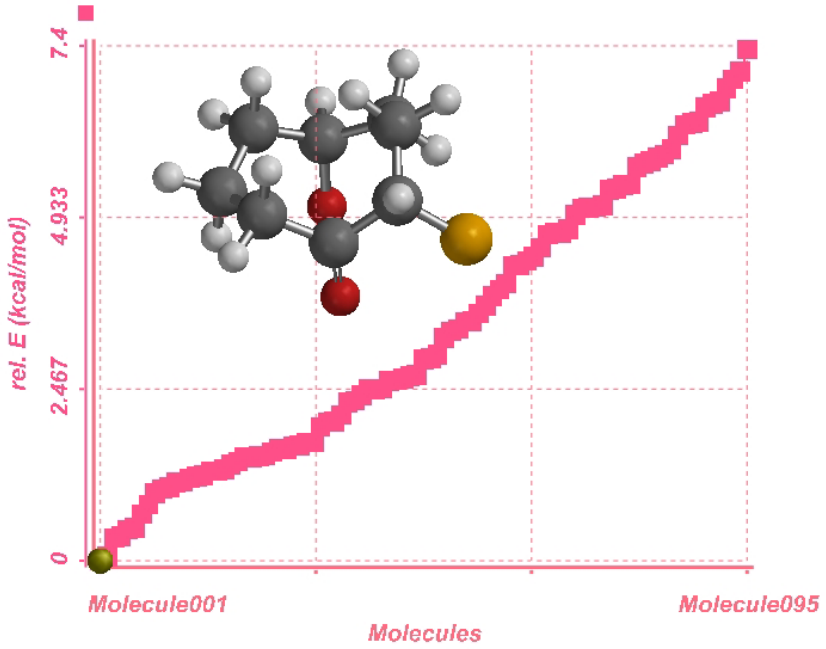

Figure 7.16: Energy profile of the conformer distribution for *endo*-conformer of **4** at MMFF level.

7.5.1 Structural features

The presence of the Br atom in **4** and **4a** has increased the calculation time so we have judiciously taken only few conformers for optimistaion at higher level of theory. The selected conformers **42** – **45** (Table 7.19) were optimised at the B3LYP/6-31+G* level of theory. For the Br atom in **4** the Stuttgart/Dresden effective core potentials (ECPs) SDD,[185] which were augmented with d polarisation functions, were employed. These ECPs include relativistic contributions of the fast moving inner shells electrons, which are important for atoms beyond the third row of the periodic table. Such basis sets have been used for halogen containing molecules.[186, 187] The

presence of the Br atom is expected to hinder the proximity of the reacting groups. But the geometrical non-bonded parameters (Table 7.19) show that in conformers **42** – **44** the reacting atoms are in close proximity with each other.

Table 7.19: Important geometrical parameters investigated in **42** – **45** and relative energies including the zero point energy calculated with respect to conformer **46** (gas phase). [Distances (Å); angles (°), rel. energies (kcal mol^{-1})].

Molecular structure	**Geometrical parameters**			
	$\mathbf{d_o}$	$\mathbf{d_1}$	$\boldsymbol{\theta_o}$	Δ_o
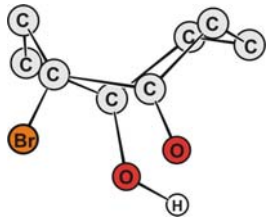 **42** (10.378)	2.880	3.270	92.0	0.044
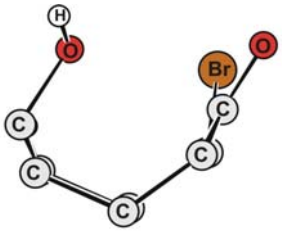 **43** (13.171)	2.591	3.186	100.1	0.083
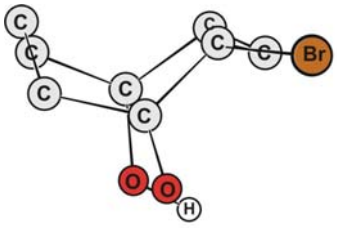 **44** (8.806)	2.864	3.269	96.7	0.019
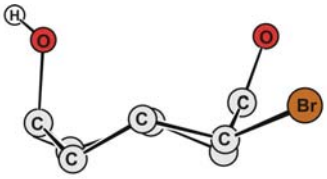 **45** (9.457)	3.543	3.478	91.9	0.021

In these conformers the C···C distance d_1 is less than the vdW distance. The approach angle θ_O of the nucleophilic O atom is also near to the Bürgi trajectory[167] defined for the nucleophilic attack. This implies that the atoms on opposite side of the ring in **43** are in close proximity with each other which is an important requirement for hemiacetal formation.

7.5.2 Bonding and interactions

The close proximity of atoms does not imply that the molecular orbitals on the atoms involved for cyclisation have strong interactions. Thus, natural bond orbital (NBO) and atoms in molecules (AIM) analyses for conformers **42** – **45** were done (Tables 7.20 and 7.21). It is interesting to note that in conformer **43** (*bb*) the stabilisation energy $E^{(2)}$ associated with donation of electrons from the filled non-bonding nucleophilic oxygen n_O to the empty electrophilic carbonyl carbon $\pi^*_{C=O}$ orbital is 4.71 kcal mol^{-1}. The electron occupancy of the $\pi^*_{C=O}$ orbital in **43** is maximal (0.094 e) and minimal (0.075 e) in **45**.

Table 7.20: Natural bond order (NBO) analysis of conformers **42** – **45**. $E^{(2)}$ (kcal mol^{-1}) is the second order perturbation energy between Φ_i and Φ_j; E_j-E_i (a.u.) is the energy difference between NBOs Φ_i and Φ_j; F_{ij} (a.u.) is the Fock matrix element; only energies greater than the default threshold 0.5 kcal mol^{-1} are included in the table.

	Interaction	**Second-order Interaction**			**Occupancy (ρ)**	
		$\mathbf{E^{(2)}}$	$\mathbf{E_j-E_i}$	$\mathbf{F_{ij}}$	$\mathbf{n_O \rightarrow \pi^*_{C=O}}$	
42	$\mathbf{n_O \rightarrow \pi^*_{C=O}}$	1.14	0.33	0.017	1.953	0.081
43	$\mathbf{n_O \rightarrow \pi^*_{C=O}}$	4.71	0.37	0.038	1.938	0.094
44	$\mathbf{n_O \rightarrow \pi^*_{C=O}}$	1.11	0.34	0.017	1.954	0.081
45	$\mathbf{n_O \rightarrow \pi^*_{C=O}}$	----	----	----	1.958	0.075

A summary of AIM calculations for conformers **42** – **45** is given in Table 7.21. The analysis shows that there are electronic interactions between donor and acceptor units in conformers **42** and **43**. Conformer **44** and **45** show no interaction in NBO and AIM analyses. It indicates that conformer **45** does not contribute in hemiacetal formation.

Table 7.21: Properties (a.u.) calculated at bond critical point in electron density for conformers **42** – **45**. [$\nabla^2\rho$: Laplacian of the electron density; ε: ellipticity; H(r): sum of kinetic and potential energy densities].

	Bond	$\nabla^2\rho$	ε	H(r)
42	O···C=O	0.038	0.223	-0.008
43	O···C=O	0.062	0.076	-0.015
44	O···C=O	-----	-----	-----
45	O···C=O	-----	-----	-----

7.5.3 Reaction energies

The molecular mechanics calculations have generated only three possible conformers for **4a** (Figure 7.17). Conformer **46** (*cc*) was found to be the global minimum (Figure 7.18). It is 5.4 and 5.2 kcal mol^{-1} more stable than **47** (*bc*) and **48** (*bc*), respectively. This energy difference is the amount of energy required or released to flip a methylene group up or down, i.e., going from *cc* (**46**) to *bc* (**47** or **48**) or reverse. The energies of hydroxy-ketone conformers **42** – **45** are quite high as compared to the corresponding hemiacetal conformers **46** – **48**. Thus, we can say that energetically hemiacetal formation is favoured. For comparison neither experimental nor theoretical studies of the relative stabilities of **4** and **4a** are reported. So from the results obtained here we consider that the Br atom at the α position to the carbonyl carbon drives the equilibrium in forward direction rather than reverse.

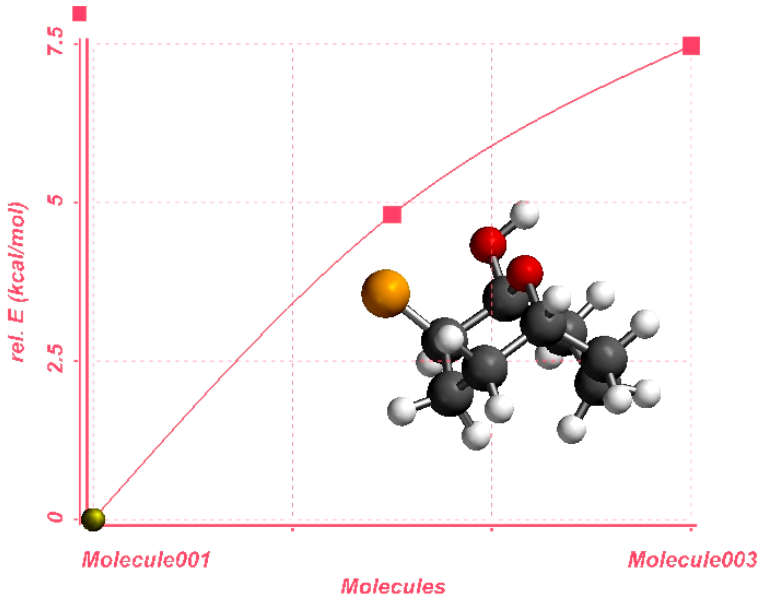

Figure 7.17: Energy profile of the conformer distribution for **4a** at MMFF level.

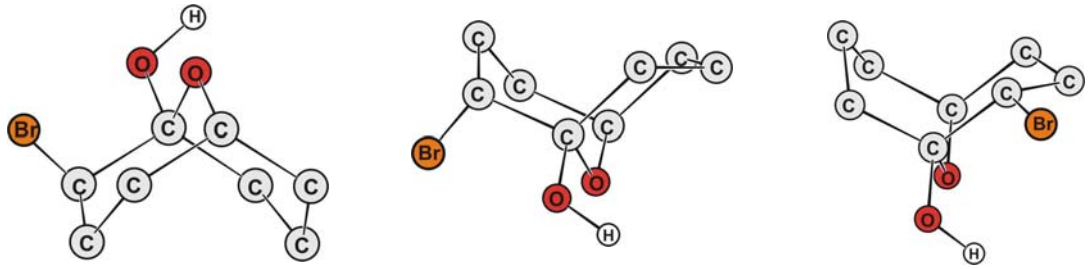

46 (0.000) **47** (5.352) **48** (5.198)

Figure 7.18: Schematic representation of the low energy conformers of hemiacetal **3a**. Relative energies (kcal mol^{-1}) are given in parentheses.

7.5.4 Transition-state calculations

We have located only two transition-state structures (**49** and **50**) on the potential energy surface (Figure 7.19). The activation energy for the cyclisation **42** (*bc*) → **47** (*bc*) *via* transition-state **49** (*bc*) is 39.1 kcal mol^{-1}. The energy barrier in cyclisation **43** (*cc*) → **46** (*cc*) *via* transition-state **50** (*cc*) is 38.2 kcal mol^{-1}. The activation barriers for the hemiacetal formation in **4** are similar to that calculated in **1**. The O(4)···C(1) distance in **49** (*bc*) and **50** (*cc*) are 1.618 and 1.646 Å, respectively (Table 7.22). The other distances and angles of the four-membered cyclic structure in **49** and **50** differ slightly. But these small differences resulted in higher energy of the transition-state **49** (*bc*) as compared to **50** (cc) by 2.7 kcal mol^{-1}.

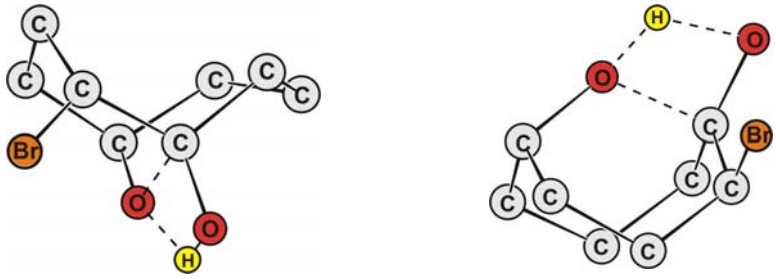

49 (-1585) **50** (-1591)
(2.721) (0.000)

Figure 7.19: Calculated transition-states **49** and **50** for the uncatalysed hemiacetal formation reaction. Imaginary frequencies (cm^{-1}) and relative energies (kcal mol^{-1}) are given in parentheses.

Table 7.22: Geometrical parameters [distances (Å) and angles (°)] of the four-membered cyclic structure in the transition-states **49** and **50**.

	49	**50**
O(4)···C(1)	1.618	1.646
C(1)···O(2)	1.313	1.314
O(2)···H(3)	1.446	1.454
H(3)···O(4)	1.136	1.135
O(4)–C(1)–O(2)	92.9	92.2
C(1)–O(2)–H(3)	77.8	78.2
O(2)–H(3)–O(4)	110.9	111.3
H(3)–O(4)–C(1)	75.8	75.5
O(2)–C(1)–O(4)–H(3)	12.7	13.3

7.5.5 Thermodynamic analysis

The energy difference between conformers **43** and **46** is -8.6 kcal mol^{-1}. In case of **4** and **4a** we do not have experimental results for comparison. To explore the equilibrium between **4** and **4a** we have analysed the thermodynamic data obtained from frequency calculations done on conformers **42**, **43**, **46** and **47**. The reaction enthalpies, ΔH°, free energy changes, ΔG°, the entropy changes, ΔS°, and the corresponding equilibrium constants for the cyclisation processes **42** → **47** and **43** → **46** are shown in Table 7.23. The free energy change, ΔG°, in going from **43** → **46** is -3.9 kcal mol^{-1} and ΔH° is negative (-5.7 kcal mol^{-1}). The ΔS° value is more unfavourable in **42** → **47**.

Table 7.23: Thermodynamic parameters for the processes **42** → **47** and **43** → **46**. [Reaction enthalpy (kcal mol^{-1}); free energy change (kcal mol^{-1}); entropy change (cal mol^{-1} K^{-1})]

	ΔG°	**ΔH°**	**ΔS°**	K_{eq}
42 → 47	4.45	1.89	-8.59	5.5×10^{-4}
43 → 46	-3.91	-5.71	-6.04	7.3×10^{2}

7.5.6 Solvent mediated calculations for the tautomeric equilibrium (4 ⇌ 4a)

The energy profile for **43** → **46** *via* transition-state **50** in gas phase, water and chloroform is shown in Figure 7.20. The activation energy calculated for **43** → **46** is least in the gas phase and it is highest in water. The transannular product **4a** is more stable even in water. This implies that **4a** is more favoured than **4**.

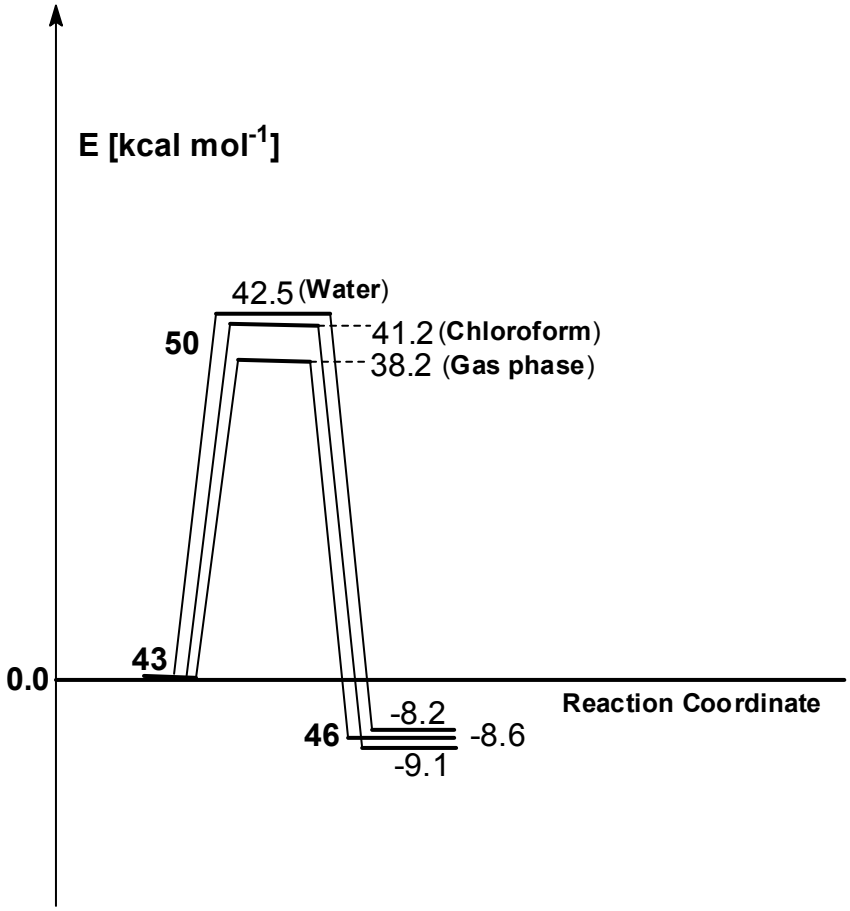

Figure 7.20: Energy profile diagram showing transannular hemiacetal formation (**43** → **46**) *via* transition-state **50** in gas phase, chloroform and water.

7.6 Results for model compound 5

Ten-membered rings possess a complex multidimensional potential energy hypersurface (PEHS).[188-190] A complete analysis of the different conformations adopted by these rings has been particularly challenging. Because of these reasons until now the role of conformation in transannular reactions such as hemiacetal formation by theoretical models has not been studied in **5**. The molecular mechanics calculations done on *endo*-conformer of **5** have generated 100 conformers (Figure 7.21). To our surprise only four conformers have an *endo*-orientation of the OH group.

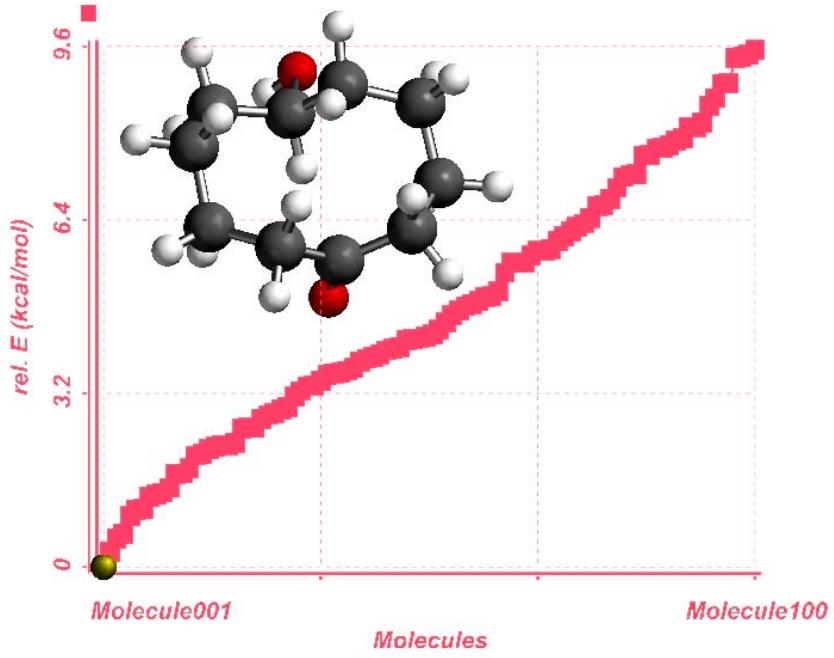

Figure 7.21: Energy profile of the conformer distribution for the *endo*-conformer of **5** at MMFF level.

7.6.1 Structural features

The most stable conformer is boat-chair-boat (*bcb*).[188-190] Spectroscopic (NMR and IR) as well as dipole measurements have indicated that in solution there is a mixture of several conformers such as crown and the highly symmetrical twist-chair-chair-chair (*tccc*) plays the main part.[189, 191] In solid state[58] **5** exits in *bcb* conformation with *exo*-orientation of the OH group. For the present investigations we have taken only *endo*-conformers **51** – **54** (Table 7.24).

Table 7.24: Important geometrical parameters investigated in **51** – **54** and relative energies including the zero point energy calculated with respect to conformer **55** (gas phase). [Distances (Å); angles (°), rel. energies (kcal mol^{-1})].

Molecular structure	**Geometrical parameters**			
	d_o	d_1	θ_o	Δ_o
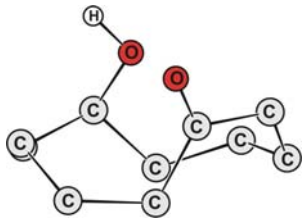 **51** (10.265)	2.787	3.967	95.1	0.047
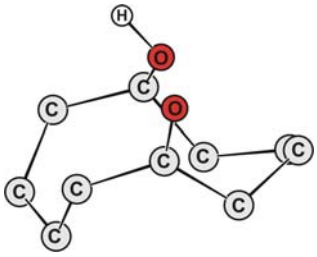 **52** (16.224)	2.585	3.487	93.1	0.066
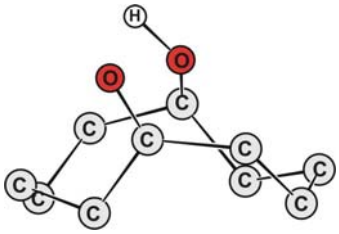 **53** (10.638)	3.156	3.942	78.3	0.022
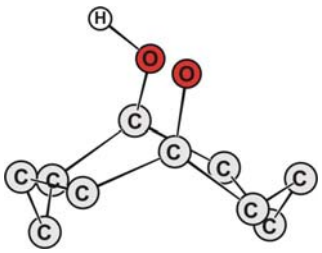 **54** (8.078)	2.513	3.479	94.0	0.068

The most stable *endo*-conformer **54** is not *bcb* but *cbc*. The distance between the electrophilic C and the nucleophilic O atoms in conformers **51** – **54** is 2.8, 2.6, 3.2 and 2.5 Å, respectively. These distances are less than the sum of vdW radii (3.2 Å) of carbon and oxygen atoms except in **53** where the distance is close to this value.
The angle of approach of the nucleophile θ_O in **51**, **52** and **54** is consistent with the reported[168, 169] nucleophilic attack angle. The carbonyl carbon shows pyramidalisation in all conformers towards the nucleophilic centre from the plane of three neighbouring bonded atoms. The deviation Δ_O in **52** and **54** is 0.066 and 0.068 Å, respectively. Conformers **51**, **52** and **54** offer the optimal orientation of the two functional groups for the intramolecular interactions at a short distance as compared to conformer **53**.

7.6.2 Bonding and interactions

In conformer **53** the distance d_O is large (>3 Å). This indicates that intramolecular interaction is less probable. This is further evident from the absence of the second order interaction between the donor and acceptor orbitals (Table 7.25). In **52** and **54** due to the short transannular distance between the functional groups strong interaction is expected. The stabilisation energies $E^{(2)}$ associated with the donation of electrons from the filled non-bonding nucleophilic oxygen n_O to the empty electrophilic carbonyl carbon $\pi^*_{C=O}$ orbital in **52** and **54** are 5.45 and 4.04 kcal mol^{-1}, respectively. The electron occupancy in the the $\pi^*_{C=O}$ orbital in **54** is greater than in **52**. This implies that there is more electron transfer from $n_O \rightarrow \pi^*_{C=O}$ in **54** than in **52**. The second order perturbation interaction energy between donor and acceptor orbitals is highest in conformer **54**. As a result the donation of electron from $n_O \rightarrow \pi^*_{C=O}$ is maximal.

Table 7.25: Natural bond order (NBO) analysis of conformers **51** – **54**. $E^{(2)}$ (kcal mol^{-1}) is the second order perturbation energy between Φ_i and Φ_j; E_j-E_i (a.u.) is the energy difference between NBOs Φ_i and Φ_j; F_{ij} (a.u.) is the Fock matrix element; only energies greater than the default threshold 0.5 kcal mol^{-1} are included in the table.

	Interaction	**Second-order Interaction**			**Occupancy (ρ)**	
		$E^{(2)}$	E_j-E_i	F_{ij}	$n_o \rightarrow \pi^*_{c=o}$	
51	$n_o \rightarrow \pi^*_{c=o}$	1.77	0.36	0.023	1.951	0.092
52	$n_o \rightarrow \pi^*_{c=o}$	4.04	0.40	0.036	1.943	0.099
53	$n_o \rightarrow \pi^*_{c=o}$	-----	-----	------	1.957	0.077
54	$n_o \rightarrow \pi^*_{c=o}$	5.45	0.41	0.043	1.937	0.107

Further, atoms in molecule (AIM) calculations were performed on conformers **51** – **54** to support the presence of electronic interactions between the donor and acceptor groups. A summary of the density analysis is provided in Table 7.26. A bond critical point corresponding to O···C=O interaction has been observed in **51** and **54** confirming that these conformers induce an interaction between OH and C=O in the ground state. These interactions probably are responsible for the initiation of the cyclisation reaction. The electron density and the energy associated at the bond critical points in **54** are much stronger than in **51**. These results indicate that conformer **54** probably plays a major role in the cyclisation.

Table 7.26: Properties (a.u.) calculated at bond critical point in electron density for conformers **51** – **54**. [$\nabla^2\rho$: Laplacian of the electron density; ε: ellipticity; H(r): sum of kinetic and potential energy densities].

	Bond	$\nabla^2\rho$	**ε**	**H(r)**
51	O···C=O	0.046	0.519	-0.010
52	O···C=O	-----	-----	-----
53	O···C=O	-----	-----	-----
54	O···C=O	0.073	0.134	-0.018

7.6.3 Reaction energies

The molecular mechanics calculations have generated 40 conformers for **5a** (Figure 7.22). Out of these only ten conformers were optimised at higher level of theory. Conformer **55** was found to be the global minimum (Figure 7.23). It is 8.0 kcal mol^{-1} more stable than the low energy conformer **54** of 6-hydroxycyclodecanone (**5**). These results support the experimental findings according to which the hemiacetal **5a** is favoured in a non-polar solvent.

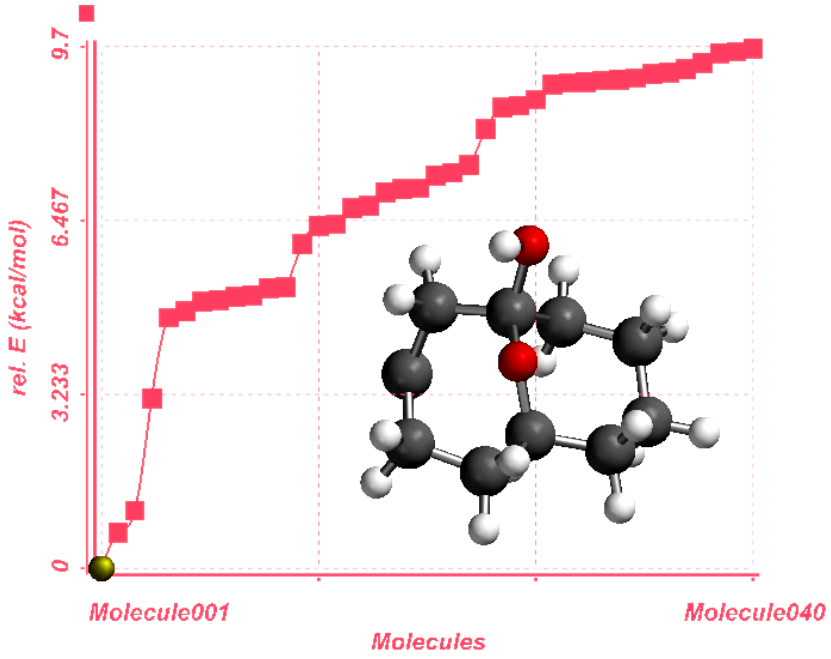

Figure 7.22: Energy profile of the conformer distribution for **5a** at MMFF level.

7.6.4 Transition-state calculations

The uncatalysed hemiacetal formation in **5** is expected to take place *via* a four-membered cyclic structure similar to model compounds **1** – **4**. The transition-state is expected to consist of a host of geometries[192] since the ten-membered ring is very flexible and a number of low energy interconversion pathways leading to the hemiacetal are possible. We have located three transition-states (**65** – **67**) on the potential energy surface (Figure 7.24). All transition-states are characterised by a single imaginary frequency. The *preferred* transition-state is **66** since it has the lowest energy. The activation energy is 36.9 kcal mol^{-1} for **54** → **55** *via* transition-state **66**.

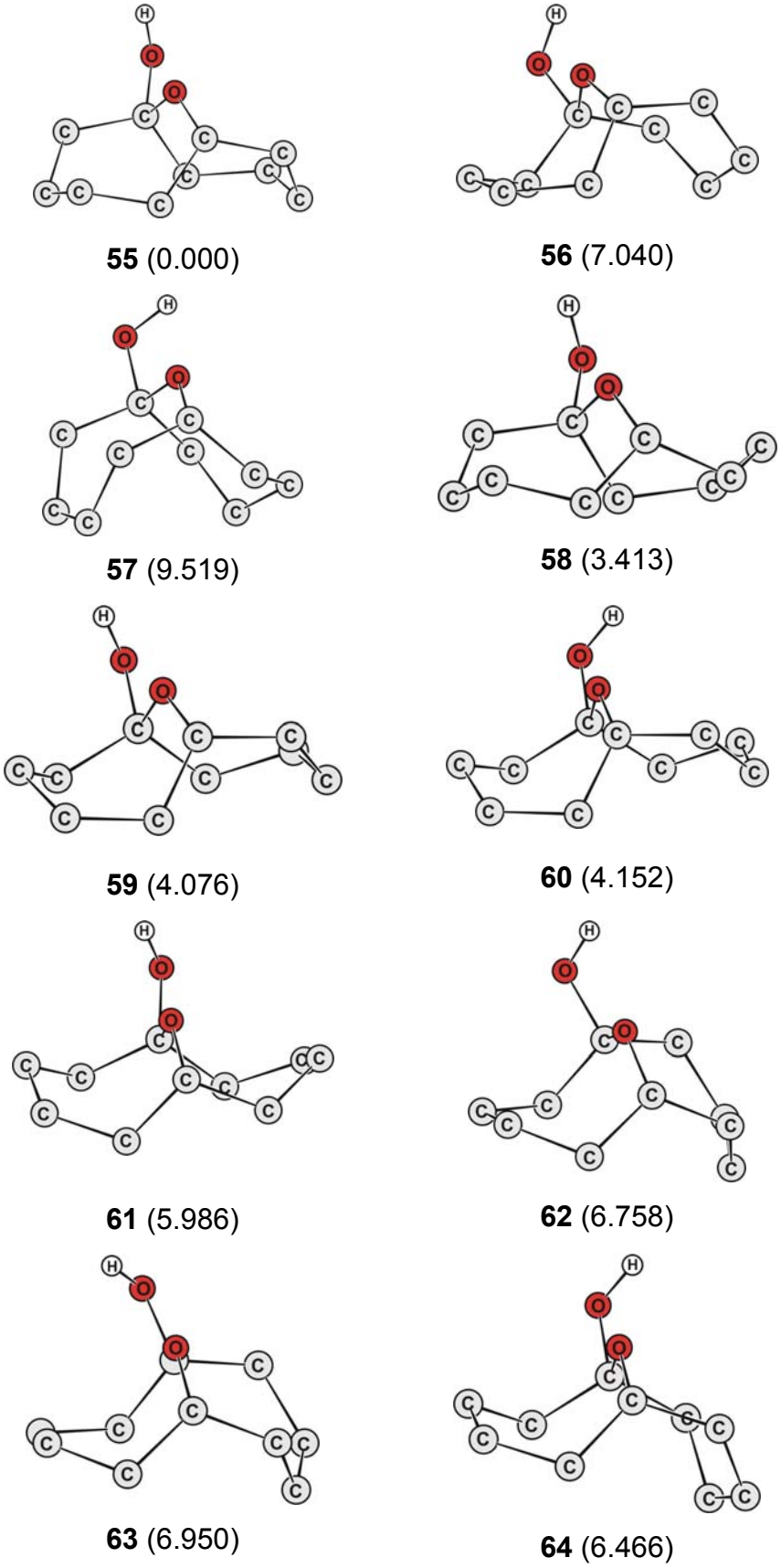

55 (0.000)

56 (7.040)

57 (9.519)

58 (3.413)

59 (4.076)

60 (4.152)

61 (5.986)

62 (6.758)

63 (6.950)

64 (6.466)

Figure 7.23: Schematic representation of the low energy conformers of hemiacetal **5a**. Relative energies (kcal mol^{-1}) are given in parentheses.

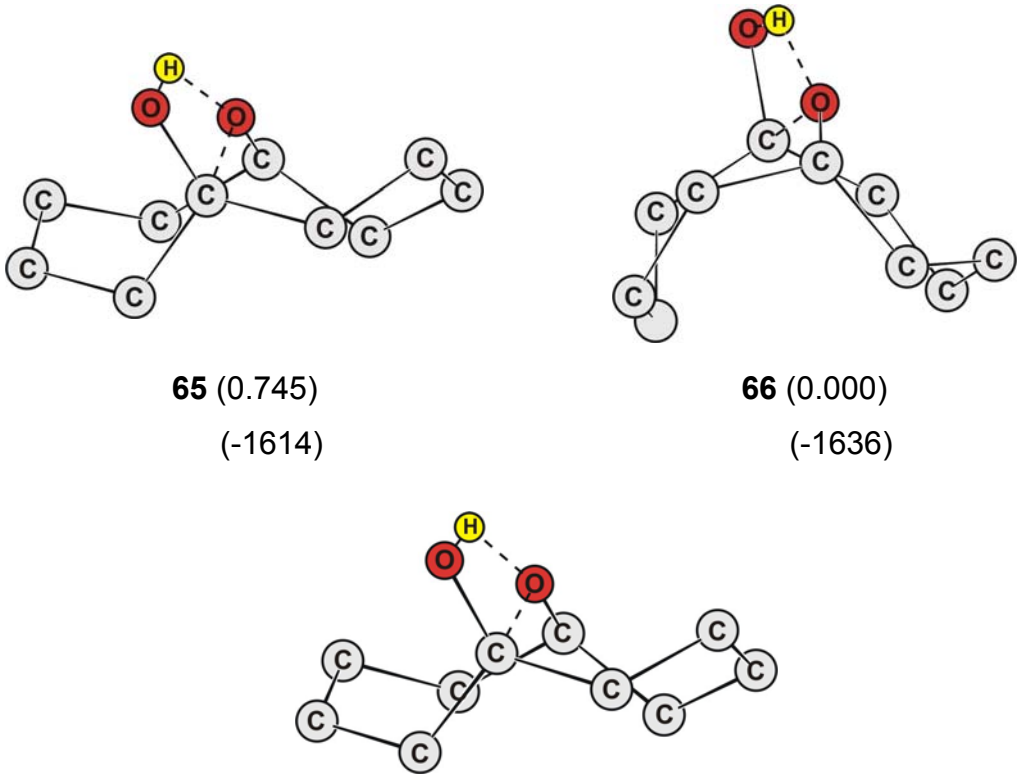

65 (0.745)
(-1614)

66 (0.000)
(-1636)

67 (0.758)
(-1609)

Figure 7.24: Calculated transition-states **65** – **67**, relative energies (kcal mol^{-1}) and imaginary frequencies (cm^{-1}) for the uncatalysed transannular hemiacetal formation in model compound **5**.

Interestingly, the geometrical parameters of the four-membered cyclic structure in transition-states **65** – **67** are similar to those of the transition-state (**6**) located for the intermolecular reaction between formaldehyde and water (Figure 6.1 and Table 6.1).

Table 7.27: Geometrical parameters [distances (Å) and angles (°)] of the four-membered cyclic structure in the transition-states **65** – **67**.

	65	**66**	**67**
O(4)···C(1)	1.684	1.698	1.680
C(1)···O(2)	1.321	1.324	1.322
O(2)···H(3)	1.384	1.358	1.386
H(3)···O(4)	1.148	1.161	1.149
O(4)–C(1)–O(2)	90.0	89.9	90.1
C(1)–O(2)–H(3)	79.8	80.2	79.7
O(2)–H(3)–O(4)	115.2	117.0	115.0
H(3)–O(4)–C(1)	72.8	71.5	73.0
O(2)–C(1)–O(4)–H(3)	-8.8	-8.9	11.0

7.6.5 Thermodynamic analysis

The energy difference between conformers **54** and **55** is -8.1 kcal mol^{-1}. Experimentally, it has been found that the equilibrium between **5** and **5a** shifts completely towards **5** in water.[58] But in case of non-polar solvents the hemiacetal **5a** is more favoured than **5**. To explore the equilibrium between **5** and **5a** we have analysed the thermodynamic data obtained from frequency calculations done on conformers **54** and **55**. Relevant results are summarised in Table 7.28.

Table 7.28: Thermodynamic parameters for the process **54** → **55**. [Reaction enthalpy (kcal mol^{-1}); free energy change (kcal mol^{-1}) and entropy (cal mol^{-1} K^{-1})].

	ΔG^o	ΔH^o	ΔS^o	K_{eq}
54 → **55**	-7.02	-8.81	-6.00	1.4×10^5

The free energy change, ΔG°, is -7.0 kcal mol^{-1} and ΔH° is negative (-8.8 kcal mol^{-1}). The negative value of ΔS° (-6.0 cal mol^{-1} K^{-1}) is consistent with the cyclisation process. There is a decrease in randomness, i. e., entropy, as **5a** is formed. The equilibrium constant is five orders of magnitude in powers of ten towards the product for **54** → **55** indicating that the reaction is almost complete.

7.6.6 Solvent mediated calculations for the tautomeric equilibrium (5 ⇌ 5a)

The activation energies in the gas phase, chloroform and water are shown in Figure 7.25. The activation barrier is least in the gas phase. Conformer **55** for hemiacetal (**5a**) is 8.1 kcal mol^{-1} more stable than the starting conformer **54** of 6-hydroxycyclodecanone (**5**). It is reported[58] that the equilibrium favours tautomer **5** exclusively in water. It is likely that intermolecular interactions in solvents like water may dominate possible intramolecular effects. The activation barrier in water is maximal (40.8 kcal mol^{-1}). In water hemiacetal **55** is only 7.1 kcal mol^{-1} more stable than **54**.

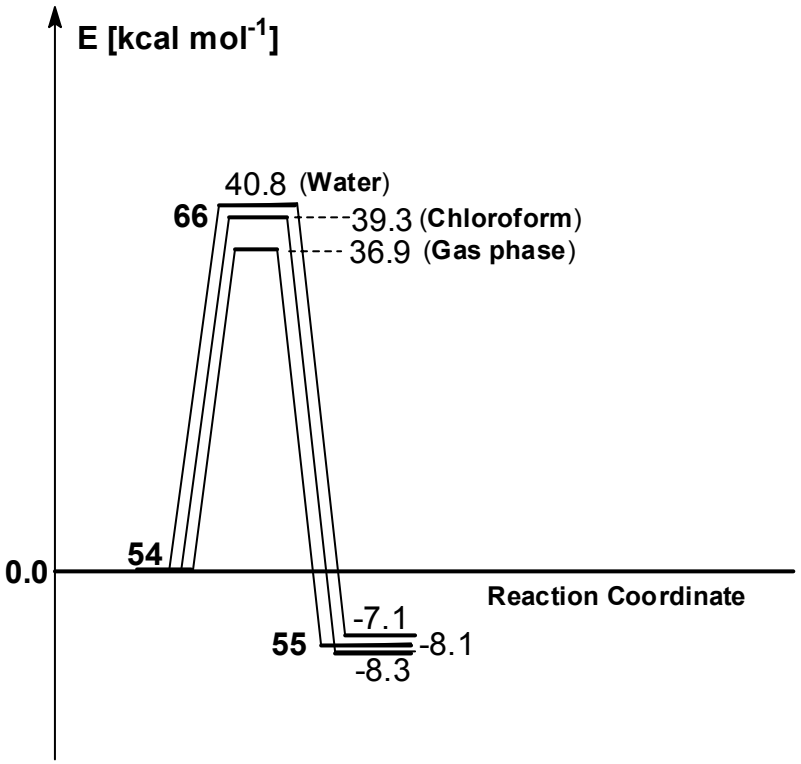

Figure 7.25: Energy profile diagram showing transannular hemiacetal formation **(54 → 55)** *via* transition-state **66** in gas phase, chloroform and water.

7.7 Discussion

It was the main purpose of this investigation to study the conformational properties of **1** – **5** and to find out how the conformations are related to transannular hemiacetal formation. Depending on the relative geometric orientation of the reacting groups, transannular orbital interactions between the frontier molecular orbitals (FMOs) n_O and $\pi^*_{C=O}$ are possible. The eight-membered ring system **1** has the largest transannular interaction and presents optimal conditions for the "contact" of substituents in the positions 1 and 5. For system **2** the interactions are less because of the change in the position of the OH group. In case of **3** the interactions are larger than in **2** because of the presence of a double bond which leads to close proximity of atoms. In **4** the Br atom does not seem to hinder the transannular interactions to a greater extent. The calculated NBO interaction is found to be strongest (5.45 kcal mol^{-1}) in the *preferred* starting conformer **54** of model compound **5**. The stabilisation energy $E^{(2)}$ associated with the donation of electrons from the filled non-bonding nucleophilic oxygen n_O to the empty electrophilic carbonyl $\pi^*_{C=O}$ orbital is 3.59, 1.78, 2.67 and 4.71 kcal mol^{-1} in conformers **13**, **23**, **33** and **43**, respectively, of model compounds **1** – **4**.

The process of cyclisation involves a concerted nucleophilic addition and transfer of a proton. The intramolecular nucleophilic addition reaction takes place *via* a four-membered cyclic transition-state leading to hemiacetal formation. The calculated energy barriers for **21** → **29**, **33** → **38**, **8** → **7** and **54** → **55** are 35.2, 36.5, 37.2 and 36.9 kcal mol^{-1}, respectively. The energy barrier for **13** → **18** and **43** → **46** is the same (38.2 kcal mol^{-1}). The activation energy required for hemiacetal formation both in **1** and **4** is higher than in model compounds **2**, **3** and **5**. This can be explained on the basis of strained transition-states in the former cases.

The geometrical parameters of transition-states **41** and **32** are similar (Tables 7.17 and 7.11). The O(4)···C(1) distance in **41** is 1.700 Å which is close to the corresponding distance (1.729 Å) found in **32**. But in case of **20** (Table 7.6) the O(4)···C(1) distance is 1.644 Å. The distance between the hydrogen atom transferred as proton is 1.350 and 1.329 Å in **41** and **32**, respectively. In contrast, this distance is large (1.449 Å) in **20**. Interestingly, the geometrical parameters of the four-membered cyclic structure in transition-states **65** – **67** (Table 7.27) are similar to those of **6**

located for the intermolecular reaction between formaldehyde and water (Figure 6.1 and Table 6.1).

In a hydroxy-ketone there is one C=O bond and one O-H bond whereas in a hemiacetal there are two C-O bonds and one O-H bond. Thermodynamic data obtained from Hessian studies also support these findings. The *preferred* starting conformers for cyclisations **13** → **18**, **43** → **46** and **54** → **55** are less stable, i.e., 8.5, 8.6 and 8.1 kcal mol^{-1}, respectively, than the corresponding hemiacetals in the gas phase. This implies thermodynamically that *preferred* products in **1**, **4** and **5** are **1a**, **4a** and **5a**. On the contrary, hemiacetals **2a** and **3a** are only 3.6 and 4.6 kcal mol^{-1} more stable than the *preferred* starting conformers **21** and **33**, of **2** and **3** respectively. But interestingly, **46** is 8.2 kcal mol^{-1} more stable than **43** in water whereas **18** is only 4.9 kcal mol^{-1} more stable than **13**. The comparison of stability of **46** and **18** in water shows that the former is more stable even in this solvent. Hence, the transannular product **4a** is more stable and favoured as compared to the open form **4** even in water. The energy difference between **21** and **29** (3.6 kcal mol^{-1}) is less as compared to **13** and **18** (8.5 kcal mol^{-1}) in the gas phase. But interestingly, the difference in energy between **21** and **29** (3.4 kcal mol^{-1}) does not change markedly in water.

The experimental results reveal that only 88% of tautomer **5a** exist in hexane and **1a** is favoured exclusively even in D_2O at room temperature. The solvent plays an important role in deciding the conformations responsible for the transannular interactions. Intermolecular interactions in solvents like water may dominate possible intramolecular effects. Since continuum models are not able to handle specific solvent effects, we consider these results as semi-quantitative. The stability of **1a** may be due to the formation of more stable six-membered rings which gives rigidity to the structure as compared to the seven-membered rings formed in **5a**. Unlike expected the results obtained here show that in compound **4** the Br atom at α to the carbonyl group drives the equilibrium in the forward direction rather than reverse. However, for the sake of comparison neither experimental nor theoretical studies of the relative stabilities of **4** and **4a** are reported. Among *cc* and *bc* conformations of **1a** and **4a**, *cc* is found to be most stable. All the structural factors, i.e., conformation, strain, and thermodynamics factors favour cyclisation.

.

8 Acid-catalysed transannular 1,5-hydride shift in 1

As we have found in preceding chapters (5 and 7) transannular hemiacetal formation is a function of the ring skeleton. In addition to this reaction another competing transannular reaction is hydride shift. The phenomenon of transannular hydride shift in cycloalkane rings (C_8 to C_{10}) involving carbocation intermediates was first observed by Prelog,[54] Cope[40] and their respective co-workers. In medium-ring compounds generally solvolysis leads to the unexpected products which are derived from the transannular hydride shift. Solvolysis studies of *cis*-cyclooctene oxide (**68**) reported earlier[40] have shown that the transannular products **69** – **71** are formed by 1,5- and 1,3-hydride shifts (Schemes 8.1 and 8.2). The expected product of solvolysis is *trans*-1,2-cyclooctanediol (**72**).

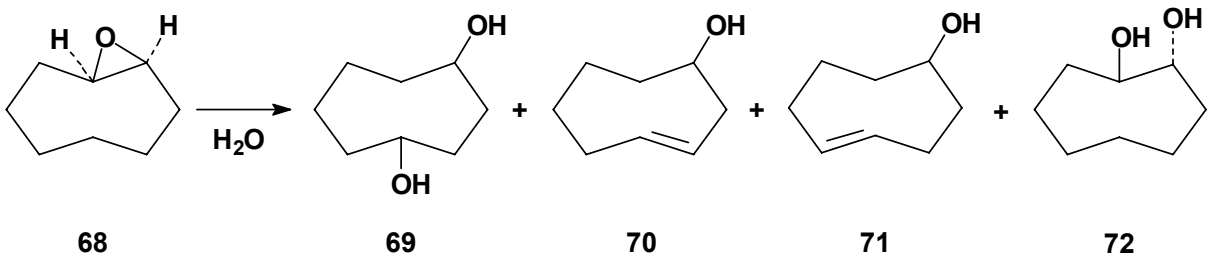

Scheme 8.1: Solvolysis of *cis*-cyclooctene oxide.

It has been reported[40] that in the reaction of *trans*-1,2-dibromocyclooctane with silver acetate in acetic acid, i.e., S_N1 reaction conditions, exclusively transannular products are formed. On the other hand, S_N2 reaction conditions, i.e., reaction with tetraethylammonium acetate in acetone, lead to the expected products formed by substitution and elimination. These results support the idea that the hydride shift is favoured by the formation of carbenium ions.

Sorensen and co-workers[67] in 1978 have first obtained NMR evidence for the existence of a μ-hydrido-bridged structure (Figure 8.1). In such structures a hydrogen atom is bridging between the two carbocation centres present on opposite side of the ring. Further these bridged cations were treated as open three-centre two-electron (3c-2e) σ-resonance systems.[70] But occurrence of such structures in hydride shift rearrangements of carbocations was proposed earlier.[193]

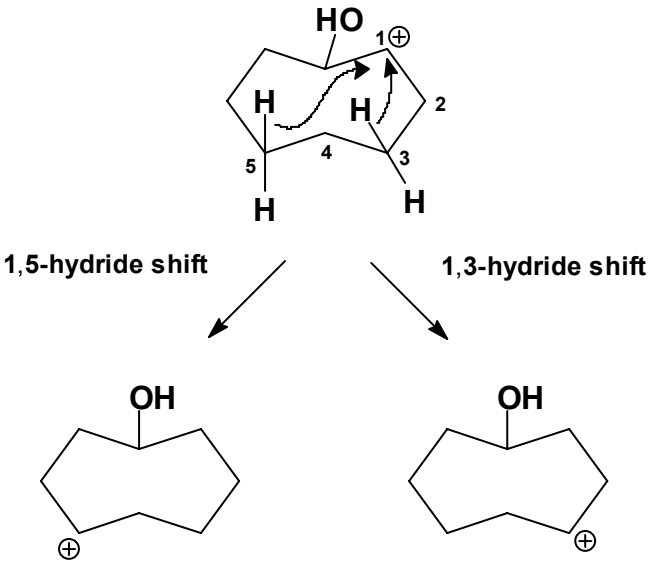

Scheme 8.2: Possible pathways for the transannular hydride shift in cyclic eight-membered carbenium ions.

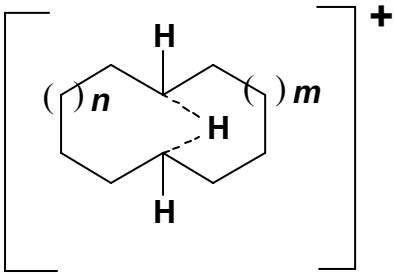

n = m = 1
n = 2, m = 0

Figure 8.1: Cyclodecyl cation possessing μ-hydrido-bridging.

Over the last few decades, transannular hydride shift reactions have held the interests of chemsits, both as subject to investigate transannular interactions and mechanism of transannular reactions.[75, 194-203] A number of examples are reported in the literature related to degenerate and non-degenerate rearrangements of compounds containing functional groups such as carbonyl and hydroxy taking place in the presence of acid[58, 71, 74, 204] or base.[194, 195, 198, 205-208] But until now a transannular hydride shift has not been reported in 5-hydroxycyclooctanone in the presence of acid or base. Presence of hydroxy-ketone **1** in D_2O at higher temperatures (Table 5.1) has given us a hope that this property can be exploited for the reactions of the carbonyl group.

Deuterium- and tritium-labelled organic compounds have become increasingly important for the role they play in mechanistic and structure determination studies. Deuterium labeling has already been exploited for studying transannular hydride shift reactions in various systems.[40, 205]

In this chapter we describe an investigation of the transannular 1,5-hydride shift in **1** in the presence of acid (Scheme 8.3). To study the effect of concentration of acid and temperature on the reaction rate *in situ* NMR experiments were planned. This was done on the basis of following assumptions:

a) Compound **1a** is soluble in water.

b) At higher temperature, equilibrium exists between **1a** and **1**.

c) In addition to transannular 1,5-hydride shift another competing reaction is hemiacetal formation. The formation and breaking of the oxo-bridge in **1a** is catalysed by acid. So it is expected that in the presence of acid and D_2O an equilibrium exists between **1a** and **1** even at room temperature.

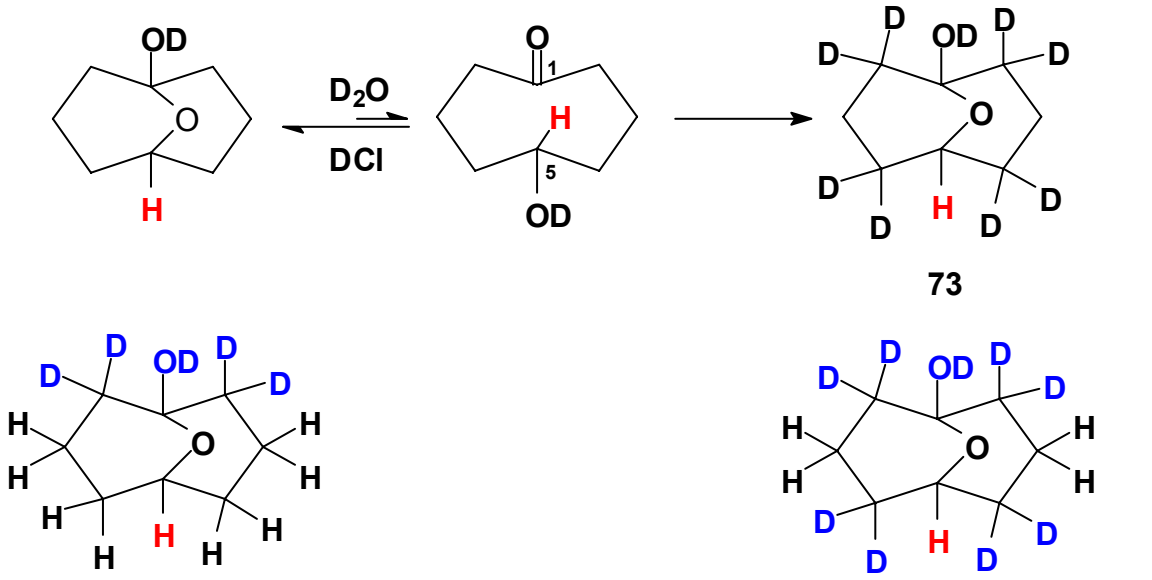

Scheme 8.3: Transannular 1,5-hydride shift in **1** in the presence of DCl in D_2O.

8.1 NMR experiment in the presence of 12.0 M DCl in D_2O

For an *in situ* NMR experiment 12.0 M DCl in D_2O was added to a clean dry NMR tube containing **1a**. Initial spectra (^{1}H- and ^{13}C-NMR) were recorded immediately after mixing the reactants at room temperature. The ^{1}H- and ^{13}C-NMR spectra for **1a** recorded at different times are shown in Figures 8.2 and 8.3, respectively.

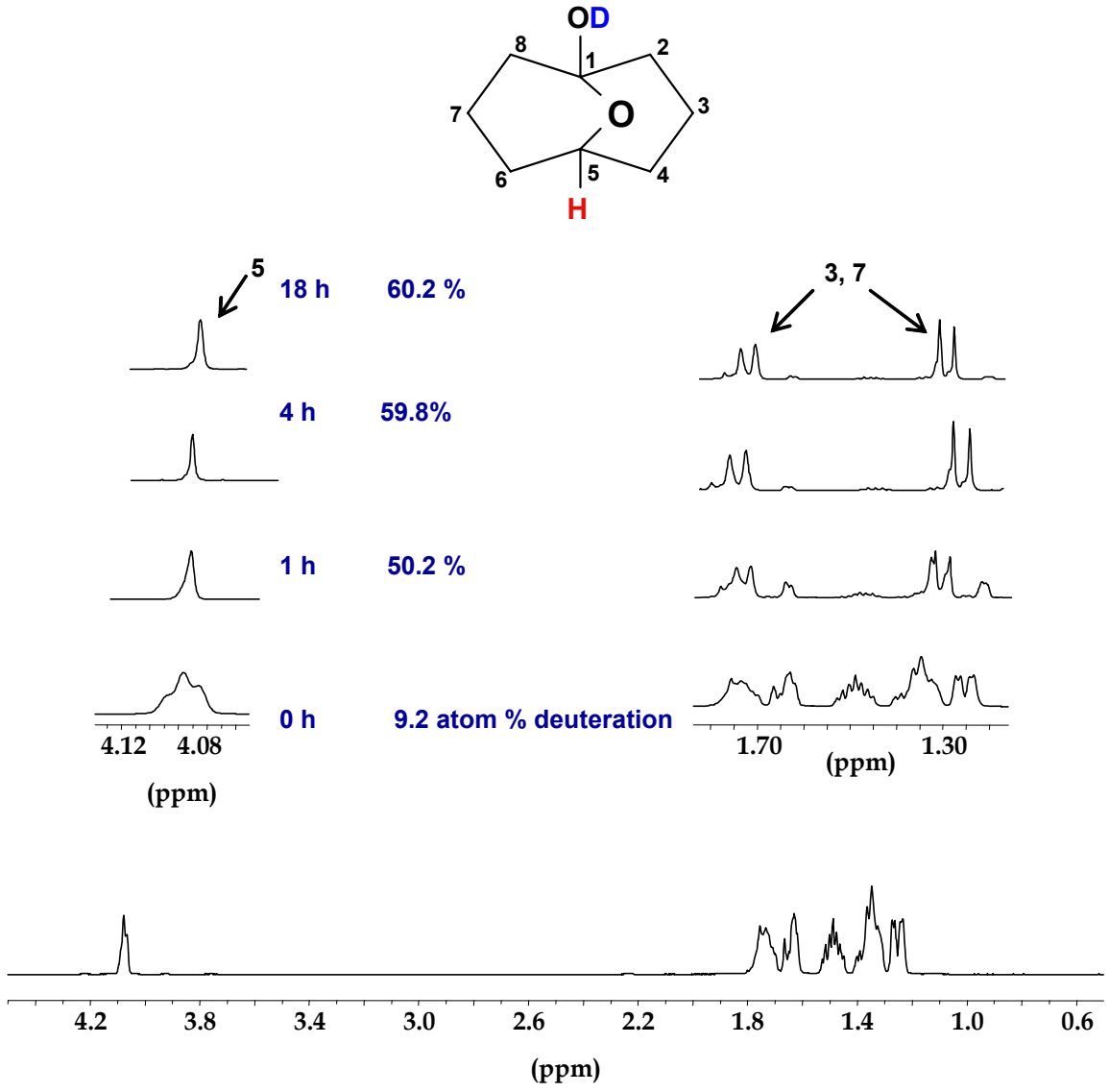

Figure 8.2: ^{1}H-NMR spectra for **1a** undergoing H/D exchange in 12.0 M DCl in D_2O at RT.

The assignment for the complex multiplet signals for the twelve methylene protons in tautomer **1a** was done on the basis of a combination of 2-D ^{13}C-/^{1}H-NMR correlation spectra recorded in $CDCl_3$ for **1a**. The signals for the protons at C-4 and C-6 appeared in the region δ 1.23 – 1.40 and 1.45 – 1.53 ppm. The signals for the

protons at C-3 and C-7 appeared as complex multiplets at δ 1.32 –1.40 and 1.63 – 1.76 ppm. The signals for the rest of eight protons of the ring come as complex multiplets at δ 1.23 –1.76 ppm. The most downfield signal was assigned to the methine proton at δ 4.08 ppm.

The ^{1}H-NMR spectrum recorded immediately after mixing the reactants revealed 9.2 atom % deuteration in the region δ 1.23 – 1.76 ppm. Simultaneously the triplet at δ 4.08 ppm broadened. The calculation of deuteration was based on the assumption that out of twelve methylene protons eight were exchanged with deuterium atoms (Scheme 8.3). After 1 h the spectrum was recorded again and the deuteration was found to increase to 50.2 atom %. In addition, the triplet signal was changed to a singlet. After 4 h, the spectrum appeared simple. The multiplet signals for the twelve methylene protons were replaced by two doublets at δ 1.32 and 1.73 ppm. The amount of deuteration was 59.8 atom %. In the next 14 h the deuteration reached a constant level of 60.2 atom %.

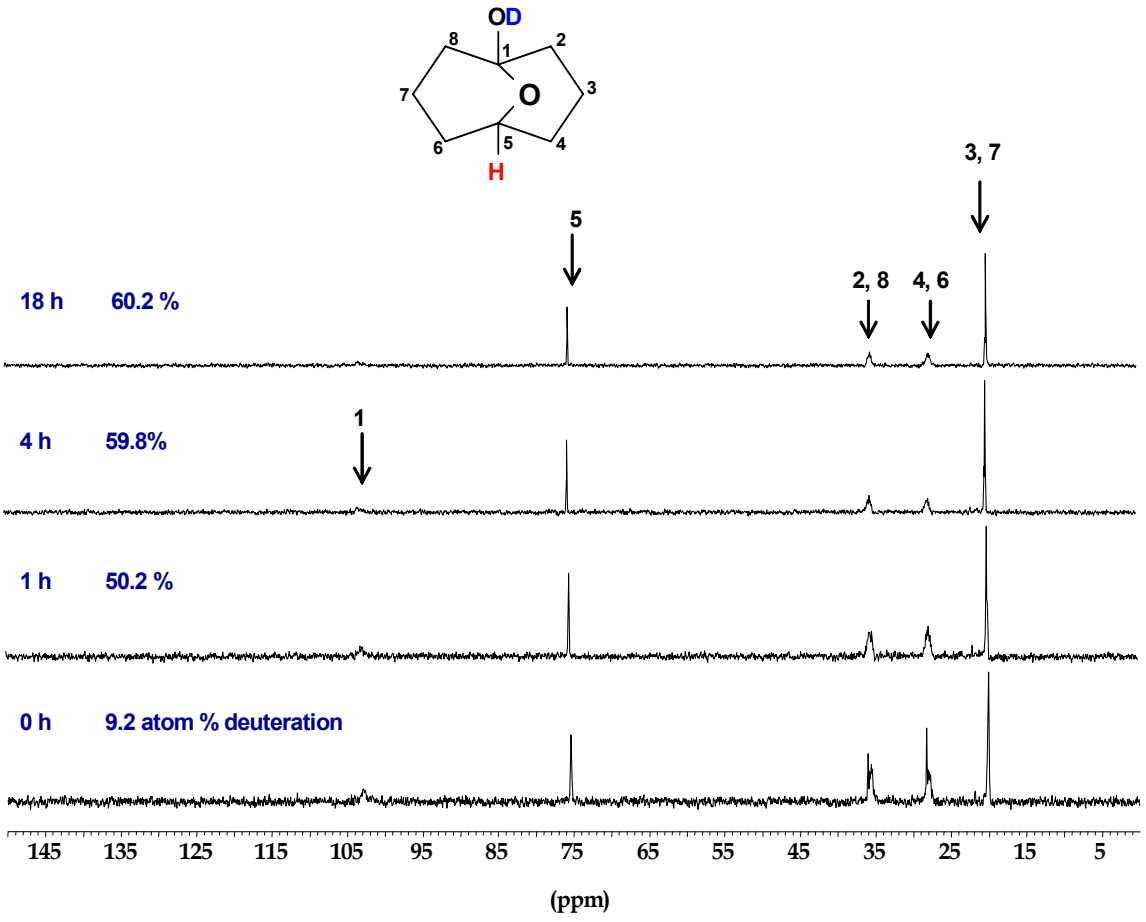

Figure 8.3: ^{13}C-NMR spectrum for **1a** undergoing H/D exchange in 12.0 M DCl in D_2O at RT.

Because of the symmetry of **1a** there are five signals in the ^{13}C-NMR spectrum. At 0 h, the signal for C-3 and C-7 was most upfield and appeared at δ 20.10 ppm (Figure 8.3). The original singlet signal for C-4 and C-6 in the C-H decoupled ^{1}H-NMR spectrum changed to a weak multiplet at δ 28.26 ppm because of ^{13}C-D coupling. The signals for C-5 and C-1 appeared also as multiplets of low intenstity at δ 75.37 and 102.01 ppm. After an interval of 1 h the signals for C-4, C-6, C-2 and C-8 become weak clusters with low intensities whereas the signal for C-1 disappeared. Two signals at δ 20.29 (C-3, C-7) and 73.65 ppm (C-5) remained after an interval of 18 h. The important inference from this experiment is that the hydrogen atoms exchange with deuterium atoms only at C-2, C-4, C-6 and C-8. Thus, the final spectra both ^{1}H- and ^{13}C-NMR correspond to **73** (Scheme 8.3).

8.2 NMR experiment with 7.9 M DCl in D_2O in the presence of an internal standard

Further studies were performed with an acid concentration of 7.9 M in the presence of 1,4-dioxane as an internal standard at different temperatures. Equimolar amounts of 1,4-dioxane and **1a** were taken for the NMR experiment. The ^{1}H-NMR spectra are shown in Figure 8.4. The signal of the protons of 1,4-dioxane appear at δ 3.75 ppm. The triplet signal for H-5 at δ 4.34 ppm changed to a singlet after 208 h. The quantitative analysis has shown that the relative intensity of H-5 was 0.97 at 0 h. After 208 h the intensity of H-5 proton was 1.01. This change in intensity is considered to be within the error limit. The multiplet signal at δ 1.57 – 2.12 ppm changed to two doublets at δ 1.68 and 2.10 ppm. The deuteration after 208 h was 62.6 atom %. These results are in agreement with our expectation that proton H-5 is not exchanging.

The NMR experiment was repeated at higher temperature. In a clean dry NMR tube containing a solution of equimolar amounts of **1a** and 1,4-dioxane, 7.9 M DCl in D_2O was added. Immediately after mixing, the NMR spectrum was recorded (0 h). The broad triplet signal at δ 4.32 ppm corresponds to H-5 (Figure 8.5) and its relative intensity with respect to the signal for 1,4-dioxane is 0.97. The NMR tube was heated for 10 min at 100 ºC in a water bath. The signal at δ 4.32 ppm became a singlet and the intensity of H-5 increased to 1.01. This implies that H-5 is not exchanging with deuterium even on heating. The multiplet assigned to protons at C-2, C-3, C-4, C-6,

C-7 and C-8 in the region δ 1.57 – 2.13 ppm become two doublets at δ 1.65 and 2.07 ppm corresponding to H-3 and H-7 of two methylene groups. The deuterium incorporation was 59.9 atom %.

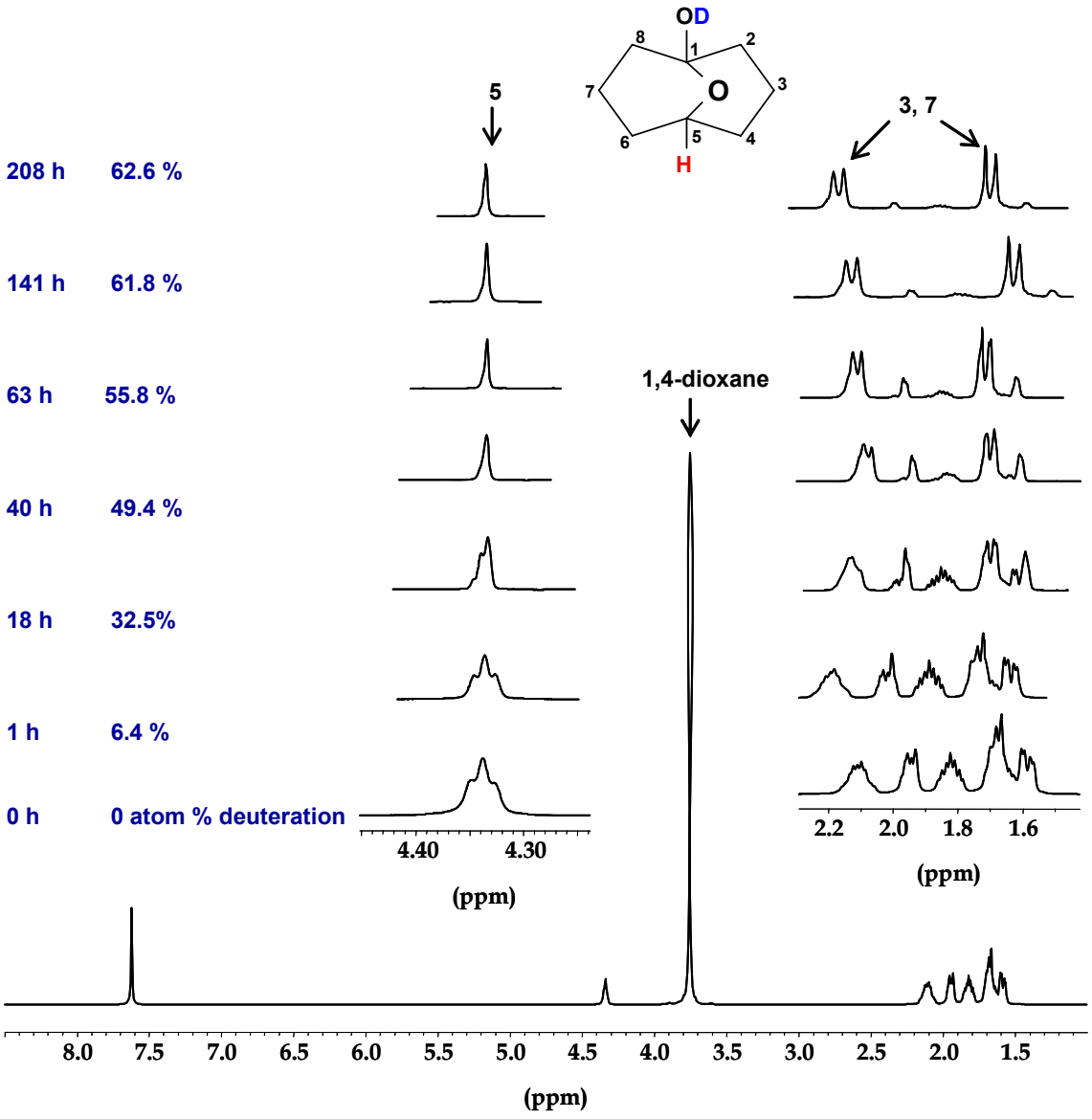

Figure 8.4: ^{1}H-NMR spectra for **1a** undergoing H/D exchange in 7.9 M DCl in D_2O at RT with 1,4-dioxane as a standard.

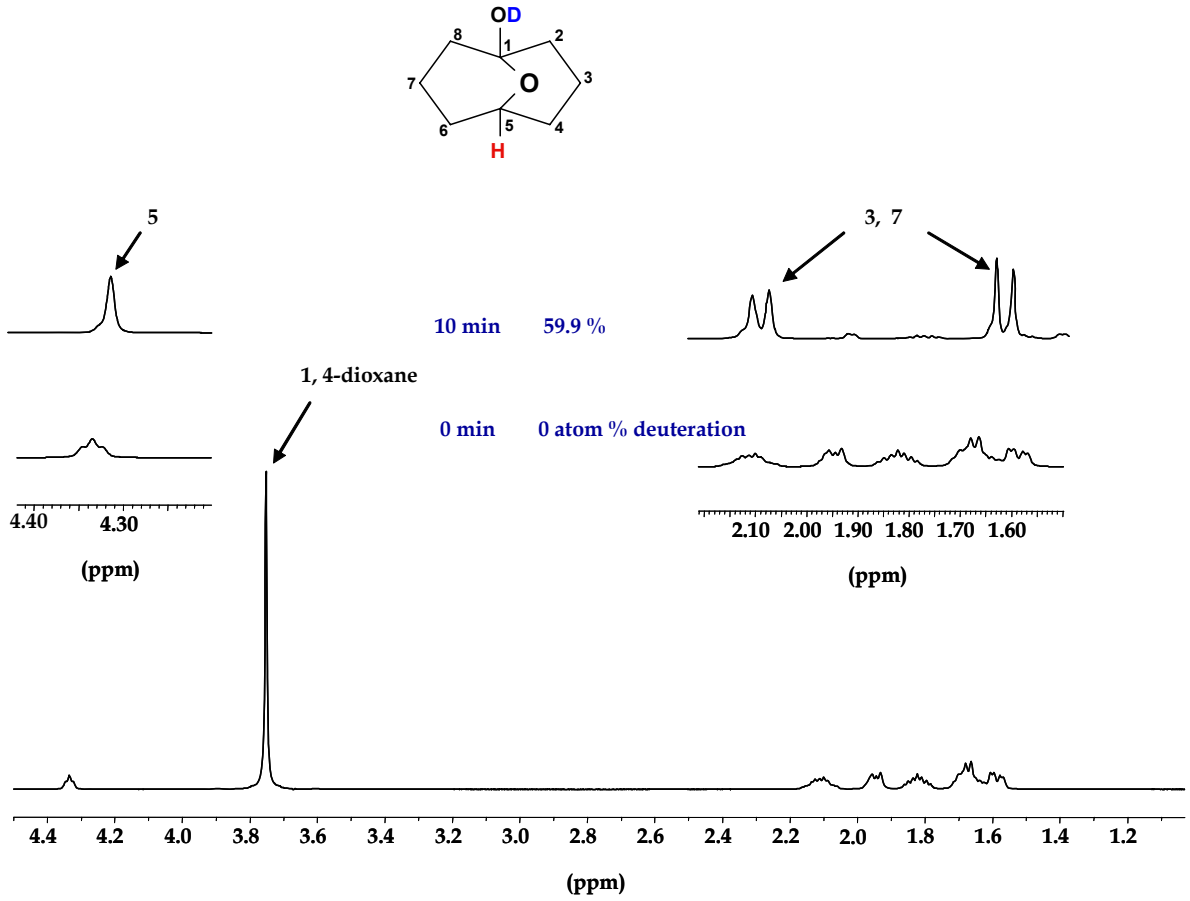

Figure 8.5: ^{1}H-NMR spectra for **1a** undergoing H/D exchange in 7.9 M DCl in D_2O at 100 ºC with 1,4-dioxane a standard.

8.3 NMR experiment in the presence of 3.4 M DCl in D_2O

The ^{1}H- and ^{13}C-NMR spectra for **1a** in 3.4 M DCl in D_2O at room temperature are shown in Figures 8.6 and 8.7. The symmetric triplet signal of H-5 in tautomer **1a** at δ 4.34 ppm changed slowly to a broad singlet in 13 d 18 h. The signal becomes a singlet due to small coupling with the neighbouring deuterium atoms at C-4 and C-6. The deuteration was 45.8 atom %. This implies that the protons H-4 and H-6 were exchanged with deuterium atoms. The multiplet pattern at δ 1.61 – 2.20 ppm for methylene protons at C-2, C-4, C-6 and C-8 changed to predominately two doublets in 23 d and 19 h. The deuteration in the end (23 d 19 h) of experiment was found to be 56.3 atom %.

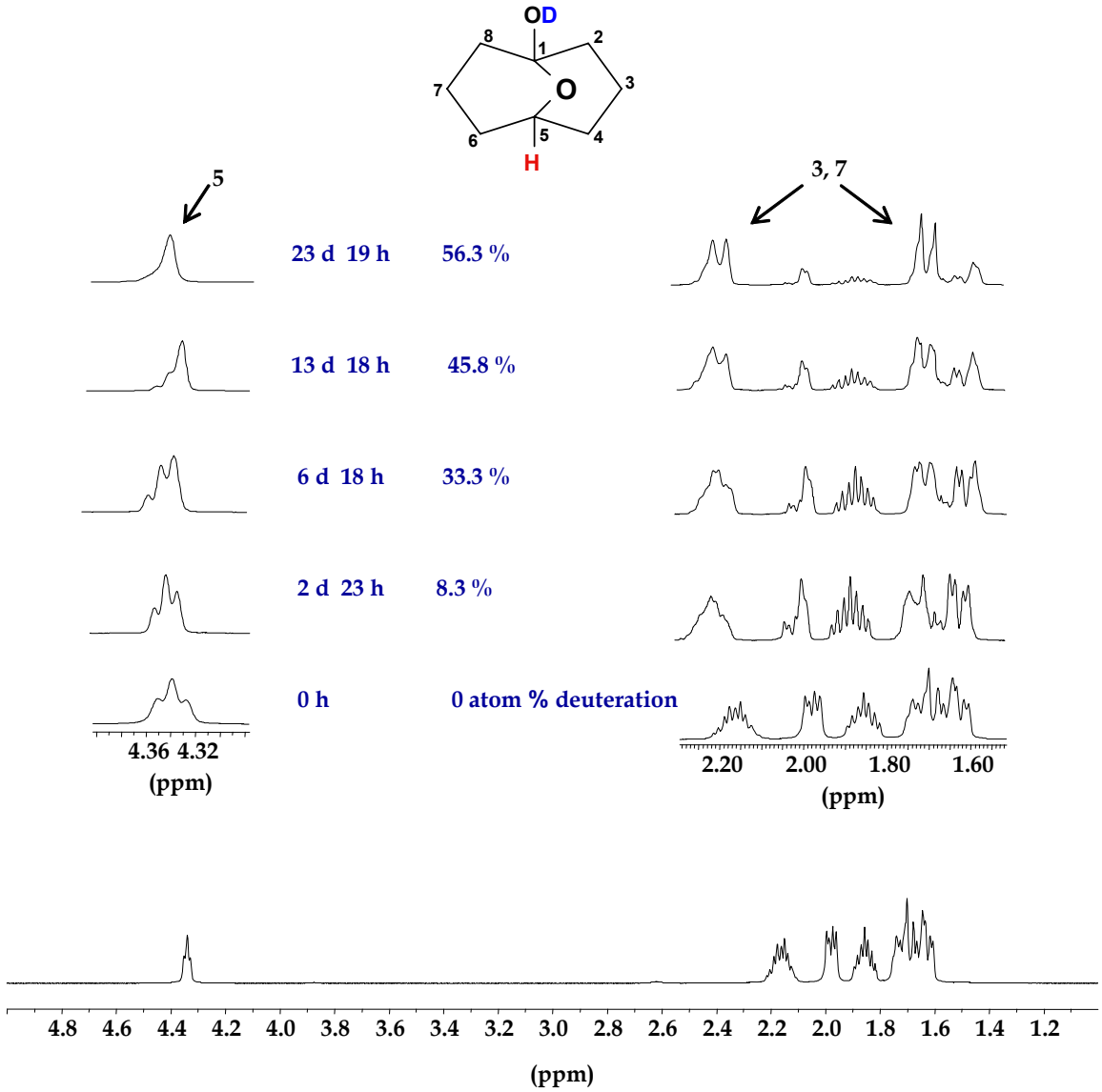

Figure 8.6: ^{1}H-NMR spectra for **1a** undergoing H/D exchange in 3.4 M DCl in D_2O at RT.

The ^{13}C-NMR spectrum shows four well defined signals (Figure 8.7). The most upfield signal at δ 19.20 ppm represents C-3 and C-7. The signal at δ 27.04 ppm for C-4, C-6 and the signal at δ 34.73 ppm for C-2, C-8 became weak clusters in 23 d 19 h. These shapes are due to the exchange of protons with deuterium atoms on the corresponding carbon atoms. The intensity of the signal at δ 72.84 ppm corresponding to C-5 is reduced to a large extent. This implies that deuterium atoms were present at α postions to C-5, i.e., C-4 and C-6. The results obtained from both ^{1}H- and ^{13}C-NMR can be explained by the mechanism based on intramolecular 1,5-hydride shift (Scheme 8.4).

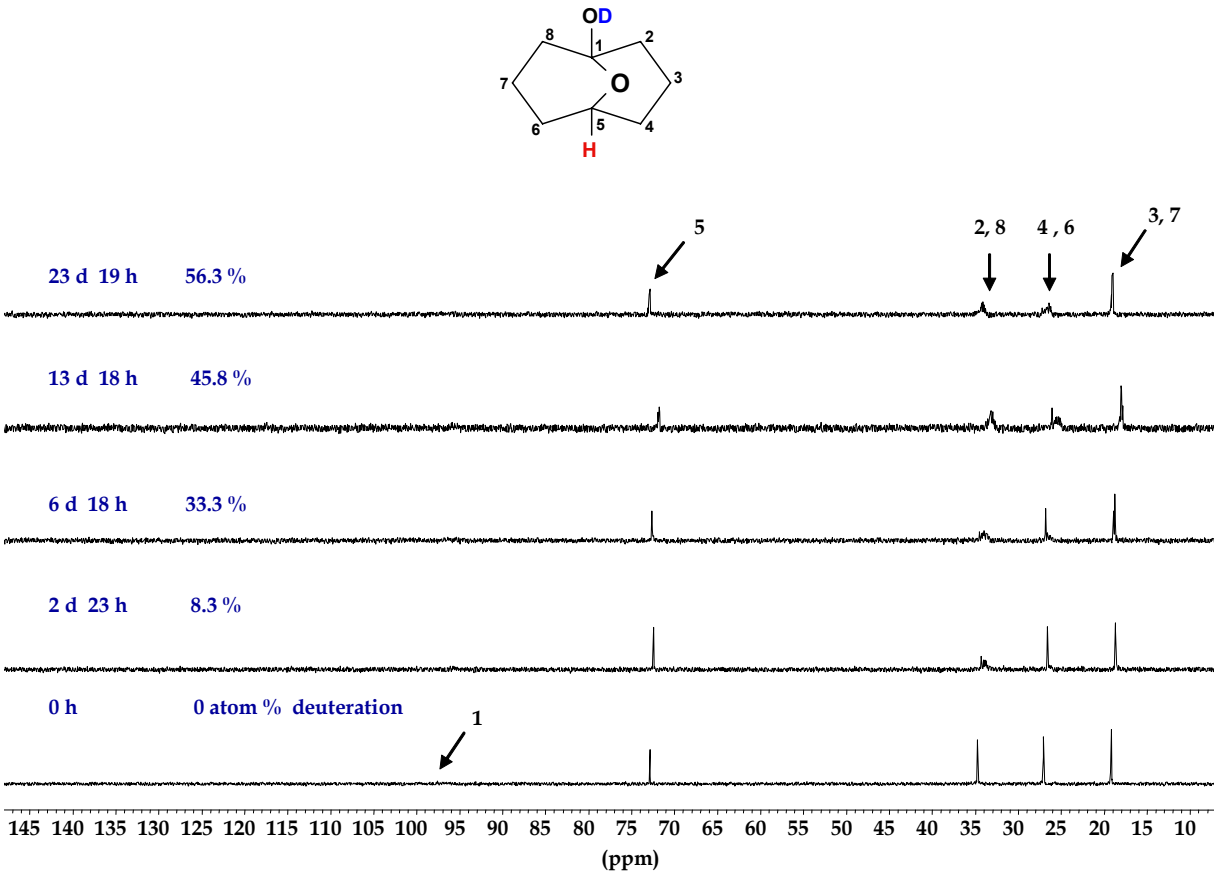

Figure 8.7: ^{13}C-NMR spectra for **1** undergoing H/D exchange in 3.4 M DCl in D_2O at RT.

8.4 Mechanism for the acid-catalysed transannular 1,5-hydride shift

The surprising results described in the previous sections indicate that there exists a mechanism which permits exchange of protons at C-2, C-4 C-6 and C-8 with deuterium in **1a**. Based on the deuteration experiments reported here and in the literature[58] a mechanism was postulated to explain these findings (Scheme 8.4).

a. The formation and breaking of the oxo-bridge in **1a** is catalysed by acid. The hydroxy group or the ethereal oxygen is more basic[204] by 3-4 pK_a units than the carbonyl oxygen. This implies that protonation preferentially occurs at the alcohol or ethereal oxygen.[204] Protonation of the ethereal oxygen leads to opening of **1a** to **1**. Due to the presence of acid **1a** opens to hydroxy-ketone **1** in D_2O at room temperature. This leads to exchange of the α protons with deuterium atoms by enolisation (Appendix 14.2). As a result the complex

multiplet region in the ^{1}H-NMR spectra became relatively simple at 0 h. In the ^{13}C-NMR spectra the signal corresponding to C-2 and C-8 became a weak cluster, whereas the signal for C-1 disappeared. These observations can only be explained by keto-enol tautomerism.

b. Due to the protonation of the carbonyl carbon an electrophilic centre is generated. The methine hydrogen atom from C-5 shifts to the electrophilic centre as hydride. As a result protons H-5 and H-6 are exchanged with deuterium by a keto-enol process. When all the adjacent hydrogen atoms are replaced by deuterium atoms the triplet signal becomes a singlet because of small H-D coupling. The number and position of the deuterium atom incorporation ruled out the possibility of hydride shift from other positions except C-5. The mechanism discussed above accounts for the NMR signals obtained in deuteration experiments reported here. These results can be explained by a mechanism based on a transannular 1,5-hydride shift (Scheme 8.4).

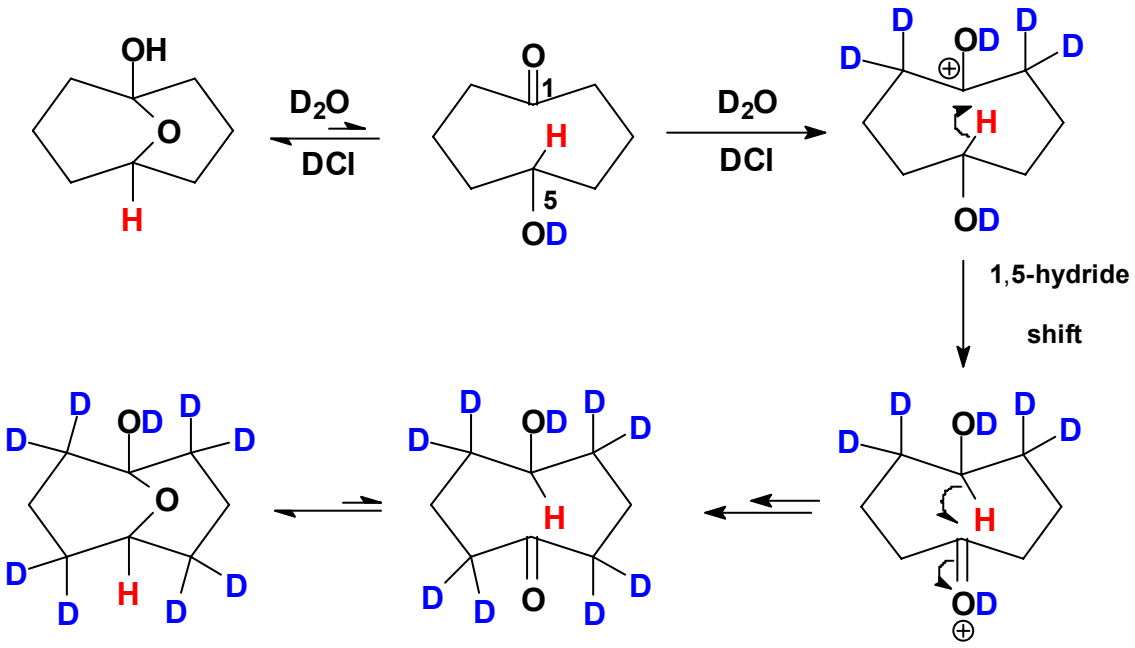

Scheme 8.4: Possible mechanism for H/D exchange and acid-catalysed transannular 1,5-hydride shift in **1**/**1a**.

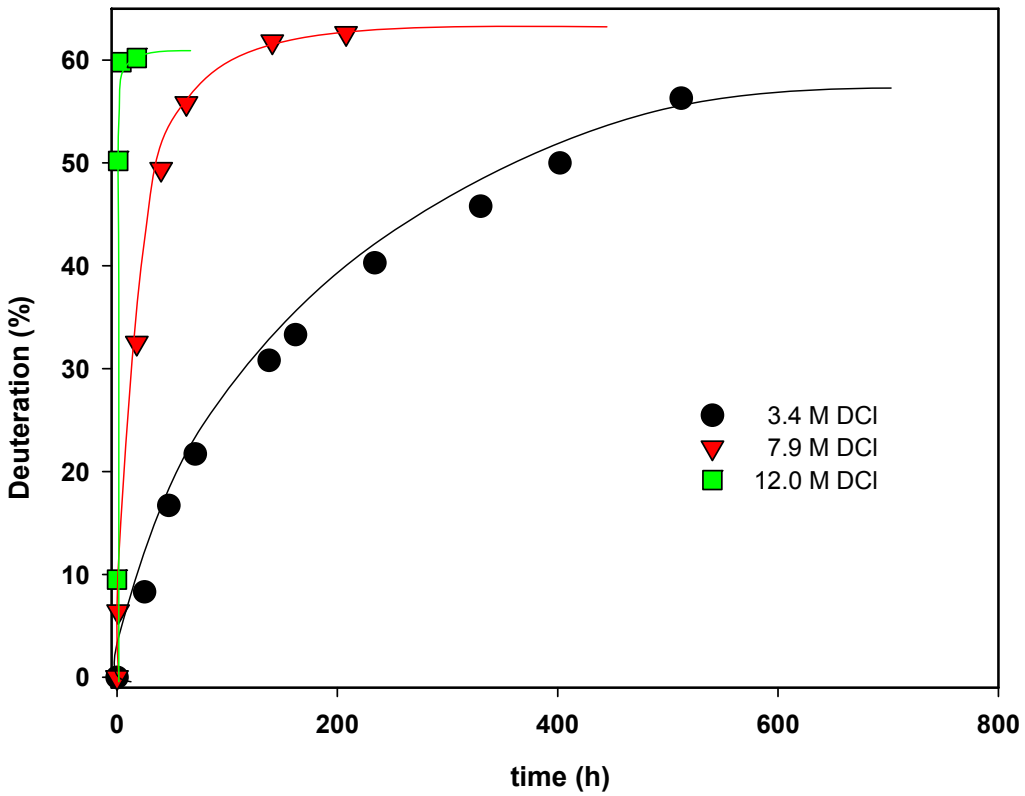

Figure 8.8: Plots of atom % deuteration in **1a** as function of time at different concentrations of DCl in D_2O solution at RT.

The plot of atom % deuteration versus time is shown in Figure 8.8. The rate of exchange of the protons with deuterium atoms is fast under strong acidic conditions but decreases remarkably with decrease in the acid concentration. However, at higher temperatures the possibility of a fast rate of the transannular 1,5-hydride shift at low acid concentration cannot be ruled out. The graph shows that the transannular 1,5-hydride shift is dependent on the acid concentration.

8.5 Conclusion

The NMR experiments have clearly shown that the transannular 1,5-hydride shift occurs in the presence of acid. The rate of the reaction is dependent on the concentration of the acid and the temperature. The reaction is fastest at a concentration of 12.0 M and decreases as the concentration decreases from 7.9 to 3.4 M DCl in D_2O.

9 Base-catalysed transannular 1,5-hydride shift in 1

In the classical Meerwein-Ponndorf-Verley (MPV) reduction a metal alkoxide transfers hydride reversibly to a carbonyl acceptor either inter- or intra-molecularly, thus aiding the oxidation-reduction of a carbinol-carbonyl pair (Scheme 9.1).[209] It is characterised by an especially mild nature of reaction conditions, excellent yields and high selectivity.[210] Many alkoxides are effectively utilized in these redox processes.[210, 211]

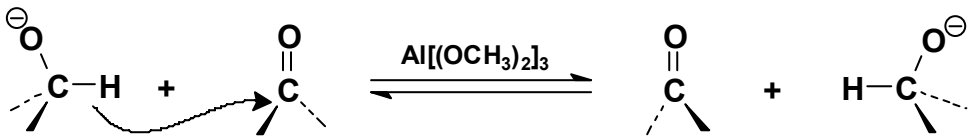

Scheme 9.1: Oxidation-reduction of a carbinol-carbonyl pair in the presence of aluminium alkoxide.

One such example[205] is the rearrangement of **75** to **76** (Scheme 9.2). In this compound 1,4-hydride shift occurs when **74** is converted to the alkali metal salt **75** in DMSO. Relative rates of transannular 1,4-hydride shift were found to be dependent on the counter metal ions.

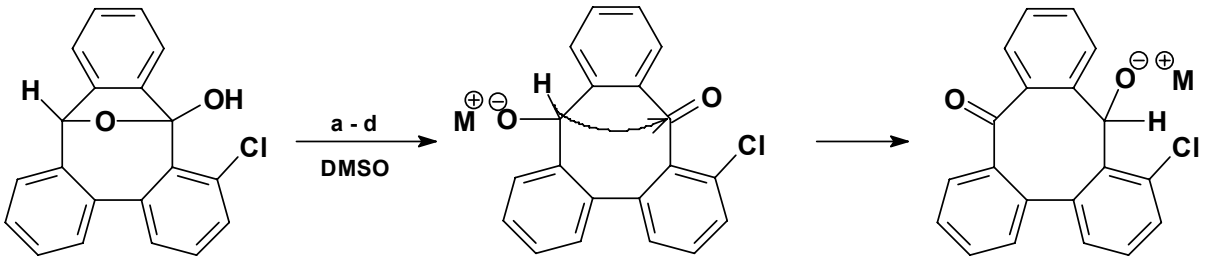

74 **75** **76**

M^+: a = Li^+, b = Na^+, c = K^+, d = Cs^+

Scheme 9.2: Intramolecular transannular 1,4-hydride shift in the presence of alkali metal salts.

A number of studies on rationally designed substrates have been reported by Watt and co-workers.[194] The substrates are rigid and the hydrogen atom is held within

spatial proximity of the electrophilic centre (carbonyl carbon) and is unable to escape. Rigidity of the system seemed to ease the hydride shift.

Not much is known about the degenerate transannular hydride shift in flexible medium-ring hydroxy-ketones.[58] In such substrates competitive reactions such as internal hemiacteal formation are equally possible. The NMR studies carried out for **1a** in the presence of acid has revealed the existence of the intramolecular 1,5-hydride shift. In this chapter we present NMR studies on the base-catalysed transannular 1,5-hydride shift.

9.1 NMR experiment in the presence of 1.30 M NaOD

The initial NMR experiment was done in 1.30 M NaOD in D_2O. In the ^{1}H-NMR spectrum a broad signal at δ 4.08 ppm was assigned to H-5 (Figure 9.1). The complex multiplet at δ 1.36 – 1.93 ppm is assigned to the twelve methylene protons. The deuteration was 14.3 atom % at 0 h. The deuteration percentage was calculated in a similar way as discussed in chapter 8. After 4 h the multiplet region was replaced by two broad doublets at δ 1.46 and 1.91 ppm corresponding to methylene protons at C-3 and C-7. The broad doublet corresponding to the methine proton H-5 became a singlet (δ 4.06 ppm). The degree of deuteration was 55.8 atom %. It increased further to 56.6 atom % within 23 h. No major change was observed in the spectra during a time interval between 4 to 23 h.

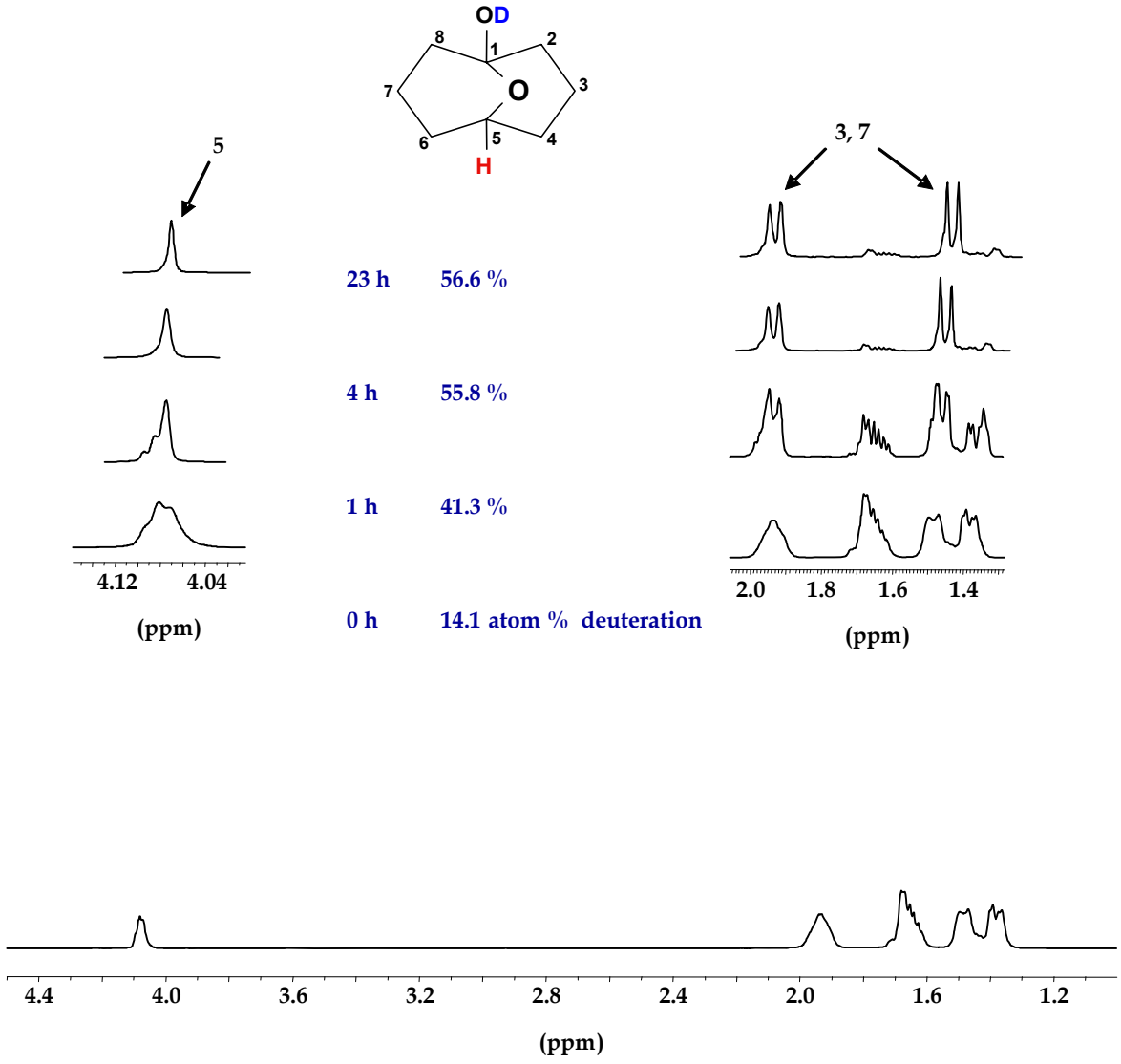

Figure 9.1: ^{1}H-NMR spectra for **1a** undergoing H/D exchange in the presence of 1.30 M NaOD in D_2O at RT.

The ^{13}C signals corresponding to C-2, C-8, C-4, C-6, and C-1 were reduced in heights as compared to the signal for C-5 after 23 h (Figure 9.2). The deuteration is 56.6 atom % after 23 h.

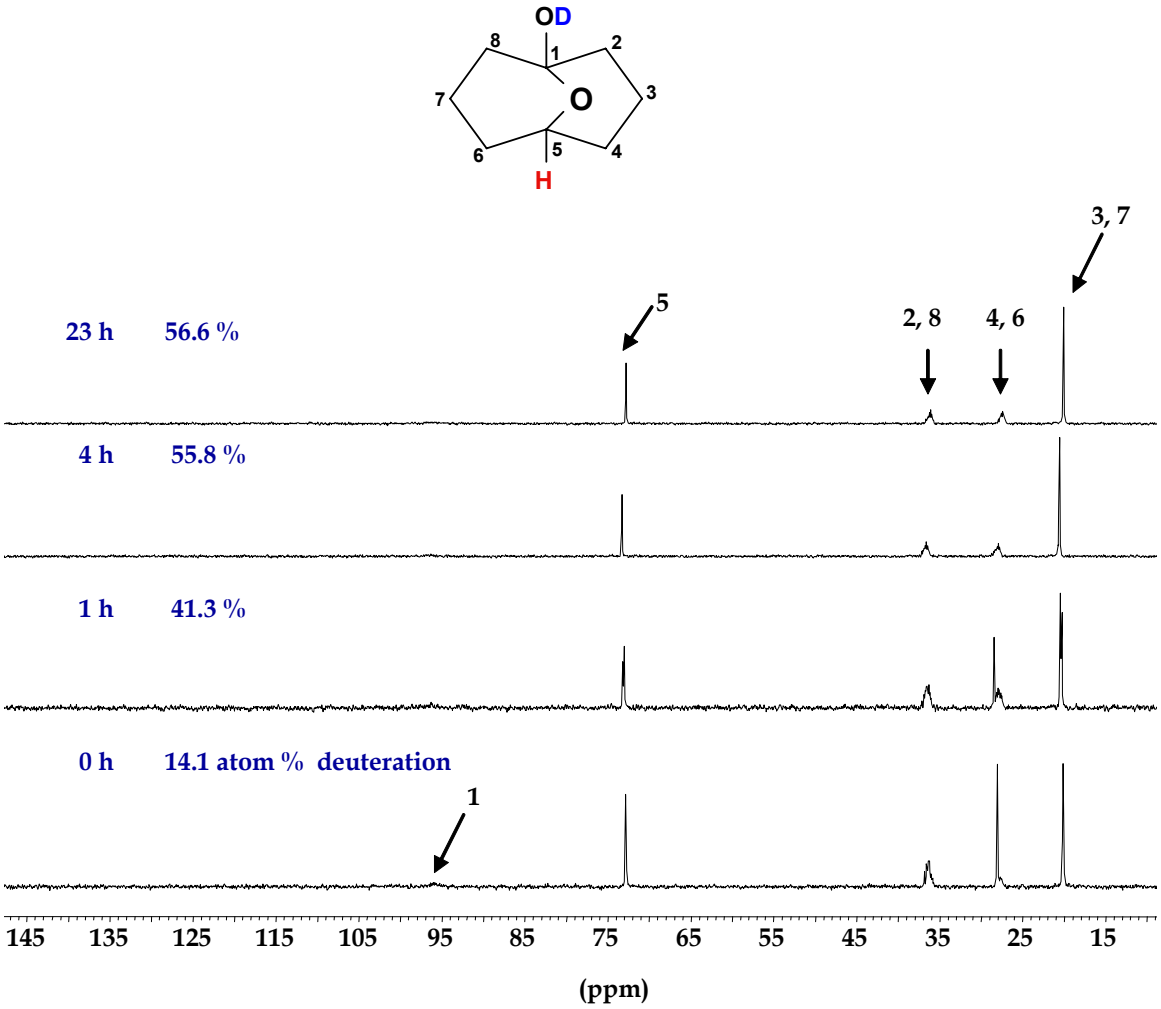

Figure 9.2: ^{13}C-NMR spectra for **1a** undergoing H/D in the presence of 1.30 M NaOD in D_2O at RT.

9.2 NMR experiment in the presence of 0.65 M NaOD

The ^{1}H- and ^{13}C-NMR spectra recorded for the solution of **1a** containing 0.65 M NaOD in D_2O are given in Figures 9.3 and 9.4. The signal of the methine proton H-5 appeared at δ 4.08 ppm as triplet whereas the signal for twelve methylene protons appeared as a complex multiplet at δ 1.35 – 1.93 ppm. The degree of deuteration was 12.9 atom % at 0 h.

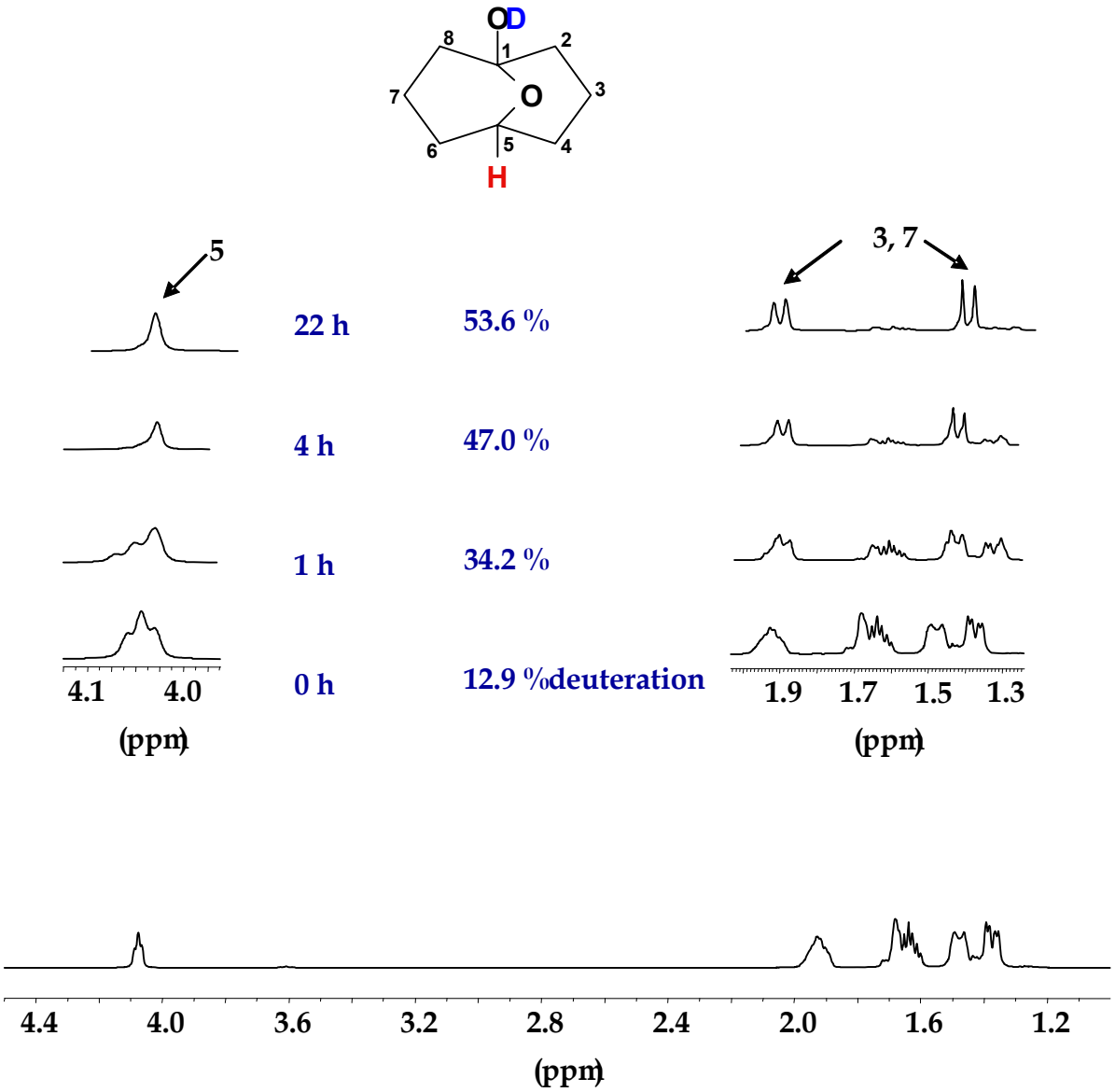

Figure 9.3: ^{1}H-NMR spectra for **1a** undergoing transannular 1,5-hydride shift in 0.65 M NaOD in D_2O at RT.

The degree of deuteration after 22 h was found to be 53.6 atom %. The spectrum became rather simple showing two doublets at δ 1.45 and 1.90 ppm. The signal corresponding to the methine proton H-5 reduced to a singlet. The ^{13}C-NMR spectrum (Figure 9.4) also shows the splitting patterns and low intensity of the signals corresponding to C-2, C-8, C-4, C-6, C-1 and C-5.

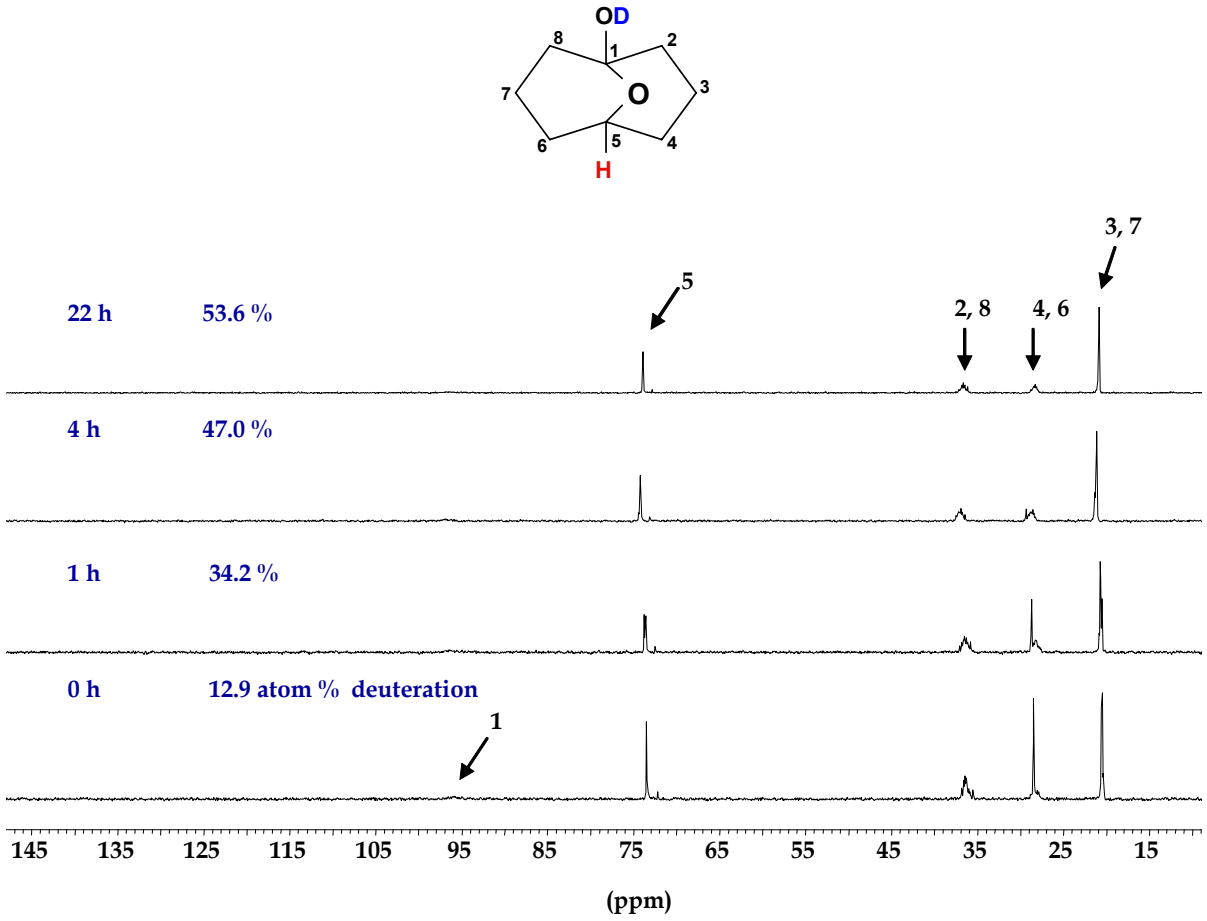

Figure 9.4: ^{13}C-NMR spectra for **1a** undergoing transannular 1,5-hydride shift in 0.65 M NaOD in D_2O at RT.

9.3 Mechanism for the base-catalysed transannular 1,5-hydride shift

The transannular 1,5-hydride shift in the presence of base is expected in **1a**. The oxo-bridge in **1a** breaks in the presence of base and thus the open form, i.e., 5-hydroxycyclooctanone (**1**) is available in solution (Scheme 9.3). The carbonyl carbon in **1** undergoes a nucleophilic attack by the potential hydride, i.e., the methine hydrogen atom present at C-5. The presence of the metal counterion facilitates the cleavage of the C-H bond[212] (discussed in detail in chapter 10). The occurrence of transannular 1,5-hydride shift in **1** is established by the fact that eight hydrogen atoms (at C-2, C-4, C-6 and C-8) are exchanged for deuterium. The exchange of protons at the α carbons to the carbonyl carbon in presence of base is due to keto-enol tautomerism (Appendix 14.3).

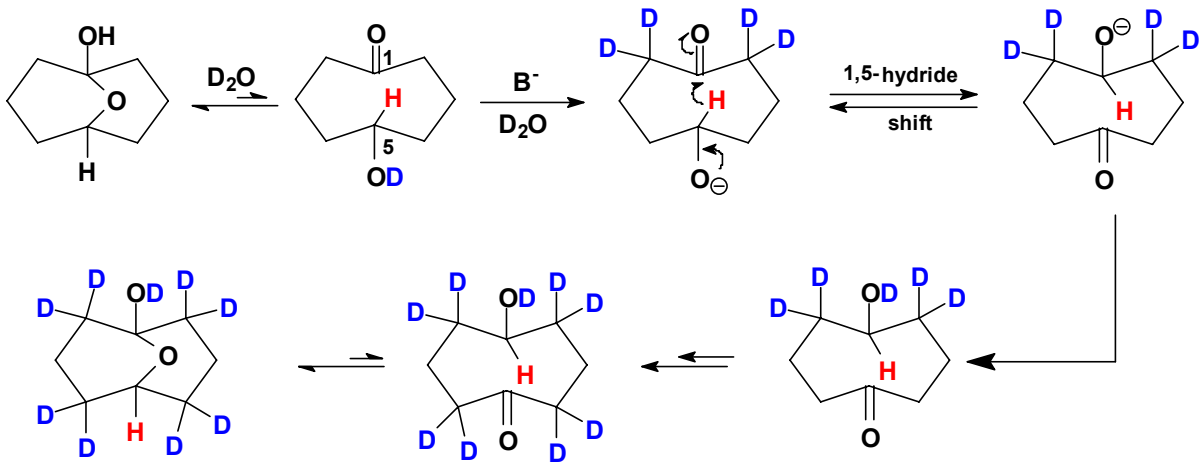

Scheme 9.2: Proposed mechanism for the base-catalysed transannular 1,5-hydride shift in **1**.

The plot showing deuteration versus time at NaOD 1.30 and 0.65 M concentrations reveals that the rate of deuteration depends on the concentration of the base (Figure 9.5). This implies that the rate of the transannular 1,5-hydride shift depends on the concentration of the base.

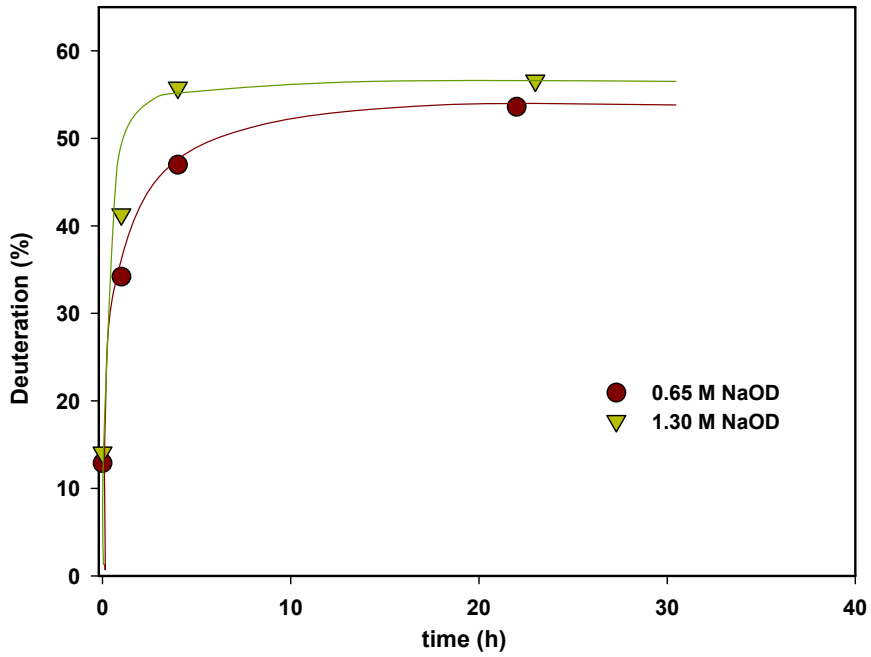

Figure 9.5: Plots of atom % deuteration in **1** as function of time at different concentration of NaOD in D_2O solution.

9.4 Conclusion

The NMR experiments carried out for **1a** in the presence of base have clearly shown that the transannular 1,5-hydride shift occur at room temperature in D_2O. The rate depends on the concentration of the base.

10 Transannular hydride shift: Theoretical mechanistic study

10.1 Introduction

The occurrence of 1,5- and 1,6-hydride shift[58] in **1** (chapters 8 and 9) and **5**, respectively, have been well-established. Similar experimental studies are not yet reported for systems **2** and **4**. On the other hand experimental and theoretical studies regarding inter- and intramolecular 1,4-hydride shift have been reported for a number of systems.[74, 208, 213] These were mostly rigid, for example, intramolecular 1,4-hydride in polycyclic hydroxy-ketones.[74] The conformation of the imbedded 4-hydroxycyclohexanone in the polycyclic hydroxy-ketone is fixed, i.e., boat. It is known that competitive inter- and intramolecular hydride shift occurs in 4-hydroxycyclohexanone in the presence of base.[199, 213] Reaction centres in rigid molecules are fixed with respect to the remainder of the molecular skeleton. Hence, perturbations due to conformational changes are effectively diminished or removed. This simplifies the understanding of the reactions taking place and of structure property relationships.

For the 1,x-hydride shift (x = 4 – 6) in model systems **1**, **2**, **4** and **5** questions regarding the relative importance of factors such as proximity between the methine hydrogen and the carbonyl carbon atom are not yet clear. In addition to the geometric factors, experimental conditions such as use of acid or base or solvent are interesting factors to study. With this aim we have carried out an intensive theoretical investigation on model compounds **1**, **2**, **4**, and **5** (Scheme 10.1).

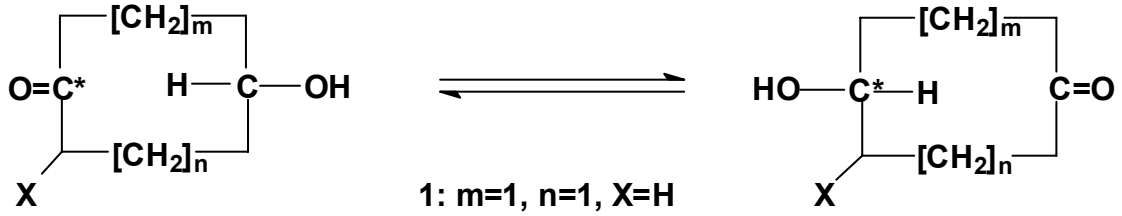

1: m=1, n=1, X=H
2: m=2, n=0, X=H
4: m=1, n=1, X=Br
5: m=2, n=2, X=H

Scheme 10.1: General representation for the degenerate and non-degenerate oxidation-reduction rearrangement involving intramolecular transannular 1,x-hydride shift (x = 4 – 6).

The selected conformers were optimised at the B3LYP/6-31+G* level of theory. To represent hydride properly p-polarisation for the H atom is needed, so single point calculations were carried out at the B3LYP/6-31+G** level. The 1,x-hydride transfer (x = 4 – 6) reaction pathway for the model compounds was studied for the uncatalysed, acid- (simulated with protonated oxygen of the carbonyl group) and base-catalysed reaction (simulated by replacing OH with OLi).

10.2 Results for the intermolecular hydride shift in the prototype system

10.2.1 Structural features

For a comparative study, first we have investigated the prototype system methanol (**77**) and formaldehyde (Table 10.1). The base-catalysed reactions are simulated by replacing OH by OLi, i.e., **77li** (Table 10.1). The bond distances and angles change in **77li**. The C-H* bond length increases from 1.092 (**77**) to 1.107 Å (**77li**). The C-O bond length decreases from 1.425 (**77**) to 1.381 (**77li**) Å. The C-O bond length in **77li** is less than a C=O bond length. The angle H–O–C (109.1°) in **77** changes to linear Li–O–C (180.0°) in **77li**. The presence of a metal counterion can generate an incipient hydride upon formation of the metal alkoxide from the respective alcohol due to reorganisation of atomic charges, molecular geometries and weakening of the C-H bond.[214] Earlier studies reported by Steigerwald *et al*.[212] have also shown that the C-H bond in methanol is weakened on going to the corresponding alkali methoxide by 10 to 12 and 17 kcal mol^{-1} on going to the anion.

10.2.2 Transition-state calculations

For simiplicity and better understanding of the intramolecular hydride shift we have calculated the transition-state **78** (Figure 10.1) for the reaction between formaldehyde and methanol (**77**). The transfer of the hydrogen atoms proceeds through a highly symmetric six-membered ring. The transition-state located is consistent with the structure reported in the literature.[215] A large single imaginary vibrational frequency in the direction of the reaction coordinate was found. The large value indicates a curved energy surface. The activation energy for the reaction with respect to the isolated reactants is 26.4 kcal mol^{-1} (Figure 10.2). The strain energy (645.0 kcal mol^{-1}) of the transition-state is calculated (at the MMFF level) by fixing the six-membered ring structure.

Table 10.1: Important geometrical parameters [bond distances (Å) and angle (°)] for **77** and **77li** (gas phase).

Molecular structure	Geometrical parameters			
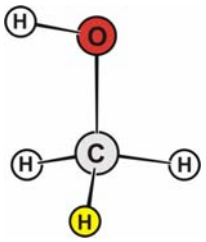 **77**	**C–H**	1.092		
	C–O	1.425	**H–O–C**	109.1
	O–H	0.965		
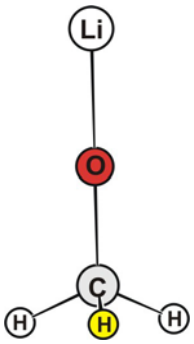 **77li**	**C–H**	1.107		
	C–O	1.381	**Li–O–C**	180.0
	O–Li$^+$	1.600		

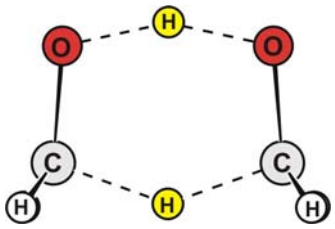

78 (-1537)

(**i**)

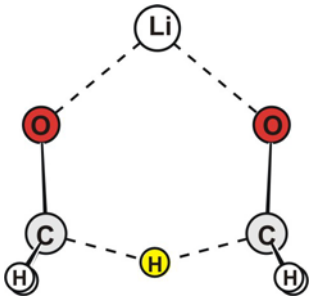

78li (-478)

(**ii**)

Figure 10.1: Calculated transition-states **78** and **78li** for the intermolecular hydride transfer between i) formaldehyde and methanol (**77**), ii) formaldehyde and lithium methoxide (**77li**). Imaginary frequencies (cm^{-1}) are given in parentheses.

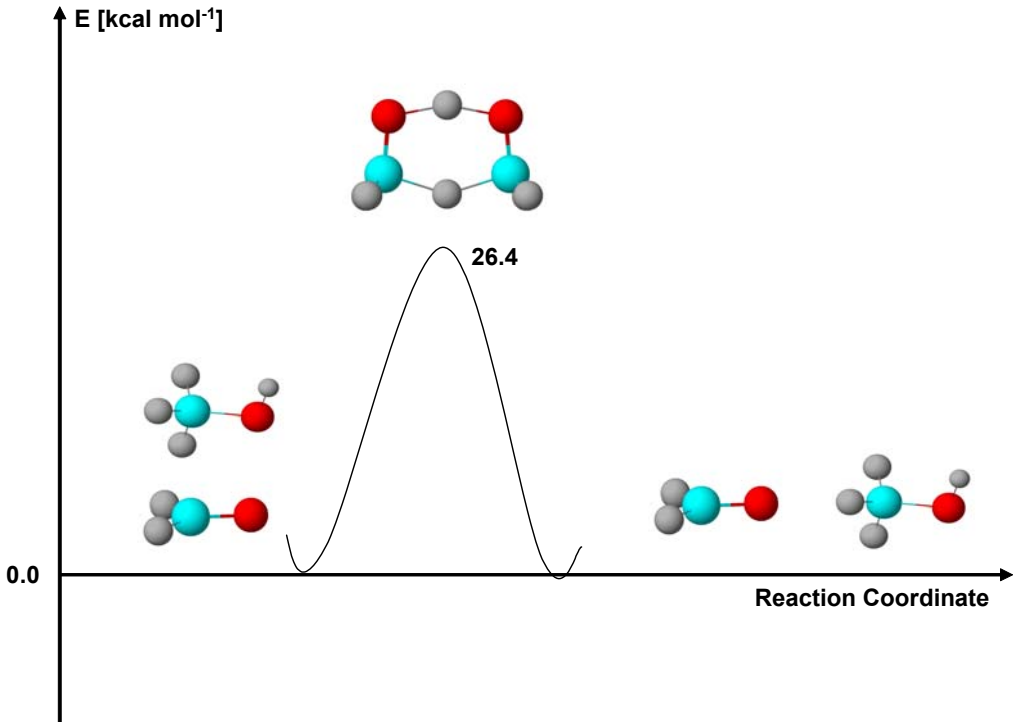

Figure 10.2: Energy profile for the gas phase reaction of formaldehyde and methanol (**77**).

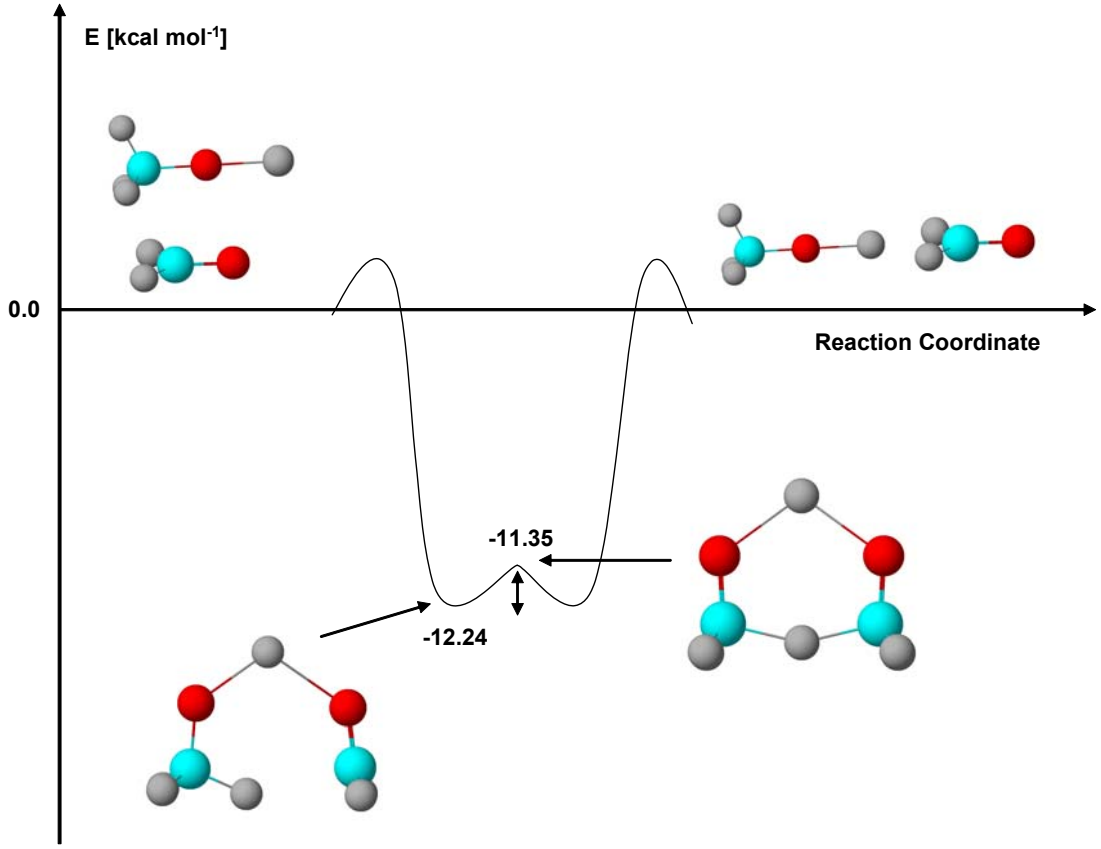

Figure 10.3: Energy profile for the gas phase reaction of formaldehyde and lithium methoxide (**77li**).

The transition-state **78li** calculated for the reaction between formaldehyde and lithium methoxide (**77li**) is shown in Figure 10.1. Both experimental and theoretical evidences suggest that the reaction proceeds through coordination of the metal ion simultaneously with both oxygens of the carbinol-carbonyl pair leading to a six-membered cyclic transition-state.[74, 194, 198, 199, 208, 216-218] A low energy complex **79li** (Figure 10.4) was located between formaldehyde and the lithium methoxide (**77li**). The calculation has shown the absence of an imaginary vibrational frequency for the complex **79li**. It is 12.2 kcal mol^{-1} more stable than the isolated reactants (Figure 10.3). The activation barrier for the hydride transfer is merely 0.9 kcal mol^{-1}. An interesting thing to note here is that both transition-states **78** and **78li** are symmetric (Figure 10.4). The partially formed C···H bonds are equally long in **78** and **78li**. In **79li** the six-membered ring is not symmetric.

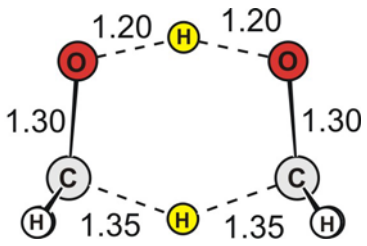

78

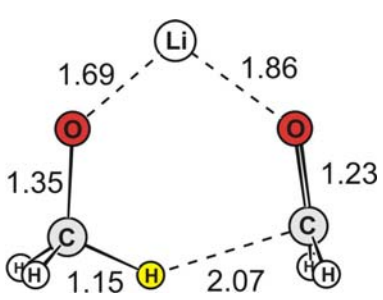

79li

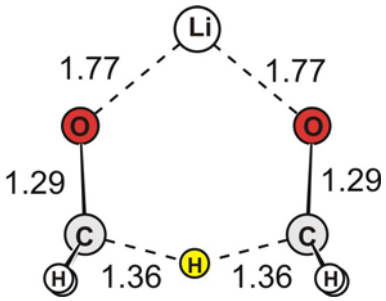

78li

	78	**79li**	**78li**
C–H–C	141.2	150.0	138.1

Figure 10.4: Important distances (Å) and angle (°) of the six-membered cyclic structure in **78**, **78li** and **79li**.

The angle between the migrating hydrogen and the carbinol-carbonyl carbon atoms are 141.2°, 150.0° and 138.1° in **78**, **79li** and **78li**, respectively. But for the intermolecular hydride shift a linear approach of hydride is reported.[219]

The natural charge distribution on the atoms involved in the formation of the six-membered ring is given in Figure 10.5. The charge on the migrating hydrogen atom in **78**, **79li** and **78li** is 0.168, 0.116 and 0.145 e, respectively. This is consistent with the literature[197] that the charge on the migrating hydrogen atom is not negative. Houk *et al.*[218] have reported that the charge on the transferring hydride is only -0.1 to -0.2 e. There is little hydride character on the migrating hydrogen and the transition-state is tight for methoxide and formaldehyde. The charge is very little, clearly pointing towards a very flat transition-state structure. The charge on the migrating hydrogen is less positive in **79li** than in **78** and **78li**. The charges on the carbon atoms in **78li** are less negative than in **78**.

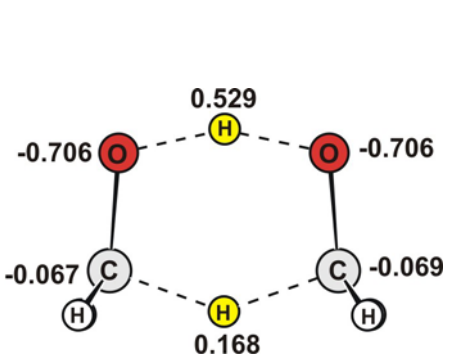

78

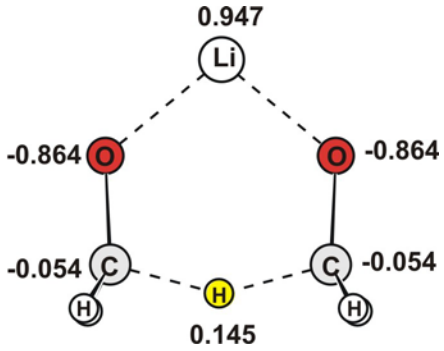

78li

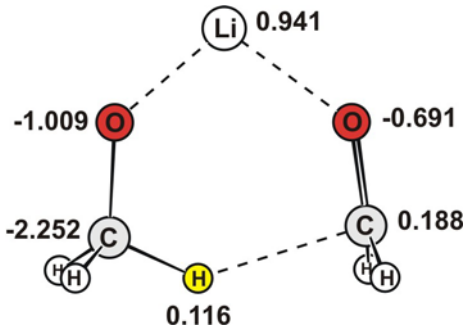

79li

Figure 10.5: Natural charge (e) distribution on the atoms involved in the formation of a six-membered ring during intermolecular hydride shift in transition-states **78**, **78li** and complex **79li**.

10.3 Results for the transannular 1,5-hydride shift in model compound 1

Initially a conformational search (at MMFF level) available in Spartan04 was carried out since model compound **1** is flexible. The number of conformers generated was 55 (Figure 10.6). Out of these only four were selected on the basis of the proximity of the reacting atoms, i.e., carbonyl carbon and methine hydrogen atom. The four unique conformers **80** – **83** are illustrated in Table 10.2.

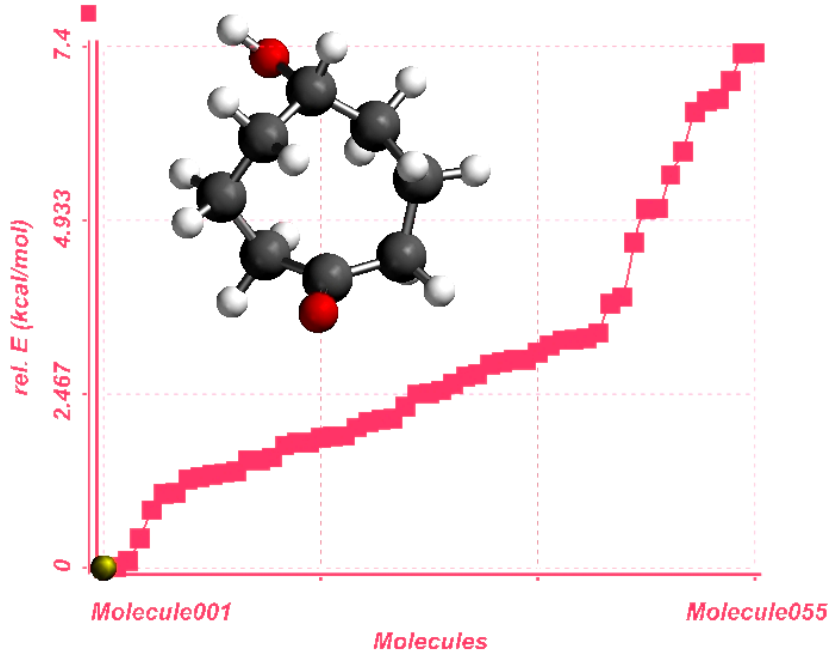

Figure 10.6: Energy profile of the conformer distribution for the *exo*-conformer of **1** at MMFF level.

10.3.1 Structural features and energetics

The interaction of the reacting atoms depends on the distance and the angle of attack between the reacting atoms in the starting conformers. The various geometric parameters related to the nucleophilic attack are shown in Scheme 10.2. The nucleophilic approach trajectory is described in terms of the attack angle θ_H between the developing C···H bond and the C=O bond. Due to the close nucleophilic approach of the hydride the carbonyl carbon atom becomes pyramidal which is denoted by Δ_H. The distance between the methine hydrogen and the carbonyl carbon atom is denoted by d_H. The other parameters of interest are the distances C-O (d_2), C···C (d_3) and C-H (d_4).

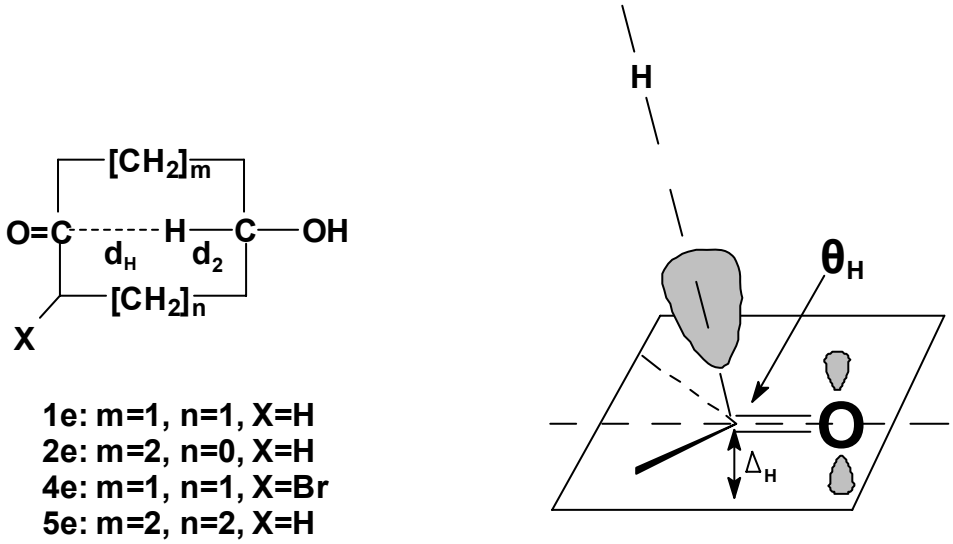

1e: m=1, n=1, X=H
2e: m=2, n=0, X=H
4e: m=1, n=1, X=Br
5e: m=2, n=2, X=H

Scheme 10.2: Important geometrical parameters such as non-bonded distance (d_H), angle of attack (θ_H) and deviation of the carbonyl carbon atom from its plane (Δ_H) in *exo*-conformers of model compounds **1**, **2**, **4** and **5**.

The chosen conformers **80** – **83** were characterised and it was found that they differ in energy as well as in proximity of the atoms required for nucleophilic attack (Table 10.2). The most stable conformer is **81** which is boat-chair (*bc*) and this is in agreement with the reported most stable conformation for the cyclooctanone.[189, 220] The least stable conformer is **82** (boat-boat, *bb*). The vdW distance between the carbon and the hydrogen atoms is 2.95 Å. The reacting groups, i.e., H and >C=O in **82** are in the closest proximity (2.4 Å). The distance d_H is maximum in **80**. The close approach of the nucleophile leads to the greater development of non-planarity of the carbonyl system in **82** (Δ_H = 0.038 Å).

Table 10.2: Important geometrical parameters in **80** – **83** and relative energies including the zero point energy (gas phase). [Distances (Å); angles (°), rel. energies (kcal mol^{-1})].

Molecular structure		Geometrical parameters		
			θ_H	Δ_H
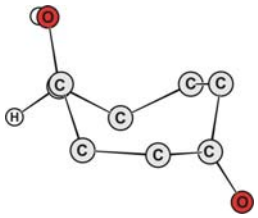 **80** (1.877)	d_H	4.306	117.7	0.007
	d_2	1.438		
	d_3	3.593		
	d_4	1.103		
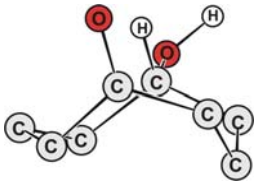 **81** (0.000)	d_H	2.643	89.8	0.008
	d_2	1.441		
	d_3	3.113		
	d_4	1.002		
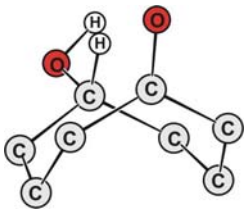 **82** (3.375)	d_H	2.425	94.1	0.038
	d_2	1.439		
	d_3	3.009		
	d_4	1.099		
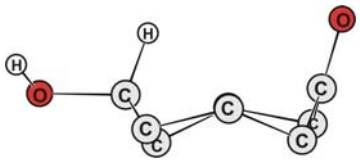 **83** (1.655)	d_H	3.051	88.9	0.016
	d_2	1.443		
	d_3	3.278		
	d_4	1.102		

In **82** the C-H bond length d_4 is 1.099 Å and this is similar to the C-H bond length in a secondary alcohol.[221] The attacking angle θ_H is 94.1° in **82**. Comparison of the geometrical parameters reported here for conformers **80** – **83** clearly indicates that the conformer **82** allows the best interaction for the methine hydrogen and the $\pi^*_{C=O}$ of the electrophilic carbonyl C atom for a nucleophilic attack.

10.3.2 Bonding and interactions

Natural bond orbital analysis was performed for the interaction between the methine hydrogen and carbonyl carbon atom in all the optimised conformers **80** – **83** in their respective ground states (Table 10.3). The comparison is made with respect to the second order interaction between the donor and acceptor orbitals. Conformers **80** and **83** do not show any interaction between the donor and acceptor orbitals. The second order energy is only 0.51 kcal mol^{-1} in **81**. The interaction between $\sigma_{C\text{-}H}$ and $\pi^*_{C=O}$ is maximal, i.e., 1.33 kcal mol^{-1} in **82**. This leads to increase in the occupancy of $\pi^*_{C=O}$ to 0.089 e.

Table 10.3: Natural bond order (NBO) analysis of conformers **80** – **83**. $E^{(2)}$ (kcal mol^{-1}) is the second order perturbation energy between Φ_i and Φ_j; E_j-E_i (a.u.) is the energy difference between NBOs Φ_i and Φ_j; F_{ij} (a.u.) is the Fock matrix element; only energies greater than the default threshold 0.5 kcal mol^{-1} are included in the table.

	Interaction	**Second-order Interaction**			**Occupancy (ρ)**	
		$E^{(2)}$	E_j-E_i	F_{ij}	$\sigma_{C\text{-}H}$	$\pi^*_{C=O}$
80	$\sigma_{C\text{-}H} \rightarrow \pi^*_{C=O}$	----	----	----	1.978	0.078
81	$\sigma_{C\text{-}H} \rightarrow \pi^*_{C=O}$	0.51	0.52	0.015	1.980	0.085
82	$\sigma_{C\text{-}H} \rightarrow \pi^*_{C=O}$	1.33	0.52	0.024	1.974	0.089
83	$\sigma_{C\text{-}H} \rightarrow \pi^*_{C=O}$	----	----	----	1.972	0.084

To simulate the acidic conditions we have taken the corresponding protonated optimised conformers **80a** – **83a** (Table 10.4). It is well known that protonation of the oxygen atom of a carbonyl group initiates nucleophilic attack and transfer of hydride from a nonactivated CH group to a carbenium ion can occur with great rapidity.[222] Moreover, carbocations are generally known to undergo inter- and intramolecular hydride shift reactions from carbon-hydrogen donors. In conformers **80a** and **83a** interaction between donor and acceptor is found to be absent. The second order interaction between donor and acceptor orbital in conformer **82a** is strongest, i.e., 6.55 kcal mol^{-1}. The second order interaction energy is about 5 times greater in the protonated conformer **82a** than in the neutral conformer **82**. The electron population in $\pi^*_{C=O}$ of **82a** is 0.275 e as compared to low occupancy (0.089 e) in **82**. In the

protonated *bc* conformer **81a** the second order interaction energy is large (1.48 kcal mol^{-1}) as compared to the corresponding neutral conformer **81** (0.51 kcal mol^{-1}).

Table 10.4: Natural bond order (NBO) analysis of protonated conformers **80a** – **83a**. $E^{(2)}$ (kcal mol^{-1}) is the second order perturbation energy between Φ_i and Φ_j; E_j-E_i (a.u.) is the energy difference between NBOs Φ_i and Φ_j; F_{ij} (a.u.) is the Fock matrix element; only energies greater than the default threshold 0.5 kcal mol^{-1} are included in the table.

	Interaction	**Second-order Interaction**			**Occupancy (ρ)**	
		$E^{(2)}$	E_j-E_i	F_{ij}	σ_{C-H}	$\pi^*_{C=O}$
80a	$\sigma_{C-H} \rightarrow \pi^*_{C=O}$	----	----	----	1.979	0.230
81a	$\sigma_{C-H} \rightarrow \pi^*_{C=O}$	1.48	0.38	0.022	1.971	0.237
82a	$\sigma_{C-H} \rightarrow \pi^*_{C=O}$	6.55	0.40	0.048	1.923	0.275
83a	$\sigma_{C-H} \rightarrow \pi^*_{C=O}$	----	----	----	1.983	0.081

The basic conditions for the 1,5-hydride shift reaction were simulated by replacing the hydrogen atom in the hydroxy group by a Li^+ counter metal ion (Table 10.5). Instead of other alkali ions such as K^+ or Na^+ we have taken Li^+ in order to save computation time. Again there is no interaction found between the donor and acceptor orbitals for conformers **80li** and **83li**, whereas the second order interaction energies are 0.67, 1.68 kcal mol^{-1} in **81li** and **82li**, respectively. The $\pi^*_{C=O}$ electron population is maximal, i.e., 0.095 e, in **82li**. These results show that the donor-acceptor interactions are strongest when the carbonyl oxygen atom is protonated, i.e., in acidic conditions. Lithium metal is a weak Lewis base. The experimental and theoretical studies reported before have clearly shown that the rate of hydride shift depends on the metal counter ion used to generate the metal alkoxide from the corresponding alcohol.[205, 214] Under all conditions, i.e., neutral, acidic and basic, conformers *bc* and *bb* have donor-acceptor interactions at the ground state. The energy difference between *bc* and *bb* is low enough to allow interconversion at room temperature.

Table 10.5: Natural bond order (NBO) analysis of lithiated conformers **80li – 83li**. $E^{(2)}$ (kcal mol^{-1}) is the second order perturbation energy between Φ_i and Φ_j; E_j-E_i (a.u.) is the energy difference between NBOs Φ_i and Φ_j; F_{ij} (a.u.) is the Fock matrix element; only energies greater than the default threshold 0.5 kcal mol^{-1} are included in the table.

	Interaction	**Second-order Interaction**			**Occupancy (ρ)**	
		$E^{(2)}$	E_j-E_i	F_{ij}	$\sigma_{C\text{-}H}$ →	$\pi^*_{C=O}$
80li	$\sigma_{C\text{-}H} \rightarrow \pi^*_{C=O}$	----	----	----	1.973	0.086
81li	$\sigma_{C\text{-}H} \rightarrow \pi^*_{C=O}$	0.67	0.49	0.016	1.975	0.089
82li	$\sigma_{C\text{-}H} \rightarrow \pi^*_{C=O}$	1.68	0.49	0.026	1.966	0.095
83li	$\sigma_{C\text{-}H} \rightarrow \pi^*_{C=O}$	----	----	----	1.979	0.082

10.3.3 Transition-state calculations

The optimised conformers **81** and **82** showing the donor-acceptor interactions between the electrophilic and nucelophilic units in their respective ground state were selected for the calculation of transition-states. The oxidation-reduction process in conformers **81** and **82** is similar to the dihydrogen transfer between ketone and alcohol (Table 10.6). On the potential energy surface several transition-state structures are possible because of the flexibility of the carbocyclic ring and a large number of low energy interconverting conformers. It is very difficult to simulate the real situation for the transannular 1,5-hydride process occurring in an eight-membered cyclic hydroxy-ketone. We have only calculated transition-states **84** and **85** with starting conformers **81** and **82**, respectively.

The transition-states **84** and **85** have *bc* and *bb* conformations, respectively. The transfer of the methine hydrogen to the carbonyl carbon atom and the hydroxy hydrogen to the oxygen atom of the carbonyl group took place *via* a symmetric six-membered ring irrespective of the conformation of the ring. It is similar to the six-membered ring structure in **78** (Figure 10.4). Both transition-states **84** and **85** are characterised by a single imaginary frequency corresponding to the motion of the hydrogen atom between the two carbon atoms. An interesting result is the similar activation energies for **81** → **84** and **82** → **85**.

Table 10.6: Calculated transition-states **84** and **85** for the uncatalysed hydride shift. Imaginary frequencies (cm^{-1}) and activation barriers including the zero point energy (kcal mol^{-1}) are given.

Transition-state structure	Reactants	ΔE_{act}
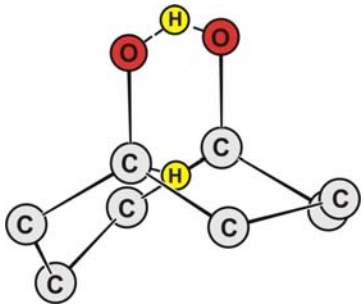 **84** (-1401)	**Conformer 81**	46.581
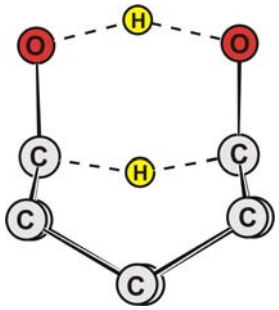 **85** (-1432)	**Conformer 82**	46.569

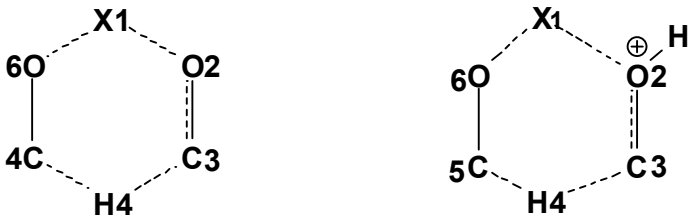

Figure 10.7: Representation of a six-membered cyclic transition-state in hydride shift reaction.

The six-membered ring of the reacting atoms is represented in Figure 10.7. The natural charges distribution on the atoms involved in the formation of the six-

membered cycle is given in Table 10.7. The charge on H(4) in **84** and **85** is 0.218 e. C(3) has a higher positive charge in **84a** and **85a** than in **84** and **85**, respectively.

Table 10.7: Natural charge (e) distribution on the atoms of the six-membered ring in transition-states **84**, **85**, **84a** and **85a** (see Figure 10.7).

	H(1)	O(2)	C(3)	H(4)	C(5)	O(6)
84	0.522	-0.743	0.311	0.218	0.311	-0.743
85	0.522	-0.723	0.293	0.218	0.317	-0.723
84a	0.568	-0.674	0.534	0.233	0.129	-0.724
85a	0.565	-0.673	0.527	0.228	0.136	-0.721

Table 10.8: Important geometrical parameters [distances (Å) and angles (°)] of the six-membered ring in transition-states **84** and **85**. Atom numbers are depicted in Figure 10.7.

	84	**85**
H(1)···O(2)	1.237	1.242
O(2)···C(3)	1.318	1.319
C(3)···H(4)	1.205	1.198
H(4)···C(5)	1.205	1.198
C(5)···O(6)	1.318	1.319
O(6)···H(1)	1.237	1.242
C(3)···C(5)	2.364	2.362
C(5)–H(4)–C(3)	157.5	160.5
O(2)–C(3)–H(4)	102.1	100.9
O(6)–C(5)–H(4)	102.1	100.9
H(1)–O(6)–C(5)	102.7	102.4
H(1)–O(2)–C(3)	102.7	102.4
O(6)–H(1)–O(2)	152.9	152.8

The various geometric parameters of the six-membered ring in **84** and **85** are compared (Table 10.8). The partially formed C(3)···H(4) and C(4)···H(5) bonds are 1.205 and 1.198 Å in **84** and **85**, respectively. According to Bürgi *et al.*[168] the

minimum energy position for a hydride in a nucleophilic attack is at a distance of 1.9 Å (as the hydride is approaching or leaving) in the plane perpendicular to the carbonyl group running through the carbonyl carbon atom. Such a motion of the hydride in medium-rings can create non-bonded repulsions and can lead to a rise of the energy barrier during hydride migration.

The tight geometry of the transition-state leads to non-bonded repulsions and this results in a higher activation barrier. Further evidence for the non-bonded repulsion in transition-states **84** and **85** was obtained by strain energy calculations at the MMFF level. The strain energies for **84** and **85** are 763.5 and 791.1 kcal mol^{-1}, respectively. The most constrained transition-state conformation is *bb* (**85**). About 27.6 kcal mol^{-1} of strain energy is released when a methylene group flips on going from the *bb* (**85**) to the *bc* (**84**) conformation. The calculated activation barriers give a semi-quantitative picture since the calculation was done in the gas phase in absence of a catalyst and solvent.

The NMR results reported in chapters 8 and 9 clearly show the transannular 1,5-hydride shift in 5-hydroxycyclooctanone in the presence of acid or base in water. The NBO analysis of the optimised conformers **81a** and **82a** has clearly shown the increase in donor-acceptor interactions when the carbonyl oxygen atom is protonated (Table 10.4). There are many examples of carbocations undergoing fast degenerate rearrangements through intramolecular hydride shifts due to their shallow potential energy surfaces.[223] The transition-states corresponding to conformers **81a** and **82a** were calculated (Table 10.9). The activation energy is 4.7 kcal mol^{-1} lower for **82a** → **85a** than **82** → **85**. The activation energy is 1.17 kcal mol^{-1} higher in the *bb* (**82** → **85**) than in the *bc* conformation (**81a** → **84a**). The $\Delta G^{\#}$ value found experimentally for the 1,5-hydride shift in the 2,4,4,6-tetramethylheptyl cation is 21.8 kJ mol^{-1} at -122 ºC and 5.0 kJ mol^{-1} in the 2,6-dimethyl-2-heptyl cation.[224] The low barriers were considered either due to a presumably linear or a less strained six-membered transition-state.

The transition-states **84a** and **85a** are very unsymmetrical as is indicated by the difference in bond angles and lengths of the atoms involved in six-membered cycle (Table 10.10). The migrating hydrogen is localised on C(3) rather than forming a symmetrical three-centre two-electron (3c-2e) bond as reported by Sorensen and McMurry.[72, 225]

The angle C(5)–H(4)–C(3) in **84a** and **85a** is 163.7° and 168.6°, respectively (Table 10.10). This implies that the transfer of hydride is almost linear and this is consistent with the reported[215, 219, 226-228] predicted preference. The transannular hydride shifts were considered to have transition-states which resemble μ-hydrido-briged carbocation structures.[67] Kirchen and Sorensen[67] have given NMR evidence for the presence of stable 1,5-hydride-briged cyclooctyl cations.

The natural charges on the atoms involved in 1,5-hydride shift in transition-states **84a** and **85a** are shown in Table 10.7. The natural charge on the shifting hydrogen atom H(4) are positive, i.e., 0.233 and 0.228 e in **84a** and **85a**,[197] respectively.

Table 10.9: Transition-states **84a** and **85a** with activation barriers including the zero point energy (kcal mol^{-1}) and imaginary frequencies (cm^{-1}) with respect to conformers **81a** and **82a**.

Transition-state structure	Reactants	ΔE_{act}
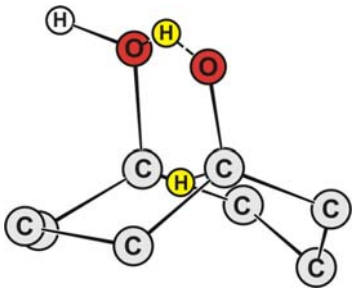 **84a** (-579)	**Conformer 81a**	40.732
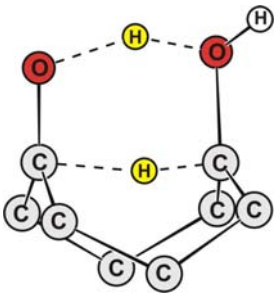 **85a** (-771)	**Conformer 82a**	41.903

Attempts were made to calculate transition-states starting with conformers **81li** and **82li** at the B3LYP/6-31+G* level. But frequency calculation showed absence of

imaginary frequency, thus characterising these structures as stationary structures. Despite much effort, no transition-state structure was located at B3LYP/6-31+G* level. On the other hand, Hartree-Fock (HF/6-31G**) optimisation was successful in search of transition-states **84li** and **85li** (Table 10.11). The structures obtained were connected to the minimum-energy conformations **81li** and **82li** on the potential energy surface. The imaginary frequencies correspond to the hydride motion along the reaction coordinate. It is highly possible that the reaction takes place with the initial formation of a low energy complex in which the Li ion is coordinated with both carbinol-carbonyl oxygen atoms. But we were not able to locate such a low energy complex. The activation barriers are 19.3 and 18.8 kcal mol^{-1} for **81li** → **84li** and **82li** → **85li**, respectively. The activation energy calculated (B3LYP/6-31+G*//HF/6-31G**) for **81li** → **85li** is 4.3 kcal mol^{-1}. According to variable temperature ^{1}H-NMR studies[206] on 7-*exo*-hydroxybicyclo[3.3.1]nonan-3-one the activation energy [$\Delta G^{\ddagger}$ (113 °C)] is 19.4 ± 0.2 kcal mol^{-1} for 1,5-hydride shift.

Table 10.10: Important geometrical parameters [distances (Å) and angles (°)] of the six-membered ring in transition-states **84a** and **85a**. Atom numbers are depicted in Figure 10.7.

	84a	**85a**
H(1)···O(2)	1.402	1.391
O(2)···C(3)	1.268	1.274
C(3)···H(4)	1.451	1.427
H(4)···C(5)	1.068	1.067
C(5)···O(6)	1.493	1.491
O(6)···H(1)	1.123	1.140
C(3)···C(5)	2.494	2.482
C(5)–H(4)–C(3)	163.7	168.6
O(2)–C(3)–H(4)	98.3	95.7
O(6)–C(5)–H(4)	95.9	94.3
H(1)–O(6)–C(5)	103.7	102.6
H(1)–O(2)–C(3)	106.1	106.7
O(6)–H(1)–O(2)	151.9	151.8

Table 10.11: Transition-states **84li** and **85li**, activation barriers including zero point energy (kcal mol^{-1}), imaginary frequencies (cm^{-1}), for the 1,5-hydride shift in conformers **81li** and **82li** (HF/6-31G**).

Transition-state structure	Reactants	ΔE_{act}
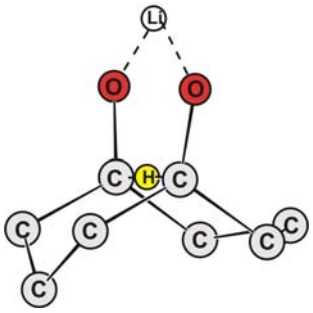 **84li** (-480)	**Conformer 81li**	19.339
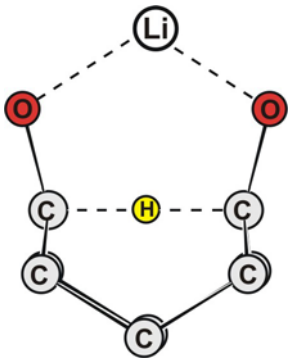 **85li** (-495)	**Conformer 82li**	18.785

Table 10.12: Important geometrical parameters [distances (Å) and angles (°)] in **84li** and **85li** for the intramolecular 1,5-hydride shift reaction. Atom numbers are depicted in Figure 10.7.

	84li	**85li**
H(1)···O(2)	1.845	1.857
O(2)···C(3)	1.287	1.289
C(3)···H(4)	1.217	1.219
H(4)···C(5)	1.217	1.219
C(5)···O(6)	1.287	1.289
O(6)···H(1)	1.845	1.857
C(3)···C(5)	2.432	2.436
C(5)–H(4)–C(3)	177.4	177.3
O(2)–C(3)–H(4)	104.8	104.5
O(6)–C(5)–H(4)	104.8	104.5
H(1)–O(6)–C(5)	108.3	106.4
H(1)–O(2)–C(3)	108.3	106.4
O(6)–H(1)–O(2)	113.8	115.5

According to literature[219] intermolecular hydride shift is linear as compared to the intramolecular hydride shift.[199, 229, 230] But the angle C(5)–H(4)–C(3) is slightly linear in **84li** and **85li** (Table 10.12).

The natural charge distribution on the atoms involved in the six-membered ring is given in Table 10.13. The migrating hydrogen H(4) in transitions-states **84li** and **85li** has positive charge.

Table 10.13: Natural charge (e) distribution on the atoms of six-membered ring in transition-states **84li** and **85li** (B3LYP/6-31+G**/HF/6-31+G**) (see Figure 10.7).

	X(1)	O(2)	C(3)	H(4)	C(5)	O(6)
84li	0.936	-0.882	0.307	0.185	0.307	-0.882
85li	0.933	-0.878	0.302	0.186	0.302	-0.878

10.4 Results for the transannular 1,4-hydride shift in model compound 2

The studies for the transannular 1,4-hydride shift were undertaken in conjunction with our efforts directed toward understanding the effect of the position of the functional group. The theoretical results for 5-hydroxycyclooctanone (**1**) have shown a high activation barrier for 1,5-hydride shift in the absence of acid or base in the gas phase. The large barriers were due to the presence of strain in the transition-states. It seems that the geometric parameters play an important role in determining the activation barriers of 1,5-hydride shift. These results have prompted us to carry out a computational study of the feasibility of 1,4-hydride shift in the eight-membered cyclic hydroxy-ketone **2** since experimental and theoretical investigations are not yet reported for this compound.

10.4.1 Structural features and energetics

A conformational search was performed as described in previous chapters to locate the lower energy conformers available for flexible 4-hydroxycyclooctanone with *exo*-orientation of the OH group. This search has generated 91 conformers (Figure 10.8). A number of conformers were optimised but out of these only five low energy conformers **86** – **90** were taken for further study (Table 10.14).

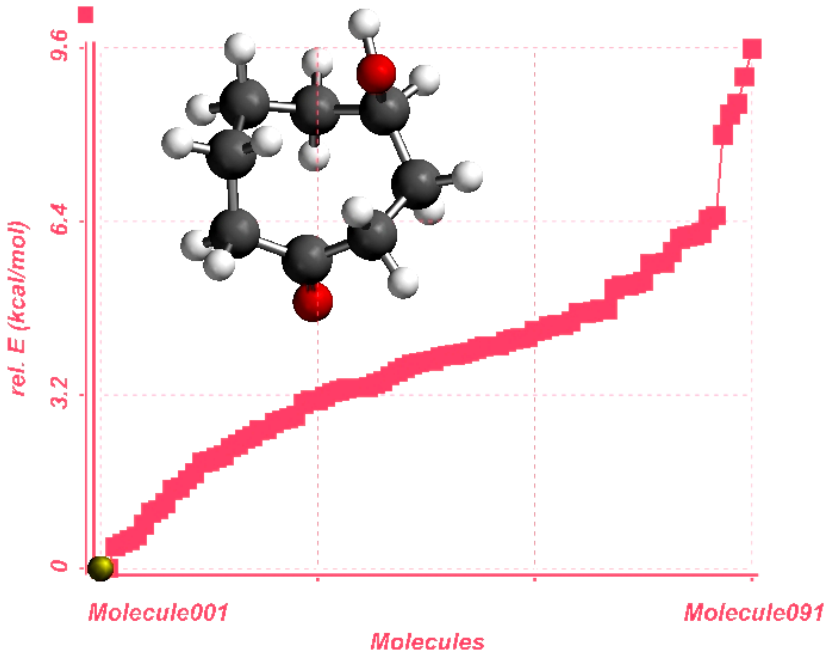

Figure 10.8: Energy profile of the conformer distribution for the *exo*-conformer of **2** at MMFF level.

The lowest energy conformer is **86**. Conformers **87** and **90** are only 0.621 and 0.659 kcal mol^{-1}, respectively, higher in energy than **86**. Investigation of the structural features of **86** and **87** reveal that the angle of attack θ_H by the potential methine hydride to the carbonyl carbon atom is found to be 90.6° and 91.0°, respectively. These values are in close agreement with the results of studies on compounds with a carbonyl group in the vicinity of a base in the crystal structure.[74] The distance d_H between the hydrogen atom and the carbonyl carbon is 2.61 and 2.65 Å in **86** and **87**, respectively, which is less than the corresponding vdW distance, i.e., 2.90 Å. Conformer **88** has highest energy among the optimised conformers. The distance d_H is least 2.425 Å. The Δ_H is maximal (0.015 Å) in **88**. Non-bonded atoms interact strongly when their distance is less than the sum of vdW radii. It is more likely that 1,4-hydride shift occurs in conformers **86** – **88** with ease than in the other conformers. In **89** and **90** the important structural parameters d_H, θ_H and Δ_H do not indicate facile 1,4-hydride shift. The d_H distances are near the sum of vdW radii of carbon and oxygen atoms.

Table 10.14: Important geometrical parameters in **86** – **90** and calculated relative energies including the zero point energy (gas phase). [Distances (Å); angles (°), rel. energies (kcal mol^{-1})].

Molecular structure		Geometrical parameters		
			θ_H	Δ_H
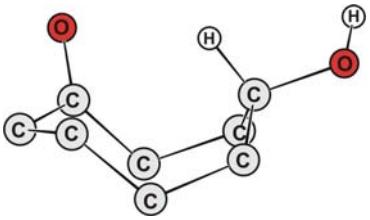 **86** (0.000)	d_H	2.614	90.6	0.004
	d_2	1.438		
	d_3	2.968		
	d_4	1.101		
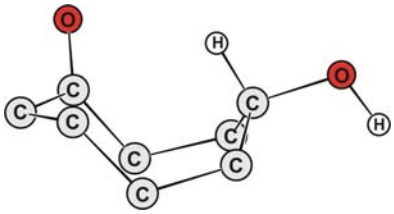 **87** (0.621)	d_H	2.651	91.0	0.003
	d_2	1.437		
	d_3	2.984		
	d_4	1.095		
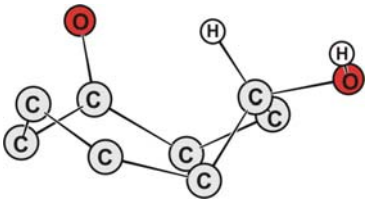 **88** (2.479)	d_H	2.425	95.8	0.015
	d_2	1.438		
	d_3	3.020		
	d_4	1.100		
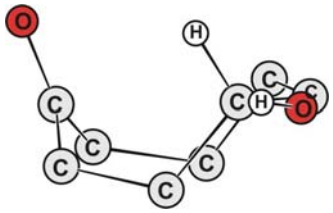 **89** (1.186)	d_H	2.830	85.0	0.000
	d_2	1.440		
	d_3	3.067		
	d_4	1.102		
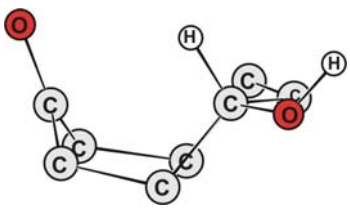 **90** (0.659)	d_H	2.814	84.6	0.003
	d_2	1.440		
	d_3	3.052		
	d_4	1.101		

10.4.2 Bonding and interactions

It is clear that the elucidation of interaction between the methine hydrogen and carbonyl carbon atom in their respective ground state in optimised conformers **86** – **90** can help us to better understand the role of conformation in transannular 1,4-hydride shift (Table 10.15). In all selected conformers interaction between $\sigma_{C\text{-}H}$ and $\pi^*_{C=O}$ is absent. Accordingly, the occupancy of $\pi^*_{C=O}$ remained low.

Table 10.15: Natural bond order (NBO) analysis of conformers **86** – **90**. $E^{(2)}$ (kcal mol^{-1}) is the second order perturbation energy between Φ_i and Φ_j; E_j-E_i (a.u.) is the energy difference between NBOs Φ_i and Φ_j; F_{ij} (a.u.) is the Fock matrix element; only energies greater than the default threshold 0.5 kcal mol^{-1} are included in the table.

	Interaction	**Second-order Interaction**			**Occupancy (ρ)**	
		$E^{(2)}$	E_j-E_i	F_{ij}	$\sigma_{C\text{-}H}$	$\pi^*_{C=O}$
86	$\sigma_{C\text{-}H} \rightarrow \pi^*_{C=O}$	---	---	---	1.978	0.082
87	$\sigma_{C\text{-}H} \rightarrow \pi^*_{C=O}$	----	----	----	1.970	0.079
88	$\sigma_{C\text{-}H} \rightarrow \pi^*_{C=O}$	----	----	----	1.982	0.079
89	$\sigma_{C\text{-}H} \rightarrow \pi^*_{C=O}$	----	----	----	1.982	0.077
90	$\sigma_{C\text{-}H} \rightarrow \pi^*_{C=O}$	----	----	----	1.982	0.077

Table 10.16: Natural bond order (NBO) analysis of protonated conformers **86a** – **90a**. $E^{(2)}$ (kcal mol^{-1}) is the second order perturbation energy between Φ_i and Φ_j; E_j-E_i (a.u.) is the energy difference between NBOs Φ_i and Φ_j; F_{ij} (a.u.) is the Fock matrix element; only energies greater than the default threshold 0.5 kcal mol^{-1} are included in the table.

	Interaction	**Second-order Interaction**			**Occupancy (ρ)**	
		$E^{(2)}$	E_j-E_i	F_{ij}	$\sigma_{C\text{-}H}$	$\pi^*_{C=O}$
86a	$\sigma_{C\text{-}H} \rightarrow \pi^*_{C=O}$	0.74	0.40	0.016	1.977	0.227
87a	$\sigma_{C\text{-}H} \rightarrow \pi^*_{C=O}$	0.92	0.39	0.018	1.968	0.226
88a	$\sigma_{C\text{-}H} \rightarrow \pi^*_{C=O}$	----	----	----	1.982	0.216
89a	$\sigma_{C\text{-}H} \rightarrow \pi^*_{C=O}$	----	----	----	1.975	0.217
90a	$\sigma_{C\text{-}H} \rightarrow \pi^*_{C=O}$	----	----	----	1.982	0.211

As expected, protonation of the oxygen atom of the carbonyl group can catalyse the nucleophilic attack and transfer of methine hydrogen. The NBO analysis of the protonated optimised conformers **86a** – **90a** is given in Table 10.16. In the most stable conformer **86a** the second order interaction energy between the donor and the acceptor orbital is 0.74 kcal mol^{-1}. In **87a** the interaction between donor and acceptor is maximal, i.e., 0.92 kcal mol^{-1}. The electron population in $\pi^*_{C=O}$ has increased from 0.082 (**86**) to 0.227 e (**86a**) and from 0.079 (**87**) to 0.226 e (**87a**) on protonation.
The NBO analysis of the optimised conformers **86li** – **90li** is given in Table 10.17. These conformers were obtained by replacing OH by OLi. The second order interaction energy between the donor and acceptor orbitals has not changed significantly on replacing OH by OLi. An interaction has been observed only in optimised conformers **86li** and **87li**. Interestingly, the second order interaction energy between the donor and acceptor orbitals is the same, i.e., 0.58 kcal mol^{-1} in both conformers. The electron population in $\pi^*_{C=O}$ of conformers **86li** and **87li** is 0.086 e and this is less than in **86a** and **87a**.

Table 10.17: Natural bond order (NBO) analysis of lithiated conformers **86li** – **90li**. $E^{(2)}$ (kcal mol^{-1}) is the second order perturbation energy between Φ_i and Φ_j; E_j-E_i (a.u.) is the energy difference between NBOs Φ_i and Φ_j; F_{ij} (a.u.) is the Fock matrix element; only energies greater than the default threshold 0.5 kcal mol^{-1} are included in the table.

	Interaction	**Second-order Interaction**			**Occupancy (ρ)**	
		$E^{(2)}$	E_j-E_i	F_{ij}	σ_{C-H}	$\pi^*_{C=O}$
86li	$\sigma_{C-H} \rightarrow \pi^*_{C=O}$	0.58	0.49	0.015	1.973	0.086
87li	$\sigma_{C-H} \rightarrow \pi^*_{C=O}$	0.58	0.49	0.015	1.973	0.086
88li	$\sigma_{C-H} \rightarrow \pi^*_{C=O}$	----	----	----	1.976	0.085
89li	$\sigma_{C-H} \rightarrow \pi^*_{C=O}$	----	----	----	1.978	0.080
90li	$\sigma_{C-H} \rightarrow \pi^*_{C=O}$	----	----	----	1.978	0.080

10.4.3 Transition-state calculations

For the intramolecular degenerate 1,4-hydride shift we have located a stationary structure **91** characterised as transition-state (Table 10.18). The single imaginary vibrational frequency corresponds to the migratory hydrogen atom between the atoms C(1) and C(4) in structure **91**. The activation barrier with respect to the starting conformer **90** is very high, i.e., 52.2 kcal mol^{-1}. This energy barrier is much larger than found in 1,5-hydride shift (Table 10.6).

On protonation of the carbonyl oxygen atom the activation energy has further reduced to 35.7 kcal mol^{-1} (Table 10.18). It is lowered by 16.3 kcal mol^{-1}. The calculated energy barrier for 1,4-hydride shift in 2,5-dimethyl-2-hexyl cation at MP4/6-311G(d,p)//MP2/6-311G(d,p) level is 7.5 kcal mol^{-1}.[231] One of the reasons of a high activation barrier in the neutral reaction as compared to the acid-catalysed reaction is because the carbonyl carbon atom is a poor acceptor of hydride. On protonation the electrophilicity of the carbonyl carbon atom increases thus it can accept hydride better.

Table 10.18: Transition-states **91**, **91a** and **91li**, activation barriers including the zero point energy (kcal mol^{-1}), imaginary frequencies (cm^{-1}) for the intramolecular 1,4-hydride shift.

Transition-state structure	Reactants	ΔE_{act}
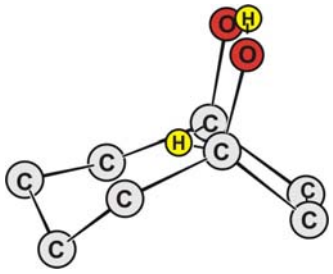 **91** (-1517)	**Conformer 86**	52.2
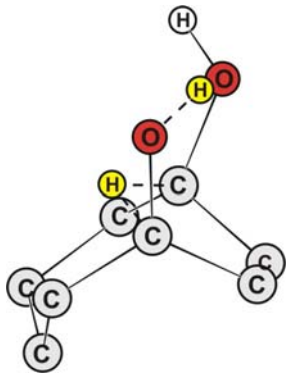 **91a** (-1310)	**Conformer 86a**	35.7
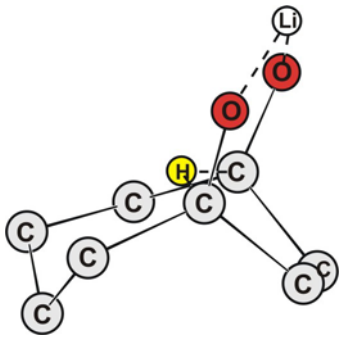 **91li** (-876)	**Conformer 86li**	7.6

The activation barrier in the presence of the metal ion has decreased dramatically to 7.6 kcal mol^{-1}. It seems that the lithium ion has stablised the transition-state by electrostatic attraction with the oxygen atoms thus leading to the relaxation of non-bonded repulsion between the atoms. An activation energy [$\Delta G^{\ddagger}$ (48ºC)] of 24.0 kcal

mol^{-1} is reported[205] for 1,4-hydride shift. The low activation barrier for the 1,4-hydride shift in the presence of the lithium ion is due to the easy hydride transfer on conversion to alkoxide.[212] But the second order interaction energy between the donor and acceptor orbitals in **90li** (Table 10.17) is small as compared to the protonated conformer **90a** (Table 10.16). This implies that there may be formation of a low energy complex which eases the 1,4-hydride shift. All our attempts to calculate such a low energy complex failed. The migration of the potential hydride to the carbonyl carbon is accompanied by simultaneous bond formation of the lithium ion with the oxygen atoms resulting in an unsymmetrical six-membered ring. A number of studies[232] have shown that the transition-state for the hydride shift in hydroxy-ketones in the presence of a metal ion goes through a symmetrical but not an unsymmetrical six-membered ring. The formation of an unsymmetrical six-membered ring in the transition-state is not reported.

Table 10.19: Important geometrical parameters [distances (Å) and angles (°)] of the six-membered ring in **91**, **91a** and **91li**. Atom numbers are depicted in Figure 10.7.

	91	**91a**	**91li**
H(1)···O(2)	1.249	1.272	1.835
O(2)···C(3)	1.317	1.269	1.314
C(3)···H(4)	1.233	1.867	1.241
H(4)···C(5)	1.241	1.070	1.322
C(5)···O(6)	1.316	1.514	1.296
O(6)···H(1)	1.240	1.264	1.861
C(5)···C(3)	2.268	2.444	2.382
C(5)–H(4)–C(3)	132.9	109.7	136.6
O(2)–C(3)–H(4)	101.1	78.6	104.1
O(6)–C(5)–H(4)	100.3	94.5	103.2
H(1)–O(6)–C(5)	100.5	150.0	107.8
H(1)–O(2)–C(3)	101.2	109.3	107.6
O(6)–H(1)–O(2)	151.0	150.0	112.7

The partial bonds C(3)···H(4) and H(4)···C(5) are unequal, i.e.,1.233 and 1.241 Å, respectively (Table 10.19). The C(3)···H(4)···C(5) group is bent, i.e., 132.9º. The

atoms H(1), O(2), C(3), H(4), C(5) and O(6) forming a six-membered cyclic structure are not truly coplanar in **91**.

The atomic charges computed by the natural population analysis on the atoms involved in forming a six-membered ring during synchronous transfer of the potential hydride H(4) and the hydrogen atom of the hydroxy group are listed in Table 10.20. The natural charge on the potential hydride H(4) in **91** is 0.226 e. This charge increases to 0.241 e on protonation of the carbonyl carbon atom (**91a**). The charge on the carbonyl carbon atom becomes a maximum, i.e., 0.674 e, in **91a**. On the contrary, the charge is least, i.e., 0.192 e, on H(4) in **91li**.

Table 10.20: Natural charge (e) distribution on the atoms of the six-membered ring in transition-states **91**, **91a** and **91li**.

	X(1)	O(2)	C(3)	H(4)	C(5)	O(6)
91	0.524	-0.733	0.322	0.226	0.312	-0.738
91a	0.560	-0.653	0.674	0.241	0.038	-0.742
91li	0.939	-0.893	0.276	0.192	0.349	-0.854

10.5 Results for the transannular 1,5-hydride shift in model compound 4

We have investigated in this section the effect of a halogen atom on the intramolecular 1,5-hydride shift in model compound **4**. It is interesting to study the detailed geometry around the reacting atoms in the transannular shift. The number of low energy conformers in **4** is 91 (Figure 10.9). Only three conformers in which Br and methine H atom are *cis* to each other (isomerism discussed in section 7.5) were selected on the basis of proximity of the reacting atoms. The selected conformers **92** – **94** (Table 10.21) were optimised at the B3LYP/6-31+G* level of theory. For the Br atom in **4** the Stuttgart/Dresden effective core potentials (ECPs) SDD,[185] which were augmented with d polarisation functions, were employed.

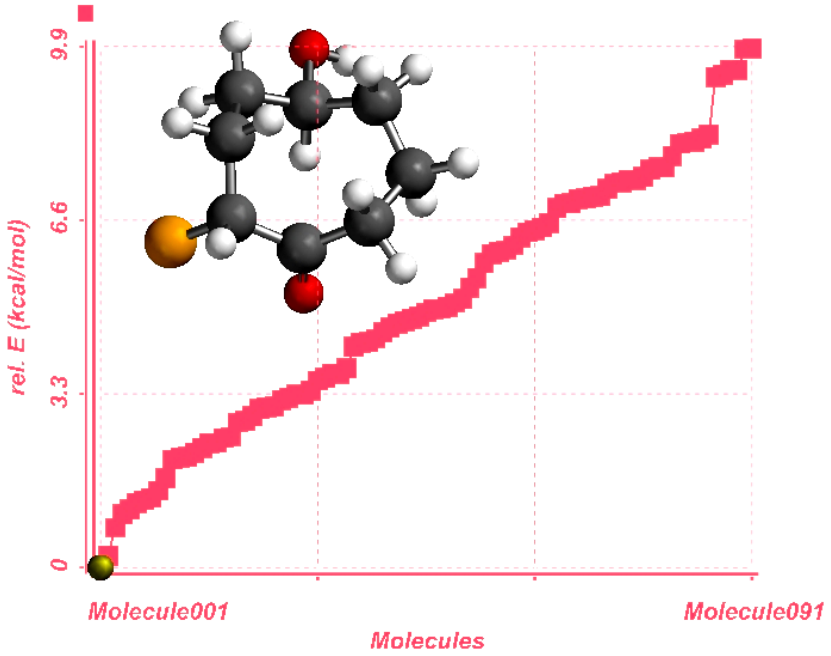

Figure 10.9: Energy profile of the conformer distribution for the *exo*-conformer of **4** at MMFF level.

10.5.1 Structural features and energetics

The most stable conformer is **92** (*bc*) (Table 10.21). This is in agreement with the reported most stable conformer for cyclooctanone.[189, 220] The second most stable conformer is **94** (*crown*). It is 0.66 kcal mol^{-1} higher in energy than **92**. The third conformer is **93** (*bb*). The reacting groups, i.e., H and >C=O, in **93** are in the closest proximity, i.e., 2.433 Å. The distance d_H is maximal in **94**. The close approach of the nucleophile leads to greater d_H, values, i.e., 0.038 and 0.037 Å, in **93** and **94**, respectively.

Table 10.21: Important geometrical parameters in **92** – **94** and relative energies including the zero point energy (gas phase). [Distances (Å); angles (°), rel. energies (kcal mol^{-1})].

Molecular structure	**Geometrical parameters**			
			θ_H	Δ_H
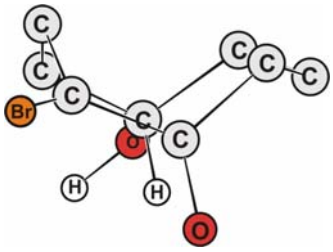 **92** (0.000)	d_H	2.620	86.6	0.009
	d_2	1.439		
	d_3	3.091		
	d_4	1.100		
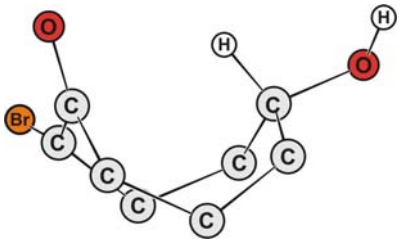 **93** (4.182)	d_H	2.433	89.5	0.038
	d_2	1.438		
	d_3	2.982		
	d_4	1.098		
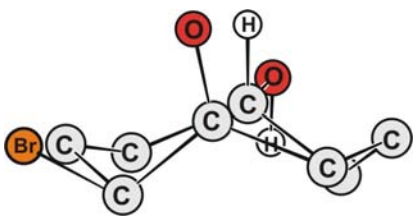 **94** (0.660)	d_H	2.901	81.9	0.037
	d_2	1.441		
	d_3	3.170		
	d_4	1.101		

10.5.2 Bonding and interactions

Natural bond orbital analysis was carried out to explore the interaction between the reacting groups in conformers **92** – **94** in their respective ground states (Table 10.22). Conformers **92** and **93** show interactions between the donor and acceptor orbitals whereas conformer **94** does not show an interaction. The second order energy is large in **93** (1.19 kcal mol^{-1}) than in **92** (0.54 kcal mol^{-1}).

In the protonated optimised conformers (Table 10.23) an interaction between the donor and acceptor is found in **92a** (*bc*) and **93a** (*bb*). The second order interaction in conformers **92a** and **93a** is 1.52 and 9.45 kcal mol^{-1}, respectively. The interaction is strongest in **93a**. The electron population in $\pi^*_{C=O}$ in **93a** is 0.302 e.

Table 10.22: Natural bond order (NBO) analysis of conformers **92** – **94**. $E^{(2)}$ (kcal mol^{-1}) is the second order perturbation energy between Φ_i and Φ_j; E_j-E_i (a.u.) is the energy difference between NBOs Φ_i and Φ_j; F_{ij} (a.u.) is the Fock matrix element; only energies greater than the default threshold 0.5 kcal mol^{-1} are included in the table.

	Interaction	**Second-order Interaction**			**Occupancy (ρ)**	
		$E^{(2)}$	E_j-E_i	F_{ij}	σ_{C-H}	$\pi^*_{C=O}$
92	$\sigma_{C-H} \rightarrow \pi^*_{C=O}$	0.54	0.51	0.015	1.981	0.081
93	$\sigma_{C-H} \rightarrow \pi^*_{C=O}$	1.19	0.51	0.022	1.975	0.083
94	$\sigma_{C-H} \rightarrow \pi^*_{C=O}$	----	----	----	1.983	0.086

Table 10.23: Natural bond order (NBO) analysis of protonated conformers **92a** – **94a**. $E^{(2)}$ (kcal mol^{-1}) is the second order perturbation energy between Φ_i and Φ_j; E_j-E_i (a.u.) is the energy difference between NBOs Φ_i and Φ_j; F_{ij} (a.u.) is the Fock matrix element; only energies greater than the default threshold 0.5 kcal mol^{-1} are included in the table.

	Interaction	**Second-order Interaction**			**Occupancy (ρ)**	
		$E^{(2)}$	E_j-E_i	F_{ij}	$\sigma_{C-H} \rightarrow \pi^*_{C=O}$	
92a	$\sigma_{C-H} \rightarrow \pi^*_{C=O}$	1.52	0.39	0.023	1.970	0.220
93a	$\sigma_{C-H} \rightarrow \pi^*_{C=O}$	9.45	0.39	0.057	1.901	0.302
94a	$\sigma_{C-H} \rightarrow \pi^*_{C=O}$	----	----	----	1.979	0.015

The natural bond order analysis of the conformers optimised with Li is given in Table 10.24. Again conformer **93li** has the strongest second order interaction energy, i.e., 1.88 kcal mol^{-1}. The electron population of $\pi^*_{C=O}$ in **93li** is 0.092 e. The comparison of NBO analysis shows that the protonation of the carbonyl oxygen leads to the strongest acceptor-donor interaction.

Table 10.24: Natural bond order (NBO) analysis of lithiated conformers **92li** – **94li**. $E^{(2)}$ (kcal mol^{-1}) is the second order perturbation energy between Φ_i and Φ_j; E_j-E_i (a.u.) is the energy difference between NBOs Φ_i and Φ_j; F_{ij} (a.u.) is the Fock matrix element; only energies greater than the default threshold 0.5 kcal mol^{-1} are included in the table.

	Interaction	**Second-order Interaction**			**Occupancy (ρ)**	
		$E^{(2)}$	E_j-E_i	F_{ij}	$\sigma_{C\text{-}H} \rightarrow$	$\pi^*_{C=O}$
92li	$\sigma_{C\text{-}H} \rightarrow \pi^*_{C=O}$	0.65	0.48	0.016	1.975	0.084
93li	$\sigma_{C\text{-}H} \rightarrow \pi^*_{C=O}$	1.88	0.48	0.027	1.965	0.092
94li	$\sigma_{C\text{-}H} \rightarrow \pi^*_{C=O}$	----	----	----	1.979	0.086

10.5.3 Transition-state calculations

The optimised conformers **92** (*bc*) and **93** (*bb*) have been considered for transition-state calculations. The transition-state **95** (*bc*) is 46.8 kcal mol^{-1} higher in energy with respect to the conformer **92** (Table 10.25). The energy barrier is 43.0 kcal mol^{-1} for the pathway **93**→ **96**. In both conformers 1,5-hydride shift occurs through a six-membered ring. The transition-states **95** and **96** are characterised by a single imaginary vibrational frequency. The vibrational mode is associated with the movement of the hydrogen atom between the two carbon atoms. The large energy barrier for the 1,5-hydride shift may be due to non-bonded repulsions which prevent conformer **95** and **96** to attain low energy transition-states. This is further supported by the high strain energy (763.9 kcal mol^{-1}) calculated at MMFF level for the transition-state **95**. The activation energies calculated for **92a** → **95a** and **93a** → **96a** are 43.8 and 37.4 kcal mol^{-1}, respectively (Table 10.25). The calculation for the transition-state **96li** was carried out at HF/6-31G** (Table 10.26).

Table 10.25: Transition-states, activation barriers including zero point energy (kcal mol^{-1}) and imaginary frequencies (cm^{-1}) for the intramolecular 1,5-hydride shift.

Transition-state structure	Reactants	ΔE_{act}
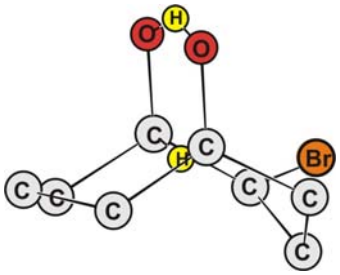 **95** (-1402)	**Conformer 92**	46.786
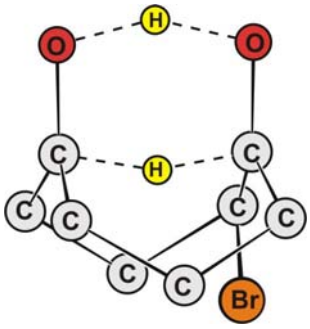 **96** (-1426)	**Conformer 93**	42.957
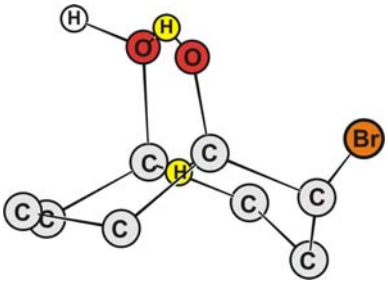 **95a** (-749)	**Conformer 92a**	43.763
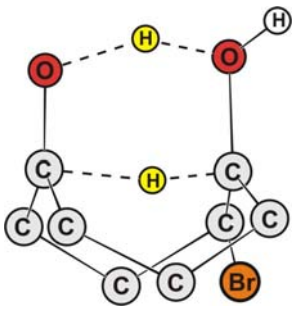 **96a** (-847)	**Conformer 93a**	37.420

Table 10.26: Calculated (HF/6-31G**) transition-state **96li**, activation barrier including zero point energy (kcal mol $^{-1}$) and imaginary frequency (cm^{-1}).

Transition-state structure	Reactants	ΔEact
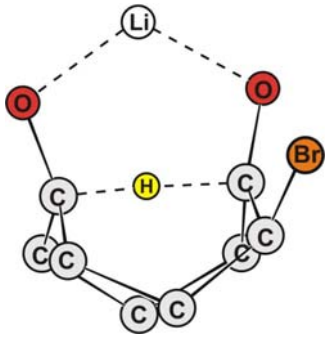 **96li** (-423)	**Conformer 93li**	17.411

Table 10.27: Important geometrical parameters [distances (Å) and angles (°)] of the six-membered ring in transition-states **95** and **96**. Atom numbers are depicted in Figure 10.7.

	95	**96**
H(1)···O(2)	1.242	1.231
O(2)···C(3)	1.309	1.317
C(3)···H(4)	1.196	1.206
H(4)···C(5)	1.214	1.197
C(5)···O(6)	1.314	1.316
O(6)···H(1)	1.231	1.250
C(5)···C(3)	2.364	2.366
C(5)–H(4)–C(3)	157.6	160.3
O(2)–C(3)–H(4)	102.3	100.6
O(6)–C(5)–H(4)	101.7	101.1
H(1)–O(6)–C(5)	103.1	102.4
H(1)–O(2)–C(3)	102.8	103.0
O(6)–H(1)–O(2)	152.4	152.7

The important geometric parameters of the six-membered ring in the transition-states **95** and **96** are given in Table 10.27. As expected both transition-states are symmetric. The C(5)···H(4)···C(3) angle in **95** and **96** is 157.6° and 160.3°,

respectively. This implies that the migrating hydrogen adopts a nearly linear trajectory. The the transition-states **95a** and **96a** (Tables 10.28) are unsymmetric. The C(3)···H(4) bonds in **95a** and **96a** are 1.434 and 1.433 Å, respectively. On the other hand, the C(5)···H(4) bonds in **95a** and **96a** are 1.072 and 1.066 Å, respectively. The C(5)···H(4)···C(3) angles in **95a** and **96a** are 163.5° and 168.5°, respectively. The transition-state **96li** calculated at HF/6-31G** is a little unsymmetric as expected. Interestingly, the C(5)···H(4)···C(3) angle in **96li** is 176.5º.

Table 10.28: Important geometrical parameters [distances (Å) and angles (°)] of the six-membered ring in the transition-states **95a**, **96a** and **96li**. Atom numbers are depicted in Figure 10.7.

	95a	**96a**	**96li**
H(1)···O(2)	1.377	1.378	1.930
O(2)···C(3)	1.263	1.274	1.255
C(3)···H(4)	1.434	1.433	1.303
H(4)···C(5)	1.072	1.066	1.157
C(5)···O(6)	1.484	1.484	1.306
O(6)···H(1)	1.140	1.149	1.836
C(5)···C(3)	2.480	2.486	2.459
C(5)–H(4)–C(3)	163.5	168.5	176.5
O(2)–C(3)–H(4)	98.4	95.0	103.6
O(6)–C(5)–H(4)	95.9	94.6	105.3
H(1)–O(6)–C(5)	103.7	102.3	105.0
H(1)–O(2)–C(3)	106.1	107.5	105.7
O(6)–H(1)–O(2)	151.3	151.7	115.0

The natural charges distribution on the atoms involved in the formation of the six-membered ring is given in Table 10.29. The charge on H(4) is positive in all calculated transition-states.

Table 10.29: Natural charge (e) distribution on the atoms of six-membered ring in transition-states **95**, **96**, **95a**, **96a** and **96li**.

	H(1)	O(2)	C(3)	H(4)	C(5)	O(6)
95	0.523	-0.721	0.295	0.216	0.323	-0.733
96	0.522	-0.723	0.293	0.218	0.317	-0.723
95a	0.567	-0.656	0.521	0.229	0.139	-0.719
96a	0.566	-0.670	0.535	0.233	0.128	-0.721
96li	0.935	-0.829	0.353	0.1881	0.247	-0.900

10.6 Results for the transannular 1,6-hydride shift in model compound 5

We have undertaken computational studies on **5** in order to advance our understanding of the effect of ring size on the transannular hydride shift. A number of studies mainly experimental, have been reported[54, 68, 71, 233, 234] in which ten-membered compounds undergo transannular 1,5- or 1,6-hydride shifts. The detailed experimental investigation[58] reported recently has established an acid-/base-catalysed degenerate oxidation-reduction process in 6-hydroxycyclodecanone *via* a transannular 1,6-hydride shift. The inter-[235] and intramolecular[54, 71, 234] hydride transfer has been studied in various systems. A number of transition-state modelling studies[218, 232, 236] for the hydride transfer are reported but such studies are lacking for **5**. The main reason is the flexibility of the ring skeleton in the ten-membered cyclic compounds. We have presented here the results for the degenerate 1,6-hydride shift in the unsubstituted ten-membered cyclic hydroxy-ketone (**5**). The number of conformers generated (at MMFF level) is 100 (Figure 10.10). At room temperature conformers are in a state of rapid conformational equilibrium.

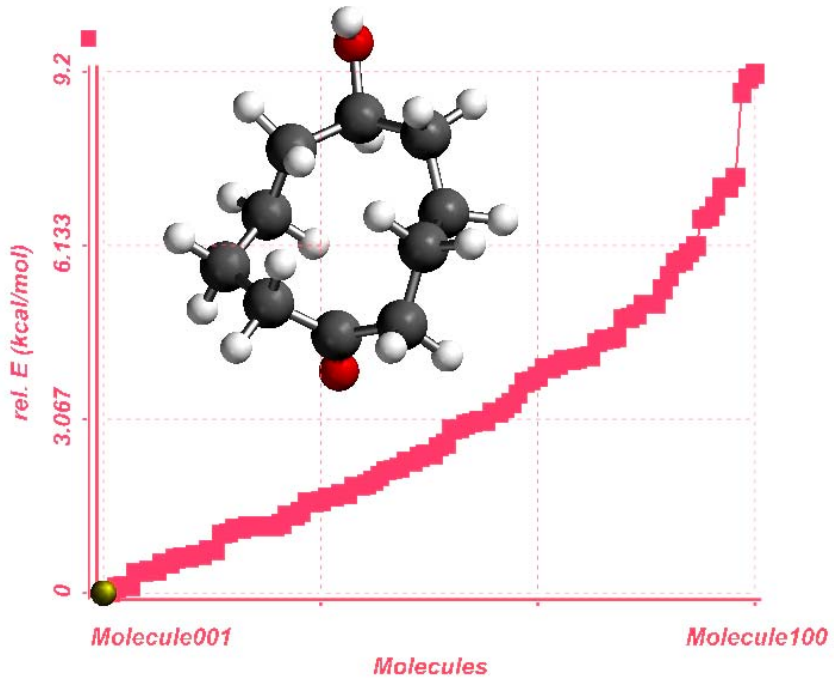

Figure 10.10: Energy profile of the conformer distribution for the *exo*-conformer of **5** at MMFF level.

10.6.1 Structural features and energetics

The optimised conformers **97** – **101** with important geometrical features are given in Table 10.30. The most stable conformer is **99**. Here the ring skeleton acquires *bcb* conformation (**99**) which is consistent with the X-ray structure reported.[58] The conformers **97** and **100** are < 1.0 kcal mol^{-1} higher in energy than the conformer **99**. The least stable conformer is **98**. In the low energy conformers **97** and **100** the distance d_H is 2.52 and 2.54 Å, respectively. The distance d_H is 2.52 Å in **99**. The distance between the methine hydrogen and the carbonyl carbon atom d_H is less than the vdW radii in the selected optimised conformers. The angle of attack θ_H is 74.4°, 74.1° and 73.3°, in **97**, **99** and **100**, respectively. These angles are less than the attacking angles reported.[168] This implies that the directionality of the nucleophile is not appropriate for an attack. The deviation of the planarity of the carbonyl group Δ_H is 0.00 Å in **99**. It implies that a small transannular distance is not the only deciding factor for a transannular reaction. Δ_H is 0.02 Å in **97** and **100**. The results obtained here show that the transannular interactions depend on all geometric parameters.

Table 10.30: Important geometrical parameters in **97** and **98** and relative energies (including the zero point energy) with respect to conformer **99** (gas phase). [Distances (Å); angles (°); rel. energies (kcal mol^{-1})].

Molecular structure		Geometrical parameters		
			θ_H	Δ_H
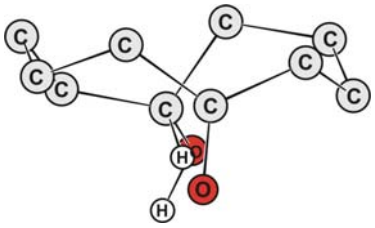 **97** (0.063)	d_H	2.523	74.4	0.018
	d_2	1.441		
	d_3	3.243		
	d_4	1.095		
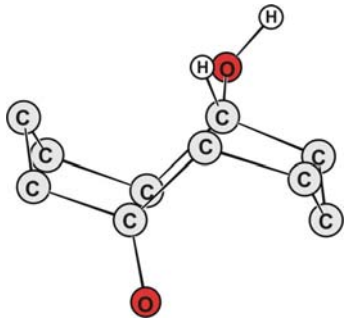 **98** (9.024)	d_H	2.543	73.1	0.003
	d_2	1.442		
	d_3	3.246		
	d_4	1.095		
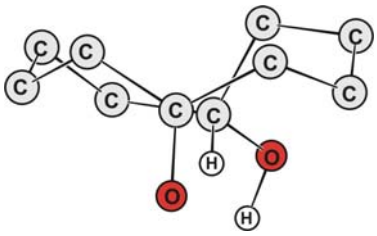 **99** (0.000)	d_H	2.519	74.1	0.000
	d_2	1.441		
	d_3	3.238		
	d_4	1.095		
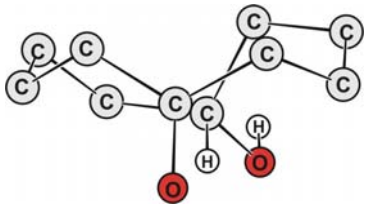 **100** (0.612)	d_H	2.542	73.3	0.019
	d_2	1.438		
	d_3	3.240		
	d_4	1.091		
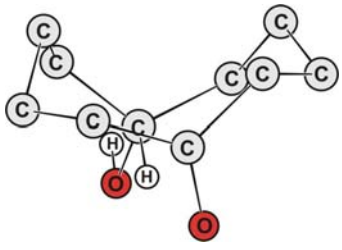 **101** (3.975)	d_H	2.684	67.5	0.003
	d_2	1.442		
	d_3	3.473		
	d_4	1.092		

10.6.2 Bonding and interactions

The NBO analysis of conformers **97** – **101** is shown in Table 10.31. An interaction between the methine hydrogen and the carbonyl carbon atom is absent in the conformers. Out of the protonated optimised conformers **97a** – **101a** (Table 10.32) the interaction between the donor and acceptor orbitals is absent only in **101a**. The second order interaction between the donor and acceptor orbitals in conformers **97a** and **100a** are strong, i.e., 1.08 and 0.95 kcal mol^{-1}, respectively, as compared to the rest of conformers. The electron population of $\pi^*_{C=O}$ in **97a** is maximal (0.240 e).

Table 10.31: Natural bond order (NBO) analysis of conformers **97** – **101**. $E^{(2)}$ (kcal mol^{-1}) is the second order perturbation energy between Φ_i and Φ_j; E_j-E_i (a.u.) is the energy difference between NBOs Φ_i and Φ_j; F_{ij} (a.u.) is the Fock matrix element; only energies greater than the default threshold 0.5 kcal mol^{-1} are included in the table.

	Interaction	**Second-order Interaction**			**Occupancy (ρ)**	
		$E^{(2)}$	E_j-E_i	F_{ij}	σ_{C-H}	$\pi^*_{C=O}$
97	$\sigma_{C-H} \rightarrow \pi^*_{C=O}$	----	----	----	1.979	0.091
98	$\sigma_{C-H} \rightarrow \pi^*_{C=O}$	----	----	----	1.979	0.090
99	$\sigma_{C-H} \rightarrow \pi^*_{C=O}$	----	----	----	1.979	0.091
100	$\sigma_{C-H} \rightarrow \pi^*_{C=O}$	----	----	----	1.969	0.090
101	$\sigma_{C-H} \rightarrow \pi^*_{C=O}$	----	----	----	1.969	0.090

Table 10.32: Natural bond order (NBO) analysis of protonated conformers **97a** – **101a**. $E^{(2)}$ (kcal mol^{-1}) is the second order perturbation energy between Φ_i and Φ_j; E_j-E_i (a.u.) is the energy difference between NBOs Φ_i and Φ_j; F_{ij} (a.u.) is the Fock matrix element; only energies greater than the default threshold 0.5 kcal mol^{-1} are included in the table.

	Interaction	**Second-order Interaction**			**Occupancy (ρ)**	
		$E^{(2)}$	E_j-E_i	F_{ij}	σ_{C-H}	$\pi^*_{C=O}$
97a	$\sigma_{C-H} \rightarrow \pi^*_{C=O}$	1.08	0.39	0.019	1.970	0.240
98a	$\sigma_{C-H} \rightarrow \pi^*_{C=O}$	0.75	0.39	0.016	1.973	0.231
99a	$\sigma_{C-H} \rightarrow \pi^*_{C=O}$	0.78	0.39	0.017	1.973	0.239
100a	$\sigma_{C-H} \rightarrow \pi^*_{C=O}$	0.95	0.39	0.018	1.965	0.231
101a	$\sigma_{C-H} \rightarrow \pi^*_{C=O}$	----	----	----	1.972	0.226

Table 10.33: Natural bond order (NBO) analysis of lithiated conformers **97li** – **102li**. $E^{(2)}$ (kcal mol^{-1}) is the second order perturbation energy between Φ_i and Φ_j; E_j-E_i (a.u.) is the energy difference between NBOs Φ_i and Φ_j; F_{ij} (a.u.) is the Fock matrix element; only energies greater than the default threshold 0.5 kcal mol^{-1} are included in the table.

	Interaction	**Second-order Interaction**			**Occupancy (ρ)**	
		$E^{(2)}$	E_j-E_i	F_{ij}	$\sigma_{C\text{-}H} \rightarrow \pi^*_{C=O}$	
97li	$\sigma_{C\text{-}H} \rightarrow \pi^*_{C=O}$	----	----	----	1.977	0.084
98li	$\sigma_{C\text{-}H} \rightarrow \pi^*_{C=O}$	----	----	----	1.972	0.091
99li	$\sigma_{C\text{-}H} \rightarrow \pi^*_{C=O}$	----	----	----	1.972	0.091
100li	$\sigma_{C\text{-}H} \rightarrow \pi^*_{C=O}$	----	----	----	1.972	0.091
101li	$\sigma_{C\text{-}H} \rightarrow \pi^*_{C=O}$	----	----	----	1.977	0.084
102li	$\sigma_{C\text{-}H} \rightarrow \pi^*_{C=O}$	17.71	0.43	0.081	1.861	0.267

Interesting results were obtained on replacing the hydrogen atom of the –OH group by a lithium ion. The second order interactions were absent between the donor and the acceptor orbitals in conformers **97li** – **102li** (Table 10.33). In addition to these conformers a low energy complex **102li** was located on the potential energy surface. The second order interaction energy between the donor and acceptor orbital is maximal, i.e., 17.7 kcal mol^{-1} in **102li**. The electron population in $\pi^*_{C=O}$ shows a large increase, i.e., 0.267 e, as compared to the other conformers. The electron population in $\sigma_{C\text{-}H}$ decreased to 1.861 e. This implies that the low energy complex formed in the presence of the metal counterion assists in the transannular 1,6-hydride shift.

10.6.3 Transition-state calculations

The activation energy calculated for **97** → **103** is 28.0 kcal mol^{-1} (Table 10.34). The strain energy calculated for **96** is 653.8 kcal mol^{-1}. The low value of strain energy indicates less strain in the transition-state **103**. These findings support the experimental results reported for the 1,6-hydride shift in 6-hydroxycyclodecanone.[58]
The activation barrier is reduced to 7.3 kcal mol^{-1} for **97a** → **103a**. In a base catalysed reaction a low energy complex **102li** was located. This complex goes to a

degenerate product, i.e., 6-hydroxycyclodecanone, *via* a very low energy barrier of 0.1 kcal mol^{-1} (Figure 10.11).

Table 10.34: Transition-states **103**, **103a** and **103li**, activation barriers including zero point energy (kcal mol^{-1}) and imaginary frequencies (cm^{-1}).

Transition-state structure	Reactants	ΔE_{act}
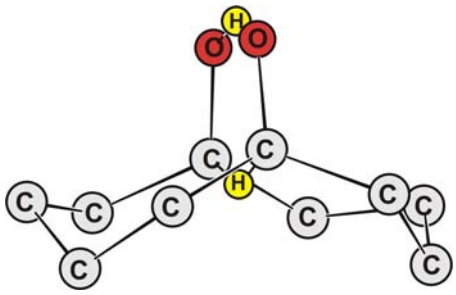 **103** (-1427)	**Conformer 97**	27.960
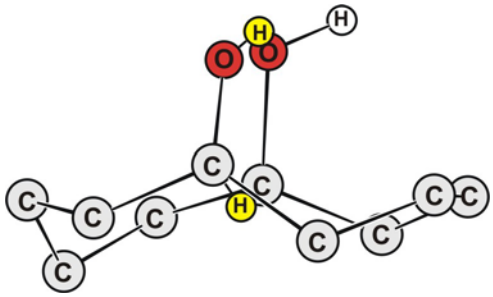 **103a** (-701)	**Conformer 97a**	7.295
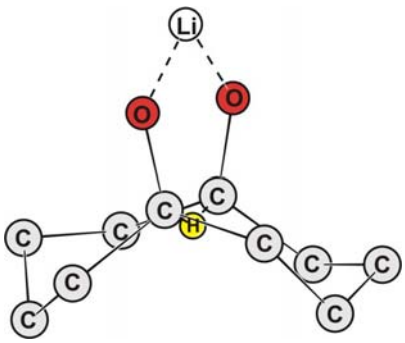 **103li** (-350)	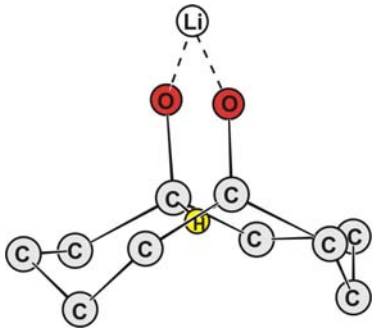 **102li**	0.102

The 1,6-hydride shift occurs through the formation of a six-membered cycle. The distance between C(5)···C(3) is 2.534 Å in **103** (Table 10.35). The migrating hydrogen easily forms a bridge between the opposite carbon atoms resulting in the formation of a 3c-2e bond. A number of ten-membered compounds containing such a

bond were prepared[69] and studied.[71] The shorter distances can have symmetric arrangements with strong 3-centre bonding as compared to the larger distances.[237] The distances C(3)···H(4), H(4)···C(5) and C(5)···C(3) in **103a** are 1.857 1.088 and 2.801 Å, respectively. This implies that the bridging hydrogen atom is localised on one of the carbon atom. The six-membered ring in transition-states **103** and **103li** (Table 10.35) are symmetrical with respect to the two C(3)···H(4) and H(4)···C(5) distances. The remaining angles and partial bond distances in the two halves of the transition-state structures **103** and **103li** are similar. The important difference between the six-membered ring in **103**, **103a** and **103li** is that the C···H···C fragment is symmetrical in **103** and **103li** but unsymmetrical in **103a**.

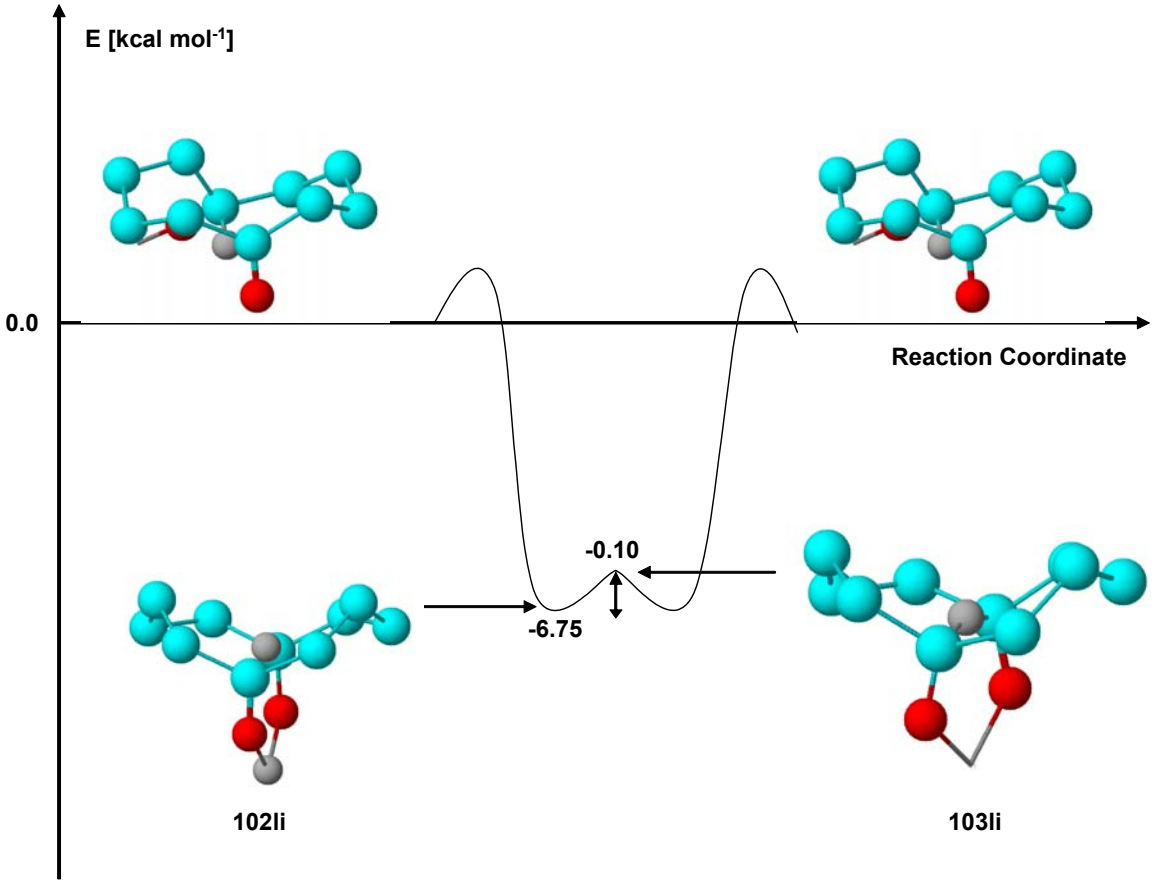

Figure 10.11: Energy profile for the lithium ion-catalysed 1,6-hydride shift.

Table 10.35: Important geometrical parameters [distances (Å) and angles (°)] of the six-membered ring in transition-states **103**, **103a**, **102li** and **103li**. Atom numbers are depicted in Figure 10.7.

	103	**103a**	**102li**	**103li**
X(1) ··O(2)	1.206	1.180	1.717	1.198
O(2)···C(3)	1.313	1.269	1.354	1.318
C(3)···H(4)	1.327	1.857	1.141	1.318
H(4)···C(5)	1.318	1.088	1.753	1.327
C(5)···O(6)	1.318	1.491	1.252	1.313
O(6)···X(1)	1.198	1.241	1.835	1.206
C(5)···C(3)	2.534	2.801	2.818	2.533
C(5)–H(4)–C(3)	146.7	142.8	152.9	146.7
O(2)–C(3)–H(4)	102.7	94.3	99.3	102.5
O(6)–C(5)–H(4)	102.5	102.5	108.7	102.7
X(1)–O(6)–C(5)	106.2	105.7	123.9	106.1
X(1)–O(2)–C(3)	106.1	112.5	128.6	106.2
O(6)–H(1)–O(2)	44.2	154.8	106.4	155.6

The natural charge distribution on the atoms forming the six-membered ring show that the potential hydride H(4) transferred is positive in **103**, **103a** and **103li** (Table 10.36). The charges on the six-atoms in complex 1**02li** are shown in Figure 10.12. The charge on the migrating hydrogen atom H(4) is 0.142 e. This charge is less positive than found in **103li**. The charges on the carbinol-carbonyl atoms are 0.138 and 0.541 e.

Table 10.36: Natural charge (e) distribution on the six-membered ring in transition-states **103**, **103a** and **103li**.

	X(1)	O(2)	C(3)	H(4)	C(5)	O(6)
103	0.531	-0.734	0.329	0.183	0.323	-0.736
103a	0.559	-0.676	0.656	0.211	0.100	-0.748
103li	0.944	-0.886	0.310	0.155	0.341	-0.878

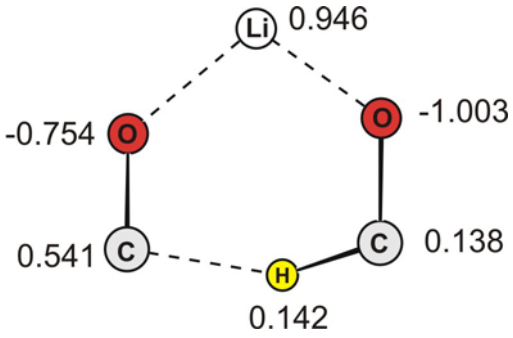

Figure 10.12: Natural charge (e) distribution on the atoms involved in the formation of the six-membered ring in complex **102li**.

10.7 Discussion

In the preceding sections transannular 1,x-hydride shifts (x = 4 – 6) in model systems **1**, **2**, **4** and **5** have been investigated by theoretical methods. A number of interestings results were obtained. These include the effect of protonation of the carbonyl oxygen atom on the donor-acceptor interactions. The strongest second order interaction energy (9.45 kcal mol^{-1}) is found in **93a** (Table 10.23). The interactions between the reacting atoms in the absence of acid or base are observed in the conformers of **1** and **4** in their respective ground states (Tables 10.3 and 10.22). Such donor-acceptor interactions are found to be absent in the optimised low energy conformers of **2** and **5** (Tables 10.15 and 10.32). In addition to these observations other geometrical properties of the selected conformers have been investigated. Based on all results a general statement can be made that the eight-membered cyclic hydroxy-ketones with substituents at positions 1 and 5 show strong transannular interactions in their respective ground states.

The most stable conformer is *bc* both in **1** (**81**) and **5** (**92)**. This is in agreement with the reported most stable conformer for cyclooctanone.[189, 220] The most stable conformer reported[58] for the ten-membered cyclic hydroxy-ketone (**5**) is *bcb*. The optimised conformer **99** is also *bcb* (Table 10.31).

Transition-state modeling was carried out on the most suitable starting conformers in neutral and acid-/base-catalysed conditions. In the uncatalysed degenerate 1,x-hydride shift (x = 4 – 6) reaction the potential energy profile has global minima that correspond to the two interchanging hydroxy-ketones and a high lying transition-state corresponding to symmetrical (in **1**, **4** and **5**) or unsymmetrical (in **2**) structures.The calculated activation barriers for **81** → **84** and **82** → **85** are the same, i.e., 46.6 kcal mol^{-1} (Table 10.6). This energy is 20.2 kcal mol^{-1} higher than that of the energy required for the intermolecular hydride shift in the formaldehyde and methanol system (**78**) (Figure 10.2). The activation barrier for **86** → **91** is 52.2 kcal mol^{-1} (Table 10.18). In model system **2** (**86** → **91**) the activation barrier for the uncatalysed 1,4-hydride shift is 5.6 kcal mol^{-1} higher than that for the 1,5-hydride shift in model compound **1** (**81** → **84** or **82** → **85**). One of the key results is that the activation barriers for the 1,6-hydride shift (28.0 kcal mol^{-1}) and the intermolecular hydride shift (26.4 kcal mol^{-1}) are similar. These energy barriers are much lower than found for the 1,4- and 1,5-hydride shift in eight-membered ring systems **1** and **2**.

There are significant differences between the transition-states for the intramolecular (**84** and **85**) and intermolecular hydride shift (**78**). These differences include short C···H···C bonds (1.198 Å) in **84** and **85** (Table 10.8). This leads to tight transition-states **84** and **85**. In contrast, the transition-state **78** (Figure 10.4) is rather flexible because of the two long C···H bonds (1.349 Å) and a bent C···H···C angle (141.0º). The transition-state modeling for the 1,4-hydride shift has revealed interesting features of the six-membered cyclic structure **91** formed. Unlike the symmetric planar six-membered cyclic structures in **84** and **85** the shift of the hydrogen takes place through a non-planar unsymmetric structure in **91**. Moreover, the C(3)···H(4) and C(5)···H(4) bonds distances are 1.233 and 1.241 Å, respectively in **91** (Table 10.19). The C(5)···C(3) distances in **84**, **85**, **91**, **95**, **96** and **103** are 2.364, 2.363, 2.268 and 2.534 Å, respectively. The shorter C(5)···C(3) distance can have a symmetric geometry of the C(5)···H···(C3) with strong three-centre bonding as compared to the geometry with larger distance.[237] The geometric parameters of the six-membered ring of **103** (Table 10.36) are more close to the corresponding parameters found in **78** (Figure 10.4) rather than the parameters for the six-membered ring for the transannular 1,5-hydride shift (Table 10.8).

Further evidence for the non-bonded repulsion was obtained by the strain energy calculations at the MMFF level (Spartan04) of the transition-states. The strain energies were calculated by fixing the six-membered ring structure. The calculated strain energies for **78**, **84**, **85**, **91** and **103** are 645.0, 763.5, 791.1, 730.7 and 653.8 kcal mol^{-1}, respectively. In the intermolecular hydride shift there are no strong steric effects operating against the formation of a six-membered ring during the hydrogen atom transfer. The most constrained transition-state conformation is *bb* (**85**) and 27.6 kcal mol^{-1} of strain is released when a methylene group flips resulting the *bc* conformation. The tight transition-state leads to non-bonded repulsions between the atoms and this result in higher activation barrier.

The acid-catalysed 1,5-hydride shift occurs through unsymmetrical six-membered cyclic transition-states **84a** and **85a** (Table 10.9). The activation barriers are about 5.0 kcal mol^{-1} lower than in the uncatalysed 1,5-hydride shift. The energy barriers reduce by 16.5 kcal mol^{-1} when the transition-state for 1,4-hydride shift is modelled in the presence of acid (Table 10.18). The energy barrier for **93a** → **96a** is about 4.5 kcal mol^{-1} (Table 10.25) lower than for **82a** → **85a** (Table 10.9).

The activation barrier is drastically reduced to 0.9 kcal mol^{-1} (Figure 10.3) in the intermolecular hydride shift in the presence of lithium as counterion. There is formation of a low energy complex **79li** due to the electrostatic attraction of the lithium ion with the oxygen atoms of the carbinol-carbonyl pair. The activation barriers reduce both for 1,5- and 1,4-hydride shift. The degenerate transannular 1,4-hydride shift is highly assisted by the metal counterion.[199] In model system **5** the 1,6-hydride shift occurs through an initial formation of a low energy complex (**102li**) with an activation barrier of 0.1 kcal mol^{-1} (Figure 10.11). Our study demonstrated the significance of a metal counterion in lowering the activation barriers.

Another interesting result is that the natural charge on the migrating hydrogen H(4) remained positive in both inter- and intramolecular hydride shift. The transition-state for the transannular hydride shift studied here is likely to resemble the starting conformer. Thus, it might be anticipated that knowledge of the starting conformations would be of great predictive value. The tight transition-state in 1,5-hydride shift in 5-hydroxycyclooctanone (**1**) indicates that it is less likely that solvent molecules such as water participate in the transition-state formation. The role of a catalytic amount of water in dihydrogen transfer between formaldehyde and methanol has already been reported.[238] The calculated enthalpic barriers for the uncatalysed and catalysed process were found to be similar. This implies that the reaction is not catalysed by the presence of water. Here for the simplicity of calculation we have investigated the transannular hydride shift without taking solvent molecule into consideration.

11 Preparation of keto-ethers *via* non-classical protection method

In the preceding chapters we have carried out both theoretical and experimental investigations on **1** and only theoretical on **2**, **4** and **5** for the transannular 1,x-hydride shift (x=4 – 6). In the present work an application of the transannular 1,5-hydride shift in **1** is presented and discussed. The protection and deprotection of functional groups and functional group interconversion (FGI) methodologies constitute very important steps in organic synthesis. Unfortunately, often the transannular interactions in medium-ring compounds lead to unwanted products (such as hemiacetal) derived from the transannular reactions. Since **1** exists as its hemiacetal **1a** many routinely employed strategies towards the functionalisation and ring expansions fail due to the transannular interactions between >C=O and –OH. An independent existence of a hydroxy and a carbonyl group in an eight-membered ring can greatly ease the methodologies for the synthesis of certain natural products by FGI startegies or ring enlargement. As an example of an important functional group the hydroxy group is protected as an ether. In the synthesis of Pentalenene[59] (Figure 11.1), the OH group of **1** was protected by *t*-butyldimethylsiloxy (TBDMS), i.e., through classical method.
The transannular hydride shift has already been exploited for the protection of the hydroxy group in 6-hydroxycyclodecanone by non-classical methods.[58, 68] But no such attempts have been reported yet for the protection of the hydroxy group in eight-membered hydroxy-ketones. We wish to report here the protection of the hydroxy group in **1** by a non-classical method.

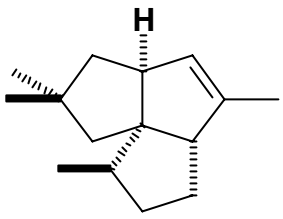

Figure 11.1: Pentalenene, a natural product used as an antibiotic antifungal metabolite.

11.1 Protection reactions with alcohols

The first reaction was planned with an easily available alcohol that can also be used as a solvent. So methanol was considered to be best choice for the preparation of the keto-ether. The procedure involved simply refluxing of **1a** with methanol in the presence of 0.02 M HCl (Scheme 11.1). The progress of the reaction was monitored by TLC. Only two spots, non-polar and polar, assumed to be corresponding to ketal (**114**) and **1a**, were observed. The reaction was stopped after 18 h when no further change was observed. The reaction was repeated under similar conditions with double concentration of acid, i.e., 0.04 M HCl (Scheme 11.1). TLC showed the appearance of a new compound more polar than the ketal **114**. No change in intensity of the spots was observed after 26 h. Work up was done by extracting the product with diethyl ether. The compounds **113** and **114** were obtained as a mixture by column chromatography (dichloromethane:methanol, 95:5/v:v) as a colourless oil. **113** and **114** do not differ significantly in polarity on TLC. The compounds were then fully characterised by spectroscopic methods.

The IR spectrum of the mixture is shown in Figure 11.2. The strong absorption peak at 1697 cm^{-1} corresponds to a carbonyl group. This is an indication of the presence of **113** in the mixture. Formation of ketal **114** from the hemiacetal **1a** on reaction with methanol in the presence of acid is expected since it is a known reaction.

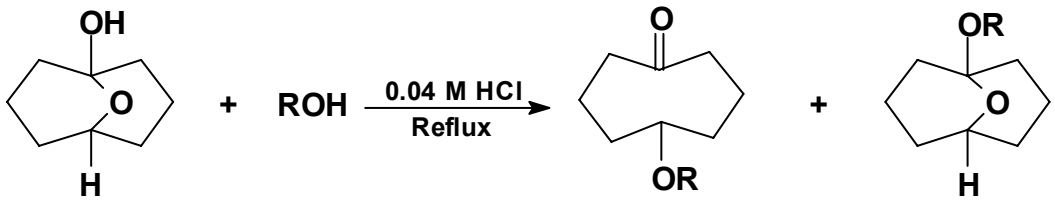

1a **R = Methyl** **113** **114**

Scheme 11.1: Reaction of **1a** with methanol.

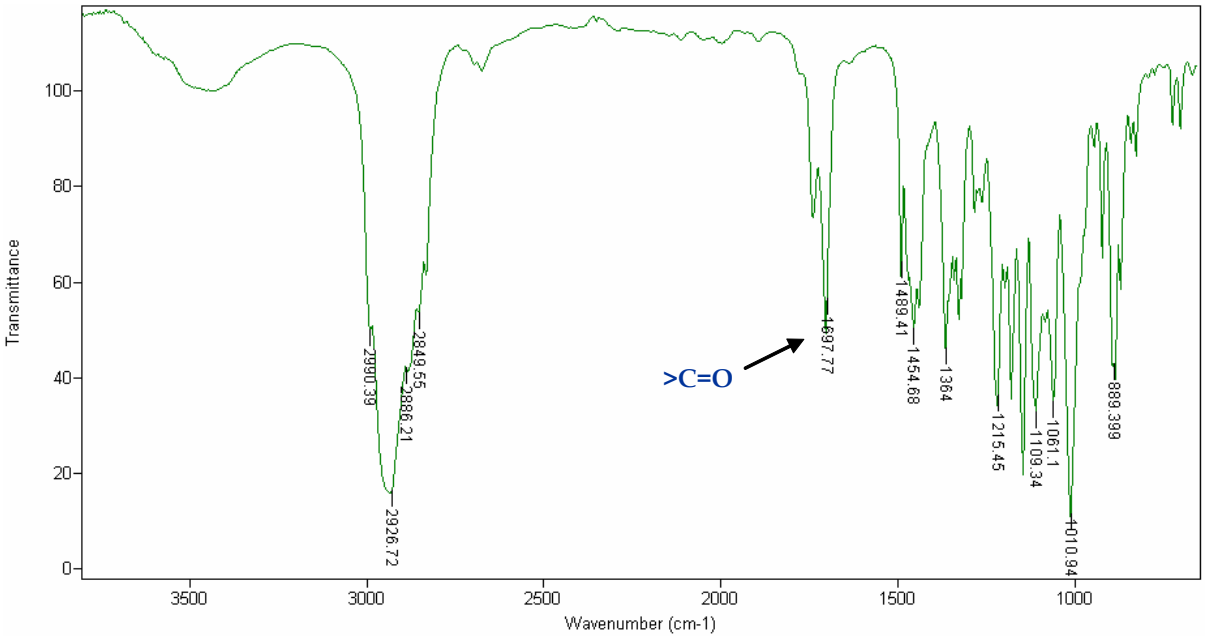

Figure 11.2: IR spectrum (NaCl plates) of the mixture of **113** and **114** obtained on refluxing **1a** with methanol in the presence of 0.04 M HCl.

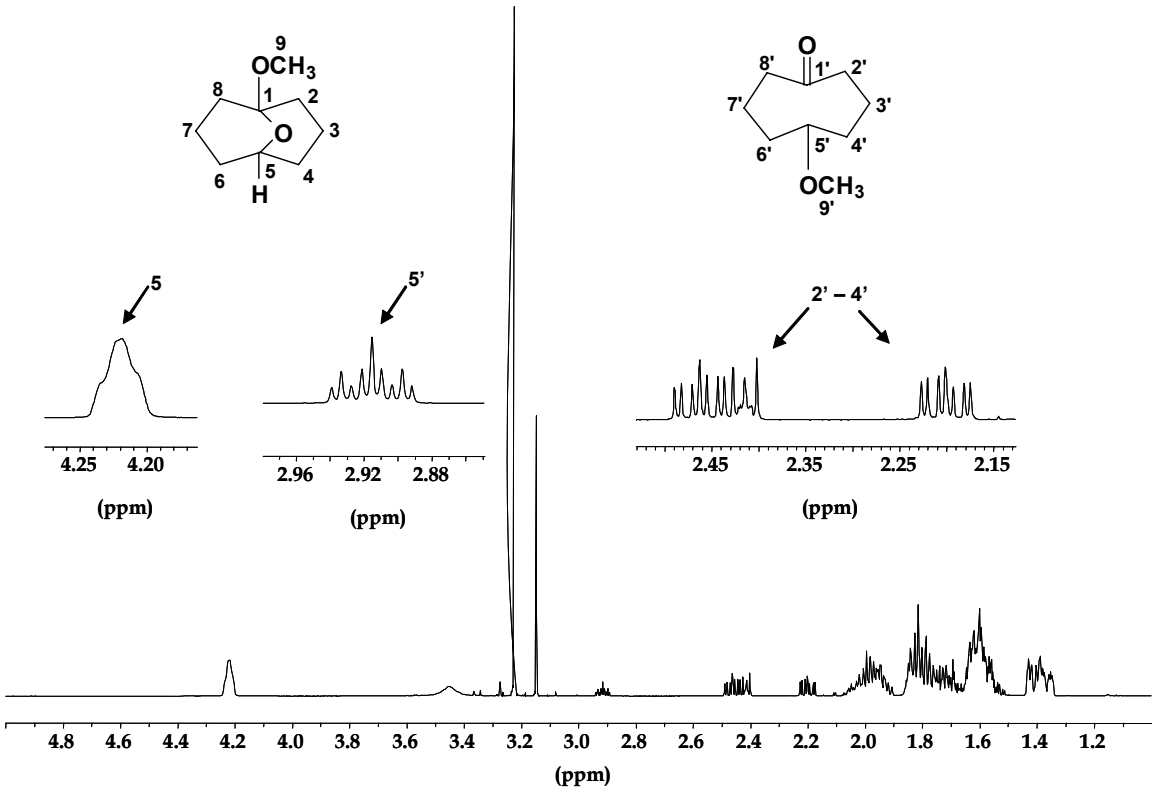

Figure 11.3: ^{1}H-NMR spectrum recorded in $CDCl_3$ of the mixture of **113** and **114** obtained on refluxing **1a** with methanol in the presence of 0.04 M HCl.

To futher support the presence of **113** in the mixture we have recorded ^{1}H- and ^{13}C-NMR spectra. The ^{1}H-NMR spectrum is given in Figure 11.3. The most downfield broad singlet signal at δ 4.22 ppm is assigned to H-5 in **114**. In **1a** the signal for H-5 appears as a triplet. It implies that the conformation for **114** may be different from the conformation of **1a**. The complex multiplet signal at δ 2.89 – 2.94 ppm is assigned to H-5' in **113**. The upfield shift of H-5' can be explained by shielding due to the magnetic anisotropic effect generated by the carbonyl group. The protons α to the carbonyl carbon are expected to appear at δ 2.17 – 2.23 and 2.40 – 2.49 ppm. The eight ring protons at C-3, C-4, C-6 and C-7 appear as a multiplet at δ 1.35 – 2.08 ppm. As expected, the twelve methylene protons of **114** come as a complex multiplet in the region δ 1.35 – 2.08 ppm. There are two singlets at δ 3.15 and 3.22 ppm for the OCH_3 and OCH_3' protons, respectively.

The diagnostic signal in the ^{13}C-NMR spectrum of **113** is that of the carbonyl carbon at δ 216.61 ppm. The signal for C-5' appears at δ 71.48 ppm. The diagnostic signals for **114** are at δ 96.19 and 72.31 ppm for C-1 and C-5, respectively. In ^{13}C-DEPT 135 spectra the signals for the methine and methyl carbons appear as positive peaks, whereas the signals for methylene carbons appear as negative peaks. We expect two positive signals for CH one each in **113** (C-5') and **114** (C-5). The methoxy carbons (C-9' and C-9) also appear as postive peaks. Together we expect four signals as positive peaks and this is consistent with the number of signals obtained. The signals at δ 71.49 and 72.32 ppm are assigned to C-5' and C-5 in **113** and **114**, respectively. The peaks at δ 55.93 and 48.11 ppm are assigned to C-9' and C-9, respectively. The negative signals correspond to the methylene groups of **113** and **114**.

The molecular formula of the compounds **113** and **114** was established to be $C_9H_{16}O_2$ by high-resolution mass spectra at m/z 156.1142 (calcd. m/z 156.1150). The major fragments observed in the MS spectrum corresponds to [M-CO] and acylium ion for **113**. It is established that the ions at m/z 128 and 55 correspond to elemental composition consistent with fragments [M^+-CO] and [$C_3H_3O^+$], respectively.

The ratio of intensities of H-5' (**113**) and H-5 (**114**) calculated from the ^{1}H-NMR spectrum is 17:83. The major product is **114**. The competing reaction during the protection of the hydroxy group is the formation of the ketal. The formation of ketal is S_N1 type reaction. Thus, the rate of reaction is independent of the nucleophile but depends on the concentration of the reactant. The experimental and theoretical

results are in accord with the fact that the hemiacetal **1a** is more stable than **1**. It implies that the availability of **1a** in the reaction mixture is larger than that of **1**. Thus, the rate of nucleophilic attack of alcohol on the hemiacetal is faster. The rate of reaction and the stablility of the so formed ketal make it the major product. Although acetal formation is an equilibrium process, in this case it seems that the thermodynamic stability of the ketal drives the equilibrium more in the forward direction. More generally, this can be explained on the basis of the finding of Wiberg *et al.*[154] that hemiacetal formation is favoured over hydration by 4-5 kcal mol^{-1}. The conversion of the hemiacetal to the acetal leads to a further stabilisation by 4-5 kcal mol^{-1}. This appears to be a general effect of replacing OH by OR.

The alcohol selected for the next reaction is ethanol (Scheme 11.2). In this case formation of keto-ether was also not observed at 0.02 M HCl concentration. Further the reaction was carried out with double HCl concentration. The structures of **115** and **116** were rigorously confirmed by spectroscopic techniques. The presence of a strong absorption band at 1704 cm^{-1} in the IR spectrum indicates the presence of **115** (Figure 11.4). The ^{1}H-NMR spectrum of the mixture of **115** and **116** is given in Figure 11.5. In **116** H-5 appears as a broad triplet at δ 4.25 ppm. The diagnostic signal for **115** appears at δ 3.02 – 3.07 ppm for H-5'. The signal at δ 216.52 ppm in the ^{13}C-NMR spectrum is assigned to the carbonyl carbon atom, i.e., C-1'. In ^{13}C-DEPT 135 spectra two positive signals are expected for methine hydrogen atoms in **115** (C-5') and **116** (C-5). The methoxy carbons (C-10' and C-10) also appear as postive peaks. This is consistent with the number of signals obtained. The signals at δ 77.92, 71.54, 15.54 and 15.98 ppm are assigned to C-5', C-5, C-10' and C-10, respectively in **115** and **116**. The negative signals correspond to the methylene groups of **115** and **116**.

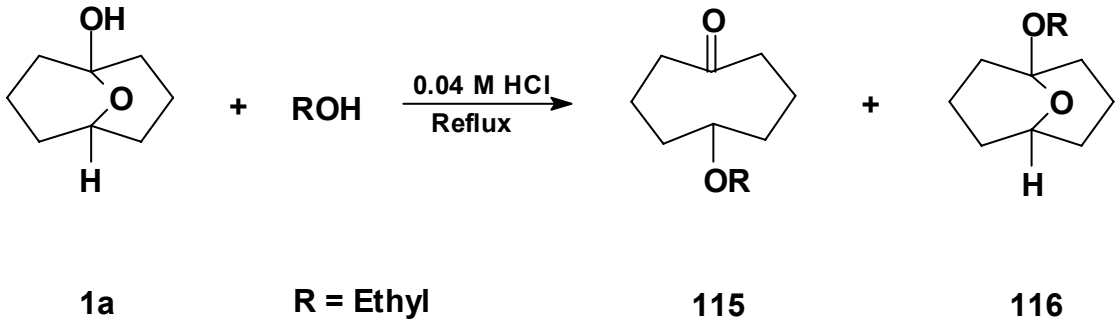

1a **R = Ethyl** **115** **116**

Scheme 11.2: Reaction of **1a** with ethanol.

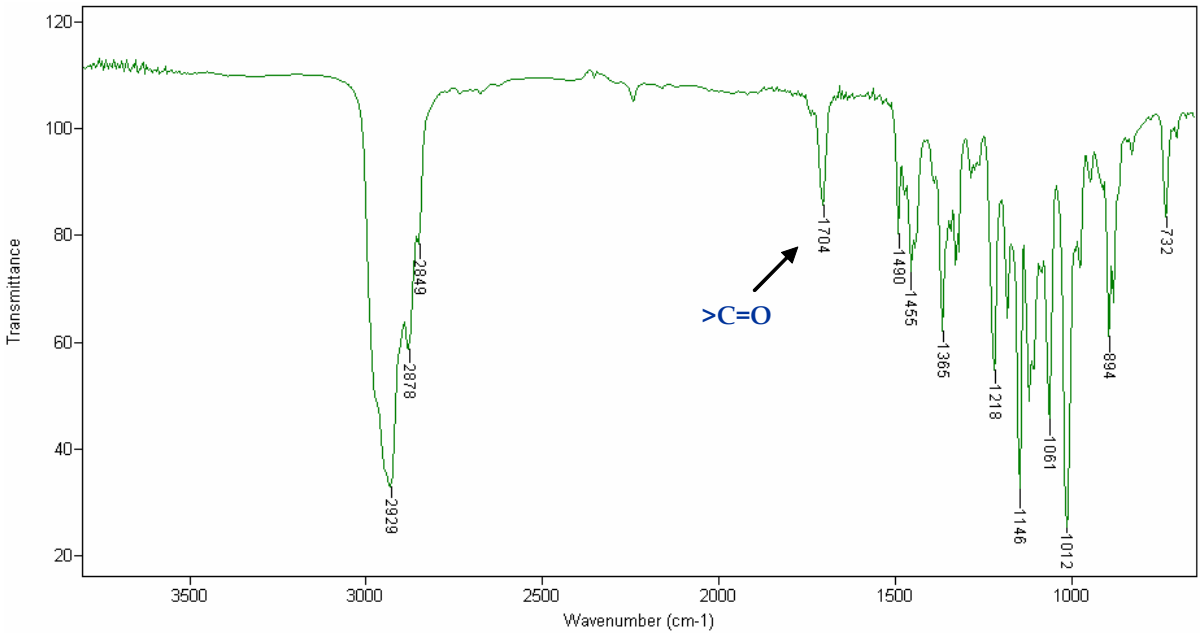

Figure 11.4: IR spectrum of the mixture of **115** and **116** obtained on refluxing **1a** with ethanol in the presence of 0.04 M HCl.

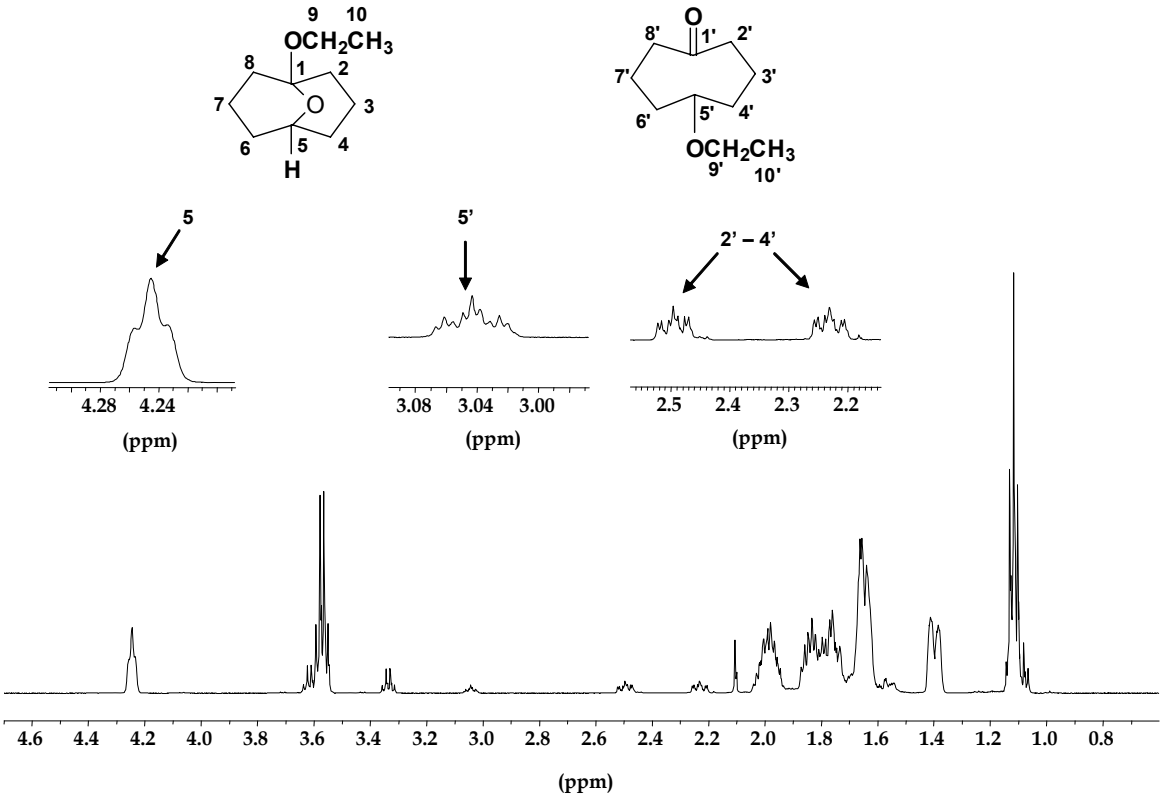

Figure 11.5: ^{1}H-NMR spectrum of the mixture of **115** and **116** obtained on refluxing **1a** with ethanol in the presence of 0.04 M HCl.

The molecular formula of the compounds **115** and **116** was established as $C_{10}H_{18}O_2$ by the high-resolution mass spectra at m/z 170.1304 (calcd. m/z 170.1307). The ions

at m/z 142 and 55 correspond to the elemental composition consistent with fragments [M^+-CO] and [$C_3H_3O^+$]. From the ^{1}H-NMR spectrum the ratio of **115**:**116** was calculated from the intensity ratio of the peaks corresponding to H-5' and H-5 as 11:89.

The next alcohol selected for the protection reaction is 2-bromobenzyl alcohol with a bulky aromatic group. A similar procedure as described above was followed for preparing the keto-ether. Compound **1a** was refluxed with 2-bromobenzyl alcohol in the presence of 0.04 M HCl in acetonitrile as solvent (Scheme 11.3). The products **117** and **118** were characterised by standard spectroscopic methods. The ratio of intensities of H-5' and H-5 calculated from ^{1}H-NMR is 31:69. The IR spectrum of **117** (Figure 11.6) shows the presence of the carbonyl stretching frequency (1700 cm^{-1}). The diagnostic signal for **117** appears at δ 3.31 ppm for H-5' (Figure 11.7). In **118** H-5 appears as a triplet at δ 4.33 ppm. The signal at δ 216.19 ppm is assigned to the carbonyl carbon atom. In the ^{13}C-DEPT 135 spectra two positive signals corresponding to the methine hydrogen atoms in **117** and **118** were observed. The signals at δ 69.91 and 78.41 ppm are assigned to C-5' and C-5 in **117** and **118**, respectively. The molecular formula of the compound **117** and **118** was established to be $C_{15}H_{19}O_2$ by the high-resolution mass spectra at m/z 310.0568 (calcd. m/z 310.0568). The ions at m/z 170 and 55 correspond to the elemental composition consistent with fragments [$C_7H_5Br^+$] and [$C_3H_3O^+$].

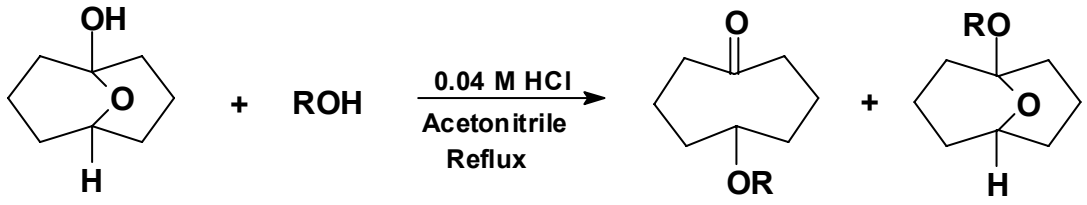

1a **R = 2-Bromobenzyl** **117** **118**

Scheme 11.3: Reaction of **1a** with 2-bromobenzyl alcohol.

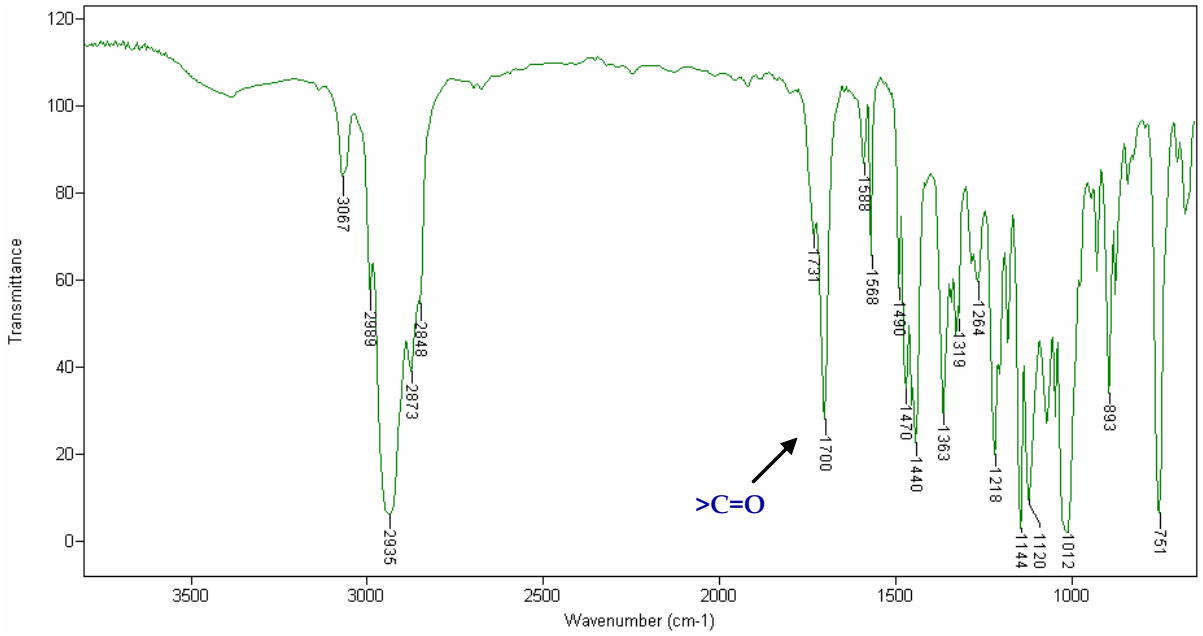

Figure 11.6: IR spectrum of the mixture of **117** and **118** obtained on refluxing **1a** with 2-bromobenzyl alcohol in the presence of 0.04 M HCl.

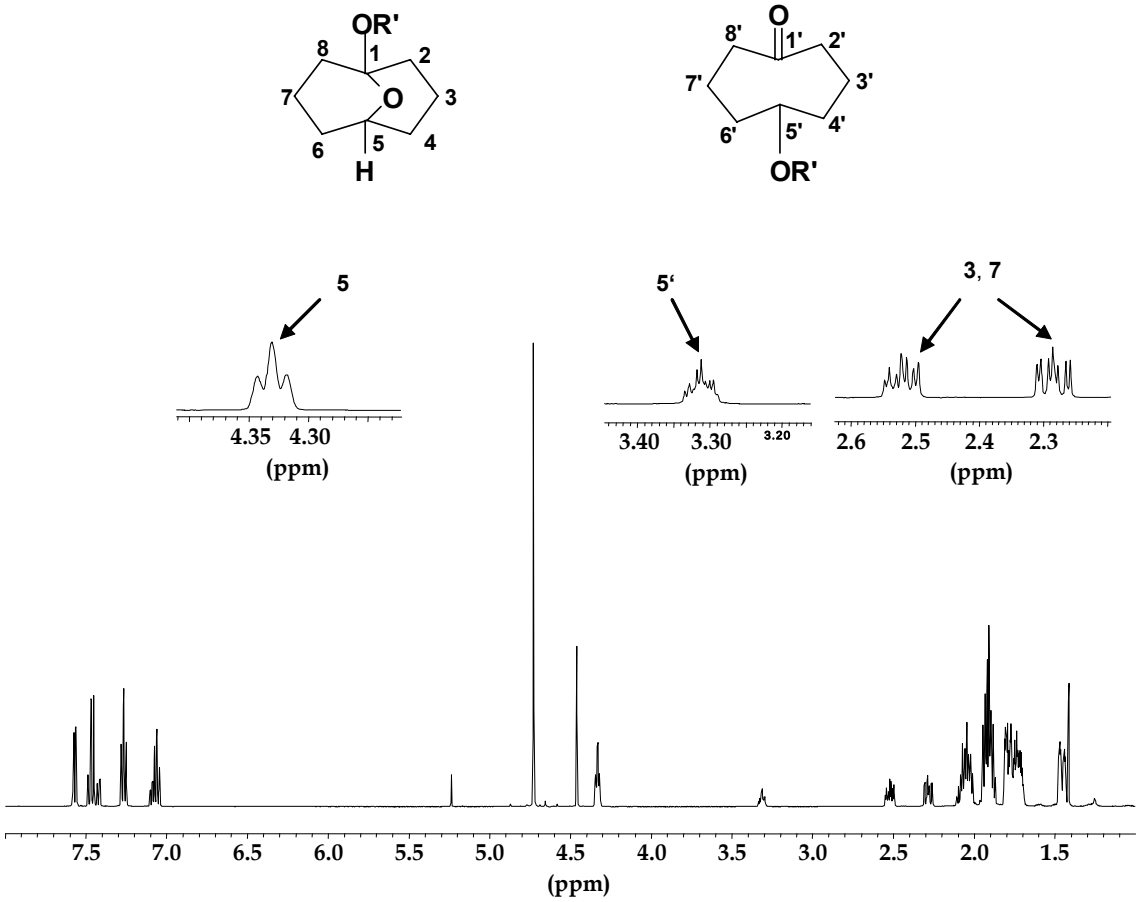

Figure 11.7: ^{1}H-NMR spectrum of the mixture of **117** and **118** obtained on refluxing **1a** with 2-bromobenzyl alcohol in the presence of 0.04 M HCl.

The molecules posses a 9-oxabicyclo[3.3.1]nonane unit with a *cc* conformation Figure 11.8 and the crystal structure reveals hydrogen bonding in the packing of the molecules (Figure 11.9). The low yields of keto-ethers obtained for the reaction between **1a** and alcohol are rationalised on the basis that the starting material exist predominately as hemiacetal (**1a**) not hydroxy-ketone (**1**). An interesting result is that HCl concentration of 0.04 M is the minimum required for preparing keto-ethers by this procedure.

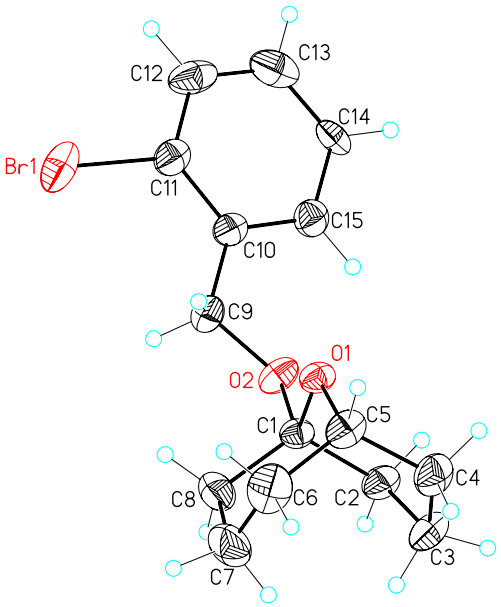

Figure 11.8: Perspective drawing of **118** as determined by X-ray analysis.

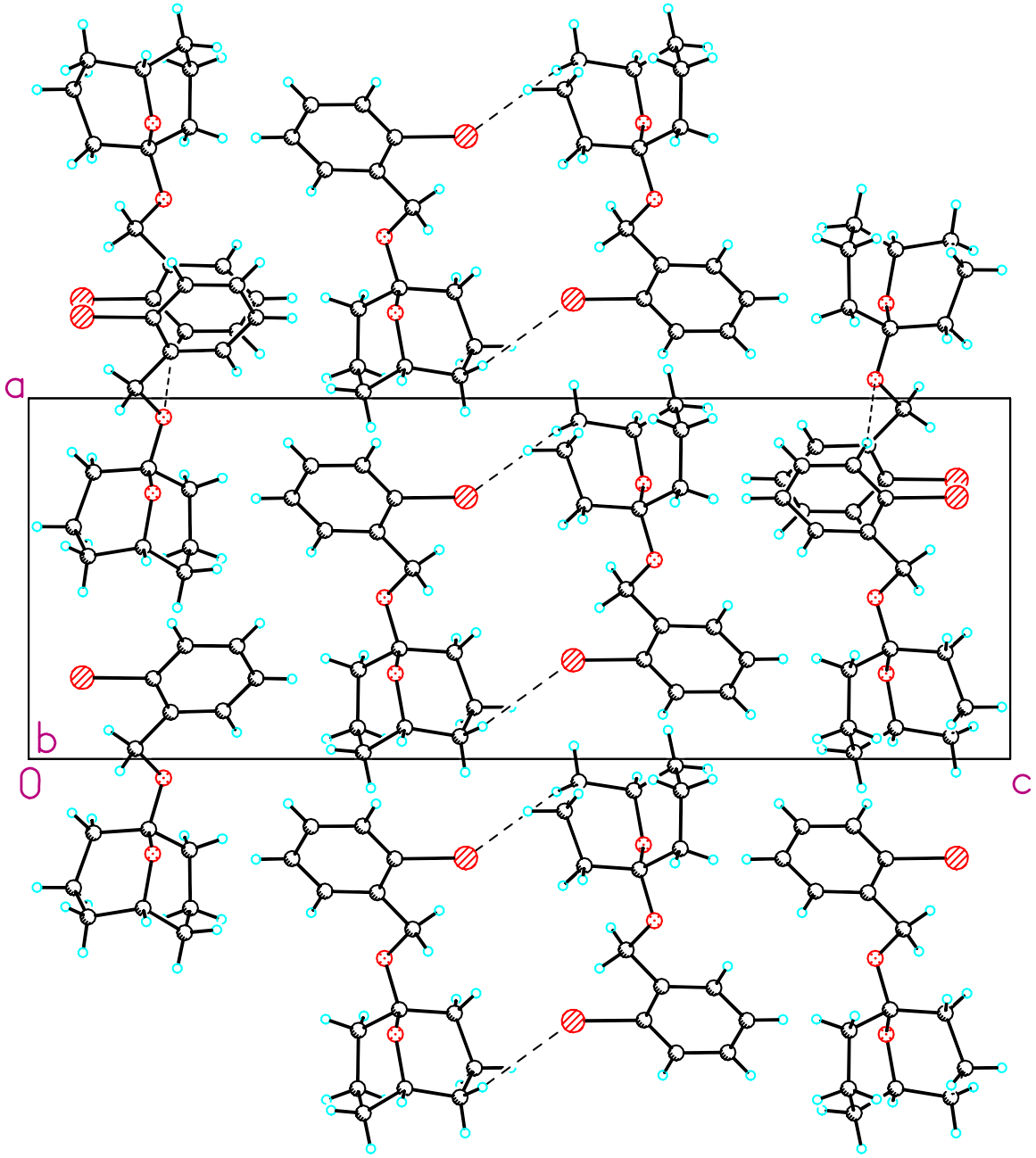

Figure 11.9: Stereoview of the packing of molecules in the crystal structure of **118**.

It has been shown in chapters 8 – 10 that a transannular 1,5-hydride shift occurs in **1a** in the presence of acid or base. Based on the literature[58] and existence of transannular hydride shift in **1** probable mechanism for the formation of keto-ether is shown in Scheme 11.4. The breaking of the oxo-bridge is catalysed by acid which leads to an equilibrium between **1a** and **1**. The carbonyl group present in **1** gets protonated in the presence of acid. Thus, an electrophilic centre at the carbonyl

carbon atom is generated. This initiates the nucleophilic attack by the alcohol present in the reaction mixture on the carbonyl carbon atom. The key step in this mechanism is the transannular 1,5-hydride shift. This step is followed by removal of water and a keto-ether is formed.

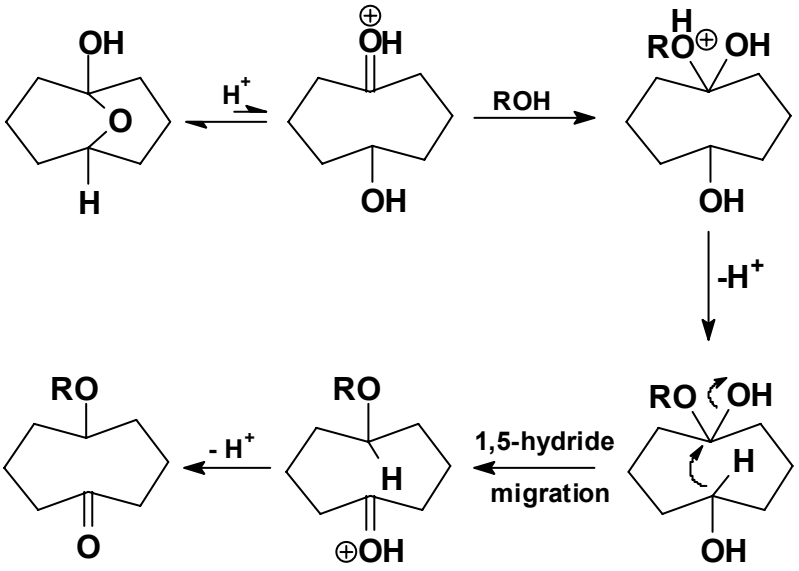

Scheme 11.4: Possible mechanism for the protection of the hydroxy group in **1** on treatment with alcohol in the presence of acid *via* transannular 1,5-hydride shift.

To gain further support for the formation of keto-ether *via* transannular 1,5-hydride shift we have tried to protect the hydroxy group of cyclooctanol (Scheme 11.5). The reaction of cyclooctanol with methanol was attempted following similar reaction conditions as described above. However, the IR and NMR spectra showed only unreacted starting material. Thus, simply heating two alcohols in the presence of acid does not yield the ether.

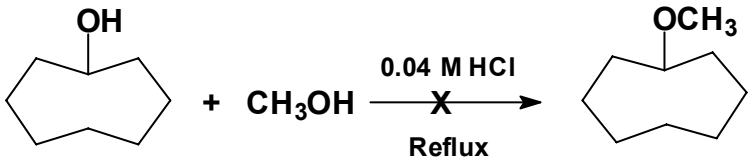

Scheme 11.5: Reaction of cyclooctanol with methanol.

11.2 Protection reaction in solid state

The solvent is important in driving the equilibrium in either direction between the tautomers **1** or **1a** (see chapter 5). In order to investigate the role of solvent in the preparation of the keto-ether we have planned a solid state reaction using 2-bromobenzyl alcohol (Scheme 11.6). A mixture of one equivalent of **1a** and ten equivalents of 2-bromobenzyl alcohol and a catalytic amount of *p*-toluenesuphonic acid (*p*-TSA) was grinded finely using mortar and pestle. The mixture so obtained was kept at room temperature for 70 h. The reaction mixture was grinded after intervals of 12 h and progress of the reaction was monitored by TLC. The products obtained on workup of the reaction mixture showed absence of carbonyl absorption in the IR spectrum clearly indicating absence of keto-ether **117**.

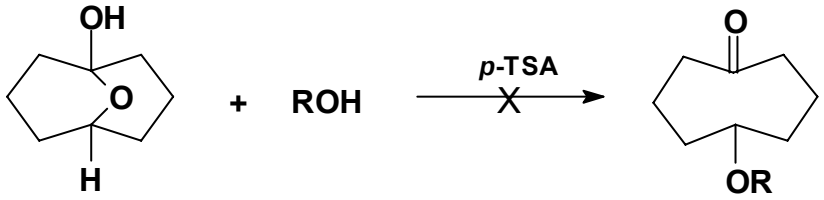

1a **R = 2-Bromobenzyl** **117**

Scheme 11.6: Solid state reaction of **1a** with 2-bromobenzyl alcohol in the presence of *p*-TSA.

Futher evidence for this result was obtained from ^{1}H-NMR spectroscopy. It has been already shown that in the solid state **1a** is in a *cc* conformation. The existence of the open form **1** is ruled out and there is no possiblity of transannular 1,5-hydride shift in solvent free reactions. Thus, the keto-ether is not formed under these conditions.

11.3 Protection reaction under microwave radiation

A surprising phenomenon was observed [58] during the synthesis of the keto-ether of 6-hydroxycyclodecanone (**5**) under microwave radiations. Reaction of benzyl alcohol, 6-hydroxycyclodecanone, water and a catalytic amount of acid (Scheme 11.7) lead not only to the expected keto-ether (**119**), but also another compound characterised

as 6-(6'-oxocyclodecanyloxy) cyclodecanone (**120**). The compound so formed is considered to be the result of a coupling reaction of two molecules.

We have planned a similar reaction for the synthesis of a keto-ether in water. Equimolar amounts of **1a** and benzyl alcohol were taken in an Erlenmeyer flask. To this mixture was added 0.19 M HCl along with 20 equivalents of water. The reaction mixture was irradiated with microwave waves at 660 W for 15 min. The product indicated absence of keto-ether. The reaction was repeated with double concentration of acid but after workup starting materials were recovered.

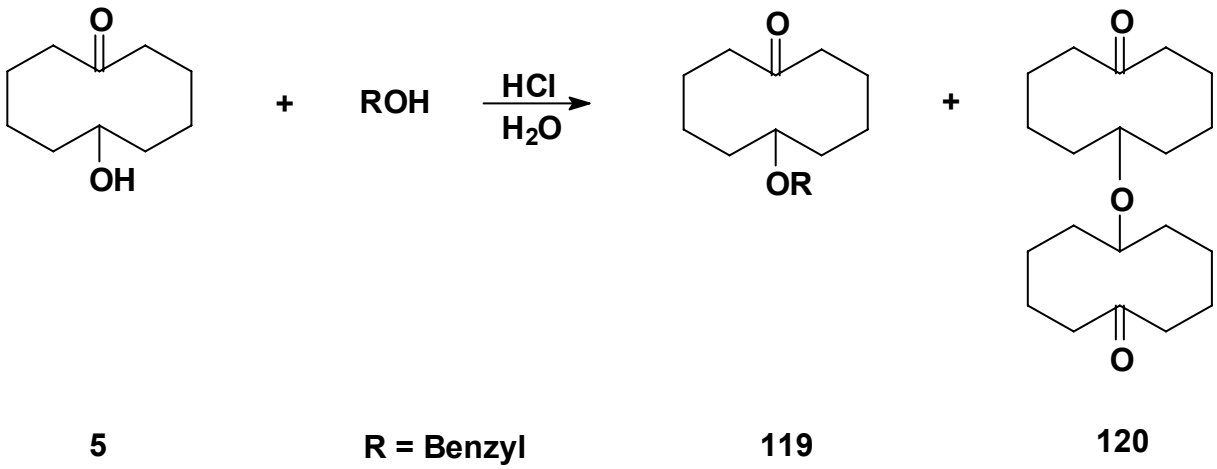

5 **R = Benzyl** **119** **120**

Scheme 11.7: Reaction of **5** with benzyl alcohol in water under microwave radiation.

11.4 Conclusion

The encouraging results obtained here can be extrapolated to various medium-ring substrates containing similar functionalities. The main advantages of the approach based on the transannular 1,5-hydride shift for the keto-ether preparation are low costs and simple reaction conditions. Yield may be improved, for example, by removing reaction water. But the major limitation of this method is that the main product is the ketal instead of the keto-ether in alcohols such as methanol and ethanol. However, reactions with alcohols such as 2-bromobenzyl alcohol give good yield of keto-ether.

12 Summary and outlook

To what extent are transannular reactions of medium-ring compounds are dependent on their conformations and to what extent can reaction conditions and other factors such as ring size and substituents partially or completely control the transannular interaction? These questions have been investigated with experimental and theoretical studies in this work. A comprehensive study of hemiacetal formation and 1,x-hydride shift (x = 4 – 6) has been carried out for model compounds **1** – **5** in order to elucidate the influence of different factors such as ring size, presence of a C=C double bond and substituents on these transannular reactions.

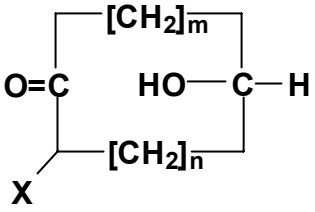

1: m=1, n=1, X=H
2: m=2, n=0, X=H
4: m=1, n=1, X=Br
5: m=2, n=2, X=H

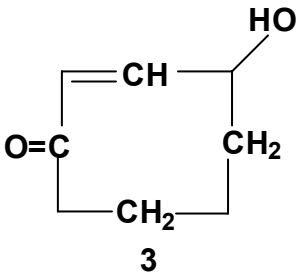

3

The theoretical and NMR investigations on **1** – **3** indicate that the eight-membered disubstituted compounds present the optimal conditions for the 'contact' of substituents in the positions 1 and 5 for the transannular interactions resulting in transannular products. The X-ray crystal structures have clearly shown that compounds **1** and **3** exist as hemiacetals. The experiments clearly indicate highly dynamic behaviour of these molecules and the existence of equilibrium between tautomers especially in protic solvents, i.e., DMSO-d_6 and D_2O, which have not been reported before. The tautomeric equilibrium between **1** and its transannular product drives in the direction of hemiacetal in a range of polar and non-polar solvents. But remarkably, the combined effect of solvent polarity and temperature drives the equilibrium in the reverse direction to a significant extent. The equilibrium constant K_{eq} for forward reaction is reduced to 16.5 in DMSO-d_6 at 403 K and 31.3 in D_2O at 323 K. In the case of **2**, the transannular hemiacetal is only ≤1 % in D_2O at higher temperature. In contrast, in compound **3** the hemiacetal is favoured exclusively in benzene-d_6 at 298 and 343 K.

The experimental findings for the tautomeric equilibrium of compounds **1** – **5** are substantiated by theoretical investigations. The present results represent the first

comparison of transannular hemiacetal formation as a function of conformation in eight- and ten-membered hydroxy-ketones. Since these compounds possess very complex multidimensional potential energy hypersurfaces (PEHS), the choice of good starting geometries for these molecules was facilitated by applying molecular mechanics. The starting geometries referred as *preferred* starting conformer are selected on the basis of factors such as proximity of the reacting groups and energetics. Detailed conformational and energetic investigations carried out using DFT theory shows that the *preferred* starting conformer of **1**, **4** and **5** are 8.5, 8.6 and 8.1 kcal mol^{-1}, respectively, less stable than the corresponding hemiacetals in the gas phase. It implies thermodynamically *preferred* products in **1**, **4** and **5** are **1a**, **4a** and **5a**. In case of **2** and **3** the *preferred* starting conformers are only 3.6 and 4.6 kcal mol^{-1} less stable that the corresponding hemiacetals. The calculated (B3LYP/6-31+G*) activation barriers for hemiacetal formation in **1**, **2**, **3**, **4** and **5** are 38.2, 35.2, 36.5, 38.2 and 36.9 kcal mol^{-1}, respectively, in the gas phase. The transannular hemiacetal formation occurs through a four-membered cyclic transition-state which is most tight in **2**. The activation barriers calculated using continuum solvation models (PCM) were not significantly different from the gas phase calculations. It is obvious that the theoretical models used are not able to handle specific solvent effects, so we consider results obtained for hemiacetal formation in water and chloroform semi-quantitatively.

The experimental data show that the transannular 1,5-hydride shift is catalysed both by base and acid. A comparative theoretical study of the transannular 1,4-, 1,5- and 1,6-hydride shifts in compounds **1**, **2**, **4** and **5** shows consensus with the experimental findings that the presence of a metal counterion or acid lowers the activation barriers. In all cases, the reaction proceeds through a hexagonal transition-state structure. The calculated (B3LYP/6-31+G*) activation barriers for 1,5-, 1,4- and 1,6-hydride shift in compounds **1**, **2**, **4** and **5** are 46.6, 52.2, 43.0 and 28.0 kcal mol^{-1}, respectively, for the uncatalysed reaction. One of the key results is that the activation barriers for 1,6-hydride shift in **5** (28.0 kcal mol^{-1}) and the corresponding intermolecular hydride shift (26.4 kcal mol^{-1}) in the methanol and formaldehyde model system are very similar in the uncatalysed reactions. Moreover, the characteristics of the six-membered cycle formed in transition-state structure of 1,6-hydride shift is similar to the six-membered cycle formed in the intermolecular hydride shift between formaldehyde and methanol.

The potential energy profiles for the degenerate 1,4-, 1,5- and 1,6-hydride shifts correspond to the two interchanging hydroxy-ketones and a high lying unsymmetrical transition structure for interconversion of **2** and **6**, respectively and symmetrical transition structures for interconversion of **1** and **4**, respectively. In the presence of a metal counterion, the transannular 1,6-hydride shift and the intermolecular hydride shift took place *via* low energy complexes. The low energy complexes are formed by the electrostatic attraction of metal counterion with carbonyl oxygen atom. It is highly likely that similar intermediates are involved in 1,4- and and 1,5-hydride shifts too, but attempts to locate similar low energy complexes in **1**, **2** and **4** all failed. The transition-state formed in the acid catalysed reaction in **5** can best be described as a localised C-H-bridged cation with a facile 1,6-hydride shift. The transition-states for the transannular hemiacetal formation and 1,x-hydride shift are likely to closely resemble the *preferred* starting conformer. Thus, it might be anticipated that knowledge of the *preferred* starting conformations would be of great predictive value in determining the type of reaction systems **1** – **5** undergo.

For the first time the synthetic potential of transannular 1,5-hydride shift in preparing keto-ethers by reaction of **1** with alcohols in presence of 0.04 M HCl is investigated. This method is attractive for the reasons that it is unexpensive and the hydroxy group can be easily deprotected. However, a major limitation of this method is that the yield of keto-ether of **1** with alcohols such as methanol and ethanol is low. On the other hand, reactions with alcohols such as 2-bromobenzyl alcohol give good yields of the keto-ether.

The transannular reactions in hydroxy-ketones reported in the present study seem to serve as good models, in terms of electronic structure and geometry, for the transition-state of transannular hemiacetal formation and hydride shift reactions in medium-ring compounds. Our results suggest that such reactions, particularly hydride shift, can be exploited *via* easy protection and deprotection of hydroxy groups in the synthesis of important target molecule. Thus, the underlying chemistry of transannular reactions in certain medium-rings reasonably offers potential as a strategic element in the synthesis of polycyclic natural products. It is anticipated that the knowledge obtained in these experiments can be fruitfully applied to the goals for the synthesis of medium rings and the chemistry related to these experiments.

13 Experimental section

13.1 General

13.1.1 Drying and purification of solvents

The solvents tetrahydrofuran (THF), diethyl ether were dried by distillation over sodium-benzophenone. Dried solvents were stored and transferred under argon. Dichloromethane (DCM) and toluene were dried over calcium hydride (CaH_2) and later stored under argon.

13.1.2 Thin layer and column chromatography

Analytical thin-layer chromatography (TLC) was conducted on standard commercial aluminium sheets pre-coated with silica gel 60 (Merck, 230 – 400) using either DCM/methanol or hexane/ethyl acetate or diethyl ether/petroleum ether in different proportions as the eluent. UV light (λ = 254 or 366 nm) was used to visualise the TLC. Column chromatography was performed on Roth silica gel (70 – 230 mesh).

13.1.3 General procedure for photooxygenation

To a solution of *cis*,*cis*-1,3-cyclooctadiene, hematoporphyrin and acetone a gentle steam of dry O_2 gas was bubbled. The reaction mixture was simultaneously irradiated with a 75 W halogen lamp. The temperature of the reaction mixture was maintained at room temperature by cooling with an ice bath. The reaction was monitored by gas chromatography. Special precautions have been taken to control the temperature since the peroxides so formed can explode when over heated.

13.1.4 General procedure for microwave and solid state reactions

The microwave oven used for reactions was a Sharp R-33ST domestic oven. The frequency of microwaves produced is 2450 MHz. For solid state reactions the reactants were powdered together using a mortar and pestle. The reaction mixture was stored under vaccum.

13.2 Analytical methods

13.2.1 NMR spectra

^{1}H-NMR Spectra were recorded using a Bruker Avance 500 (DRX) spectrometer.The following frequencies were used: 499.7 MHz (^{1}H), 125.7 MHz (^{13}C). The spectra were measured as solution in a 5 mm tube at different temperatures in different solvents. The chemical shifts are reported in units of parts per million (%) relative to tetramethylsilane (^{1}H, ^{13}C) as internal standard. Coupling constants *J* are given in Hz. The chemical shifts are expressed as δ (parts per million). The signal characteristics are described using standard abbreviations: s (singlet), d (doublet), dd (doublet of doublet), t (triplet), q (quartet), m (multiplet), br (broad), vbr (very broad). In ^{13}C-DEPT 135 spectra, CH_3, CH_2, CH, C are used to indicate methyl, methylene, methine and quaternary carbons. One- and two-dimensional such as ^{1}H-^{1}H, ^{1}H-^{13}C correlation were determined using the same instrument.

13.2.2 Vibrational spectra

FTIR spectra were recorded on a Bio-Rad FT-IR-spectrometer FTS 135. The neat compounds were taken as film on NaCl pellets in the region 4000 to 650 cm^{-1}. The spectra for solid compounds were measured using KBr pellets. The absorptions are assigned as s (strong), m (medium), w (weak), br (broad) and v (very). The vibrational modes v (valence stretching) and δ (deformation) are also assigned.

13.2.3 Melting points

Melting points (uncorrected) were determined with an Electrothermal 9100 apparatus.

13.2.4 Mass spectra

High-resolution mass spectra (HRMS) were obtained with a Fisons Instruments VG Pro-Spec 3000. The intensities are reported as a percentage relative to the base peak after the corresponding *m/z* value.

13.2.5 X-ray crystallography

The accurate structure determinations were carried out with a Siemens P4 diffractometer. The instrument is computer controlled and used graphite monochromated Mo-K·radiation. Siemens SADABS program is used for the absorption correction. Crystallographic data and details of refinement are reported in X-ray Tables (ref. Appendix 14.1). The accurate structure determinations were carried out with a Siemens SMARTCCD area detector system. The structures were solved by direct methods. The refinements based on *F*2 were performed by the full-matrix least-squares method with the crystallographic software SHELXTL program.

13.3 Materials

Commerically available reagents (Aldrich, Sigma and Fluka) cyclooctanol, cyclooctanone, *cis*-1,5-cyclooctanediol, chromium(VI) oxide, *cis*,*cis*-1,3-cyclooctadiene, azodicarbonamide, triethylamine, benzyl alcohol, 2-bromobenzyl alcohol, 3-bromobenzyl alcohol, 4-bromobenzyl alcohol 4-nitrobenzyl alcohol, deuterium chloride, 35 *wt.* % solution in D_2O (99 atom % D), deuterated solvents, hematoporhyrin, were used without purification.

13.4 Synthesis and characterisation of model compound 1a (1 ⇌ 1a)[128]

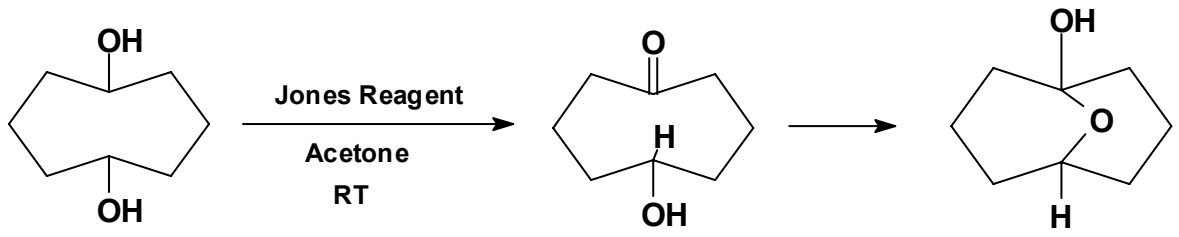

1 **1a**

A round bottom flask (250 mL) equipped with stirring bar was charged with *cis*-1,5-cyclooctanediol (5.0 g, 35.7 mmol) and acetone (100 mL). The contents were stirred at room temperature. Freshly prepared Jones reagent (6.7 g chromium (VI) oxide, 5.5 mL conc. H_2SO_4 and 10.0 mL H_2O) was added dropwise until the red colour persists. The amount of Jones reagent added was 4.8 mL. Isopropanol (2.0 mL) was added to quench the excess of oxidising reagent. The contents were stirred for an additional

30 min. A green colored salt was formed. The acetone layer was decanted and the salt was washed with dichloromethane (2 x 5 mL). The solvent was evaporated under reduced pressure. The residue was extracted with dicholromethane (3 x 10 mL) and dried over sodium sulphate. A pale white solid was obtained after removal of the solvent. The compound was purified by sublimation at 35 °C and pressure 0.15 hPa (lit[128] 0.2 torr at 65 ºC). A white solid compound was obtained. The compound was dissolved in hexane and crystallised by slow evaporation. X-ray structure of **1a** and details of crystallographic data are presented in Figure 4.1 and Appendix 22.1.1.

Yield: (2.8 g, 19.7 mmol) 56 % [Lit.[128] 81 %]

M.p.: 99-100°C [Lit.[128] 100-102°C].

IR (KBr): ν [cm^{-1}] = 3341 brs (OH), 2944 s (CH_2), 1151 s (C-O-C), 1211 s (C-OH).

13.5 Synthesis and characterisation of model compound 2a (2 ⇌ 2a)[129, 130]

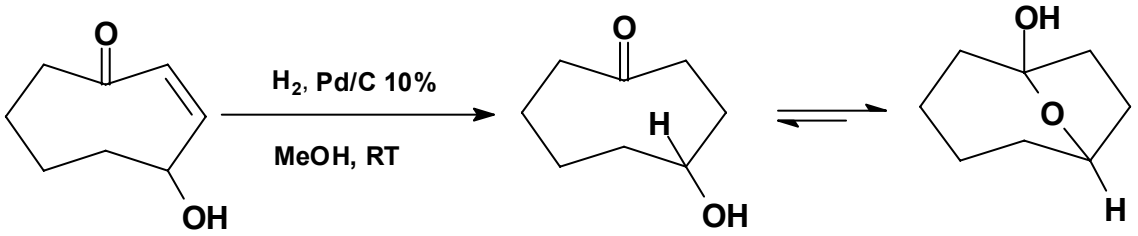

3 **2** **2a**

A solution of 4-hydroxycyclooct-2-enone (**3**, 3.6 g, 25.7 mmol) was shaken in methanol in the presence of 10% palladium on charcoal (360.0 mg) under 3.0 x 10^5 Pa hydrogen pressure for 24 h. The suspension was filtered and the solvent was evaporated under reduced pressure. The compound obtained was a yellow oil.

Yield: (2.0 g, 14.3 mmol) 55 %

IR (KBr): ν [cm^{-1}] = 3419 brs (OH), 2932 s (CH_2), 1699 s (>C=O), 1151 s (C-O-C), 1211 s (C-OH).

13.6 Synthesis and characterisation of model compound 3a (3 ⇌ 3a)[129, 131]

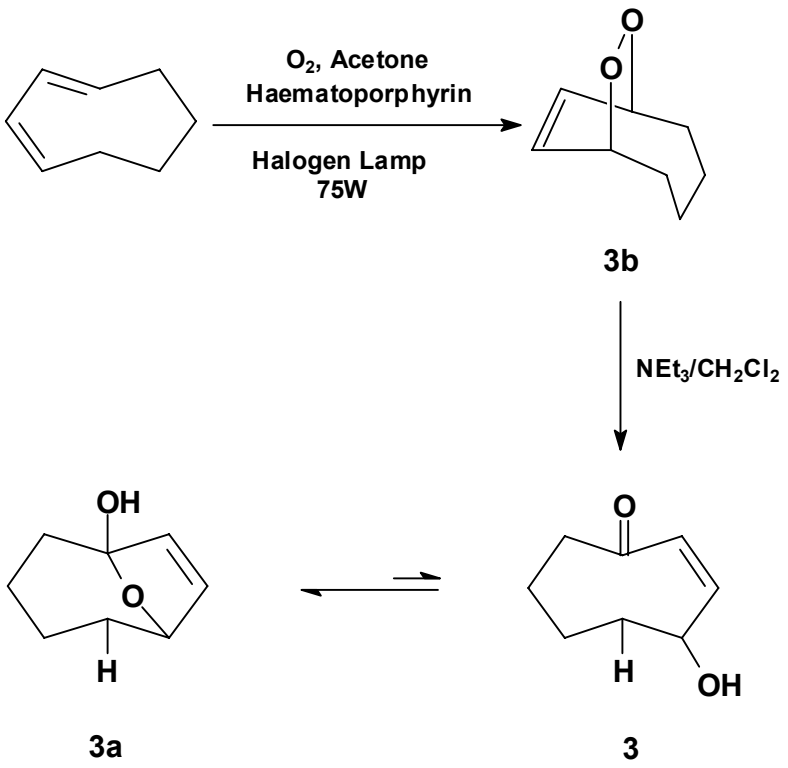

To a stirred solution of *cis*,*cis*-1,3-cyclooctadiene (20.9 g, 193.0 mmol) in acetone (840 mL) and haematoporphyrin (487.0 mg, 1.7 mmol) oxygen gas was bubbled gently. The reaction mixture was simultaneously irradiated with a 75 W halogen lamp. The evaporation of solvent was minimised by cooling the reaction mixture in an ice bath. The temperature was maintained near to room temperature. The colour of the reaction mixture changed to brown yellow. Progress of reaction was monitored with gas chromatography. After 8 d the reaction was stopped. The solvent was removed under reduced pressure at room temperature. Care has been taken during removal of solvent since peroxides are explosive in nature. A brown yellow oil was obtained in 14 % yield (2.7 g, 19.3 mmol). The compound so obtained was characterised by spectroscopy and used for the next step without further purification. To a solution of **3b** (2.7 g, 19.3 mmol) in dichloromethane (90 mL) a solution of triethylamine (5.4 mL, 38.9 mmol) in dicholoromethane (38 mL) was added slowly with stirring. The addition was done at 0°C. After completion of addition, the reaction mixture was refluxed for 24 h. The solvent was removed under reduced pressure to give a pale yellow oil. Column chromatography was done using dichloromethane:methanol (95:5/v:v) mixture as eluent. The product was a white solid. The compound was crystallised

from ethyl acetate. X-ray structure of **3a** and details of crystallographic data are presented in Figure 4.3 and Appendix 22.1.2.

Yield: (1.6 g, 11.4 mmol) 67 % [Lit.[129] 78 %]

M.p.: 92-93°C [Lit.[63] 92-93°C].

IR (KBr): ν [cm^{-1}] = 3308 brs (OH), 2926 s (CH_2), 1069 s (C-O-C), 1211 s (C-OH).

13.7 Synthesis and characterisation of ethers 113 and 114

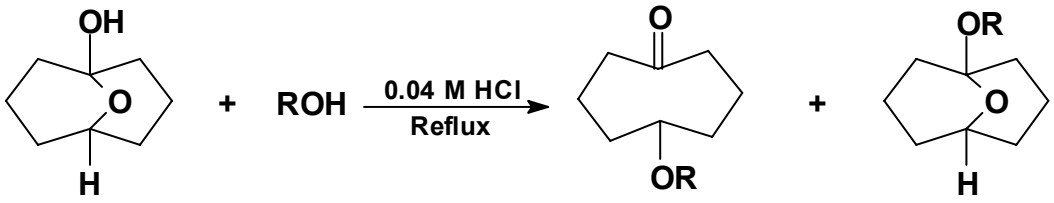

1a **R = Methyl** **113** **114**

In a 100 mL round bottom flask charged with **1a** (2.0 g, 13.7 mmol) a solution of 0.3 mL conc. HCl in 90 mL of methanol was added. The reaction was monitored with TLC (dichloromethane:methanol, 95:5/v:v). The mixture was refluxed for 26 h. The mixture was treated with 30 mL diethyl ether. Washing of reaction mixture was done repeatedly with water and $NaHCO_3$ solution. The solution was dried over anhydrous Na_2SO_4 and evaporated under reduced pressure giving a brown yellow oil. The oil was purified by column chromatography (dichloromethane:methanol, 95:5/v:v). A mixture of **113** and **114** as a colorless oil (350.0 mg, 18 %) was obtained. The ratio of **113**:**114** calculated from the intensities of H-5' and H-5 in ^{1}H-NMR spectra is 17:83 in $CDCl_3$.

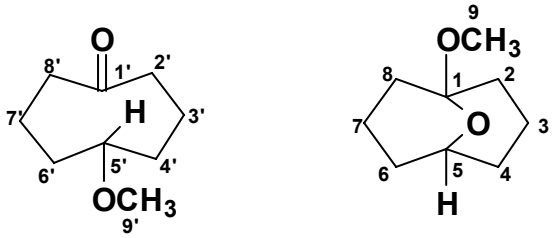

113 **114**

^{1}H-NMR-Spectrum for **113** ($CDCl_3$, 500 MHz): δ [ppm] = 1.35 – 2.07 (m, 8 H, H-3', H-4', H-6' and H-7'), 2.17 – 2.23 and 2.40 – 2.49 (m, 4 H, H-2', H-8'), 2.89 – 2.94 (m, 1 H, H – 5'), 3.15 (s, 3 H, H-9').

^{13}C-NMR-Spectrum for **113** ($CDCl_3$, 500 MHz): δ[ppm] = 216.61 (C-1'), 71.48 (C-5'), 55.94 (C-9'), 42.13 (C-2', C-8'), 33.16 (C-4', C-6'), 20.52 (C-3', C-7').

IR (KBr) for **113**: ν [cm^{-1}] = 2933 s, 2879 s (CH), 2848 m (OCH_3), 1700 s (C=O), 1490 m, 1455 m δ [$(CH)_{aliph.}$)].

Mass spectrum for **113**: $^{m}/_{z}$ (%) = 156 (17) [M^+], 128 (13) [M^+-CO], 55 (100) [$C_3H_3O^+$].

^{1}H-NMR-Spectrum for **114** ($CDCl_3$, 500 MHz): δ [ppm] = 1.35 – 2.07 (m, 12 H, H-2 – H-4 and H-6 – H-8), 3.22 (s, 3 H, H-9), 4.22 (s, 1 H, H-5).

^{13}C-NMR-Spectrum for **114** ($CDCl_3$, 500 MHz): δ [ppm] = 96.19 (C-1), 72.31 (C-5), 48.11 (C-9), 36.13 (C-2, C-8), 28.20 (C-4, C-6), 22.81 (C-3, C-7).

IR (KBr) for **114**: ν [cm^{-1}] = 2933s, 2879 s (CH), 2848 m (OCH_3), 1490 m, 1455 m δ [$(CH)_{aliph.}$)], 1147 s (C-O-C).

Mass spectrum for **114**: $^{m}/_{z}$ (%) = 156 (17) [M^+], 128 (13) [M^+-C_2H_4], 74 (49) [M^+-C_6H_{10}].

13.8 Synthesis and characterisation of ethers 115 and 116

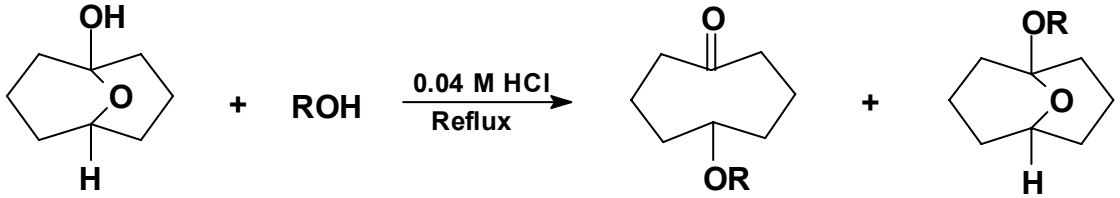

1a **R = Ethyl** **115** **116**

In a 250 mL round bottom flask charged with **1a** (4.4 g, 31.0 mmol) a solution of 0.3 mL conc. HCl in 90 mL of ethanol was added. The mixture was refluxed for 28 h. The mixture was treated with 30 mL diethyl ether and washed repeatedly with water and $NaHCO_3$ solution. The solution was dried over anhydrous Na_2SO_4 and evaporated under reduced pressure giving a brown yellow oil. The oil was purified by column chromatography (dichloromethane:methanol, 95:5/v:v). A mixture of **115** and **116** as colorless oil (1.2 g, 27 %) was obtained. The ratio of **115**:**116** calculated from the intensities of H-5' and H-5 in ^{1}H-NMR spectra is 11:89.

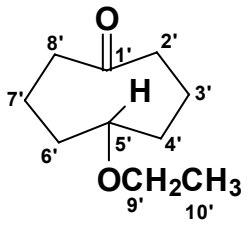

115

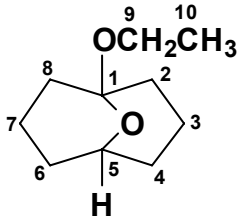

116

^{1}H-NMR-Spectrum for **115** ($CDCl_3$, 500 MHz): δ [ppm] = 1.11 (t, J = 7.1 Hz, 3 H H-10'), 1.54 – 2.04 (m, 8 H, H-3', H-4', H-6', H-7'), 2.20 – 2.26 and 2.47 – 2.52 (m, 4 H, H-2', H-8'), 3.02 – 3.07 (m, 1 H, H – 5'), 3.31 – 3.57 (m, 2 H, H-9').

^{13}C-NMR-Spectrum for **115** ($CDCl_3$, 500 MHz): δ [ppm] = 216.52 (C-1'), 77.92 (C-5'), 56.05 (C-9'), 42.26 (C-2', C-8'), 33.89 (C-4', C-6'), 23.03 (C-3', C-7'), 15.54 (C-10').

IR (KBr) for **115**: ν [cm^{-1}] = 2929 s, 2878 s (CH), 2848 m (OCH_2CH_3), 1704 s (C=O), 1490 w, 1455 w, δ [$(CH)_{aliph.}$)].

Mass spectrum for **115**: $^m/_z$ (%) = 170 (54) [M^+], 142 (22) [M^+-CO], 55 (93) [$C_3H_3O^+$].

^{1}H-NMR-Spectrum for **116** ($CDCl_3$, 500 MHz): δ [ppm] = 1.17 (t, J = 7.1 Hz, 3 H, H-10), 1.38 – 2.04 (m, 12 H, H-2 – H-4 and H-6 – H-8), 3.55 – 3.59 (m, 2 H, H-9), 4.25 (t, 1 H, H - 5).

^{13}C-NMR-Spectrum for **116** ($CDCl_3$, 500 MHz): δ[ppm] = 96.30 (C-1), 71.54 (C-5), 55.85 (C-9), 33.36 (C-2, C-8), 28.35 (C-4, C-6), 20.00 (C-3, C-7), 15.98 (C-10).

IR (KBr) for **116**: ν [cm^{-1}] = 2929s, 2878 s (CH), 2848 m (OCH_2CH_3), 1146 s (C-O-C), 1490 w, 1455 w δ [$(CH)_{aliph.}$)].

Mass spectrum for **116**: $^m/_z$ (%) = 170 (54) [M^+], 142 (22) [M^+-C_2H_4], 88 (100) [M^+-C_6H_{10}].

13.9 Synthesis and characterisation of ethers 117 and 118.

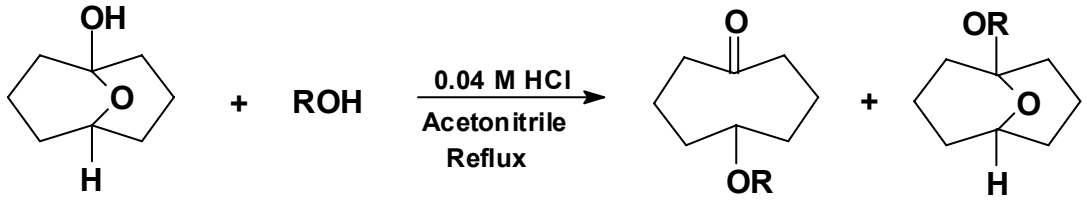

1a **R = 2-Bromobenzyl** **117** **118**

In a 250 mL round bottom flask charged with **1a** (6.0 g, 42.3 mmol) a solution of 0.6 mL conc. HCl in 180 mL of acetonitrile was added. To the obtained solution was added 2-bromobenzyl alcohol (9.5 g, 50.8 mmol). The molar ratio of **1a**:2-bromobenzyl alcohol was kept 1:1.2. The mixture was refluxed for 50 h. The resulting cooled mixture was treated with 30 mL diethyl ether, followed by washing with water and $NaHCO_3$ solution. The combined extracts were dried over anhydrous Na_2SO_4 and evaporated under reduced pressure giving a yellow oil. The oil was purified by column chromatography (dichloromethane:methanol, 95:5/v:v). A mixture of **117** and **118** as colorless oil (3.9 g, 65 %) was obtained. The ratio of **117**:**118** calculated from the ratios of intensities of H-5' and H-5 in ^{1}H-NMR spectra is 31:69 in $CDCl_3$. The mixture was dissolved in hexane and crystallised. X-ray crystallography reveals that crystals correspond to compound **118**.

M.p. of **118**: 51-52º.

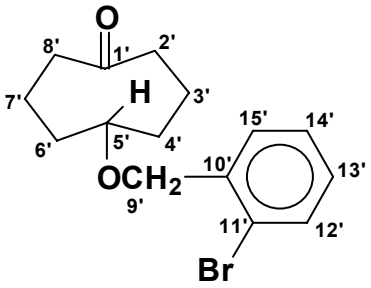

117

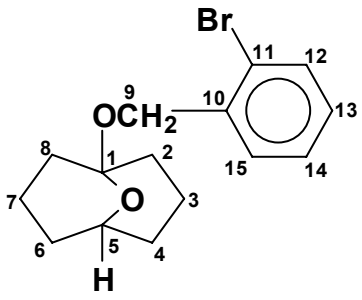

118

^{1}H-NMR-Spectrum for **117** ($CDCl_3$, 500 MHz): δ [ppm] = 1.43 – 1.44 (m, 8 H, H-3', H-4', H-6' and H-8'), 2.26 – 2.31 and 2.50 – 2.55 (m, 4 H, H-2', H-8'), 3.31 (m, 1 H, H-5'), 4.46 (s, 2 H, H-9'), 7.04 – 7.58 (m, 4H, H-12' – H-15').

^{13}C-NMR-Spectrum for **117** ($CDCl_3$, 500 MHz): δ [ppm] = 216.52 (C-1'), 132.29 (C-11'), 128.93 (C-12'), 128.69 (C-15'), 127.28 (C-13', C-14'), 69.91 (C-5'), 42.13 (C-2', C-8'), 34.61 (C-4', C-6'), 26.86 (C-3', C-7').

IR (KBr) for **117**: ν [cm^{-1}] = 3067 w [$(CH)_{arom.}$)], 2989 s, 2935 s, 2873 m (CH), 2848 m (OCH_2-), 1700 s (C=O), 1588 w, 1585 s (C=C), 1490 s, 1470 s, δ [$(CH)_{aliph.}$)], 751 s (1,2-disubstituted benzene).

Mass spectrum for **117**: $^{m}/_{z}$ (%) = 310 (14) [M^+], 141 (38) [M^+-2-bromobenzyl], 95 (14) [$C_7H_{11}^+$], 55 (28) [$C_3H_3O^+$], 170 (100) [$C_7H_5Br^+$].

^{1}H-NMR-Spectrum for **118** ($CDCl_3$, 500 MHz): δ [ppm] = 1.45 – 2.11 (m, 12 H, H-2 – H-4 and H-6 – H-8), 4.73 (s, 2 H, H-9), 4.73 (s, 2 H, H-9), 7.04 – 7.58 (m, 4H, H-12 – H-15).

^{13}C-NMR-Spectrum for **118** ($CDCl_3$, 500 MHz): δ [ppm] = 131.94 (C-11), 128.69 (C-12), 128.13 (C-15), 127.19 (C-13, C-14), 96.30 (C-1), 78.41 (C-5), 33.41 (C-2, C-8), 28.35 (C-4, C-6), 20.00 (C-3, C-7), 15.98 (C-10).

IR (KBr) for **118**: ν [cm^{-1}] = 3067 w [$(CH)_{arom.}$)], 2989 s, 2935 s, 2873m (CH), 2848 m (OCH_2-), 1588 w, 1585s (C=C), 1490 s, 1470 s, δ [$(CH)_{aliph.}$)], 1147 s (C-O-C), 751 s (1,2-disubstituted benzene).

Mass spectrum for **118**: $^m/_z$ (%) = 310 (14) [M^+], 141 (38) [M^+-2-bromobenzyl], 170 (100) [$C_7H_5Br^+$], 181 (35) [M^+-C_6H_{10}]

13.10 Attempts to synthesis ether of cyclooctanol

In a 100 mL round bottom flask charged with cyclooctanol (2.0 g, 35 mmol) a solution of 0.3 mL conc. HCl in 90 mL of methanol was added. The mixture was refluxed for 28 h. The product was extracted with 25 mL diethyl ether. The compound obtained was washed with water and $NaHCO_3$ solution. The solution was dried over anhydrous Na_2SO_4 and evaporated under reduced pressure. Only unreacted cyclooctanol could be identified by ^{1}H-NMR and IR spectroscopy.

13.11 Attempts to synthesis keto-ether of 1a in solid state

A mixture of **1a** (200 mg, 1.4 mmol), 2-bromobenzyl alcohol (2.6 g, 14. 1 mmol) and *p*-toluenesulphonic acid (*p*-TSA, 26.8 mg, 0.14 mmol) was powdered using mortar and pestle. The powdered mixture was kept at room temperature for 70 h. The reaction mixture was grinded after an intervals of 12 h. Progress of the reaction was monitored by TLC. A single non-polar spot as compared to the starting material was observed. The mixture was treated with 20 mL diethyl ether. It was followed by washing with water and $NaHCO_3$ solution. The solution was dried over anhydrous Na_2SO_4 and evaporated under the reduced pressure. The compound obtained showed absence of an absorption corresponding to the carbonyl group in the IR spectrum clearly indicating absence of the keto-ether. Futher support for this result was obtained from ^{1}H-NMR spectroscopy.

13.12 Attempts to synthesis keto-ether of 1a in water.

A mixture of equimolar amounts of **1a** (100 mg, 0.7 mmol) and benzyl alcohol (75.0 mg, 0.7 mmol) was taken in an Erlenmeyer flask. To this mixture was added HCl (0.3 ml, 0.19 M) along with water (20 mL, 1.4 mmol). The reaction mixture was irradiated with microwave waves at 660 W for 15 min. The mixture was treated with 15 mL

diethyl ether, followed by washing with water and $NaHCO_3$ solution. The resulting solution was dried over anhydrous Na_2SO_4. The compound recovered after evaporation under the reduced pressure was starting material.

13.13 NMR experiments for the tautomeric equilibrium between 1 and 1a in solvents of different polarities

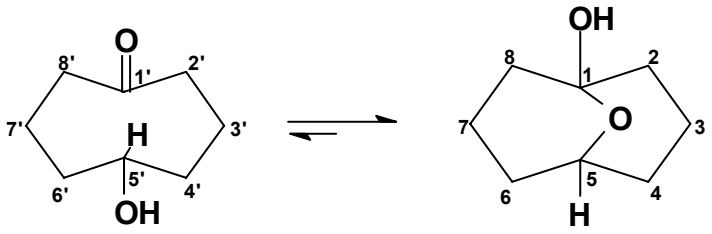

1 **1a**

Solutions were prepared by dissolving approximately 80.0 mg (70 mmol) of **1a** in solvents (approximately 0.15 mL) of different polarities. The spectra were recorded at different temperatures.

^{1}H-NMR-Spectrum ($CDCl_3$, 500 MHz, 25 °C): δ [ppm] = 1.49 – 2.16 (m, 12 H, H-2 – H-4, H-6 – H-8), 2.51 (brs, exch –OH), 4.33 (t, 1 H, H-5).

^{13}C-NMR-Spectrum ($CDCl_3$, 500 MHz, 25 °C): δ [ppm] = 93.86 (C-1), 72.67 (C-5), 36.44 (C-2, C-8), 28.37 (C-4, C-6), 20.72 (C-3, C-7).

^{1}H-NMR-Spectrum ($CDCl_3$, 500 MHz, 50 °C): δ [ppm] = 1.49 – 2.16 (m, 12 H, H-2 – H-4, H-6 – H-8), 2.51 (brs, exch –OH), 4.31 (t, 1 H, H-5).

^{1}H-NMR-Spectrum (THF-d_8, 500 MHz, 25 °C): δ [ppm] = 1.44 – 2.14 (m, 12 H, H-2 – H-4, H-6 – H-8), 2.51 (brs, exch –OH), 4.13 (t, 1 H, H-5).

^{1}H-NMR-Spectrum (ethanol-d_6, 500 MHz, 25 °C): δ [ppm] = 1.50 – 2.17 (m, 12 H, H-2 – H-4, H-6 – H-8), 3.32 (brs, exch –OH), 4.22 (t, 1 H, H-5).

^{1}H-NMR-Spectrum (acetonitrile-d_3, 500 MHz, 25 °C): δ [ppm] = 1.47 – 2.14 (m, 12 H, H-2 – H-4, H-6 – H-8), 3.53 (brs, exch –OH), 4.18 (t, 1 H, H-5).

^{1}H-NMR-Spectrum (acetonitrile-d_3, 500 MHz, 70 °C): δ [ppm] = 1.49 – 2.15 (m, 12 H, H-2 – H-4, H-6 – H-8), 3.27 (brs, exch –OH), 4.20 (t, 1 H, H-5).

^{1}H-NMR-Spectrum (DMSO-*d*$_6$, 500 MHz, 25 °C): δ [ppm] = 1.42 – 2.07 (m, 12 H, H-2 – H-4, H-6 – H-8), 5.62 (brs, exch –OH), 4.12 (t, 1 H, H-5).

^{1}H-NMR-Spectrum (DMSO-*d*$_6$, 500 MHz, 50 °C): δ [ppm] = 1.42 – 2.06 (m, 12 H, H-2 – H-4, H-6 – H-8), 5.48 (brs, exch –OH), 4.12 (t, 1 H, H-5).

^{1}H-NMR-Spectrum (DMSO-*d*$_6$, 500 MHz, 100 °C): δ [ppm] = 1.42 – 2.03 (m, 12 H, H-2 – H-4, H-6 – H-8), 2.19 – 2.48 (m, 4 H, H-2' – H-8'), 3.44 (vbr m, 1 H, H-5'), 4.14 (t, 1 H, H – 5), 5.18 (brs, exch –OH).

^{1}H-NMR-Spectrum (DMSO-*d*$_6$, 500 MHz, 130 °C): δ [ppm] = 1.43 – 2.05 (m, 12 H, H-2 – H-4, H-6 – H-8), 2.22 – 2.50 (m, 4 H, H-2', H-8'), 2.86 (brs, exch -OH), 3.47 (vbr m, 1 H, H-5'), 4.16 (t, 1 H, H-5).

^{1}H-NMR-Spectrum (D_2O, 500 MHz, 25 °C): δ [ppm] = 1.59 – 2.21 (m, 12 H, H-2 – H-4, H-6 – H-8), 4.32 (t, 1 H, H-5).

^{1}H-NMR-Spectrum (D_2O, 500 MHz, 50 °C): δ [ppm] = 1.83 – 2.46 (m, 12 H, H-2 – H-4, H-6 – H-8), 2.60 – 2.66 and 2.89 – 2.95 (m, 4 H, H-2', H-8'), 3.79 (vbr m, 1 H, H-5'), 4.58 (t, 1 H, H-5).

^{1}H-NMR-Spectrum (D_2O, 500 MHz, 90 °C): δ [ppm] = 2.17 – 2.77 (m, 12 H, H-2 – H-4, H-6 – H-8), 2.99 – 3.04 and 3.22 – 3.27 (m, 4 H, H-2', H-8'), 4.19 (vbr m, 1 H, H-5'), 4.93 (t, 1 H, H-5).

13.14 NMR experiments for the tautomeric equilibrium between 2 and 2a in solvents of different polarities

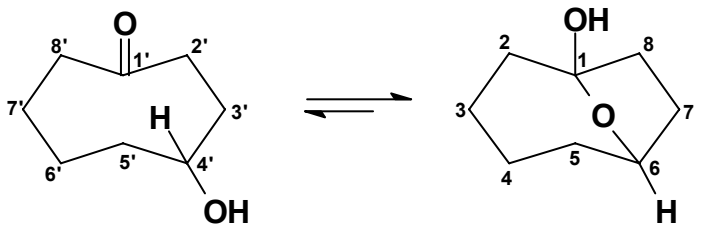

2 **2a**

^{1}H-NMR-Spectrum for **2** (CCl_4, 500 MHz, 25 °C): δ [ppm] = 1.50 – 2.69 (series of m, 12H), 4.35 (brs, exch –OH), 3.96 – 4.00 (m, 1 H, H-4').

^{1}H-NMR-Spectrum for **2a** (CCl_4, 500 MHz, 25 °C): δ [ppm] = 1.50 – 2.69 (series of m, 12H), 4.35 (brs, exch –OH), 4.62 – 4.67 (m, 1 H, H-6).

^{1}H-NMR-Spectrum for **2** (C_6D_6, 500 MHz, 25 °C): δ [ppm] = 1.00 – 2.31 (series of m, 12H), 4.38 (brs, exch –OH), 3.63 (vbr m, 1 H, H-4').

^{1}H-NMR-Spectrum for **2a** (C_6D_6, 500 MHz, 25°C): δ [ppm] = 1.00 – 2.31 (series of m, 12H), 4.38 (brs, exch –OH), 4.30 – 4.38 (m, 1 H, H-6).

^{1}H-NMR-Spectrum for **2** ($CDCl_3$, 500 MHz, 25 °C): δ [ppm] = 1.20 – 2.44 (series of m, 12H), 3.00 (brs, exch –OH), 3.62 (vbr m, 1 H, H-4').

^{13}C-NMR-Spectrum for **2** ($CDCl_3$, 500 MHz, 25 °C): δ [ppm] = 21.75, 28.62, 30.39, 39.29, 40.72 (6 x CH_2), 70.54 (C-4), 217.36 (C-1).

^{1}H-NMR-Spectrum for **2a** ($CDCl_3$, 500 MHz, 25 °C): δ [ppm] = 1.20 – 2.44 (series of m, 12H), 3.00 (brs, exch –OH), 4.36 – 4.40 (m, 1 H, H-5).

^{13}C-NMR-Spectrum for **2** and **2a** ($CDCl_3$, 500 MHz, 25 °C): δ [ppm] = 23.23, 23.70, 31.11, 36.27, 37.03, 41.55 (6 x CH_2), 76.90 (C-6), 108.19 (C-1).

^{1}H-NMR-Spectrum for **2** (DMSO-*d_6*, 500 MHz, 25 °C): δ [ppm] = 1.27 – 2.42 (series of m, 12H), 3.35 (brs, exch –OH), 3.59 – 3.64 (m, 1 H, H-4').

^{1}H-NMR-Spectrum for **2a** (DMSO-*d_6*, 500 MHz, 25 °C): δ [ppm] = 1.27 – 2.42 (series of m, 12H), 3.35 (brs, exch –OH), 4.31 – 4.35 (m, 1 H, H-6).

^{1}H-NMR-Spectrum for **2** (DMSO-*d_6*, 500 MHz, 50 °C): δ [ppm] = 1.26 – 2.50 (series of m, 12H), 5.61 (brs, exch –OH), 3.69 (vbr m, 1 H, H-4').

^{1}H-NMR-Spectrum for **2a** (DMSO-*d_6*, 500 MHz, 50 °C): δ [ppm] = 1.26 – 2.50 (series of m, 12H), 5.61 (brs, exch –OH), 4.33 – 4.36 (m, 1 H, H-6).

^{1}H-NMR-Spectrum for **2** (DMSO-d_6, 500 MHz, 100 °C): δ [ppm] = 1.30 – 2.50 (series of m, 12H), 5.28 (brs, exch –OH), 3.64 – 3.68 (m, 1 H, H-4').

^{1}H-NMR-Spectrum for **2a** (DMSO-d_6, 500 MHz, 100 °C): δ [ppm] = 1.26 – 2.50 (series of m, 12H), 5.28 (brs, exch –OH), 4.33 – 4.37 (m, 1 H, H-6).

^{1}H-NMR-Spectrum for **2** (D_2O, 500 MHz, 25 °C): δ [ppm] = 1.41 – 2.61 (series of m, 12H), 3.86 – 3.91 (m, 1 H, H-4').

^{1}H-NMR-Spectrum for **2a** (D_2O, 500 MHz, 25 °C): δ [ppm] = 1.41 – 2.61 (series of m, 12H), 4.52 – 4.55 (m, 1 H, H-6).

^{1}H-NMR-Spectrum for **2** (D_2O, 500 MHz, 50 °C): δ [ppm] = 1.69 – 2.87 (series of m, 12H), 4.11 – 4.16 (m, 1 H, H-4').

^{1}H-NMR-Spectrum for **2** (D_2O, 500 MHz, 90 °C): δ [ppm] = 2.13 – 3.23 (series of m, 12H), 5.16 (brs, exch –OH), 4.48 – 4.52 (m, 1 H, H-4').

13.15 NMR experiments for the tautomeric equilibrium between 3 and 3a in solvents of different polarities

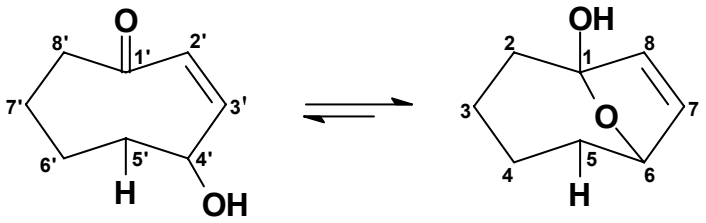

3 **3a**

^{1}H-NMR-Spectrum for **3a** (C_6D_6, 500 MHz, 25 °C): δ [ppm] = 1.16 – 1.90 (m, 7 H), 2.15 – 2.20 (m, 1 H), 4.82 (dddd, J= 8.0, 3.0, 1.4, 1.5 Hz, 1H, H-6), 5.51 (dd, J = 4.0, 1.8, Hz, 1 H, H-7), 5.54 (dd, J = 4.5, 1.3 Hz, 1 H, H-8).

^{1}H-NMR-Spectrum for **3a** (C_6D_6, 500 MHz, 70 °C): δ [ppm] = 1.12 – 1.81 (m, 7 H), 2.00 – 2.06 (m, 1 H), 4.75 (dddd, J= 8.0, 3.0, 1.4, 1.4 Hz, 1 H, H-6), 5.48 (dd, J = 4.5, 1.3 Hz, 1 H, H-7), 5.51 (dd, J = 4.0, 1.8 Hz, 1 H, H-8).

^{1}H-NMR-Spectrum for **3** ($CDCl_3$, 500 MHz, 25 °C): δ [ppm] = 1.45 – 1.67 (m, 6 H), 2.54 (vbr m, 1 H, H-8'), 2.45 (brs, exch –OH), 2.65 – 2.72 (m, 1 H, H-8'), 5.19 (vbr m, 1 H, H-4'), 6.15 (dd, J = 5.7, 3.8, 1.9 Hz, 1 H, H-3'), 6.31 (dd, J = 12.9, 5.6 Hz, 1 H, H-2').

^{1}H-NMR-Spectrum for **3a** ($CDCl_3$, 500 MHz, 25 °C): δ [ppm] = 1.42 – 1.68 (m, 5 H), 1.86 – 2.02 (m, 3 H), 4.96 (dddd, J= 6.4, 3.1, 1.6, 1.6 Hz, 1 H, H-6), 5.78 (dd, J = 5.8, 1.4 Hz, 1 H, H-7), 5.96 (dd, J = 5.8, 1.9 Hz, 1 H, H-8).

^{13}C-NMR-Spectrum ($CDCl_3$, 500 MHz, 25 °C) for **3**: δ [ppm] = 22.26, 22.91, 33.80, 42.21, (4 X CH_2), 69.65 (C-4'), 131.88 (C-3'), 147.67 (C-2').

^{13}C-NMR-Spectrum ($CDCl_3$, 500 MHz, 25 °C) for **3a**: δ [ppm] = 23.05, 23.75, 33.43, 39.10 (4 X CH_2), 81.54 (C-6), 111.47 (C-1), 132.65 (C-7), 134.30 (C-8).

^{1}H-NMR-Spectrum for **3** ($CDCl_3$, 500 MHz, 50 °C): δ [ppm] = 1.43 – 1.70 (m, 6H), 2.56 (vbr m, 1 H, H-8'), 2.74 (brs, exch –OH), 5.14 (vbr m, 1 H, H-4'), 6.17 (dd, J = 5.7, 3.8, 1.9 Hz, 1 H, H-3'), 6.30 (dd, J = 12.6, 5.6 Hz, 1H, H-2').

^{1}H-NMR-Spectrum for **3a** ($CDCl_3$, 500 MHz, 50 °C): δ [ppm] = 1.42 – 1.70 (m, 5 H), 1.87 – 2.02 (m, 3 H), 4.96 (dd, J= 6.4, 5.0 Hz, 1 H), 5.79 (dd, J = 5.0, 4.5 Hz, 1 H, H-3'), 6.00 (dd, J=5.8, 3.9 Hz, 1 H, H-2').

^{1}H-NMR-Spectrum for **3** (acetonitrile-d_3, 500 MHz, 25 °C): δ [ppm] = 1.42 – 1.61 (m, 6H') , 2.37 – 2.42 (m, 1 H, H-8'), 2.72 – 2.78 (m, 1 H, H-8'), 2.14 (brs, exch –OH), 5.07 – 5.14 (vbr m, 1 H, H-4'), 6.03 (dd, J = 5.8, 3.9 Hz, 1 H, H-3'), 6.26 (dd, J = 12.8, 7.3 Hz, 1 H, H-2').

^{1}H-NMR-Spectrum for **3a** (acetonitrile-d_3, 500 MHz, 25 °C): δ [ppm] = 1.42 – 1.68 (m, 5 H), 1.81 – 1.95 (m, 3 H), 4.88 (dddd, J= 6.4, 3.4, 1.6, 1.6 Hz, 1 H), 5.74 (dd, J = 5.8, 1.4 Hz, 1 H, H-7), 5.99 (dd, J = 5.8, 2.0 Hz, 1 H, H-8).

^{1}H-NMR-Spectrum for **3** (acetonitrile-d_3, 500 MHz, 70 °C): δ [ppm] = 1.43 – 1.66 (m, 6H), 2.43 (vbr m, H-8'), 2.73 (ddd, J= 13.7, 10.5, 6.6 Hz, 1 H, H-8'), 3.65 (brs, exch – OH), 5.04 (vbr m, H-4'), 5.92 (ddd, J = 9.2, 3.8, 1.6 Hz, 1 H, H-3'), 6.26 (dd, J = 12.9, 5.45 Hz, 1 H, H-2').

^{1}H-NMR-Spectrum for **3a** (acetonitrile-d_3, 500 MHz, 70 °C): δ [ppm] = 1.43 – 1.66 (m, 5H), 1.84 – 1.95 (m, 3 H), 4.90 (dddd, J= 6.4, 3.1, 1.6, 1.6 Hz, 1 H), 5.75 (dd, J = 5.7, 1.4 Hz, 1 H, H-7), 6.00 (dd, J = 5.8, 2.0 Hz, 1 H, H-8).

^{1}H-NMR-Spectrum for **3** (DMSO-d_6, 500 MHz, 25 °C): δ [ppm] = 1.33 – 1.54 (m, 6 H), 2.51 (dt, J = 7.0, 3.6 Hz, 1 H, H-8'), 2.76 (vbr m, 1 H, H-8'), 5.02 (vbr m, H-4'), 5.90 (ddd, J = 6.0, 3.8, 1.9 Hz, 1 H, H-3'), 6.29 (dd, J = 12.8, 5.6 Hz, 1 H, H-2').

^{1}H-NMR-Spectrum for **3a** (DMSO-d_6, 500 MHz, 25 °C): δ [ppm] = 1.33 – 1.55 (m, 5 H), 1.70 – 1.85 (m, 3 H), 4.96 (dddd, J= 8.0, 5.0, 3.1, 1.6, 1.6 Hz, 1 H, H-6), 5.78 (dd, J = 5.8, 1.4 Hz, 1 H, H-7), 5.99 (dd, J = 6.2, 2.4 Hz, 1 H, H-8).

^{1}H-NMR-Spectrum for **3** (DMSO-d_6, 500 MHz, 50 °C): δ [ppm] = 1.36 – 1.56 (m, 6 H) , 2.51 (dt, J = 7.4, 3.7 Hz, 1 H, H-8'), 2.74 (m, 1 H, H-8'), 5.00 (vbr m, 1 H, H-4'), 5.90 (ddd, J = 12.8, 3.8, 1.7 Hz, 1 H, H-3'), 6.38 (dd, J = 12.8, 5.5 Hz, 1 H, H-2').

^{1}H-NMR-Spectrum for **3a** (DMSO-d_6, 500 MHz, 50 °C): δ [ppm] = 1.36 – 1.59 (m, 5 H), 1.71 – 1.86 (m, 3 H), 4.96 (dddd, J= 8.0, 3.1, 1.6, 1.6 Hz, 1 H, H-6), 5.73 (dd, J = 5.8, 1.4 Hz, 1 H, H-7), 5.99 (dd, J = 6.2, 2.0 Hz 1 H, H-8).

^{1}H-NMR-Spectrum for **3** (DMSO-d_6, 500 MHz, 100 °C): δ [ppm] = 1.39 – 1.59 (m, 5 H), 1.74 – 1.88 (m, 3 H), 2.51 (dt, J = 7.5, 3.7 Hz, 1 H, H-8'), 2.71 (vbr m, 1 H, H-8'), 4.91 (m, 1 H, H-4'), 5.87 (ddd, J = 12.8, 3.4, 1.8 Hz, 1 H, H-3'), 6.38 (dd, J = 12.8, 5.3 Hz, 1 H, H-2').

^{1}H-NMR-Spectrum for **3a** (DMSO-d_6, 500 MHz, 100 °C): δ [ppm] = 1.38 – 1.70 (m, 6H), 4.85 (dddd, J= 8.1, 3.2, 1.5, 1.5 Hz, 1 H, H-6), 5.72 (dd, J = 5.8, 1.4 Hz, 1 H, H-7), 5.99 (dd, J = 5.8, 2.0 Hz, 1 H, H-8).

^{1}H-NMR-Spectrum for **3** (DMSO-d_6, 500 MHz, 130 ºC): δ [ppm] = 1.40 – 1.79 (m, 6 H), 2.51 (dt, J = 7.5, 3.7 Hz, 1 H, H-8'), 2.70 (vbr m, 1H, H-8'), 4.91 (vbr m, 1 H, H-4'), 5.87 (ddd, J = 12.8, 3.4, 1.8 Hz, 1 H, H-3'), 6.27 (dd, J = 12.9, 5.4 Hz, 1 H, H-2').

^{1}H-NMR-Spectrum for **3a** (DMSO-d_6, 500 MHz, 130 °C): δ [ppm] = 1.40 – 1.66 (m, 5 H), 1.72 – 1.91 (m, 3 H), 4.85 (dddd, J= 6.5, 3.1, 1.5, 1.5 Hz, 1 H, H-6), 5.73 (dd, J = 5.8, 1.4 Hz, 1 H, H-7), 5.86 (dd, J = 12.9, 3.1 Hz, 1 H, H-2').

^{1}H-NMR-Spectrum for **3** (D_2O, 500 MHz, 25 °C): δ [ppm] = 1.48 – 1.78 (m, 6 H), 2.49 – 2.53 (m, 1 H, H-8'), 2.84 – 2.91 (m, 1 H, H-8'), 5.23 – 5.29 (vbr m, 1 H, H-4'), 5.90 (ddd, J = 6.0, 3.8, 1.9 Hz, 1 H, H-3'), 6.29 (dd, J = 12.8, 5.6 Hz, 1 H, H-2').

^{1}H-NMR-Spectrum for **3a** (D_2O, 500 MHz, 25 °C): δ [ppm] = 1.48 – 2.78 (m, 5 H), 1.86 – 2.02 (m, 3 H), 5.03 (dd, J= 6.6, 1.6 Hz, 1 H, H-6), 5.82 (dd, J = 6.0, 1.5 Hz, 1 H, H-7), 6.13 (dd, J = 6.0, 2.0 Hz, 1 H, H-8).

^{1}H-NMR-Spectrum for **3** (D_2O, 500 MHz, 50 °C): δ [ppm] = 1.71 – 2.12 (m, 6 H), 2.76 – 2.80 (m, 1 H, H-8'), 3.08 – 3.14 (m, 1 H, H-8'), 5.45 – 5.50 (vbr m, 1 H, H-4'), 6.34 – 6.37 (m, 1 H, H-3'), 6.73 (dd, J = 12.9, 5.6 Hz, 1 H, H-2').

^{1}H-NMR-Spectrum for **3a** (D_2O, 500 MHz, 50 °C): δ [ppm] = 1.72 – 2.12 (m, 5 H), 2.14 – 2.28 (m, 3 H), 5.29 (dd, J= 6.6, 1.3 Hz, 1 H, H-7), 6.39 (dd, J = 5.9, 1.8 Hz, 1 H, H-8).

^{1}H-NMR-Spectrum for **3** (D_2O, 500 MHz, 90 °C): δ [ppm] = 2.12 – 2.39 (m, 6 H), 3.16 – 3.19 (m, 1 H, H-8'), 3.40 – 3.49 (m, 1 H, H-8'), 5.78 – 5.83 (vbr m, 1 H, H-4'), 6.70 (d, J = 13.3, 1 H, H-3'), 7.10 (vbr.dd, J = 12.9, 5.3 Hz, 1 H, H-2').

^{1}H-NMR-Spectrum for **3a** (D_2O, 500 MHz, 90 °C): δ [ppm] = 2.12 – 2.39 (m, 5 H), 2.52 – 2.60 (m, 3 H), 5.66 (d, J= 6.1 Hz, 1 H, H-7), 6.47 (d, J = 5.7 Hz, 1 H, H-8).

13.16 NMR experiments in the presence of different concentration of deuterated hydrochloric acid

13.16.1 In the presence of 3.4 M DCl in D_2O

The compound **1a** (58.0 mg, 0.41 mmol) was weighed into a 5 mm clean dry NMR tube. It is followed by addition of a solution of 3.4 M DCl in D_2O at room temperature. **1a** dissolved readily in acidic solution. Immediately, the NMR spectra were recorded. A number of spectras were recorded at different intervals. The deuteration was 56.3 atom % in 23 d 19 h.

13.16.2 In the presence of 7.9 M DCl in D_2O

The hemiacetal **1a** (68 mg, 0.48 mmol) was taken in a dry clean NMR tube. An equimolar amount of internal reference standard 1,4-dioxane (42.2 mg, 0.48 mmol)

was added to the solution followed by addition of a solution of 7.9 M DCl in D_2O. The spectrum was recorded immediately after preparing sample at room temperature. The deuteration was 58.8 atom % in 165 h.

13.16.3 In the presence of 7.9 DCl in D_2O at high temperature

A solution was prepared by dissolving 67.0 mg (0.47 mmol) of **1a** in 7.9 M DCl solution in D_2O in a clean dry NMR tube. An internal reference standard 1,4-dioxane (44 mg, 0.50 mmol) was added into the solution. A spectrum was recorded immediately. Next spectrum was measured after heating the sample at 100 ºC for 10 min. The final spectrum recorded at room temperature revealed 59.9 atom % deuteration.

13.16.4 In the presence of 12 M DCl in D_2O

A solution was prepared by dissolving **1a** (61.5 mg, 0.43 mmol) in 12 M DCl solution in D_2O. The spectrum was recorded at room temperature. The final spectrum revealed 59.9 atom % deuteration in 18 h.

13.17 NMR experiments in the presence of different concentration of base

13.17.1 In the presence of 0.65 M NaOD in D_2O

A solution was prepared by dissolving **1a** (61.5 mg, 0.43 mmol) in 0.65 M NaOD solution in D_2O. The spectrum was recorded at room temperature. The deuteration was 54.1 atom % in 22 h.

13.17.2 In the presence of 1.30 M NaOD in D_2O

A solution was prepared by dissolving **1a** (60.0 mg, 0.42 mmol) in 1.30 M NaOD solution in D_2O. The spectrum was recorded at room temperature. The deuteration was 56.8 atom % in 23 h.

14 Appendix

14.1 X-ray tables

14.1.1 Crystal data and structure refinement for 1a

Empirical formula	$C_8 H_{14} O_2$	
Formula weight	142.19 Da	
Density (calculated)	1.268 g cm^{-3}	
F (000)	312	
Temperature	426(2) K	
Crystal size	0.60 x 0.50 x 0.20 mm	
Crystal color	colorless	
Crystal description	block	
Wavelength	0.71073 Å	
Crystal system	triclinic	
Space group	$P\bar{1}$	
Unit cell dimensions	*a* = 6.7449(13) Å	α = 73.25(3)°
	b = 9.6101(19) Å	β = 85.15(3)°
	c = 12.237(2) Å	γ = 78.90(3)°
Volume	745.0(3) $Å^3$	
Z	4	
Cell measurement reflections used	4568	
Cell measurement theta min/max	2.42° to 28.27°	
Diffractometer control software	Bruker AXS SMART Vers. 5.054 1997/98	
Diffractometer measurement device	Siemens SMART CCD area detector system	
Diffractometer measurement method	Omega data collection at 0.3° scans width four runs with 600 frames, phi = 0°,90°,180°, 270°	
Theta range for data collection	1.74° to 26.40°	
Completeness to theta = 26.40°	99.8 %	
Index ranges	-8<=h<=8, -12<=k<=11, -15<=l<=15	
Computing data reduction	Bruker AXS SAINT program Vers. 6.45A	
Absorption coefficient	0.089 mm^{-1}	

Computing absorption correction	Bruker AXS SADABS program multiscan V2.03
Absorption correction details	R.H. Blessing, Acta Cryst. (1995) A51 33-38
Max. / min. transmission	0.9824 / 0.9485
R(merg) before/after correction	0.0460 / 0.0198
Computing structure solution	Bruker AXS SHELXTL Vers. 5.10 DOS/WIN95/NT
Computing structure refinement	Bruker AXS SHELXTL Vers. 5.10 DOS/WIN95/NT
Refinement method	Full-matrix least-squares on F^2
Reflections collected	8605
Independent reflections	3046 [*R* (int) = 0.0215]
Data / restraints / parameters	2488 / 0 / 176
Goodness-of-fit on F^2	1.053
Weighting details	$w = 1/ [\sigma^2 (Fo^2)+ (0.0443*P)^2+0.2073*P]$ where $P = (Fo^2+2Fc^2)/3$
Final R indices [I>2sigma(I)]	*R*1 = 0.0356, *wR*2 = 0.0903
R indices (all data)	*R*1 = 0.0456, *wR*2 = 0.0966
Extinction coefficient	0.023(4)
Largest diff. peak and hole	0.291 and -0.199 $eÅ^{-3}$
Treatment of hydrogen atoms	Riding model on idealized geometries with the 1.2 fold isotropic displacement parameters of the equivalent Uij of the corresponding carbon atom. Hydroxy hydrogen atom position taken from a Fourier-map and also refined as riding group with the 1.5 fold isotropic displacement parameters of the equivalent Uij of the corresponding oxygen atom.

14.1.2 Crystal data and structure refinement for 3a

Empirical formula	$C_8 H_{12} O_2$
Formula weight	140.18 Da
Density (calculated)	1.300 g cm^{-3}
F(000)	608
Temperature	203(2) K
Crystal size	0.37 x 0.21 x 0.07 mm

Crystal color	colorless	
Crystal description	plate	
Wavelength	0.71073 Å	
Crystal system	monoclinic	
Space group	$P2_1/c$	
Unit cell dimensions	a = 11.068(3) Å	α = 90°
	b = 5.7547(17) Å	β = 90.333(5)°
	c = 22.488(7) Å	γ = 90°
Volume	1432.4(7) $Å^3$	
Z	8	
Cell measurement reflections used	6044	
Cell measurement theta min/max	2.56° to 28.30°	
Diffractometer control software	Bruker AXS SMART Vers. 5.054 1997/98	
Diffractometer measurement device	Siemens SMART CCD area detector system	
Diffractometer measurement method	Omega data collection at 0.3° scan width four runs with 600 frames, phi = 0°,90°,180°, 270°	
Theta range for data collection	2.57° to 28.42°	
Completeness to theta = 28.42°	99.4 %	
Index ranges	-14<=h<=14, -7<=k<=7, -30<=l<=30	
Computing data reduction	Bruker AXS SAINT program Vers. 6.45A	
Absorption coefficient	0.092 mm^{-1}	
Computing absorption correction	Bruker AXS SADABS program multiscan V2.03	
Absorption correction details	R.H. Blessing, Acta Cryst. (1995) A51 33-38	
Max. / min. transmission	1.00 / 0.87	
R(merg) before/after correction	0.114 / 0.0172	
Computing structure solution	Bruker AXS SHELXTL Vers. 5.10 DOS/WIN95/NT	
Computing structure refinement	Bruker AXS SHELXTL Vers. 5.10 DOS/WIN95/NT	
Refinement method	Full-matrix least-squares on F^2	
Reflections collected	18030	

Independent reflections	3587 [*R*(int) = 0.0179]
Data / restraints / parameters	3222 / 0 / 181
Goodness-of-fit on F^2	1.061
Weighting details	$w = 1/[\sigma^2 (Fo^2)+ (0.0536*P)^2+0.4202*P]$ where $P = (Fo^2+2Fc^2)/3$
Final R indices [I>2sigma(I)]	*R*1 = 0.0356, *wR*2 = 0.0977
R indices (all data)	*R*1 = 0.0396, *wR*2 = 0.1016
Extinction coefficient	0.0036(14)
Largest diff. peak and hole	0.376 and -0.200 $eÅ^{-3}$
Treatment of hydrogen atoms	Riding model on idealized geometries with the 1.2 fold isotropic displacement parameters of the equivalent Uij of the corresponding carbon atom. Hydroxy hydrogen atom position taken from a Fourier-map and also refined as riding group with the 1.5 fold isotropic displacement parameters of the equivalent Uij of the corresponding hydroxy atom.

14.1.3 Crystal data and structure refinement for 118

Empirical formula	$C_{15} H_{19} Br O_2$	
Formula weight	311.21 Da	
Density (calculated)	1.484 g cm^{-3}	
F(000)	1280	
Temperature	173(2) K	
Crystal size	0.37 x 0.29 x 0.12 mm	
Crystal color	colorless	
Crystal description	plate	
Wavelength	0.71073 Å	
Crystal system	orthorhombic	
Space group	*Pbcn*	
Unit cell dimensions	*a* = 9.4448(4) Å	α = 90°
	b = 11.4937(5) Å	β = 90°
	c = 25.6612(12) Å	γ = 90°
Volume	2785.7(2) $Å^3$	
Z	8	
Cell measurement reflections used	7248	

Cell measurement theta min/max	2.44° to 26.05°
Diffractometer control software	Bruker AXS APEX 2 Vers. 1.0-27 2005
Diffractometer measurement device	Siemens SMART three axis goniometer with APEX II area detector system
Diffractometer measurement method	Data collection strategy APEX 2/COSMO
Theta range for data collection	1.59° to 31.55°
Completeness to theta = 31.55°	99.4 %
Index ranges	-13<=h<=13, -16<=k<=16, -33<=l<=37
Computing data reduction	Bruker AXS APEX 2 Vers. 1.0-27 2005
Absorption coefficient	2.943 mm^{-1}
Empirical absorption correction	Bruker AXS APEX 2 Vers. 1.0-27 2005
Max. / min. transmission	1.00 / 0.60
R(merg) before/after correction	0.2570 / 0.0406
Computing structure solution W95/98/NT/2000/ME	Bruker AXS SHELXTL Vers. 6.12
Computing structure refinement W95/98/NT/2000/ME	Bruker AXS SHELXTL Vers. 6.12
Refinement method	Full-matrix least-squares on F^2
Reflections collected	77762
Independent reflections	4626 [*R*(int) = 0.0531]
Data / restraints / parameters	2883 / 0 / 164
Goodness-of-fit on F^2	1.008
Weighting details	$w = 1/[\sigma^2 (Fo^2) + (0.057*P)^2+2.111*P]$ where $P = (Fo^2+2Fc^2)/3$
Final R indices [I>2sigma(I)]	*R*1 = 0.0441, *wR*2 = 0.1031
R indices (all data)	*R*1 = 0.0918, *wR*2 = 0.1242
Extinction coefficient	0.0002(2)
Largest diff. peak and hole	0.805 and -0.748 $eÅ^{-3}$
Treatment of hydrogen atoms	Riding model on idealized geometries with the 1.2 fold isotropic displacement parameters of the equivalent Uij of the corresponding carbon atom

14.2 Acid-catalysed keto-enol tautomerism

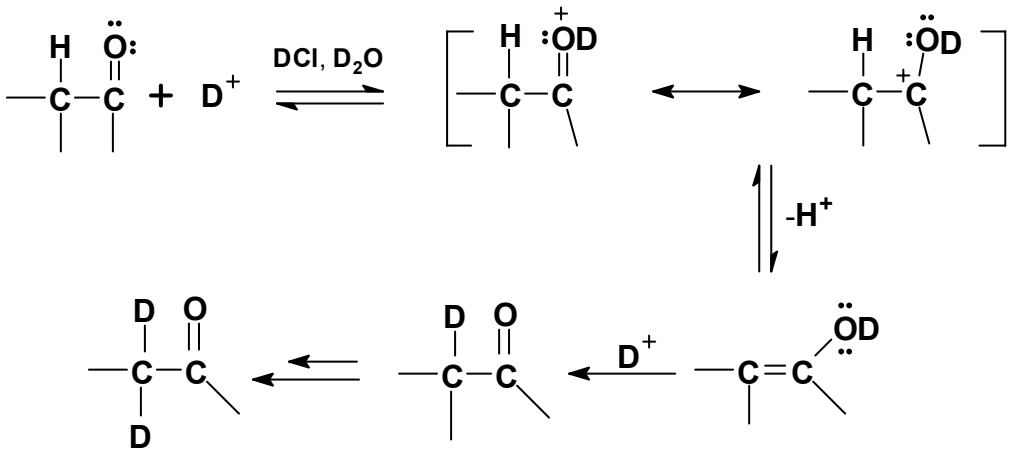

14.3 Base-catalysed keto-enol tautomerism

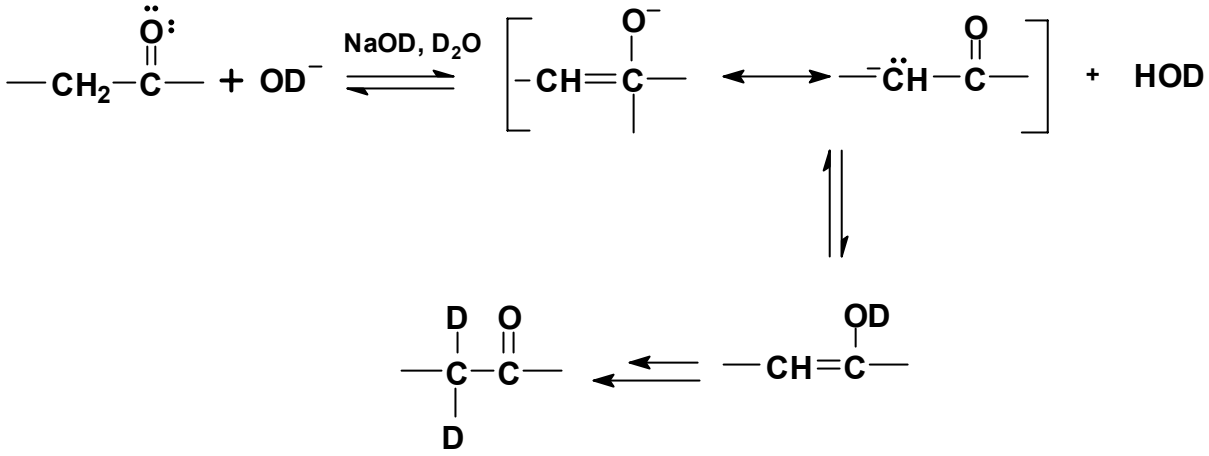

15 References

[1] G. Mehta, V. Singh, *Chem. Rev.* **1999**, *99*, 881-930.

[2] A. Pollex, M. Hiersemann, *Organic Lett.* **2005**, *7*, 5705 -5708.

[3] J. Marco-Contelles, E. DeOpazo, *J. Org. Chem.* **2002**, *67*, 3705-3717.

[4] S. A. Fakhri, A. M. Zenouz, *Molecules* **2002**, *7*, 801-805.

[5] S. L. Gwaltney II, S. T. Sakata, K. J. Shea, *J. Org. Chem.* **1996**, *61*, 7438-7451.

[6] W. Fenical, G. R. Schulte, J. Finer, J. Clardy, *J. Org. Chem.* **1978**, *43*, 3628-3630.

[7] F. Schitz, K. H. Hollenbeak, D. J. Vanderah, *Tetrahedron* **1978**, *34*, 2719-2722.

[8] E. Ayanoglu, T. Gebreyesus, C. M. Beechan, C. Djerassi, *Tetrahedron* **1979**, *35*, 1035-1039.

[9] N. Petasis, M. A. Patane, *Tetrahedron* **1992**, *48*, 5757-5821 and references therein.

[10] G. Mehta, A. N. Murthy, *J. Org. Chem* **1987**, *52*, 2875-2881.

[11] A. J. Minnaard, A. G. Stork, J. B. P. A. Wijnberg, A. DeGroot, *J. Org. Chem* **1997**, *62*, 2344-2349.

[12] K. Mori, *Acc. Chem. Res.* **2000**, *33*, 102-110.

[13] J. Limanto, M. L. Snapper, *J. Am. Chem. Soc.* **2000**, *122*, 8071-8072.

[14] L. A. Paquette, L.-Q. Sun, T. J. N. Watson, D. Friedrich, B. T. Freeman, *J. Org. Chem.* **1997**, *62*, 8155-8161.

[15] G. Mehta, K. S. Rao, *J. Org. Chem* **1988**, *53*, 425-427.

[16] L. Yet, *Tetrahedron* **1999**, *55*, 9449-9403.

[17] G. Illuminati, L. Mandolini, *Acc. Chem. Res.* **1981**, *14*, 95-102.

[18] L. A. Paquette, R. E. Hartung, J. E. Hofferberth, I. Vilotijevic, J. Yang, *J. Org. Chem.* **2004**, *69*, 2454-2460.

[19] G. Appendino, G. C. Tron, T. Jarevang, O. Sterner, *Organic Lett.* **2001**, *3*, 1609-1612.

[20] G. L. Olson, M. E. Voss, D. E. Hill, M. Kahn, V. S. Madison, C. M. Cook, *J. Am. Chem. Soc.* **1990**, *112*, 323-333.

[21] R. Griffith, J. B. Bremener, S. J. Titmuss, *J. Comput. Chem.* **1997**, *18*, 1211-1221.

[22] R. Griffith, B. F. Yates, J. B. Bremner, S. J. Titmuss, *J. Mol. Graphics and Modelling* **1997**, *15*, 91-991.

[23] C. W. Bielawski, R. H. Grubbs, *Angew. Chem. Int. Ed.* **2000**, *39*, 2903-2906.

[24] M. A. Hillmyer, W. R. Laredo, R. H. Grubbs, *Macromolecules* **1995**, *28*, 6311-6316.

[25] F. D. Suvire, L. N. Santagata, J. A. Bombasaro, R. D. Enriz, *J. Comp. Chem.* **2006**, *27*, 188-202.

[26] E. L. Eliel, N. L. Allinger, S. J. Angyal, G. A. Morrison, *Conformational Analysis*, 3rd ed., Wiley & Sons, New York, **1967**.

[27] F. A. L. Anet, *Conformational Analysis, Scope and Present limitations*, Academic Press, New York, **1971**.

[28] G. Haufe, G. Mann, *Chemistry of Alicyclic compounds*, Elsevier, Amsterdam, **1989**.

[29] M. Grossel, *Alicyclic Chemistry*, Oxford Series, New York, **1997**.

[30] J. B. Hendrickson, *J. Am. Chem. Soc.* **1967**, *89*, 7036-7043.

[31] K. B. Wiberg, *J. Org. Chem.* **2003**, *68*, 9322-9329.

[32] N. L. Allinger, M. T. Tribble, M. A. Miller, *Tetrahedron* **1972**, *28*, 1173-1179.

[33] I. Kolossvary, W. C. Guida, *J. Am. Chem. Soc.* **1993**, *115*, 2107-2119.

[34] P. Rademacher, *Chem. Soc. Rev.* **1995**, *24*, 143-150.

[35] C. E. Harding, J. G. R. Standford, *J. Org. Chem.* **1989**, *54*, 3054-3056.

[36] R. S. Glass, *Conformational Analysis of Medium Sized Heterocycles*, VCH, New York, **1988**.

[37] M. Hanack, *Conformational Theory*, Academic Press, New York, **1965**.

[38] N. J. Leonard, *Rec. Chem. Prog.* **1956**, *17*, 243-257.

[39] E. L. Eliel, S. H. Wilen, *Stereochemistry of Organic Compounds*, Wiley, New York, **1994**.

[40] A. C. Cope, M. M. Martin, M. A. McKervey, *Q. Rev. Chem. Soc.* **1966**, *20*, 119-152.

[41] J. D. Dunitz, *Perspectives in Structural Chemistry*, 2nd ed., Wiley, New York, **1968**.

[42] H. B. Bürgi, J. D. Dunitz, *Acc. Chem. Res.* **1983**, *16*, 153-161.

[43] K. M.-Majeski, M. Vinkovic, D. Skare, A. P. Marchand, *ARKIVOC* **2002**, *IV*, 30-37.

[44] Y. Senda, J. Ishiyama, S. Imaizumi, *J. Chem. Soc. Perkin Trans. 2* **1981**, 90-93.

[45] T. A. Robbins, V. T. Vien, J. W. Givens, D. A. Lightner, *J. Am. Chem. Soc.* **1992**, *114*, 10799-10810.

[46] T. Doerner, R. Gleiter, T. A. Robbins, P. Chayangkoon, D. A. Lightner, *J. Am. Chem. Soc.* **1992**, *114*, 3235-3241.

[47] R. Bishop, *Aust. J. Chem.* **1984**, *37*, 319-325.

[48] R. Bishop, G.-H. Lee, *Aust. J. Chem.* **1987**, *40*, 249-255.

[49] P. Rademacher, A. Strenge, *Eur. J. Org. Chem.* **1999**, 1601-1609.

[50] R. Gleiter, W. Schafer, *Acc. Chem. Res.* **1990**, *23*, 369-375.

[51] T.-R. Heiss, Universität Duisbürg-Essen (Germany), **1998**.

[52] V. Balaji, K. D. Jordan, R. Gleiter, G. Jahne, G. Muller, *J. Am. Chem. Soc.* **1985**, *107*, 7321-7323.

[53] V. Balaji, L. Ng, K. D. Jordan, M. N. P.-Row, H. K. Patney, *J. Am. Chem. Soc.* **1987**, *109*, 6957-6969.

[54] V. Prelog, K. Schenker, *Helv. Chim. Acta* **1952**, *35*, 2044-2053.

[55] H. C. Brown, K. Ichikawa, *Tetrahedron* **1957**, 221-230.

[56] V. Prelog, M. Kobelt, *Helv. Chim. Acta.* **1949**, *32*, 1187-1192.

[57] R. Sahil, Panjab University (India), **1989**.

[58] P. Walia, Panjab University (India), **2005**.

[59] P. Helquist, S. Zhao, G. Mehta, *Tetrahedron Lett.* **1991**, 5753-5756.

[60] P. Helquist, S. Ishii, S. Zhao, G. Mehta, C. Knors, *J. Org. Chem.* **2001**, *66*, 3449-3458.

[61] H. Suginome, Y. Kanno, A. Sasaki, K. Kobayashi, *Tetrahedron* **1991**, *47*, 7245-7258.

[62] N. A. Pegg, L. A. Paquette, *J. Org. Chem.* **1991**, *56*, 2461-2468.

[63] M. Barelle, M. Apparu, *Bull. Soc. Chim. Fr.* **1972**, 2016-2024.

[64] C. R. Smith, J. R. Malpass, *Tetrahedron Lett.* **1992**, *33*, 277-280.

[65] J.-E. Bäckvall, U. Andreasson, *Tetrahedron Lett.* **1993**, *34*, 5459-5462.

[66] W. J. Mijs, K. S. DeVries, J. G. Westra, H. A. Gaur, J. Smidt, J. Vriend, *Rec. Trav. Chim. Pays-Bas* **1968**, *87*, 580-584.

[67] R. P. Kirchen, T. S. Sorensen, *J. Am. Chem. Soc.* **1979**, *101*, 3240-3243.

[68] J. E. McMurry, T. Leckta, C. N. Hodge, *J. Am. Chem. Soc.* **1989**, *111*, 8867-8872.

[69] J. E. McMurry, T. Lectka, *Acc. Chem. Res.* **1992**, *25*, 47-53.

[70] R. P. Kirchen, N. Okayawa, K. Ranganayakulu, A. Rauk, T. S. Sorensen, *J. Am. Chem. Soc.* **1981**, *103*, 597-604.

[71] R. P. Kirchen, K. Ranganayakulu, A. Rauk, B. P. Singh, T. S. Sorensen, *J. Am. Chem. Soc.* **1981**, *103*, 588-596.

[72] R. P. Kirchen, T. S. Sorensen, K. Wagstaff, *J. Am. Chem. Soc.* **1978**, *100*, 6761-6763.

[73] R. P. Kirchen, T. S. Sorensen, *J. Chem. Soc. Chem. Comm.* **1978**, 769-770.

[74] R. Cernik, G.-A. Craze, O. S. Mills, I. Watt, S. N. Whittleton, *J. Chem. Soc. Perkin Trans. 2* **1984**, 685-690.

[75] J. E. Hofferberth, H. Y. Lo, L. A. Paquette, *Organic Lett.* **2001**, *3*, 1777-1780.

[76] P. Magnus, F. Ujjainwalla, N. Westwood, V. Lynch, *Tetrahedron* **1998**, *54*, 3069-3092.

[77] I. N. Levine, *Quantum Chemistry*, 4th ed., Prentice-Hall, New York, **1991**.

[78] A. R. Leach, *Molecular Modeling : Principles and Applications*, 2nd ed., Prentice Hall, Harlow, England, **2001**.

[79] U. Burket, N. L. Allinger, *Molecular Mechanics*, Am. Chem. Soc., Washington D.C, **1982**.

[80] W. Koch, M. C. Holthausen, *A Chemist's Guide to Density Functional Theory*, Wiley-VCH, Weinheim, **2000**.

[81] Spartan'04, Irvine, 4th ed., Wavefunction, Inc., CA.

[82] M. J. S. Dewar, W. Thiel, *J. Am. Chem. Soc.* **1977**, *99*, 4899-4907.

[83] M. J. S. Dewar, M. L. McKee, H. S. Rzepa, *J. Am. Chem. Soc.* **1978**, *100*, 3607-3607.

[84] M. J. S. Dewar, E. G. Zoebisch, E. F. Healy, *J. Am. Chem. Soc* **1985**, *107*, 3902-3909.

[85] J. J. P. Stewart, *J. Comp. Chem.* **1989**, *10*, 209-220.

[86] W. Kohn, L. J. Sham, *Phys. Rev.* **1965**, *137(6A)*, 1697-1705.

[87] A. D. Becke, *Phys. Rev. A* **1988**, *38*, 3098-3100.

[88] A. D. Becke, *J. Chem. Phys.* **1993**, *98*, 5648-5652.

[89] P. v. R. Schleyer, N. L. Allinger, T. Clark, J. Gasteiger, P. A. Kollman, H. F. Schaefer-III, P. R. Schreiner, *The Encyclopedia of Computational Chemistry*, Wiley & Sons, Chichester, U. K, **1998**.

[90] Y. Zhao, D. G. Truhlar, *J. Phys. Chem. A* **2005**, *109*, 5656-5667.

[91] A. D. Boese, J. M. L. Martin, N. C. Handy, *J. Chem. Phys.* **2003**, *119*, 3005-3014.

[92] B. G. Johnson, P. M. W. Gill, J. A. Pople, *J. Chem. Phys.* **1993**, *98*, 5612-5626.

[93] C. Lee, W. Yang, R. G. Parr, *Phys. Rev. B.* **1988**, *37*, 785-789.

[94] J. B. Foresman, A. Frisch, *Exploring Chemistry with Electronic Structure Methods*, 2nd ed., Gaussian, Inc., Pittsburg, PA, **1996**.

[95] B. J. Lynch, D. G. Truhlar, *J. Chem. Phys. A* **2001**, *105*, 2936-2941.

[96] A. E. Reed, L. A. Curtiss, F. Weinhold, *Chem. Rev.* **1988**, *88*, 899-926.

[97] A. E. Reed., R. B. Weinstock, F. Weinhold, *J. Chem. Phys.* **1985**, *83*, 735-746.

[98] L. Carballeira, I. P´erez-Juste, *J. Phys. Chem. A* **2000**, *104*, 9362-9369.

[99] S. Moon, Y. Kwon, J. Lee, *J. Phys. Chem. A* **2001**, *105*, 3221-3225.

[100] V. Pophristic, L. Goodman, *Nature* **2001**, *411*, 565-568.

[101] A. E. Reed, F. Weinhold, *Isr. J. Chem.* **1991**, *31*, 277-285.

[102] U. Salzner, P. v. R. Schleyer, *J. Org. Chem.* **1994**, *59*, 2138-2155.

[103] R. Gleiter, H. Lange, O. Borzyk, *J. Am. Chem. Soc.* **1996**, *118*, 4889-4895.

[104] S. Klod, A. Koch, E. Kleinpeter, *J. Chem. Soc. Perkin Trans. 2* **2002**, 1506-1509.

[105] F. Weinhold, P. v. R. Schleyer, *Encyclopedia of Computational Chemistry, Vol. 3*, Wiley, New York, **1998**.

[106] F. Weinhold, A. E. Reed, *J. Chem. Phys.* **1985**, *83*, 1736-1740.

[107] M. Leblanc, D. Siri, S. R. A. Marque, S. Grimaldi, D. Bertin, P. Tordo, *Int. J. Quant. Chem* **2005**, *106*, 676-685.

[108] I. V. Alabugin, M. Manoharan, T. A. Zeidan, *J. Am. Chem. Soc.* **2003**, *125*, 14014-14031.

[109] R. F. W. Bader, *Atoms in Molecules-A Quantum Theory*, Oxford, London, **1991**.

[110] R. F. W. Bader, *Acc. Chem. Res.* **1985**, *18*, 9-15.

[111] R. F. W. Bader, T. T. Nguyen-Dang, Y. Tal, *Reports on Prog. in Phys.* **1981**, *44*, 893-948.

[112] T. S. Koritsanszky, P. Coppens, *Chem. Rev.* **2001**, *101*, 1583-1627.

[113] J. D. Dunitz, A. Gavezzotti, *Angew. Chem. Int. Ed.* **2005**, *44*, 1766-1787.

[114] A. A. Korlyukov, K. A. Lyssenko, M. Y. Antipin, V. N. Kirin, E. A. Chernyshev, S. P. Knyazev, *Inorg. Chem.* **2002**, *41*, 5043-5051.

[115] K. A. Lyssenko, A. A. Korlyukov, M. Y. Antipin, S. P. Knyazev, V. N. Kirin, N. V. Alexeev, E. A. Chernysev, *Mendel. Comm.* **2000**, *3*, 83-124.

[116] K. A. Lyssenko, M. Y. Antipin, D. Y. Antonov, *CHEMPHYSCHEM* **2003**, *4*, 817-823.

[117] J. P. Anglada, B. Carles, J. M. Bofill, R. Crehuet, J. M. Poblet, *Organometallics* **1999**, *18*, 5584-5593.

[118] C. Gatti, M. Barzaghi, M. Simonetta, *J. Am. Chem. Soc.* **1985**, *108*, 878-894.

[119] R. Destro, F. Merati, *Acta Crystallogr.* **1995**, *B51*, 559-572.

[120] M. E. Gurskii, A. V. Gueiderikin, Y. N. Bubnov, M. Y. Antipin, K. A. Lyssenko, I. D. Gridnev, R. Boese, D. Blaeser, *J. Organomet. Chem.* **2001**, *636*, 3-6.

[121] R. F. W. Bader, H. Essen, *J. Chem. Phys.* **1984**, *80*, 1943-1960.

[122] R. W. F. Bader, *J. Chem. Phys. A* **1998**, *102*, 7314-7323.

[123] M. J. Frisch, G. W. Trucks, H. B. Schlegel, G. E. Scuseria, M. A. Robb, J. R. Cheeseman, V. G. Zakrzewski, J. A. Montgomery-Jr., R. E. Stratmann, J. C. Burant, S. Dapprich, J. M. Millam, A. D. Daniels, K. N. Kudin, M. C. Strain, O. Farkas, J. Tomasi, V. Barone, M. Cossi, R. Cammi, B. Mennucci, C. Pomelli, C. Adamo, S. Clifford, J. Ochterski, G. A. Petersson, P. Y. Ayala, Q. Cui, K. Morokuma, D. K. Malick, A. D. Rabuck, K. Raghavachari, J. B. Foresman, J. Cioslowski, J. V. Ortiz, A. G. Baboul, B. B. Stefanov, G. Liu, A. Liashenko, P. Piskorz, I. Komaromi, R. Gomperts, R. L. Martin, D. J. Fox, T. Keith, M. A. Al-Laham, C. Y. Peng, A. Nanayakkara, C. Gonzalez, M. Challacombe, P. M. W. Gill, B. Johnson, W. Chen, M. W. Wong, J. L. Andres, C. Gonzalez, M. Head-Gordon, E. S. Replogle, J. A. Pople, Revision A.7 ed., Gaussian, Inc., Pittsburgh, PA, **1998**.

[124] M. J. Frisch, G. W. Trucks, H. B. Schlegel, G. E. Scuseria, M. A. Robb, J. R. Cheeseman, J. A. Montgomery-Jr., T. Vreven, K. N. Kudin, J. C. Burant, J. M. Millam, S. S. Iyengar, J. Tomasi, V. Barone, B. Mennucci, M. Cossi, G.

Scalmani, N. Rega, G. A. Petersson, H. Nakatsuji, M. Hada, M. Ehara, K. Toyota, R. Fukuda, J. Hasegawa, M. Ishida, T. Nakajima, Y. Honda, O. Kitao, H. Nakai, M. Klene, X. Li, J. E. Knox, H. P. Hratchian, J. B. Cross, C. Adamo, J. Jaramillo, R. Gomperts, R. E. Stratmann, O. Yazyev, A. J. Austin, R. Cammi, C. Pomelli, J. W. Ochterski, P. Y. Ayala, K. Morokuma, G. A. Voth, P. Salvador, J. J. Dannenberg, V. G. Zakrzewski, S. Dapprich, A. D. Daniels, M. C. Strain, O. Farkas, D. K. Malick, A. D. Rabuck, K. Raghavachari, J. B. Foresman, J. V. Ortiz, Q. Cui, A. G. Baboul, S. Clifford, J. Cioslowski, B. B. Stefanov, A. L. G. Liu, P. Piskorz, I. Komaromi, R. L. Martin, D. J. Fox, T. Keith, M. A. Al-Laham, C. Y. Peng, A. Nanayakkara, M. Challacombe, P. M. W. Gill, B. Johnson, W. Chen, M. W. Wong, C. Gonzalez, J. A. Pople, Revision A.1 ed., Gaussian Inc., Pittsburgh, PA, **2003**.

[125] G.Schaftenaar, J. H. Noordik, *J. Comput.-Aided Mol. Design* **2000**, *14*, 123-134.

[126] PCMODEL, 8.0 ed., Serena Software, Bloomington, Indiana, USA, **2002**.

[127] R. Sustmann, W. Sicking, *Chem. Ber.* **1987**, *120*, 1323-1330.

[128] H. Meier, H. Peterson, *Synthesis* **1978**, 596-598.

[129] C. R. Smith, D. E. Justice, J. R. Malpass, *Tetrahedron* **1994**, *50*, 11039-11056.

[130] F. D. Boyer, T. Prange, P. H. Ducrot, *Tetrahedron Asymm.* **2003**, *14*, 1153-1159.

[131] Y. Kayama, M. Oda, Y. Kitahara, *Chem. Lett.* **1974**, *3*, 345-348.

[132] R. Bishop, W. Parker, J. R. Stevenson, *J. Chem. Soc. Perkin Trans 1* **1981**, 565-573 and references within.

[133] M. E. Gurskii, K. A. Lyssenko, A. L. Karionova, P. A. Belyakov, T. V. Potapova, M. Y. Antipin, Y. N. Bubnov, *Rus. Chem. Bull. Int. Ed. (Engl. Transl.)* **2004**, *53*, 1963-1977.

[134] N. L. Allinger, J. Allinger, *Structure of Organic Molecules*, Prentice Hall Inc., New York, **1965**.

[135] A. S. Feliciano, A. F. Barrero, M. Medarde, J. M. DelCorral, A. Aramburu, *Tetrahedron Lett.* **1985**, *26 .* 2369-2372.

[136] N. G. Ramesh, A. Hassner, *Eur. J. Org. Chem.* **2005**, 1892-1902.

[137] G. I. Glover, R. B. Smith, H. Rapoport, *J. Am. Chem. Soc.* **1965**, *87*, 2003-2010.

[138] R. C. Weast, *CRC Handbook of Chemistry and Physics*, 68th ed., CRC Press Inc. Boca Raton, Florida, **1987**.

[139] C. Reichardt, *Solvents and Solvent Effects in Organic Chemistry*, 2nd ed., VCH: Weinheim, **1988**.

[140] J. Sicher, J. Zavada, M. Svoboda, V. A. Vaver, *Chem. Comm.* **1965**, *1*, 12-12.

[141] W. C. Still, I. Galynker, *Tetrahedron* **1981**, *37*, 3981-3996.

[142] W. C. Still, *J. Am. Chem. Soc.* **1979**, *101*, 2493-2495.

[143] P. Rademacher, A. Strenge, *Eur. J. Org. Chem.* **1999**, 1611-1617.

[144] Parveen, H. Singh, T. V. Singh, P. V. Bharatam, P. Venugopalan, *J. Mol. Struct. (THEOCHEM)* **2004**, *685*, 139-145.

[145] M. W. Schmidt, K. K. Baldridge, J. A. Boatz, S. T. Elbert, M. S. Gordon, J. H. Jensen, S. Koseki, N. Matsunaga, K. A. Nguyen, S. Su, T. L. Windus, M. Dupuis, J. J. A. Montgomery, *J. Comp. Chem.* **1993**, *14*, 1347-1363.

[146] W. P. Jencks, *Catalysis in chemistry and Enzymology*, Dover Publications, Inc., New York, **1987**.

[147] V. I. Minkin, Y. B. Simkin, R. M. Minyaev, *Quantum Chemistry of Organic Compounds: Mechanism of Reactions*, Springer Verlag, Berlin, **1990**.

[148] K. N. Houk, M. N. Paddon-Row, N. G. Rondan, Y.-D. Wu, F. K. Brown, D. C. Spellmeyer, J. T. Metz, Y. Li, R. J. Lonchairch, *Science* **1986**, *231*, 1108-1117.

[149] M. T. Nguyen, G. Raspoet, L. G. Vanquickenborne, *J. Phys. Chem. A* **1997**, *101*, 7379-7388.

[150] R. M. Minyaev, E. A. Lepin, *Mendel. Comm.* **1997**, 189-191.

[151] M. T. Nguyen, A. F. Hegarty, *J. Am. Chem. Soc.* **1983**, *105*, 3811-3815.

[152] M. T. Nguyen, A. F. Hegarty, *J. Am. Chem. Soc.* **1984**, *106*, 1552-1557.

[153] S.-W. Hu, S.-M. Lü, X.-Y. Wang, *J. Phys. Chem. A* **2004**, *108*, 8485-8494.

[154] K. B. Wiberg, K. M. Morgan, H. Maltz, *J . Am. Chem. Soc.* **1994**, *116*, 11067-11077.

[155] K. P. C. Vollhardt, N. E. Schore, *Organic Chemistry*, 3rd ed., W. H. Freeman, San Francisco, **1999**.

[156] P. Zuman, *ARKIVOC* **2002**, 85-140.

[157] I. H. Williams, G. M. Maggiora, R. L. Schowen, *J. Am. Chem. Soc.* **1980**, *102*, 7831-7839.

[158] A. A. Zavitsas, M. Coffiner, T. Wiseman, L. R. Zavitsas, *J. Phys. Chem.* **1970**, *74*, 2746-2750.

[159] R. P. Bell, P. G. Evans, *Proc. Roy. Soc. (London), Ser. A* **1966**, *291*, 297-323.

[160] S. Wolfe, C.-K. Kim, Kiyull, N. Weinberg, Z. Shi, *J. Am. Chem. Soc.* **1995**, *117*, 4240-4260.

[161] L. H. Funderburk, L. Aldwin, W. P. Jencks, *J . Am. Chem. Soc.* **1978**, *100*, 5444-5459.

[162] O. N. Ventura, E. L. Coitino, K. Irving, A. Iglesias, A. Liedos, *J. Mol. Struct. (THEOCHEM)* **1990**, *69*, 427-440.

[163] O. N. Ventura, E. L. Coitino, A. Lledos, J. Bertran, *J. Comput. Chem.* **1992**, *13*, 1037-1046.

[164] T. Clark, J. Chandrasekhar, G. W. Spitznagel, P. v. R. Schleyer, *J. Comp. Chem.* **1983**, *4*, 294-301.

[165] D. A. McQuarrie, *Statistical Mechanics*, Harper & Row, New York, **1976**.

[166] R. F. W. Bader, T. T. Nguyen-Dang, *Adv. Quant. Chem.* **1981**, *14*, 63-124.

[167] H. B. Bürgi, J. D. Dunitz, E. Shefter, *J. Am. Chem. Soc.* **1973**, *95*, 5065-5067.

[168] H. B. Bürgi, J. M. Lehn, G. A. Wipff, *J. Am. Chem. Soc.* **1974**, *96*, 1956-1957.

[169] H. B. Bürgi, J. D. Dunitz, *Structure Correlation*, Verlag Chemie, Weinheim, **1994**.

[170] J. Hern'andez-Trujillo, R. F. W. Bader, *J. Phys. Chem. A* **2000**, *104*, 1779-1794.

[171] R. F. W. Bader, *Chem. Rev.* **1991**, *91*, 893-928.

[172] J. P. Krug, P. Popelier, R. F. W. Bader, *J. Phys. Chem.* **1992**, *96*, 7604-7616.

[173] A. C. Cope, M. A. Mckervey, N. M. Weinshenker, *J. Org. Chem.* **1969**, *34*, 2229-2231.

[174] S. L. Schreiber, D. B. Smith, *J. Am. Chem. Soc.* **1989**, *54*, 5994-5996.

[175] J. Tomasi, M. Persico, *Chem. Rev.* **1994**, *94*, 2027-2094.

[176] R. Cammi, J. Tomasi, *J. Comput. Chem.* **1995**, *16*, 1449-1458.

[177] C. J. Cramer, D. G. Truhlar, *Chem. Rev.* **1999**, *99*, 2161-2200.

[178] N. S. Zefirov, V. A. Palyulin, *Topics in Stereochemistry*, E. L. Eliel and S. H. Wilen, Wiley, New York, **1991**.

[179] M. Dobler, J. D. Dunitz, *Helv. Chim. Acta* **1964**, *47*, 695-704.

[180] W. A. C. Brown, G. Eglinton, J. Martin, W. Parker, G. A. Sim, *Proc. Chem. Soc.* **1964**, 57-58.

[181] W. A. C. Brown, J. Martin, G. A. Sim, *J. Chem. Soc.* **1965**, 1844-1857.

[182] H. C. Brown, G. Zweifel, *J. Am. Chem. Soc.* **1959**, *81*, 247-247.

[183] G. Eglinton, J. Martin, W. Parker, *J. Chem. Soc.* **1965**, 1243-1251.

[184] K. Y. Burshtein, A. N. Isaev, *(THEOCHEM)* **1985**, *26*, 263-268.

[185] A. Bergner, M. Dolg, W. Kuechle, H. Stoll, H. Preuss, *Mol. Phys.* **1993**, *80*, 1431-1441.

[186] Y. G. Lazarou, A. V. Prosmitis, V. C. Papadimitriou, P. Papagiannakopopulos, *J. Phys. Chem. A* **2001**, *105*, 6729-6742.

[187] R. Prosmiti, P. Villarreal, G. Delgado-Barrio, *Chem. Phys. Lett.* **2002**, *359*, 473-479.

[188] J. Dunitz, *Pure Appl. Chem.* **1971**, *25*, 495-508.

[189] F. A. L. Anet, M. S. Jacques, P. M. Henrichs, A. K. Cheng, J. Krane, L. Wong, *Tetrahedron* **1974**, *30*, 1629-1637.

[190] F. R. L. Hilderbrandt, J. D. Wieser, L. K. Montgomery, *J. Am. Chem. Soc.* **1973**, *95*, 8598-8605.

[191] T. Alvik, G. Borgen, J. Dale, *Acta Chem. Scand.* **1972**, *26*, 1805-1816.

[192] F. M. Menger, *Tetrahedron* **1983**, *39*, 1013-1040.

[193] V. Prelog, J. G. Traynham, *Molecular Rearrangements, Vol. 1*, Interscience, New York, **1963**.

[194] G.-A. Craze, I. Watt, *J. Chem. Soc. Perkin Trans. 2* **1981**, 175-184.

[195] R. W. Nagorski, J. P. Richard, *J. Am. Chem. Soc.* **2001**, *123*, 794-802.

[196] R. W. Nagorski, J. P. Richard, *J. Am. Chem. Soc.* **1996**, *118*, 7432-7433.

[197] S. Gronert, J. R. Keeffe, *J. Am. Chem. Soc.* **2005**, *127*, 2324-2333.

[198] R. Cernik, G.-A. Craze, O. S. Mills, I. Watt, *J.Chem. Soc. Perkin Trans. 2* **1982**, 361-367.

[199] E. W. Warnhoff, P. R.-Warnhoff, M. Y. H. Wong, *J. Am. Chem. Soc.* **1980**, *102*, 5956-5957.

[200] O. Tapia, R. Cardenas, J. Andres, F. Colonna-Cesari, *J . Am. Chem. Soc.* **1988**, *110*, 4046-4047.

[201] C. I. F. Watt, *Adv. Phys. Organ. Chem.* **1988**, *24*, 58-105.

[202] L. Stehelin, J. Lhomme, G. Ourisson, *J . Am. Chem. Soc.* **1971**, *93*, 1650-1657.

[203] Y. D. Wu, D. K. Lai, K. N. Houk, *J. Am. Chem. Soc.* **1995**, *117*, 4100-4108.

[204] O. S. Mills, C. I. F. Watt, S. M. Whitworth, *J. Chem. Soc. Perkin Trans. 2* **1990**, 487-497.

[205] P. T. Lansbury, F. D. Saeva, *J. Am. Chem. Soc.* **1967**, *89*, 1890-1895.

[206] R. S. Henry, F. G. Riddell, W. Parker, C. I. F. Watt, *J. Chem. Soc. Perkin Trans. 1* **1976**, 1549-1553.

[207] I. Watt, S. N. Whittleton, S. M. Whitworth, *Tetrahedron* **1986**, *42*, 1047-1062.

[208] I. H. Hiller, S. Smith, S. C. Mason, C. Whittleton, I. F. Watt, J. Willis, *J. Chem. Soc. Perkin Trans. 2* **1988**, 1345-1352.

[209] A. L. Wilds, *Organic Reactions*, 179-209.

[210] D. N. Kirk, A. Mudd, *J. Chem. Soc.* **1969**, 804-806.

[211] M. P. Doyle, C. T. West, *Stereoselective Reduction Dowden Hutchinson and Ross*, P A, Stroudsburg, **1976**.

[212] M. L. Steigerwald, W. A. Goddard, D. A. Evans, *J. Am. Chem. Soc.* **1979**, *101*, 1994-1997.

[213] E. W. Warnhoff, *Can. J. Chem* **1977**, *55*, 1653-1643.

[214] Parveen, H. Singh, P. Venugopalan, T. V. Singh, *Indian J. Chem. Soc. B* **2004**, *43A*, 233-239.

[215] Y. Brumer, M. Shapiro, P. Brumer, K. K. Baldrige, *J. Phys. Chem. A* **2002**, *106*, 9512-9519.

[216] D. Whittaker, V. J. Shiner, *J. Am. Chem. Soc.* **1969**, *91*, 394-398.

[217] G.-A. Craze, I. Watt, *J. Chem. Soc. Chem. Comm.* **1980**, 147-148.

[218] K. N. Houk, Y.-D. Wu, *J. Am. Chem. Soc.* **1987**, *109*, 906-908.

[219] B. G. Hutley, A. E. Mountain, I. H. Williams, G. M. Maggiora, R. J. Schowen, *J. Chem. Soc. Chem. Comm.* **1986**, 267-268.

[220] C. H. Langley, J.-H. Lii, N. L. Allinger, *J. Comp. Chem.* **2001**, *22*, 1451-1475.

[221] F. H. Allen, O. Kennard, D. G. Watson, L. Brammer, A. G. Orpen, R. Taylor, *J. Chem. Soc. Perkin. Trans. 2* **1987**, *12*, S1-S19.

[222] P. D. Bartlett, F. E. Condon, A. Schneider, *J. Am. Chem. Soc.* **1944**, *66*, 1531-1539.

[223] G. A. Olah, G. K. S. Prakash, J. Sommer, *Superacids, Vol. 3*, Wiley-Interscience, New York, **1985**.

[224] H.-U. Siehl, H. Walter, *J. Chem. Soc. Chem. Comm.* **1985**, 76-77.

[225] J. E. McMurry, C. N. Hodge, *J. Am. Chem. Soc.* **1984**, *106*, 6450-6451.

[226] M. C. A. Donkersloot, H. M. Buck, *J. Am. Chem. Soc.* **1981**, *103*, 6549-6554.

[227] H. S. Rzepa, J. Miller, *J. Chem. Soc. Perkin Trans. 2* **1985**, 717-723.

[228] O. Tapia, J. Andrea, J. M. Aullo, C. I. Branden, *J. Chem. Phys.* **1985**, *83*, 4673-4682.

[229] A. M. Davis, M. I. Page, S. C. Mason, I. Watt, *J. Chem. Soc. Comm.* **1984**, 1671-1672.

[230] M. G. Essig, T. T. Stevenson, F. Shatizadeh, R. E. Stenkamp, L. H. Jenson, *J. Org. Chem.* **1984**, *49*, 3652-3656.

[231] I. V. Vrceck, V. Vrceck, H.-U. Siehl, *J. Phys. Chem. A* **2002**, *106*, 1604-1611.

[232] M. J. Sherrod, F. M. Menger, *J. Am. Chem. Soc.* **1989**, *111*, 2611-2613.

[233] J. Sicher, J. Zavada, M. Svoboda, *Collect. Czech. Chem. Comm.* **1962**, *27*, 1927-1938.

[234] V. Prelog, W. Kung, *Helv. Chim. Acta* **1956**, *39*, 1394-1406.

[235] S. Danishefsky, M. Hirama, N. Fritsch, J. Clardy, *J. Am. Chem. Soc.* **1979**, *101*, 7013-7018.

[236] F. M. Menger, M. J. Sherrod, *J. Am. Chem. Soc.* **1990**, *112*, 8071-8075.

[237] R. Ponec, G. Yuzhakov, *J. Org. Chem.* **2004**, *69*, 2992-2996.

[238] M. L. Mckee, P. B. Shevlin, H. S. Rzepa, *J. Am. Chem. Soc.* **1986**, *108*, 5793-5798.

Curiculum Vitae

Personal details

Name: Parveen Choudhary Mohr

Date of birth: 01.06.1974

Place of birth Chandigarh

Nationality: Indian

Marital Status: Married

Education

1989-90 Secondary School from CBSE, New Delhi

1990-1992 Senior Secondary School from CBSE, New Delhi

1992-1996 B.Sc. Chemistry (Hon. School), Punjab University, Chandigarh

1995-1997 M.Sc. Chemistry (Hon. School), Punjab University, Chandigarh

1997-1998 Bachlor of education (Science & Mathematics), Punjab University, Chandigarh

1998-1999 Master of education, Kurukshetra University, Kurukshetra

1999-2000 NET-LECTURESHIP QUALIFIED conducted on behalf of the University Grant Commission (UGC), New Delhi

July 2000- dec 2003

Worked as Junior Research fellow in Chemistry Department of Panjab University, Chandigarh

Jan 2004 onwards

Working for doctorate thesis at University of Duisburg–Essen, Germany.

Publications

- Parveen, H. Singh, P. Venugopalan, T. V. Singh; *Indian J. Chem*. **2004**, 43A, 233-239.
- Parveen, H. Singh, T. V. Singh, P. V. Bhartam, P. Venugopalan; *J. Mol. Struct.* (Theochem), **2004**, 685, 139-145.